SEMICRYSTALLINE POLYMER-BASED AEROGELS: STRUCTURE, MORPHOLOGY AND MULTIFUNCTIONAL PROPERTIES

by

VIPIN G. KRISHNAN
Registration No: 10CC17A39011

A thesis submitted to the
Academy of Scientific and Innovative Research
for the award of the degree of
DOCTOR OF PHILOSOPHY
in
SCIENCE

Under the Supervision of
Dr. E. BHOJE GOWD

सीएसआईआर का अंतर्विषयी आयाम
Interdisciplinary face of CSIR

CSIR-National Institute for Interdisciplinary Science and Technology

(CSIR-NIIST), Thiruvananthapuram- 695 019, Kerala, India

Academy of Scientific and Innovative Research
AcSIR Headquarters, CSIR-HRDC campus, Sector 19, Kamla Nehru Nagar,
Ghaziabad, U.P.- 201002, India

February 2023

Dedicated to My Beloved Brother...

CERTIFICATE

This is to certify that the work incorporated in this Ph.D. thesis entitled *"Semicrystalline Polymer-based Aerogels: Structure, Morphology and Multifunctional Properties"* submitted by **Mr. Vipin G. Krishnan** to the Academy of Scientific and Innovative Research (AcSIR), in partial fulfilment of the requirements for the award of the **Degree of Doctor of Philosophy in Science**, embodies original research work under my supervision and guidance. We further certify that this work has not been submitted to any other University or Institution, in part or full, for the award of any degree or diploma. Research material obtained from other sources has been duly acknowledged in the thesis. Any text, illustration, table, etc., used in the thesis from other sources, have been duly cited and acknowledged.

22/02/2023

Vipin G. Krishnan

22/02/2023

Dr. E. Bhoje Gowd
(Thesis Supervisor)

Thiruvananthapuram

22nd February, 2023

i

STATEMENTS OF ACADEMIC INTEGRITY

I, **Vipin G. Krishnan,** a Ph.D. student of the Academy of Scientific and Innovative Research (AcSIR) with Registration No. 10CC17A39011 hereby undertake that the thesis entitled **"Semicrystalline Polymer-based Aerogels: Structure, Morphology and Multifunctional Properties"** has been prepared by me and that the document reports original work carried out by me and is free of any plagiarism in compliance with the UGC Regulations on *"Promotion of Academic Integrity and Prevention of Plagiarism in Higher Educational Institutions (2018)"* and the CSIR Guidelines for *"Ethics in Research and in Governance (2020)"*.

22|02|2023

Vipin G. Krishnan

Thiruvananthapuram

22nd February 2023

It is hereby certified that the work done by the student, under my supervision, is plagiarism-free in accordance with the UGC Regulations on *"Promotion of Academic Integrity and Prevention of Plagiarism in Higher Educational Institutions (2018)"* and the CSIR Guidelines for *"Ethics in Research and in Governance (2020)"*.

22|02|2023

Dr. E. Bhoje Gowd

Thiruvananthapuram

22nd February 2023

DECLARATION

I, **Vipin G. Krishnan**, bearing AcSIR Registration No. 10CC17A39011 declare

(i) that my thesis entitled, **"Semicrystalline Polymer-based Aerogels: Structure, Morphology and Multifunctional Properties"** is plagiarism free in accordance with the UGC Regulations on *"Promotion of Academic Integrity and Prevention of Plagiarism in Higher Educational Institutions (2018)"* and the CSIR Guidelines for *"Ethics in Research and in Governance (2020)"*.

(ii) that I would be solely held responsible if any plagiarised content in my thesis is detected, which is violative of the UGC regulations 2018.

22/02/2023

Vipin G. Krishnan

Thiruvananthapuram

22nd February 2023

ACKNOWLEDGEMENTS

First and foremost, I would love to put forth my profound gratitude and indebtedness to Dr. E. Bhoje Gowd, my guru and mentor, for suggesting the research problem, guiding me on the right path and reassuring my potentials. He wholeheartedly supported me through thick and thin, provided the scientific freedom of thought and action and helped me become a better researcher. It is his positive outlook and passion towards science that inspired and helped me to build confidence in my work. His teachings were prolific and his life stories were a real learning curve. "Thank you Bhoje Sir for being the person you are and inspiring young minds like me each and every day with your words and deeds. You are an absolute gem!!"

My sincere thanks go to Dr. Saju Pillai, Dr. U. S. Hareesh and Dr. Joshy Joseph, my doctoral advisory committee members, for their valuable comments, creative suggestions and fruitful discussions during each step of my research work.

I am grateful to Dr. A. Ajayaghosh and Dr. C. Anandharamakrishnan, the former and present directors of CSIR-NIIST, for providing the necessary facilities and infrastructure to carry out my thesis work. Thanks are also due to Dr. P. Prabhakar Rao, Dr. Harikrishna Bhatt, Dr. S. Savithri and Dr. M. Ravi, the heads of Materials Science and Technology Division during my tenure at CSIR-NIIST, for their valuable help in various academic and official matters.

I would like to acknowledge the former and present AcSIR coordinators, Dr. R. Luxmi Varma, Dr. C. H. Suresh and Dr. Karunakaran Venugopal, for the help rendered during my admission and all other academic activities.

Vipin G. Krishnan

x

TABLE OF CONTENTS

Chapter 2 **Nanoporous Crystalline Aerogels of Syndiotactic** **29-58**
 Polystyrene: Polymorphism, Dielectric, Thermal
 and Acoustic Properties

LIST OF ABBREVIATIONS

λ	Thermal conductivity
ρ_{ap}	Apparent density of aerogel
ρ_{pol}	Density of bulk polymer
$Đ$	Polydispersity Index
3D	Three-dimensional
APP	Ammonium polyphosphate
BET	Brunauer–Emmett–Teller
BJH	Barrett–Joyner–Halenda
CA	Citric acid
CPO	Cyclopentanone
CS	Chitosan
CVD	Chemical vapor deposition
DI	Deionised
DMF	N,N-dimethylformamide
DSC	Differential scanning calorimetry
EDS	Energy dispersive spectroscopy
EMI	Electromagnetic interference
EPE	Expanded polyethylene
EPS	Expanded polystyrene
FTIR	Fourier transform infrared spectroscopy
FWHM	Full width at half maximum
HRC	Heat release capacity
HRR	Heat release rate

IFR	Intumescent flame retardant
IR	Infrared
LbL	Layer-by-layer
LOI	Limiting oxygen index
MCC	Microscale combustion calorimetry
M_w	Weight-average molecular weight
NIPS	Non-solvent induced phase separation
PA	Phytic acid
PDLA	Poly(D-lactide)
PEC	Polyelectrolyte complex
PHB	Poly(3-hydroxybutyrate)
PHRR	Peak heat release rate
PLA	Polylactide
PLLA	Poly(L-lactide)
PPO	Polyphenylene oxide
PU	Polyurethane
PVA	Polyvinyl alcohol
SA	Sodium alginate
SAXS	Small-angle X-ray scattering
SC	Stereocomplex
SEM	Scanning electron microscopy
sPS	Syndiotactic polystyrene
TEM	Transmission electron microscopy
TGA	Thermogravimetric analysis
THF	Tetrahydrofuran

THR	Total heat release
TTPHRR	Time to peak heat release rate
UL	Underwriters laboratories
ULT	Ultra-low temperature
WAXD	Wide-angle X-ray diffraction
WAXS	Wide-angle X-ray scattering
WCA	Water contact angle
XPS	X-ray photoelectron spectroscopy

PREFACE

The global energy crisis has prompted researchers worldwide to look for energy-efficient alternatives to conventional lightweight materials in acoustic insulation, thermal insulation, packaging, electronics, environment remediation, etc. Because of their unique properties, such as low density, high specific surface area, high porosity, ultralow dielectric constant, super low thermal conductivity, low sonic velocity and so on, aerogels have gained widespread attention of scientists as well as industry. Polymer based aerogels, in particular, attracted much interest due to their superior mechanical properties and ease of processing. Semicrystalline polymers are reported to form thermoreversible gels in different organic solvents, where the connectedness between polymer chains is achieved by crystallization. Solvent extraction from the gels can be eased by exchanging the gel solvents with other green solvents. In the case of water soluble polymers, non-covalent interactions like hydrogen bonding induce gel formation. The present thesis focuses on developing polymer-based aerogels with superior properties and multi-functions by the physical gelation of polymers. In the first half, structure-morphology-property relationship in crystalline aerogels is studied. Enhancement of flame-retardant properties of polymer aerogels is another challenge, which is addressed in the second half of the thesis.

The thesis has been structured into six chapters. Chapter 1 provides a brief understanding of the history, evolution, structural aspects and properties of aerogels. Emphasis is given to polymer-based aerogels and their merits. Elaborate discussions on various gelation mechanisms in polymers and solvent extraction strategies are also provided. An entire section is dedicated to the flame-retardancy of aerogels, which

includes flammability test methods, flame-retardant mechanisms, etc. The chapter is concluded by highlighting various applications of polymer-based aerogels.

The crystal structure of semicrystalline polymers is found to influence the microstructure of aerogels, affecting most of the aerogel properties. Chapter 2 investigates the impact of structure and morphology on the thermal, mechanical, dielectric and acoustic properties of syndiotactic polystyrene (sPS) aerogels. sPS is capable of forming nanoporous crystalline forms of aerogels, namely δe and εe forms, from their respective gels. Solvent exchange and freeze-drying techniques were used to prepare hierarchically porous sPS (δe and εe) aerogels. These aerogels exhibited a difference in morphology, resulting in differences in surface areas, pore sizes, pore distributions, thermal conductivities, sound absorption coefficients, etc. The intricate polymorphic phase transition behavior of sPS crystalline nanoporous forms elucidated by X-ray diffraction furnished useful information to the existing literature on sPS. This chapter also demonstrated the excellent oil-water separation capability of sPS aerogel monoliths.

Acknowledging the growing demand for sustainable polymers, Chapter 3 reports a facile strategy for enhancing the thermal and mechanical properties of polylactide (PLA) aerogels by the supramolecular gelation of poly(L-lactide) (PLLA)/poly(D-lactide) (PDLA) blend and the subsequent stereocomplex (SC) formation between the enantiomers. In the blend gel, PLLA and PDLA crystallized independently into the corresponding crystal complex forms (ε forms) and the complete stereocomplexation was induced by thermally annealing the blend gel at 70 °C. Upon solvent exchange and freeze-drying of the crystalline pure SC gel, mechanically and thermally superior SC aerogel was furnished. The SC content in the blend gel could be tuned by varying the gel annealing temperature. Unlike the homopolymer aerogels with fibrillar network

morphologies, SC aerogel exhibited unique interconnected nodular microstructure. It is this structural evolution, both at the molecular level and the micrometer length scale, during the SC formation that instigated better thermal, mechanical and surface properties in the PLA aerogels.

Since flammability is a major limitation of polymeric materials, Chapter 4 focuses on enhancing the flame retardant properties of PLA aerogels. A sustainable and novel strategy of incorporating biobased ionic molecules into the thermoreversible gels of PLLA in a layer-by-layer (LbL) fashion during the solvent exchange process was developed in this chapter for flame retardant modification. The ionic interactions between the guest molecules (sodium alginate, chitosan and phytic acid) and the hydrogen bonding between PLLA and guest molecules favored the LbL assembly. PLLA aerogels with different sequential depositions were prepared by freeze-drying and the flammability properties were investigated. The synergetic effect of N and P rich guest biomolecules with char forming ability furnished excellent flame retardancy to the PLLA aerogels without employing any halogenated or inorganic flame retardant fillers. The protocol developed in this chapter is not limited to PLA alone; it can be used for the flame retardant modification of other semicrystalline polymers as well.

Polyvinyl alcohol (PVA) is another commercially important and widely used polymer for its biodegradability, water solubility, biocompatibility, low toxicity and low cost. Flame retardant modifications of PVA aerogels are generally achieved using inorganic fillers, but at the expense of other good properties. Chapter 5 aims at enhancing the flame retardancy of PVA aerogels by avoiding inorganic fillers and simultaneously retaining their lightweight nature, mechanical strength and acoustic properties. A completely organic and sustainable polyelectrolyte complex (PEC) made from chitosan and phytic acid was used as a flame retardant filler. Aerogels were prepared by ice

templating and freeze-drying of aqueous PVA-PEC solutions. The strong interaction between reactive PEC and PVA ensured excellent compatibility as well as interfacial adhesion of the filler, leading to flexible and strong aerogels with excellent anti-fire properties. A simple surface modification of the aerogels using silane endowed sticky hydrophobicity to the aerogels and further enhanced their flame retardancy. The salient features of the entire research work are summarised in Chapter 6, along with the perspectives for future work.

Chapter 1

Introduction

Aerogels, known as the world's lightest solid materials, are open-cell three-dimensional porous materials derived from gels in which the liquid component of the gel has been replaced with air. These materials possess outstanding properties such as extremely low density, high porosity, high specific surface area, low dielectric constant, super low thermal conductivity, and so on.[1-3] Dr. Samuel Stephen Kistler produced aerogels for the first time by the supercritical drying of a silica wet gel without destroying the gel structure and he published this work in Nature in 1931.[4] Subsequently, he synthesized aerogels from alumina, gelatine, agar, tungstic, ferric and stannic oxide, nickel tartrate, cellulose, nitrocellulose, egg albumin, etc.[4,5] In the early 1940's, the Monsanto Corp. started the commercial production of silica aerogel in a plant in Everett, Massachusetts after completing a license agreement with Dr. Kistler, and sold products for many years under the trade name "Santocel".[6,7] Monsanto continued the production of Santocel until the 1970's, and later abandoned it for reasons such as high production cost and competition from other thermal insulation materials. But not long after this, interest in aerogel was rekindled, in the late 1970's, when a group from Claude Bernard University in Lyons, France, applied sol-gel chemistry for the preparation of silica aerogels.[8] However, the major breakthrough came in 1989, when Pekala extended the techniques used to prepare inorganic aerogels for the preparation of aerogels of organic polymers, which included resorcinol-formaldehyde and melamine-formaldehyde.[9] Further, the pyrolysis of these organic aerogels led to the discovery of carbon aerogels, which opened a completely new area in aerogel research. The last decade witnessed fascinating advancements in the field of aerogels; nowadays, it is possible to make aerogels out of any material, for example, biopolymers, synthetic polymers, wood, metals, metal oxides, carbon nanotubes, graphene, boron nitride, clay, and so on.[10-18]

1.1. Definition of Aerogel

The definition of the term "aerogel" has always been controversial. Initially, only the gels dried by supercritical fluid extraction were called aerogels and the porous monoliths prepared using other drying techniques like evaporation and freeze-drying were termed as xerogels and cryogels, respectively.[19,20] However, the present-day terminology has nothing to do with the drying methods; it is rather based on material properties. The technical definition is "*an aerogel is an open-celled, mesoporous, solid foam that is composed of a network of interconnected nanostructures and that exhibits a porosity (non-solid volume) of no less than 50%*". In practice, any porous monolith, largely mesoporous (pore diameter = 2-50 nm), with low density and high specific surface area and having around 90% of its volume made up by air is treated as aerogel.[19,21] This definition can be extended further to materials which are predominantly macroporous (pore diameter > 50 nm), even though terminologies like open-cell foams or sponges sound more suitable.[22,23]

1.2. Polymer Based Aerogels

Silica aerogels are the most studied and commercialized class of aerogels and remain the standard reference material in aerogel research. Typically, silica aerogels possess 85-99.8 % porosity, specific surface area between 500 and 1200 m^2g^{-1}, bulk density as low as 0.003 gcm^{-3} and ultra-low thermal conductivity (0.005-0.1 $Wm^{-1}K^{-1}$).[24] Despite all these wonderful properties, applications of silica aerogels are limited due to their weak mechanical properties. The monolithic form is exceptionally fragile and brittle as the Si-O-Si linkages that make up their structure are weak.[3] The past few years saw a transition to polymer and polymer-inorganic hybrid aerogels and intense research is happening on these materials because of their superior mechanical performance and multifunctional

properties. This is quite evident from the increased number of publications in this area in the last eight years or so (Figure 1.1).
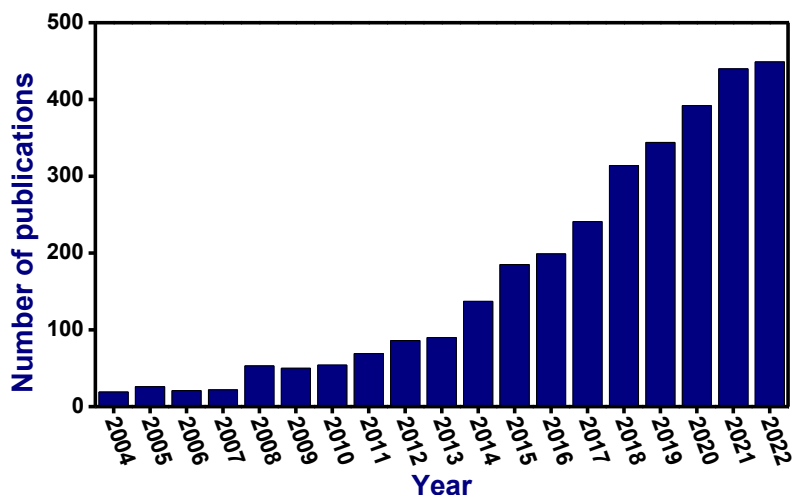
Figure 1.1. *Year-wise publications (2004–2022) with the keyword 'polymer aerogels' (Data collected on January 2023 from Web of Science).*

Polymer aerogels, unlike their silica counterparts, are mechanically robust when made in a monolithic form. They lose some of the advantages that silica provides, such as transparency and exceptionally low thermal conductivity but offer an excellent blend of properties that typically combine low thermal conductivity, energy absorption, and low density. Thus, polymer aerogels combine typical polymer properties such as low cost, robustness, durability, and easy processing with much of the extraordinary properties of inorganic aerogels. Also, some of these aerogels can offer unprecedented flexibility and the ability to be made into thin films or fibers (examples are given in Figure 1.2).[25-27] Polymer aerogels are attractive candidates for multitude of applications, including thermal energy insulation, environmental remediation, catalysis, packaging, chemical sensors, energy storage devices, etc.[18,21,26,28,29]
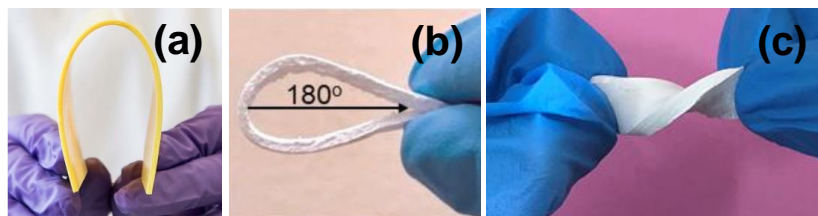
Figure 1.2. Flexible aerogels of (a) polyimide,[25] (b) polyvinyl chloride,[26] and (c) polyvinyl alcohol.

1.3. Gelation Mechanisms in Polymers

In order to develop aerogels with superior comprehensive properties using polymers, one must have a good understanding of the gel formation process in polymeric systems and the factors affecting the stability of gels. According to Almdal et al., gel is defined as *"a soft and/or solid-like substance consisting of at least two components, one of which is a liquid present in abundance."*[30] Gels are predominantly liquid by weight/volume, yet show solid-like behavior. This is because the solid component of the gel forms a three-dimensional (3D) network structure within the liquid and it is this crosslinking network within the liquid that furnishes hardness to a gel. In short, the dispersion medium in gels is solid and the dispersed phase is a liquid.

Polymeric gels consist of 3D polymer networks swollen by solvents and are mostly binary systems. The properties of polymer gels depend up on various factors such as the type of polymer, molecular weight of polymer, nature and degree of cross-linking, etc. Based on the cross-linking character, i.e., the nature of bonding in gels, polymeric gels are mainly classified into chemical gels and physical gels.[31,32]

1.3.1. Chemical Gels

Chemical gels are those formed by the covalent cross-linking between polymer chains. Typically, chemical gels are prepared by addition polymerization, condensation polymerization, free radical polymerization, or electromagnetic radiation. The former

methods involve the addition of external cross-linking agents, whereas the electromagnetic radiation induced gelation can be obtained without additional cross-linkers.[33] In any case, however, the formation of covalent connectivity between polymer chains modifies the chemical structure of the polymer and eventually affects the physical properties of the gels both at the molecular and macromolecular levels. Once chemically cross-linked, the polymer gel becomes insoluble and the cross-linking density influences many of the gel properties, such as elasticity, mechanical robustness, transport properties, etc. Since the network junction points of the chemical gels are formed by covalent bonds between either the polymers or the polymer and the cross-linker, these gels can only be damaged by bond cleavage or by thermal degradation of polymer(s).[34] Compared to physical gels, chemically cross-linked gels are stronger due to the higher strength of covalent bonds.

1.3.2. Physical Gels

Unlike chemical gels, the interconnectedness between polymer chains in physical gels is brought about by the physical aggregation of polymer chains, which includes non-covalent interactions (hydrogen bonds, ionic interactions, hydrophobic interactions, etc.), polymer chain entanglements, helix formation, complexation, crystallization, and so on. These intermolecular physical cross-links are not as strong as the covalent bonds but are strong enough to link polymer chain segments for a prolonged period of time. The lifetime of such physical gels depends mainly on temperature and similar thermodynamic variables. Since the physical bonds in these gels are not permanent in nature, most of the physical polymer gels are "thermoreversible", i.e., the junction zones of the gel network can be created or removed by cooling or heating, respectively.[35,36] Thus, a transition from gel to sol (local order to disorder) and vice-versa can be achieved with the help of temperature, as shown in Figure 1.3.
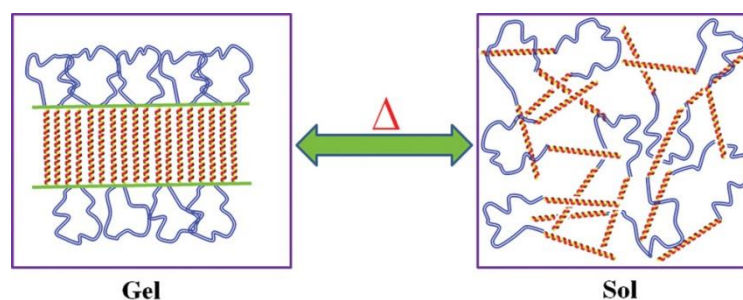
Figure 1.3. *Schematic illustration of thermoreversible gelation.*[37]

1.4. Thermoreversible Gelation in Semicrystalline Polymers

Most of the synthetic semicrystalline polymers undergo thermoreversible gelation, where the physical knots of the gel network are formed by tiny crystallites, rather than chemical or other physical bonds, as shown in Figure 1.4. In general, thermoreversible gels are obtained by cooling a mixture of two miscible entities, where one of the entities undergoes a phase transition from liquid to solid at a particular temperature called gel point and the second entity remains in the liquid state. As a result, the entity which has undergone the phase transition generates a solid framework wherein the liquid component remains confined.[38-41] In the case of polymer gels, the first entity is a polymer and the second entity is a good solvent of the polymer. Here, the gelation occurs via thermally induced phase-separation (TIPS), as the polymer-solvent affinity decreases with the decrease in temperature. By appropriately altering the temperature of a homogeneous polymer solution, liquid-liquid phase separation is induced, which leads to a polymer-rich phase and a polymer-lean phase. For semicrystalline polymers, crystallization takes place in the polymer-rich phase and this results in the gel formation as the micro-crystallites can serve as junction points for a 3D interpenetrating network structure.[42]

Though TIPS remains the most popular method for the fabrication of thermoreversible gels of polymers, phase separation and gelation of polymeric solutions can also be brought about using a non-solvent. This method is known as non-solvent

induced phase separation (NIPS). In NIPS, the polymer-rich phase is constituted by the polymer and a little solvent, similar to the TIPS method. Whereas the polymer-lean phase in NIPS consists of the non-solvent and the remaining solvent.[42,43] Therefore, it is necessary that the solvent and the non-solvent are completely miscible with each other.
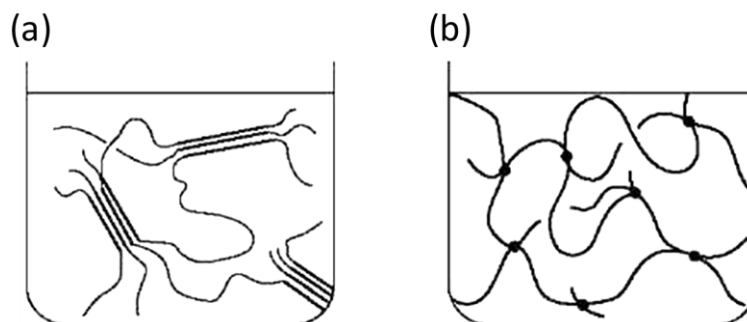
Figure 1.4. Schematic illustration of polymer gels. (a) Thermoreversible gels formed by crystalline junctions and (b) gels formed by covalent bonds.

1.5. Solvent Extraction Techniques

Solvent extraction from the gels is the key step that determines the structure, porosity, and density of aerogels. Removal of fluids from the gel should be done in such a way that the gel network is retained without structural disintegration. Drying procedures can influence the properties of final products as well as the economic scalability.[20,44] The evaporation of liquid from a porous structure can generate capillary forces at the liquid–gas–solid interfaces. Capillary pressure is inversely proportional to the pore radius.[45] Therefore, it is extremely difficult to evaporate out solvents from the nanometer sized pores of aerogels without collapsing their highly porous structures by normal drying methods. As shown in the temperature–pressure phase diagram (Figure 1.5), advanced techniques such as supercritical drying and freeze-drying can avoid the capillary forces by circumventing the liquid–gas interface.[46] Even though evaporative/ambient pressure drying is well established and industrially viable for silica aerogel production, the success rate of this method in polymer aerogel synthesis is very low and therefore, is rarely used.
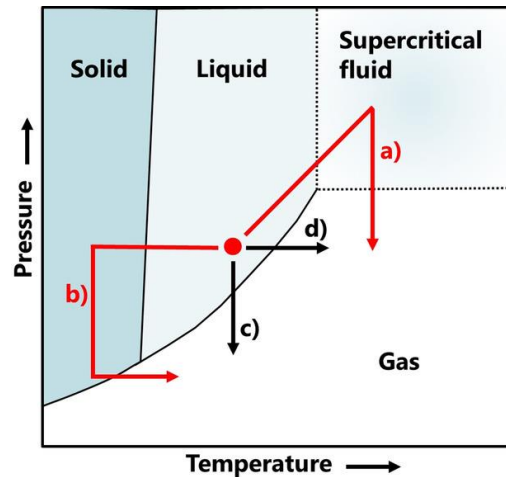
Figure 1.5. Typical temperature–pressure phase diagram showing the drying routes: a) supercritical drying, b) freeze drying, c) vacuum drying, and d) oven drying.[47]

1.5.1. Supercritical Drying

Supercritical drying takes the gel solvents above their critical temperatures and pressures to circumnavigate the liquid–gas interface. The critical point of water is too high; a temperature of 374 °C and pressure as high as 22.1 MPa must be reached to convert water into the supercritical fluid. Hence, solvents like ethanol with a lower critical point (241 °C and 6.14 MPa) were initially used as supercritical drying solvents.[4] Once the low-temperature process was introduced, CO_2 became the most favorite supercritical drying solvent due to its very low critical temperature of 31 °C (critical pressure = 7.38 MPa). The cost is also acceptable to go with the mild supercritical conditions.[48]

From the industrial point of view, the major drawback of supercritical drying is associated with the solvent exchange process, which is time consuming. Particularly, in the case of hydrogels, as the miscibility of water with CO_2 is poor under pressure, the hydrogels must be exchanged with CO_2 miscible organic solvents. The capital investments and maintenance costs for such high-pressure equipment are very high, which poses another challenge and the reduction of the same depends also on regional

laws and regulations for high-pressure gas safety. Over half of the current market requirement of silica aerogels is met by supercritical CO_2 drying of silica alcogels since it is an industrially viable process.

1.5.2. Freeze-Drying

Freeze-drying avoids the liquid–gas phase boundary by freezing of the gel liquid and the subsequent sublimation. The gel is cooled below the triple point of the pore fluid and vacuum is applied. Under isobaric conditions, the frozen gel is then subjected to controlled sublimation thereby bypassing the liquid-gas boundary to cross the solid-liquid border. This indeed can avoid the capillary forces associated with pore collapse in aerogels, making the process suitable for the preparation of porous monoliths.[49] Freeze-drying of hydrogels can be done directly; organogels should be exchanged with solvents like ethanol, methanol, water, or acetone. This technique requires high energy inputs and long drying times, which are the major drawbacks. However, freeze-drying is a safer and cheaper technique for gel drying when compared with the supercritical drying. Hence it is widely used, particularly in laboratories and has the potential to be scaled up to meet the industrial requirements.

1.6. Structure and Properties of Polymer Aerogels

Because of their unique porous structure, most aerogels possess multifunctional properties. That means an aerogel monolith has the potential to be used for various applications. The morphology and pore structure of aerogels greatly influence their properties, particularly mechanical, surface and molecular sorption properties. For example, polymer aerogels with interconnected fibrillar structures tend to have better mechanical strength than aerogels with spherulitic/globular morphology.[38,50-52] The pore size, shape and volume are key parameters in determining the physical properties of

aerogels and these could be controlled by varying the preparation conditions of the gels and aerogels. Apart from the disordered meso (2-50 nm) and macro (>50 nm) porosities, aerogels of polymers such as syndiotactic polystyrene (sPS) and polyphenylene oxide (PPO) have the ability to exhibit crystalline nanoporosity, i.e., porosity within the crystal lattice, which is of the order of less than 2 nm (microporosity).[36,53] Thus, it is possible to achieve aerogels with hierarchical porosity (Figure 1.6) using polymers. By tuning the molecular structure of polymers, morphology and porous structure, and ultimately, the physical properties of the aerogels could be tuned. The first part of the thesis explores the structure-morphology-property relationship in semicrystalline polymer aerogels.
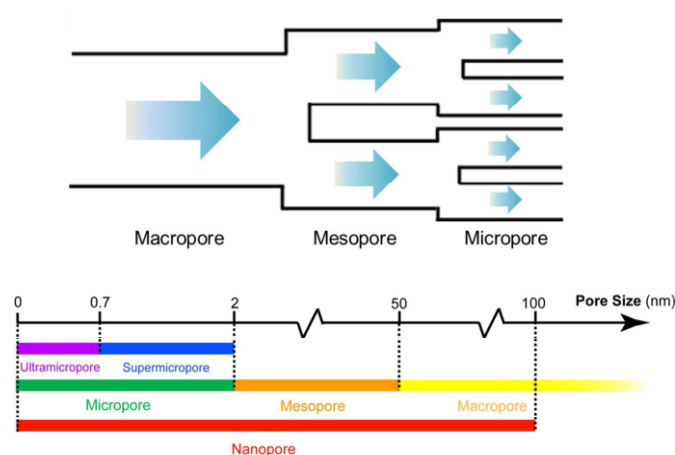
Figure 1.6. Schematic illustration of hierarchical porosity in polymer aerogels.[54]

1.7. Polymers are Flammable

Despite all the good properties, polymer aerogels still pose a serious concern that can restrict their utilization in households, transportation, or packaging; they are inherently flammable due to the organics that make up the polymer structure. On exposure to fire, polymer aerogels get ignited very easily and the flame propagates through the bulk rapidly leading to release of huge amounts of heat and smoke.[55] Compared to the bulk polymer, aerogels are even more susceptible to fire because of the air-filled cavities present in them. Heat, oxygen, and fuel are the three basic elements required for a fire to

start and sustain.[56] If either one of these elements is cut off, the flame can be ceased. Polymers, on exposure to sufficient heat, decompose gradually and release volatile products. This phenomenon is known as pyrolysis. The flammable volatiles will then mix with the atmospheric oxygen to form a combustible source. If the temperature is high enough for the autoignition, it catches fire. Combustion generates more heat, some of which is radiated onto the unburned polymer, thereby leading to further decomposition and combustion. This process of burning continues until either oxygen, heat or fuel is cut off. When exposed to fire, thermoplastic polymers tend to drip and flow, and these dripping particles can cause the additional process of flame propagation. However, thermosets do not drip and flow.[57-62] Figure 1.7 shows the scheme of polymer decomposition and combustion.
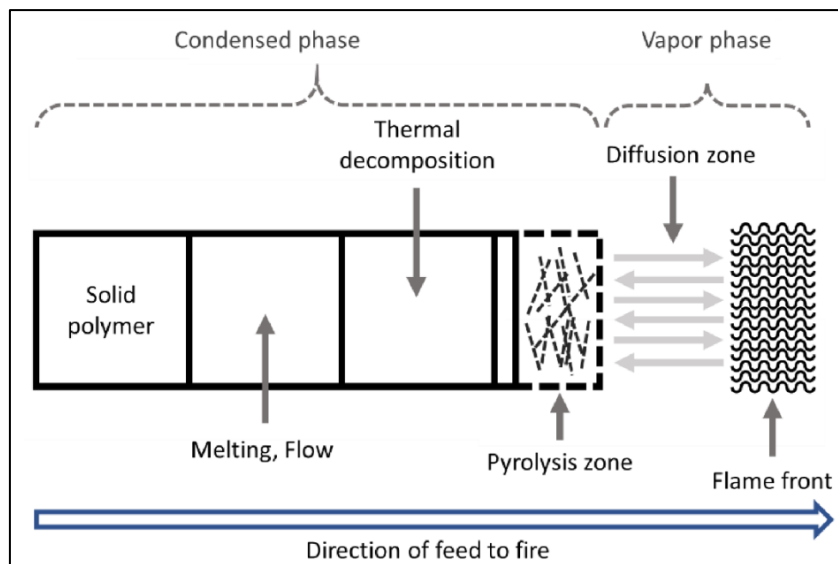
Figure 1.7. *Schematic diagram showing decomposition and combustion behavior of polymer.*[63]

The second part of the thesis focuses on improving the flame-retardancy of commercially important thermoplastic polymers-based aerogels. Therefore, it is important to highlight the standard procedures adopted for testing the flammability of polymer aerogels. Several parameters are measured, such as how readily materials get ignited, how

fast they are burning, and their behavior after burning. Limiting oxygen index, UL 94, cone calorimetry, and microscale combustion calorimetry are the most important tests for the determination of the flame behavior of polymers. But a single test alone cannot provide a comprehensive estimation of the flame-retardant character of samples since each test represents specific fire conditions that cannot be generalized for all the fire scenarios.[64] Therefore, a combination of a few of these tests is preferred for the real analysis of the flame-retardancy of polymer aerogels.

1.7.1. Limiting Oxygen Index (LOI)

LOI is the minimum percentage of oxygen required by a particular material for its combustion and an oxygen supply less than the LOI value cannot initiate the burning of that material. The oxygen content in the air is close to 21 %, which means that in an open-air situation, any material with LOI below 21 % will readily catch and sustain fire in the presence of a flame source. In the LOI test, a vertical specimen in a gas column fed with a mixed stream of oxygen/nitrogen will be ignited from the top and burned downwards to record the minimum percentage of oxygen required to initiate the burning of a specimen. The higher the number, more difficult it is for combustion to occur. However, LOI does not provide any qualitative information about the burning behavior of polymers. A material with LOI > 26 % can be considered as good flame-retardant material and a material with LOI = 21-26 % burns slowly.[65] Table 1.1 gives the LOI values of some of the common polymeric materials.

1.7.2. UL 94

UL 94 is a widely used flammability test for polymers originally designed by the Underwriters Laboratories (UL) that measures the extinguishing ability of the material after it is ignited. It involves applying flame to samples in various orientations. The

sample will be placed over the flame vertically or horizontally (vertical burn test (UL-94 V) and horizontal burn test (UL-94 HB)). For polymer aerogels, the horizontal test is generally used where the flame propagation or extinguishment after the removal of the flame source is noted, and the burning rate is calculated accordingly. On the other hand, the vertical flammability test considers several aspects, such as flame propagation time after the removal of the flame source, the quantity of specimen burned and dripping of flame particles. Accordingly, there are five standard ratings for the vertical burn test: V-2, V-1, V-0, 5VB and 5VA (from lowest to highest flame-retardancy).

Table 1.1. *LOI values of common polymeric materials.*[63,66]

Polymer	LOI (%)
Polyoxymethylene	15.7
Polyurethane foam	16.5
Cotton	16–17
Polymethyl methacrylate	17.3
Polyethylene	17.4
Polystyrene	17.6–18.3
Polycarbonate	22.5
Nylon 6	25–26
Poly(vinyl chloride)	45–49
Polytetrafluoroethylene	95.0
Polyvinyl alcohol	19
Polylactic acid	20

1.7.3. Cone Calorimetry

A conventionally used device for examining the flammability of polymers in detail and to predict their real-time fire behavior is the cone calorimeter. Cone calorimetry gives an abundance of information on various flammability parameters such as heat release rate (HRR), total heat release (THR), time to ignition, mass loss rate, total smoke release, and

effective heat of combustion.[67] The principle is based on the heat released during the ignition of the sample, which is directly related to the oxygen consumption during combustion. The specimen is placed under a conical heater and an input heat flux of 0–100 kW m^{-2} is given. The combustion products released are collected, from which the above-mentioned parameters are measured.[68] However, the specimen sizes required for testing are larger and the equipment is quite complex and requires a high cost of maintenance.[69]

1.7.4. Microscale Combustion Calorimetry (MCC)

MCC, also called pyrolysis combustion flow calorimetry, is a fast and convenient method for evaluating the flame-retardant properties with sample requirement in the scale of only milligrams, which is its major advantage over cone calorimetry. Here, milligram-sized samples are first pyrolyzed in a chamber with nitrogen or a mixed oxygen/nitrogen environment. The gases released from the combustion are oxidized in an oxygen rich environment under controlled conditions. The sample requirement in milligrams is really advantageous for screening, but phenomena like dripping, swelling, or shrinking will be missed in this process. This method cannot give the real-time fire behavior of materials as the specimen is not actually burning, instead, only the oxidation of combustion gases takes place.[70] Heat release rate (HRR) and heat release capacity (HRC) are the major parameters that can be obtained from MCC. Thus, a coupling of MCC results with either UL-94 results or LOI values, or even the cone calorimetry results, is vital to derive conclusions on the flammability of materials.

1.8. Flame Retardant Aerogels

Polymer-inorganic compositions have proven to be an effective way to improve the fire resistance of polymer aerogels. Lately, various inorganic nanofillers like silica,

MXenes, boron nitride nanosheets, hydroxyapatite nanocrystals, clay, MoS_2, etc. have been incorporated into the polymer matrix to produce aerogels with enhanced fire resistance performance.[71-74] These nanofillers act as free-radical scavengers during polymer degradation and provide mass transport barrier to oxygen and the flammable volatiles.[75] Intumescent flame retardants (IFR) have also been successfully employed to improve the flame retardancy of polymer aerogels. IFR coatings will swell and expand when heated, resulting in a charred surface layer that plays the role of a protective layer to the underlying material by preventing flame propagation.[76]

Organic or reactive flame retardants are char-type flame retardants. They prevent the release of fuel by combining it with char and form a protective char layer that can thermally insulate the underlying polymer.[77-79] The dehydration of the flame-retardant results in carbonization on the polymer surface and the char layer generated in this manner provides the flame-retardant effect to the polymer, as shown in Figure 1.8. Thus, the carbon layer acts as a barrier, and during burning, the decomposing polymer further enhances the char density/stability.[80-82]
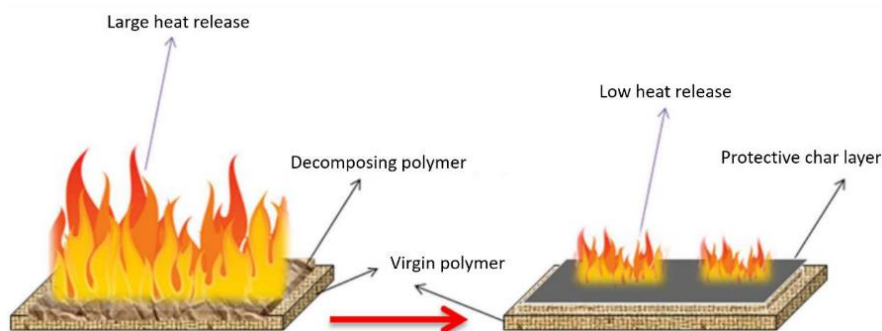
Figure 1.8. Schematic illustration of the effect of char-type flame-retardant during the burning of polymers.[83]

1.9. Applications of Polymer Aerogels

Because of their unique and extraordinary properties, polymer aerogels can find applications in numerous and diverse fields. The ultra-porous structure of aerogels

contributes to intrinsic properties such as low thermal conductivity, low sound velocity, low dielectric constant, and molecular sorption ability. However, research on polymer aerogels has not flourished extensively to the industrial scale yet, but is showing hopeful signs in recent times. The barriers to the commercialization of these wonderful materials include the time-consuming and expensive multistep production processes. Achieving structural stability in various operating environments is another challenge. In spite of all these difficulties, polymer aerogels can be tailored to suit a broad range of applications, some of which include thermal insulation, acoustic insulation, biomedical applications, packaging, environmental remediation, electronic applications, etc.[21,22,47,84-87] and we can expect some of these aerogels in the market in the near future.

1.9.1. Thermal Insulation

Thermal insulation is an important aspect when it comes to energy efficient buildings and structures and superior thermal insulation materials can effectively reduce the energy consumed for heating or cooling the buildings. The commercially available thermal insulators include silica aerogels, polyurethane (PU) foams, expanded polystyrene, mineral wool, and fiberglass. Silica aerogels are reported to have the lowest thermal conductivity (λ) (15 mWm^{-1}K^{-1}).[88] Whereas, PU foam has $\lambda \sim 21\text{–}24$ mWm^{-1}K^{-1} and the λ of mineral/glass wool and expanded polystyrene lies in the range of 32–37 mWm^{-1}K^{-1}.[89] Because of their highly mesoporous structure, aerogels possess lower thermal conductivity than the PU foams or expanded polystyrene, which are predominantly macroporous in nature. In porous materials, thermal conductivity is a sum of solid conductivity, gaseous conductivity and radiative conductivity (Figure 1.9). As the pore (mesopore) sizes in aerogels are lesser than the mean free path of gas molecules, the Knudsen effect will be induced, which can result in lower gaseous thermal conductivity.[90]

Therefore, aerogels are ideal candidates for thermal insulation applications as they can be effectively processed into panels or sheets.
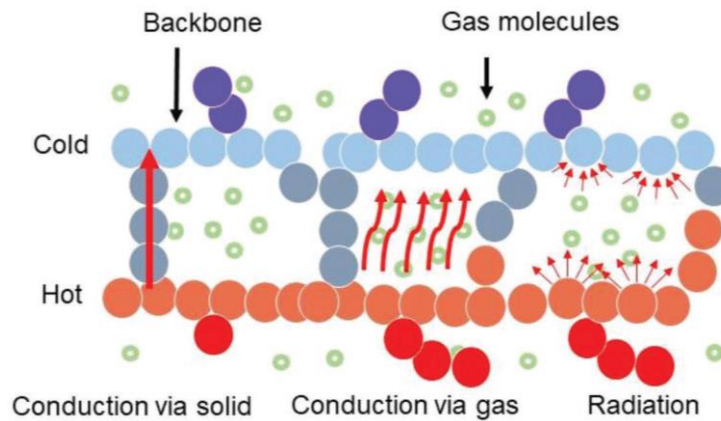
Figure 1.9. Schematic illustration of thermal transport pathways in aerogels.[26]

1.9.2. Acoustic Insulation

Soundproofing is equally important in buildings as thermal insulation, particularly in theatres and halls. The acoustic insulation ability of a particular material is measured in terms of its sound absorption coefficient, which is the ratio of absorbed sound intensity to the incident sound intensity and is a value between 0 and 1.[91] The higher the value of absorption coefficient, the greater the absorption ability. A good soundproof material should have minimum thickness and the maximum ability to absorb and attenuate sound energy of different frequencies. Conventionally, cellular concrete, asbestos, rock wool, glass wool, glass silk, mineral wool boards, cane fibre, porous tiles, gypsum plaster, etc., have been employed for sound insulation in buildings and structures. Aerogels are better acoustic insulators due to their large open-porosity and small pore sizes, which can result in multiple scattering of the incident and reflected sound waves. Also, the interconnected network structure of aerogels can cause air-viscous resistance damping, leading to the attenuation of sound energy (Figure 1.10).[92-94] Using aerogels, lightweight structures with excellent sound proofing can be achieved, but not at the cost of architectural aesthetics.
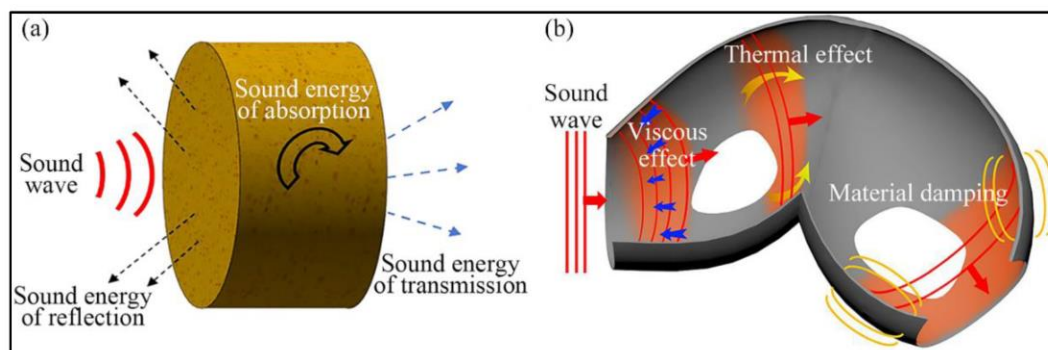
Figure 1.10. *Schematic illustration of (a) sound absorption process and (b) sound energy consumption mechanisms in aerogels.*[95]

1.9.3. Biomedical Applications

The biomedical uses of aerogels include tissue engineering scaffolds, sensing/imaging, drug delivery systems, biomedical implantable devices, etc. Biopolymer based aerogels are cytocompatible, biocompatible, and biodegradable and can be used in vivo. Biomedical scaffolds for tissue regeneration, particularly bone tissue regeneration, often use aerogel composites of polylactide and hydroxyapatite.[96,97] Aerogels prepared by freeze drying provide highly porous, elastic and interconnected network structures which are suitable for the smooth diffusion of cells and other molecules.[98] Electrically conducting polymers on conjugation with biopolymers have been reported for bio-sensing applications.[99,100] Drug delivery is another potential application; the high surface area and mesoporous structure of aerogels cater this potential.[101,102]

1.9.4. Packaging

Packaging materials have a huge market, which is currently dominated by polystyrene foams. Brittle products such as glassware, electronic goods, laboratory equipments, etc., mostly come wrapped in styrofoam. Consumers are looking for sustainable packaging alternatives which can provide mechanical protection and extend the shelf-life of packed products. Sustainable polymer aerogels can be the ideal

replacement of styrene foams in packaging industry. Because of their porous structure, lightweightedness and high surface area, aerogels provide interesting opportunities as food packages. They can simultaneously act as thermal insulators and provide protection against gases, vapors, and moisture. Bio-based hydrophobic polymers are best suited for this purpose. Aerogels can also incorporate active components which are capable of enhancing the shelf-life of the contained food by preventing microbial growth. The easy processability of aerogels into different shapes is another advantage and is crucial in packaging design.[103-105]

1.9.5. Environmental Remediation

Polymer-based aerogels are promising candidates for the removal of pollutants or contaminants from the environment. Aerogels possess huge potential in oil-water separation, CO_2 capture, air filtration, heavy metal removal from water, dye sorption, and so on, which can ultimately result in air and water purification.[106-108] The high surface area and the different levels of porosity of aerogels are particularly useful in the purification process. Biopolymers, in particular, are the favorite aerogel materials for environmental remediation because of their tuneable surface functionality. There are plenty of reports on the selective adsorption of organic solvents (potential pollutants) from water using polymer aerogels. Many of the synthetic polymers are hydrophobic in nature; the surface roughness induced by the aerogel structure can further enhance the hydrophobicity of such materials. These aerogels can selectively adsorb the oil/organic pollutants from water with very high efficiency. Biopolymer aerogels are mostly hydrophilic in nature but can be made hydrophobic using hydrophobization agents like alkyl siloxanes, alkyl aldehydes, trityl groups, etc.[109] The advantage of biopolymer aerogels is their flexibility; the oil/organic solvents can therefore be squeezed out several times from the aerogels without compromising their efficiency.

1.9.6. Electronic Applications

Aerogels have numerous applications in the field of electronics. Their nanostructure and extremely high porosity render aerogels unusual electronic and dielectric properties. The lowest ever dielectric constant reported for a solid material (close to 1.0) belongs to an aerogel.[110] In addition, aerogels possess extraordinarily large dielectric strength and dielectric resistivities, i.e., they exhibit exceptional insulating ability at very high voltages. Dielectric loss is also the bare minimum at the microwave frequency region. Some of the polymer and hybrid aerogels can be electrically conductive; some others can be photoconductive. These properties of aerogels are well exploited to furnish future energy storage materials, low dielectrics, ultra-fast electronic materials, etc.[110,111] In this era of wearable electronics, there is a huge market demand for flexible energy storage devices. Compressible and elastic aerogels with outstanding conductivity have been explored for batteries and as electrode materials for supercapacitors.

The rapid advancement in electronic communication and the widespread use of electronic devices has resulted in an undesirable phenomenon known as electromagnetic interference (EMI). In order to tackle this problem, a new class of materials called EMI shields has been developed, which can protect humans as well as devices from EM radiation pollution. Porous materials with well-interconnected network structures are preferred as EMI shields as the major mechanism of EMI-shielding involves the multiple reflections of the incoming electromagnetic waves.[112,113] Polymer aerogels can offer mechanical robustness and lightweightedness simultaneously, and the compressibility/flexibility associated with them can cater tuneable EMI shielding performance. Other applications of aerogels are as sensors, piezoelectric nanogenerators, triboelectric nanogenerators, etc.

1.10.   Scope of the Present Thesis

The preceding sections highlighted the importance of polymer-based aerogels in the upcoming days as alternatives to conventional porous materials in the construction field, packaging industry, electronics, and environmental remediation. Unlike silica or other inorganic aerogels, polymer aerogels generally possess excellent mechanical strength and the possibility for easy tuning of a wide range of properties. In this context, the present thesis provides an excellent opportunity to understand the structure-property relationship in some of the commercially important polymer aerogels. The effect of crystal structure on the morphology development in semicrystalline polymer aerogels has not been well-studied. The first half of the thesis tries to understand the role of chain packing and structural evolution on the morphology and physical properties of highly porous polymer aerogels. The second half proposes innovative and sustainable approaches to make flame retardant biodegradable aerogels. The credentials mentioned above are critical for the lab scale to industry level transition of polymer aerogels.

1.11.   References

1.   Aegerter, M. A.; Leventis, N.; Koebel, M. M.: *Aerogels handbook*; Springer Science & Business Media, **2011**.
2.   Teichner, S.; Nicolaon, G.; Vicarini, M.; Gardes, G. Inorganic oxide aerogels. *Advances in Colloid and Interface Science* **1976**, *5*, 245-273.
3.   Joseph, A. M.; Nagendra, B.; Shaiju, P.; Surendran, K.; Gowd, E. B. Aerogels of hierarchically porous syndiotactic polystyrene with a dielectric constant near to air. *Journal of Materials Chemistry C* **2018**, *6*, 360-368.
4.   Kistler, S. S. Coherent expanded aerogels and jellies. *Nature* **1931**, *127*, 741-741.
5.   Kistler, S. S. Coherent expanded-aerogels. *The Journal of Physical Chemistry* **2002**, *36*, 52-64.
6.   White, J. F. Manufacture of Silica Aerogel—Description of Process and Heat Transfer Problems. *Trans. Amer. Inst. Chem. Eng.* **1942**, *38*, 435-446.
7.   Jones, C. Santocel-a new raw material for the coating industry. *P Industry Magazine* **1947**, *62*, 390-391.
8.   Fricke, J. The unbeatable lightness of aerogels: Take 10 parts of metal oxide, 90 parts of air, mix well–and watch industry fall upon the product with glee. *New Scientist* **1993**.
9.   Pekala, R. W. Organic aerogels from the polycondensation of resorcinol with formaldehyde. *Journal of Materials Science* **1989**, *24*, 3221-3227.

10. Liu, W.; Herrmann, A.-K.; Bigall, N. C.; Rodriguez, P.; Wen, D.; Oezaslan, M.; Schmidt, T. J.; Gaponik, N.; Eychmüller, A. Noble Metal Aerogels: Synthesis, Characterization, and Application as Electrocatalysts. *Accounts of chemical research* **2015**, *48*, 154-162.

11. Li, Y.; Kang, Z.; Yan, X.; Cao, S.; Li, M.; Guo, Y.; Huan, Y.; Wen, X.; Zhang, Y. A three-dimensional reticulate CNT-aerogel for a high mechanical flexibility fiber supercapacitor. *Nanoscale* **2018**, *10*, 9360-9368.

12. Mao, J.; Iocozzia, J.; Huang, J.; Meng, K.; Lai, Y.; Lin, Z. Graphene aerogels for efficient energy storage and conversion. *Energy & Environmental Science* **2018**, *11*, 772-799.

13. Sun, H.; Xu, Z.; Gao, C. Multifunctional, ultra-flyweight, synergistically assembled carbon aerogels. *Advanced materials* **2013**, *25*, 2554-2560.

14. Benad, A.; Jürries, F.; Vetter, B.; Klemmed, B.; Hübner, R.; Leyens, C.; Eychmüller, A. Mechanical properties of metal oxide aerogels. *Chemistry of Materials* **2018**, *30*, 145-152.

15. Song, Y.; Li, B.; Yang, S.; Ding, G.; Zhang, C.; Xie, X. Ultralight boron nitride aerogels via template-assisted chemical vapor deposition. *Scientific reports* **2015**, *5*, 10337.

16. Lei, W.; Mochalin, V. N.; Liu, D.; Qin, S.; Gogotsi, Y.; Chen, Y. Boron nitride colloidal solutions, ultralight aerogels and freestanding membranes through one-step exfoliation and functionalization. *Nature communications* **2015**, *6*, 8849.

17. Madyan, O. A.; Fan, M. Hydrophobic clay aerogel composites through the implantation of environmentally friendly water-repellent agents. *Macromolecules* **2018**, *51*, 10113-10120.

18. Song, J.; Chen, C.; Yang, Z.; Kuang, Y.; Li, T.; Li, Y.; Huang, H.; Kierzewski, I.; Liu, B.; He, S. Highly compressible, anisotropic aerogel with aligned cellulose nanofibers. *ACS nano* **2018**, *12*, 140-147.

19. Pierre, A. C.; Pajonk, G. M. Chemistry of aerogels and their applications. *Chemical Reviews* **2002**, *102*, 4243-4266.

20. Zhao, S.; Manic, M. S.; Ruiz-Gonzalez, F.; Koebel, M. M. Aerogels. *The Sol‑Gel Handbook* **2015**, 519-574.

21. Noroozi, M.; Panahi-Sarmad, M.; Abrisham, M.; Amirkiai, A.; Asghari, N.; Golbaten-Mofrad, H.; Karimpour-Motlagh, N.; Goodarzi, V.; Bahramian, A. R.; Zahiri, B. Nanostructure of Aerogels and Their Applications in Thermal Energy Insulation. *ACS Applied Energy Materials* **2019**, *2*, 5319-5349.

22. Zhao, S.; Malfait, W. J.; Guerrero-Alburquerque, N.; Koebel, M. M.; Nyström, G. Biopolymer aerogels and foams: Chemistry, properties, and applications. *Angewandte Chemie International Edition* **2018**, *57*, 7580-7608.

23. Jiang, S.; Agarwal, S.; Greiner, A. Low‑density open cellular sponges as functional materials. *Angewandte Chemie International Edition* **2017**, *56*, 15520-15538.

24. Salimian, S.; Zadhoush, A.; Naeimirad, M.; Kotek, R.; Ramakrishna, S. A review on aerogel: 3D nanoporous structured fillers in polymer-based nanocomposites. *Polymer Composites* **2018**, *39*, 3383-3408.

25. Pantoja, M.; Boynton, N.; Cavicchi, K. A.; Dosa, B.; Cashman, J. L.; Meador, M. A. B. Increased flexibility in polyimide aerogels using aliphatic spacers in the polymer backbone. *ACS applied materials & interfaces* **2019**, *11*, 9425-9437.

26. Li, M.; Qin, Z.; Cui, Y.; Yang, C.; Deng, C.; Wang, Y.; Kang, J. S.; Xia, H.; Hu, Y. Ultralight and Flexible Monolithic Polymer Aerogel with Extraordinary Thermal Insulation by A Facile Ambient Process. *Advanced Materials Interfaces* **2019**, *6*, 1900314.

27. Li, X.; Dong, G.; Liu, Z.; Zhang, X. Polyimide aerogel fibers with superior flame resistance, strength, hydrophobicity, and flexibility made via a universal sol–gel confined transition strategy. ACS nano 2021, 15, 4759-4768..

28. Zhang, X.; Wang, H.; Cai, Z.; Yan, N.; Liu, M.; Yu, Y. Highly compressible and hydrophobic anisotropic aerogels for selective oil/organic solvent absorption. *ACS Sustainable Chemistry & Engineering* **2018**, *7*, 332-340.

29. Wei, T.-Y.; Lu, S.-Y.: Aerogels for Energy Saving and Storage. 2011; Vol. 33; pp 873-911.

30. Almdal, K.; Dyre, J.; Hvidt, S.; Kramer, O. Towards a phenomenological definition of the term 'gel'. *Polymer gels and networks* **1993**, *1*, 5-17.

31. Flory, P. J.: *Principles of polymer chemistry*; Cornell university press, 1953.

32. De Gennes, P.-G.; Gennes, P.-G.: *Scaling concepts in polymer physics*; Cornell university press, 1979.

33. Horkay, F.; Douglas, J. F. Polymer gels: basics, challenges, and perspectives. *Gels and other soft amorphous solids* **2018**, 1-13.

34. Osada, Y.; Khokhlov, A.: *Polymer gels and networks*; CRC Press, 2001.

35. Longo, S.; Vitillo, J. G.; Daniel, C.; Guerra, G. Monolithic aerogels based on poly (2, 6-diphenyl-1, 4-phenylene oxide) and syndiotactic polystyrene. *ACS applied materials & interfaces* **2013**, *5*, 5493-5499.

36. Daniel, C.; Alfano, D.; Venditto, V.; Cardea, S.; Reverchon, E.; Larobina, D.; Mensitieri, G.; Guerra, G. Aerogels with a microporous crystalline host phase. *Advanced materials* **2005**, *17*, 1515-1518.

37. Kotharangannagari, V. K.; Sánchez-Ferrer, A.; Ruokolainen, J.; Mezzenga, R. Thermoreversible gel–sol behavior of rod–coil–rod peptide-based triblock copolymers. *Macromolecules* **2012**, *45*, 1982-1990.

38. Daniel, C.; Dammer, C.; Guenet, J.-M. On the definition of thermoreversible gels: the case of syndiotactic polystyrene. *Polymer* **1994**, *35*, 4243-4246.

39. Guenet, J.-M.: *Thermoreversible gelation of polymers and biopolymers*; Academic Press, 1992.

40. Guenet, J.-M. Physical aspects of organogelation: A point of view. *Gels* **2021**, *7*, 65.

41. Nayak, A. K.; Das, B.: Introduction to polymeric gels. In *Polymeric gels*; Elsevier, 2018; pp 3-27.

42. Kang, J.; Gi, H.; Choe, R.; Yun, S. I. Fabrication and characterization of poly (3-hydroxybutyrate) gels using non-solvent-induced phase separation. *Polymer* **2016**, *104*, 61-71.

43. Kang, J.; Hwang, J.-Y.; Huh, M.; Yun, S. I. Porous poly (3-hydroxybutyrate) scaffolds prepared by non-solvent-induced phase separation for tissue engineering. *Macromolecular Research* **2020**, *28*, 835-843.

44. Dowson, M.; Grogan, M.; Birks, T.; Harrison, D.; Craig, S. Streamlined life cycle assessment of transparent silica aerogel made by supercritical drying. *Applied Energy* **2012**, *97*, 396-404.

45. Zarzycki, J.; Prassas, M.; Phalippou, J. Synthesis of glasses from gels: the problem of monolithic gels. *Journal of materials science* **1982**, *17*, 3371-3379.

46. Takeshita, S.; Yoda, S. Chitosan aerogels: transparent, flexible thermal insulators. *Chemistry of Materials* **2015**, *27*, 7569-7572.

47. Takeshita, S.; Zhao, S.; Malfait, W. J.; Koebel, M. M. Chemistry of chitosan aerogels: three-dimensional pore control for tailored applications. *Angewandte Chemie International Edition* **2021**, *60*, 9828-9851.

48. Tewari, P. H.; Hunt, A. J.; Lofftus, K. D. Ambient-temperature supercritical drying of transparent silica aerogels. *Materials letters* **1985**, *3*, 363-367.

49. Brinker, C. J.; Scherer, G. W.: *Sol-gel science: the physics and chemistry of sol-gel processing*; Academic press, 2013.

50. Keller, A. Introductory lecture. Aspects of polymer gels. *Faraday Discussions* **1995**, *101*, 1-49.

51. Guenet, J.-M.: *Polymer-solvent molecular compounds*; Elsevier, 2010.

52. Itagaki, H.; Tokami, T.; Mochizuki, J. A trial to clarify a cause of forming physical gels: Morphology of syndiotactic polystyrene in n-alkylbenzene. *Polymer* **2012**, *53*, 5304-5312.

53. Daniel, C.; Sannino, D.; Guerra, G. Syndiotactic polystyrene aerogels: adsorption in amorphous pores and absorption in crystalline nanocavities. *Chemistry of Materials* **2008**, *20*, 577-582.

54. Liu, T.; Zhang, F.; Song, Y.; Li, Y. Revitalizing carbon supercapacitor electrodes with hierarchical porous structures. *Journal of Materials Chemistry A* **2017**, *5*, 17705-17733.

55. Guo, W.; Liu, J.; Zhang, P.; Song, L.; Wang, X.; Hu, Y. Multi-functional hydroxyapatite/polyvinyl alcohol composite aerogels with self-cleaning, superior fire resistance and low thermal conductivity. *Composites Science and Technology* **2018**, *158*, 128-136.

56. Dewaghe, C.; Lew, C.; Claes, M.; Belgium, S.; Dubois, P.: Fire-retardant applications of polymer–carbon nanotubes composites: Improved barrier effect and synergism. In *Polymer–carbon nanotube composites*; Elsevier, 2011; pp 718-745.

57. Gao, Y.; Wu, J.; Wang, Q.; Wilkie, C. A.; O'Hare, D. Flame retardant polymer/layered double hydroxide nanocomposites. *Journal of Materials Chemistry A* **2014**, *2*, 10996-11016.

58. Matusinovic, Z.; Wilkie, C. A. Fire retardancy and morphology of layered double hydroxide nanocomposites: a review. *Journal of Materials Chemistry* **2012**, *22*, 18701-18704.

59. Morgan, A. B.; Gilman, J. W. An overview of flame retardancy of polymeric materials: application, technology, and future directions. *Fire and Materials* **2013**, *37*, 259-279.

60. Huggett, C. Estimation of rate of heat release by means of oxygen consumption measurements. *Fire and materials* **1980**, *4*, 61-65.

61. Contescu, C. I.; Adhikari, S. P.; Gallego, N. C.; Evans, N. D.; Biss, B. E. Activated carbons derived from high-temperature pyrolysis of lignocellulosic biomass. *C* **2018**, *4*, 51.

62. Aslani, A.; Mazzuca-Sobczuk, T.; Eivazi, S.; Bekhrad, K. Analysis of bioenergy technologies development based on life cycle and adaptation trends. *Renewable energy* **2018**, *127*, 1076-1086.

63. Kim, Y.; Lee, S.; Yoon, H. Fire-safe polymer composites: flame-retardant effect of nanofillers. *Polymers* **2021**, *13*, 540.

64. Fina, A.; Camino, G.; Bocchini, S. Comprehensive approach to flame-retardancy evaluation of layered silicate nanocomposites. *Polymer Green Flame Retardants* **2014**, 441-459.

65. Norouzi, M.; Zare, Y.; Kiany, P. Nanoparticles as effective flame retardants for natural and synthetic textile polymers: application, mechanism, and optimization. *Polymer Reviews* **2015**, *55*, 531-560.

66. Zhang, Y.; Xiong, Z.; Ge, H.; Ni, L.; Zhang, T.; Huo, S.; Song, P.; Fang, Z. Core–shell bioderived flame retardants based on chitosan/alginate coated ammonia polyphosphate for enhancing flame retardancy of polylactic acid. ACS Sustainable Chemistry & Engineering 2020, 8, 6402-6412.

67. Yang, X.; Zhang, W.: Flame Retardancy of Wood-Polymeric Composites. In *Polymer-Based Multifunctional Nanocomposites and Their Applications*; Elsevier, 2019; pp 285-317.
68. Lin, T. S.; Cogen, J. M.; Lyon, R. E. Correlations between microscale combustion calorimetry and conventional flammability tests for flame retardant wire and cable compounds. *Proceedings of the 56th IWCS* **2007**.
69. Mensah, R. A.; Xu, Q.; Asante-Okyere, S.; Jin, C.; Bentum-Micah, G. Correlation analysis of cone calorimetry and microscale combustion calorimetry experiments. *Journal of Thermal Analysis and Calorimetry* **2019**, *136*, 589-599.
70. Zhuge, J.; Chen, X.; KS, A.; Manica, D. P. Microscale combustion calorimeter—application and limitation. *Fire and Materials* **2016**, *40*, 987-998.
71. Sun, H.; Schiraldi, D. A.; Chen, D.; Wang, D.; Sánchez-Soto, M. Tough polymer aerogels incorporating a conformal inorganic coating for low flammability and durable hydrophobicity. *ACS applied materials & interfaces* **2016**, *8*, 13051-13057.
72. Yu, Z. L.; Yang, N.; Apostolopoulou-Kalkavoura, V.; Qin, B.; Ma, Z. Y.; Xing, W. Y.; Qiao, C.; Bergström, L.; Antonietti, M.; Yu, S. H. Fire-retardant and thermally insulating phenolic-silica aerogels. *Angewandte Chemie International Edition* **2018**, *57*, 4538-4542.
73. Wang, N.-N.; Wang, H.; Wang, Y.-Y.; Wei, Y.-H.; Si, J.-Y.; Yuen, A. C. Y.; Xie, J.-S.; Yu, B.; Zhu, S.-E.; Lu, H.-D. Robust, lightweight, hydrophobic, and fire-retarded polyimide/MXene aerogels for effective oil/water separation. *ACS applied materials & interfaces* **2019**, *11*, 40512-40523.
74. Chen, H.-B.; Liu, B.; Huang, W.; Wang, J.-S.; Zeng, G.; Wu, W.-H.; Schiraldi, D. A. Fabrication and properties of irradiation-cross-linked poly (vinyl alcohol)/clay aerogel composites. *ACS applied materials & interfaces* **2014**, *6*, 16227-16236.
75. Chen, H.-B.; Wang, Y.-Z.; Schiraldi, D. A. Preparation and flammability of poly (vinyl alcohol) composite aerogels. *ACS applied materials & interfaces* **2014**, *6*, 6790-6796.
76. Kozlowski, R.; Wesolek, D.; Wladyka-Przybylak, M.; Duquesne, S.; Vannier, A.; Bourbigot, S.; Delobel, R.: Intumescent flame-retardant treatments for flexible barriers. In *Multifunctional Barriers for Flexible Structure*; Springer, 2007; pp 39-61.
77. Choi, K.; Seo, S.; Kwon, H.; Kim, D.; Park, Y. T. Fire protection behavior of layer-by-layer assembled starch–clay multilayers on cotton fabric. *Journal of Materials Science* **2018**, *53*, 11433-11443.
78. Geoffroy, L.; Samyn, F.; Jimenez, M.; Bourbigot, S. Intumescent polymer metal laminates for fire protection. *Polymers* **2018**, *10*, 995.
79. Wu, J.-N.; Chen, L.; Fu, T.; Zhao, H.-B.; Guo, D.-M.; Wang, X.-L.; Wang, Y.-Z. New application for aromatic Schiff base: High efficient flame-retardant and anti-dripping action for polyesters. *Chemical Engineering Journal* **2018**, *336*, 622-632.
80. Kabir, I. I.; Sorrell, C. C.; Mofarah, S. S.; Yang, W.; Yuen, A. C. Y.; Nazir, M. T.; Yeoh, G. H. Alginate/polymer-based materials for fire retardancy: Synthesis, structure, properties, and applications. *Polymer Reviews* **2021**, *61*, 357-414.
81. Vahabi, H.; Rastin, H.; Movahedifar, E.; Antoun, K.; Brosse, N.; Saeb, M. R. Flame retardancy of bio-based polyurethanes: Opportunities and challenges. *Polymers* **2020**, *12*, 1234.
82. Lu, Y.; Wu, C.; Xu, S. Mechanical, thermal and flame retardant properties of magnesium hydroxide filled poly (vinyl chloride) composites: The effect of filler shape. *Composites Part A: Applied Science and Manufacturing* **2018**, *113*, 1-11.
83. Tawfik, S. Y. Flame retardants: Additives in plastic technology. *Polymers and Polymeric Composites: A Reference Series; Palsule, S., Ed* **2017**, 1-27.

84. De France, K. J.; Hoare, T.; Cranston, E. D. Review of hydrogels and aerogels containing nanocellulose. *Chemistry of Materials* **2017**, *29*, 4609-4631.

85. Hu, Y.; Chen, Z.; Zhuo, H.; Zhong, L.; Peng, X.; Sun, R. C. Advanced compressible and elastic 3D monoliths beyond hydrogels. *Advanced Functional Materials* **2019**, *29*, 1904472.

86. Feng, J.; Su, B.-L.; Xia, H.; Zhao, S.; Gao, C.; Wang, L.; Ogbeide, O.; Feng, J.; Hasan, T. Printed aerogels: Chemistry, processing, and applications. *Chemical Society Reviews* **2021**, *50*, 3842-3888.

87. Nita, L. E.; Ghilan, A.; Rusu, A. G.; Neamtu, I.; Chiriac, A. P. New trends in bio-based aerogels. *Pharmaceutics* **2020**, *12*, 449.

88. Cuce, E.; Cuce, P. M.; Wood, C. J.; Riffat, S. B. Toward aerogel based thermal superinsulation in buildings: a comprehensive review. *Renewable and Sustainable Energy Reviews* **2014**, *34*, 273-299.

89. Özlüsoylu, İ.; İstek, A. The effect of hybrid resin usage on thermal conductivity in ecological insulation panel production. In *Proceedings of the 4th International Conference on Engineering Technology and Applied Sciences. Kiev*, **2019**, 292-296.

90. Shatat, M.; Elmer, T.; Tetlow, D.; Riffat, S. The state of the art: Superinsulation construction materials under the UK's domestic energy building: Aerogel and vacuum insulation technology applications. In *14 th International Conference o n Sustainable Energy Technologies-SET*, **2015**, 25-27.

91. Peng, L.: Sound absorption and insulation functional composites. Advanced High Strength Natural Fibre Composites in Construction: Advanced High Strength Natural Fibre Composites in Construction, Research Institute of Wood Industry, Chinese Academy of Forestry, Beijing, China pp: 333–373. 2017.

92. Oh, J.-H.; Kim, J.; Lee, H.; Kang, Y.; Oh, I.-K. Directionally antagonistic graphene oxide-polyurethane hybrid aerogel as a sound absorber. *ACS applied materials & interfaces* **2018**, *10*, 22650-22660.

93. Si, Y.; Yu, J.; Tang, X.; Ge, J.; Ding, B. Ultralight nanofibre-assembled cellular aerogels with superelasticity and multifunctionality. *Nature communications* **2014**, *5*, 1-9.

94. Pinto, S. C.; Marques, P. A.; Vicente, R.; Godinho, L.; Duarte, I. Hybrid structures made of polyurethane/graphene nanocomposite foams embedded within aluminum open-cell foam. *Metals* **2020**, *10*, 768.

95. Rahimabady, M.; Statharas, E. C.; Yao, K.; Sharifzadeh Mirshekarloo, M.; Chen, S.; Tay, F. E. H. Hybrid local piezoelectric and conductive functions for high performance airborne sound absorption. *Applied Physics Letters* **2017**, *111*, 241601.

96. Reverchon, E.; Pisanti, P.; Cardea, S. Nanostructured PLLA− hydroxyapatite scaffolds produced by a supercritical assisted technique. *Industrial & engineering chemistry research* **2009**, *48*, 5310-5316.

97. Szustakiewicz, K.; Gazińska, M.; Kryszak, B.; Grzymajło, M.; Pigłowski, J.; Wiglusz, R. J.; Okamoto, M. The influence of hydroxyapatite content on properties of poly (L-lactide)/hydroxyapatite porous scaffolds obtained using thermal induced phase separation technique. *European Polymer Journal* **2019**, *113*, 313-320.

98. Kumar, M. R.; Muzzarelli, R. A.; Muzzarelli, C.; Sashiwa, H.; Domb, A. Chitosan chemistry and pharmaceutical perspectives. *Chemical reviews* **2004**, *104*, 6017-6084.

99. Li, Y.; Zhao, M.; Chen, J.; Fan, S.; Liang, J.; Ding, L.; Chen, S. Flexible chitosan/carbon nanotubes aerogel, a robust matrix for in-situ growth and non-enzymatic biosensing applications. *Sensors and Actuators B: Chemical* **2016**, *232*, 750-757.

100. Zhai, T.; Verdolotti, L.; Kacilius, S.; Cerruti, P.; Gentile, G.; Xia, H.; Stanzione, M.; Buonocore, G. G.; Lavorgna, M. High piezo-resistive performances of anisotropic composites realized by embedding rGO-based chitosan aerogels into open cell polyurethane foams. *Nanoscale* **2019**, *11*, 8835-8844.

101. Maleki, H.; Durães, L.; García-González, C. A.; Del Gaudio, P.; Portugal, A.; Mahmoudi, M. Synthesis and biomedical applications of aerogels: Possibilities and challenges. *Advances in colloid and interface science* **2016**, *236*, 1-27.

102. Martins, M.; Barros, A. A.; Quraishi, S.; Gurikov, P.; Raman, S.; Smirnova, I.; Duarte, A. R. C.; Reis, R. L. Preparation of macroporous alginate-based aerogels for biomedical applications. *The Journal of Supercritical Fluids* **2015**, *106*, 152-159.

103. Manzocco, L.; Mikkonen, K. S.; García-González, C. A. Aerogels as porous structures for food applications: Smart ingredients and novel packaging materials. *Food structure* **2021**, *28*, 100188.

104. Michaloudis, I.; Dann, B. Aer () sculpture: Inventing skies and micro-clouds into diaphanous sculptures made of the space technology nanomaterial silica aerogel. *Journal of Sol-Gel Science and Technology* **2017**, *84*, 535-542.

105. Lehtonen, M.; Kekäläinen, S.; Nikkilä, I.; Kilpeläinen, P.; Tenkanen, M.; Mikkonen, K. S. Active food packaging through controlled in situ production and release of hexanal. *Food chemistry: X* **2020**, *5*, 100074.

106. Wang, X.; Pan, Y.; Liu, X.; Liu, H.; Li, N.; Liu, C.; Schubert, D. W.; Shen, C. Facile fabrication of superhydrophobic and eco-friendly poly (lactic acid) foam for oil–water separation via skin peeling. *ACS applied materials & interfaces* **2019**, *11*, 14362-14367.

107. Mi, H.-Y.; Jing, X.; Liu, Y.; Li, L.; Li, H.; Peng, X.-F.; Zhou, H. Highly durable superhydrophobic polymer foams fabricated by extrusion and supercritical CO2 foaming for selective oil absorption. *ACS applied materials & interfaces* **2019**, *11*, 7479-7487.

108. Jiao, C.; Xiong, J.; Tao, J.; Xu, S.; Zhang, D.; Lin, H.; Chen, Y. Sodium alginate/graphene oxide aerogel with enhanced strength–toughness and its heavy metal adsorption study. *International journal of biological macromolecules* **2016**, *83*, 133-141.

109. Hayase, G.; Kanamori, K.; Abe, K.; Yano, H.; Maeno, A.; Kaji, H.; Nakanishi, K. Polymethylsilsesquioxane–cellulose nanofiber biocomposite aerogels with high thermal insulation, bendability, and superhydrophobicity. *ACS applied materials & interfaces* **2014**, *6*, 9466-9471.

110. Hrubesh, L.; Keene, L.; Latorre, V. Dielectric properties of aerogels. *Journal of materials research* **1993**, *8*, 1736-1741.

111. Hrubesh, L. *Aerogels for electronics* **1994**.

112. Chung, D. Electromagnetic interference shielding effectiveness of carbon materials. *carbon* **2001**, *39*, 279-285.

113. Pai, A. R.; Puthiyaveettil Azeez, N.; Thankan, B.; Gopakumar, N.; Jaroszewski, M.; Paoloni, C.; Kalarikkal, N.; Thomas, S. Recent Progress in electromagnetic interference shielding performance of porous polymer nanocomposites—a review. *Energies* **2022**, *15*, 3901.

Nanoporous Crystalline Aerogels of Syndiotactic Polystyrene: Polymorphism, Dielectric, Thermal and Acoustic Properties

This chapter has been adopted from the following publication

Vipin G. Krishnan, Angel Mary Joseph, Surendran K. P., and E. Bhoje Gowd*

2.1. Abstract

Hierarchically porous crystalline-nanoporous aerogels of syndiotactic polystyrene (sPS) received much attention because of their unique nanoporous structures along with meso and macro porosity. Depending on the difference in the packing of polymer chains within the crystal lattice, sPS has two nanoporous crystalline forms, namely δ and ε forms (δ_e and ε_e). In this study, we have prepared high purity nanoporous δ and ε forms of sPS aerogels from their respective gels using a solvent exchange strategy with green solvents followed by an environment-friendly freeze-drying technique. Using these highly porous aerogels, the phase transition behavior of sPS at higher temperatures was investigated. The δ_e form showed a complex phase transition behavior on heating and at a higher temperature, the γ form (obtained through an intermediate helical phase) transformed to the mixture of α and β forms. On the other hand, the ε_e form transformed directly to the γ form and on further heating, the γ form transformed exclusively to the α form. The dielectric, thermal and acoustic properties of crystalline-nanoporous aerogels were promising with ultralow dielectric constant (1.02 ± 0.02), thermal conductivity (λ) as low as 0.04 $Wm^{-1}K^{-1}$ and high sound absorption coefficient (close to 1). Moreover, these aerogels exhibited excellent oleophilicity which was demonstrated in oil/organic solvent separation experiments. These multifunctional aerogels of sPS can therefore find multitude of applications, especially in thermal and acoustic insulation and molecular sorption of oil/organic solvents.

2.2. Introduction

As elaborated in the previous chapter, aerogel monoliths based on polymers are trending nowadays in diverse fields of application such as thermal insulation, packaging, acoustic insulation, oil spill cleanup, sorbents of volatile organic compounds, antennas and electronics, etc. mainly because of their ability to surpass the drawbacks of traditional inorganic aerogels which are highly fragile and brittle.[1-11] Semi-crystalline polymers like syndiotactic polystyrene (sPS),[12-18] poly(2,6-dimethyl-1,4-phenylene) oxide (PPO),[19, 20] isotactic polypropylene,[21, 22] poly(vinylidene fluoride),[23, 24] polyethylene,[25] poly(ether ether ketone),[26, 27] etc. are capable of forming thermoreversible gels in various solvents where the junction zones of the gel network are made up of polymer crystalline phases, which provide the required robustness to the system. Among them, sPS and PPO received remarkable attention due to their ability to form physical aerogels with crystalline nanoporosity.[12, 28-37]

Guerra and co-workers reported a physically bonded aerogel of sPS using δ form gel by supercritical carbon dioxide (CO_2) extraction and it is the first example of nanoporous-crystalline aerogel of sPS.[12] Similar to δ aerogel, ε form sPS aerogels also possess crystalline nanocavities (empty spaces/nanopores within the crystal lattice) and both these phases exhibit helical trans-trans-gauche-gauche (T_2G_2) polymer chain conformation with the nanocavities being isolated in the monoclinic δ form and channel-shaped in the orthorhombic ε form, parallel to the chain axes.[12, 30, 31] Such crystalline cavities have a diameter of less than 2 nm, which together with the typical disordered amorphous mesopores (2-50 nm) and macropores (greater than 50 nm) of the aerogels render hierarchical porosity to the δ and ε sPS aerogels.[29] The polymorphism of sPS is even more complex with additional crystalline phases α and β having planar zigzag all-trans (T_4) chain conformation and γ with closely packed helical T_2G_2 chains.[16, 38-42] Most of the

reported literature on sPS aerogels focuses attention on the δ form aerogel, probably due to the complex procedures involved in the making of ε aerogel. Daniel and co-workers formulated a strategy to produce the ε aerogel in its finest crystalline purity.[30] ε aerogels prepared from the γ form aerogels by chloroform sorption/desorption, the previously known method, presented traces of γ and/or δ form.[31, 33, 37] Pure ε phase obtained in aerogels could be effectively utilized to unravel the intricate polymorphism of sPS by the systematic investigation of the structural transitions.

Rizzo et al. investigated the thermal transition behavior of ε crystalline phase of sPS using thin films and compared it with δ form.[43] Unlike the δ form, the nanoporous ε form transformed directly to the γ form on heating above 100 °C without passing through the intermediate phase (disordered helical phase). Though high temperature transitions were reported in the case of nanoporous δ form, no reports are available on the crystalline transitions at a higher temperature using the ε form. For example, Gowd et al. reported that the γ form transformed to a mixture of α and β forms for the thick δ form film or uniaxially-oriented sample (co-crystal), while a completely dried thin film (or powder) transformed exclusively to the kinetically stable α phase.[41, 42, 44-49] They have reported that the residual solvents in the amorphous phase of δ or γ form triggered the β crystal formation.[45] On the other hand, when the uniaxially oriented nanoporous δ form was used, the γ form transformed to a mixture of α and β forms at higher temperatures even though no solvent residues were there in the amorphous phase of the γ form.[41, 42] The origin of the formation of the β form at higher temperatures is unclear when the nanoporous δ form was used as a starting material. As aerogels are fully dried and no residual solvents are present, these are the right candidates to understand the phase transition behavior. In this paper, a detailed investigation was carried out on the phase transition behavior of both nanoporous δ and ε phases using aerogels.

sPS aerogels are deployed in molecular sorption, namely, volatile organic compounds absorption, adsorption of H_2, and trapping of airborne nanoparticles, mainly due to the nanosized pores possessed by them.[28, 31, 50] Nanoporous-crystalline polymer aerogels, however, have never been exploited for their low dielectric constant and thermal and acoustic insulation. The first attempt in that direction was brought off by Joseph et al. who demonstrated the ultra-low dielectric constant of sPS δ type aerogels (1.03 ± 0.02), which is the lowest value ever reported for any polymer aerogel.[29] Rossinsky et al. investigated the thermal conductivity of crystalline δ phase of sPS in the bulk, the average value was found out to be 0.2-0.3 $Wm^{-1}K^{-1}$.[51] Thermal conductivity increased with the increase in material density, which is the general trend. However, there are no reports on the thermal insulation behavior of sPS aerogels, to the best of our knowledge. The micro/meso pores in aerogels can induce a Knudsen effect which lowers the gaseous conductivity as compared to commercial thermal insulators such as expanded polystyrene, which are macroporous in nature. Also, the conduction through the condensed phase (solid conduction) will be lower in micro/mesoporous aerogels than in dense (nonporous) matrix material as the three-dimensional network structure in aerogels is composed of weakly connected nanofibers.[52-55] These features of sPS aerogels, therefore, could not only reduce the heat conduction through them but also influence their sound absorption characteristics. He et al. have shown that high porosity and small pore size of cellulose-based aerogels resulted in their excellent sound insulation performance.[6] The hydrophobic nature of sPS presents an added advantage to its aerogels in terms of water repellence and this could be extended to the selective absorption of oil/organic solvents (oleophilicity) from water mixture. Amidst other excellent thermally insulating materials or acoustic insulators, sPS aerogels thus stand out as they could combine a

whole lot of properties within a single system, which is explored in the second part of this chapter.

Herein, we proposed a sustainable method for the preparation of nanoporous ε and δ forms of sPS aerogels using freeze-drying as the solvent extraction technique. The organic solvents used for the preparation of gels were recovered completely after the solvent exchange process with green solvents (water and ethanol). Processes like the aging of gel, solvent exchange, freezing, etc. were carefully controlled to obtain samples with different porosities; the highest attained porosity is 97 %. By the controlled heating of aerogels, the phase transition behavior of nanoporous sPS δ and ε forms was investigated using wide-angle X-ray diffraction (WAXD) and differential scanning calorimetry (DSC). The nanoporous-crystalline aerogels of sPS proved to be multifaceted materials with spectacularly low values for dielectric constant (1.02 ± 0.02) and thermal conductivity (~ 0.04 $Wm^{-1}K^{-1}$), excellent acoustic insulation performance with sound absorption coefficients as high as 0.97 in the mid-frequency range and superior oil/organic solvent absorption ability. These multifunctional properties of sPS aerogels permit them to be potential alternatives to conventional materials in the fields of microelectronics, thermal management, acoustic insulation and oil/solvent spill cleanup.

2.3. Experimental Section

2.3.1. Materials

sPS (M_w: 272 000 and $Đ$: 2.28) used in this study was supplied kindly by Idemitsu Petrochemical Co., Ltd (Japan). The solvent used for δ gel preparation was a mixture of isomers of xylene, purchased from Merck, India. Chloroform provided by Sigma-Aldrich Co. and acrylonitrile purchased from TCI Co., Ltd. were used for the preparation of ε gel. Polymer and all the above solvents were used as received. The solvent exchange was done using ethanol received from S.D. Fine chemicals and distilled water.

2.3.2. Preparation of the δ Form Aerogel of sPS

δ form sPS aerogel was prepared according to our previous report.[29] Briefly, sPS pellets were dissolved in xylene by heating above 140 °C (boiling point of xylene). After complete dissolution of the polymer, the solution with a polymer concentration of 3 wt% was transferred to plastic moulds and cooled down to room temperature at a rate of 1.5 °C/min, where gelation occurred. As obtained gels were aged at room temperature for 3 h and the solvent was exchanged systematically by immersing the gel in ethanol first, followed by solvent mixtures of different volume ratios of ethanol and water and finally in water alone. A detailed description of the solvent exchange process is given the later section. The as obtained hydrogels were transferred to an ultra-low temperature (ULT) freezer preset at –60 °C, frozen for 12 h and then lyophilized. Rotary evaporation of the solvent mixtures obtained after the solvent exchange process was carried out in order to separate and recover xylene.

2.3.3. Preparation of the ε form Aerogel of sPS

The freeze-drying technique was used to prepare ε form sPS aerogel with the aid of a systematic solvent exchange procedure. To prepare ε gel of sPS, a combination of chloroform (solvent) and acrylonitrile (non-solvent) was used. sPS pellets were first dissolved completely in chloroform in a tightly sealed set up by heating above the boiling point of chloroform (60 °C). Then, a slightly hot mixture of chloroform and acrylonitrile (volume ratio 1:2) was slowly added to the polymer solution with stirring. The final solution was immediately transferred to plastic moulds and cooled to room temperature at a rate of 1.5 °C/min. The ε gel thus obtained was aged for 2 h at room temperature and subjected to solvent exchange as earlier. This is followed by freezing of hydrogel for 12 h in a ULT freezer preset at –60 °C and freeze-drying to obtain ε form sPS aerogel with 100% crystalline purity. In the final solution, the polymer concentration was 3 wt% and

the volume ratio of chloroform to acrylonitrile was 1:1. Similar to the above case, a rotary evaporator was used for the recovery of solvents (chloroform and acrylonitrile). We prepared both δ_e and ε_e aerogel samples with different shapes and dimensions for various characterizations, the largest being 5 cm × 5 cm × 2 cm in dimension.

2.3.4. Solvent Exchange Process

A systematic procedure was adopted in order to exchange the gel solvents of both δ_e and ε_e aerogels. In the first step, the organogels were fully immersed in ethanol overnight. Then, the solvents were removed by decantation. In the second step, the gels were immersed in a mixture of ethanol/distilled water (v/v 75/25) and the solvents were removed after 3 hours. Immediately, the gels were introduced into another mixture of ethanol/distilled water, with a composition of 50/50 by volume. After 3 hours, again the solvents were replaced with a fresh mixture of ethanol and distilled water. This time around, the amount of water is more in the mixture (v/v 25/75). In the final step, the gels were immersed exclusively in water and the immersion time is not more than 1 hour as a longer time in water can lead to the shrinkage of gels. Therefore, during the final step, continuous monitoring of the gels should be done. The entire solvent exchange process requires almost 24 hours for completion. Once the process is completed, the gels were transferred immediately to a ULT freezer preset at -60 °C.

2.3.5. Characterization

The total porosity of different sPS aerogel samples was determined from the density values using the following equation:

$$P = 100 \left[1 - \frac{\rho_{ap}}{\rho_{pol}} \right] \tag{1}$$

where ρ_{ap} is the mass/volume ratio (apparent density) of the prepared aerogel; volume is determined theoretically from the dimensions of the samples and ρ_{pol} is the density of the

bulk polymer. A universal testing machine (Hounsfield, H5KS UTM, Redhill, UK) with a crosshead speed of 1.3 mm min^{-1} was used for the compressive strength analysis of the aerogels and cylindrical samples with diameter to height ratio of approximately 1.5 : 1 were used for the measurements. Scanning electron microscopy was employed to examine the morphologies of various samples and the measurements were performed using a Zeiss EVO 18 cryo-SEM operating at an accelerating voltage of 15 kV. The water contact angle of the samples was measured at room temperature using an automated DSA30 Drop Shape Analyzer, KRŰSS, Germany. The measurements were carried out at different regions on the same aerogel as well as on the same region of the aerogel over a period of 15 minutes. From nitrogen adsorption-desorption isotherm (Gemini 2375, Micromeritics, Norcross, USA), the Brunauer–Emmett–Teller (BET) surface area of the porous aerogels was measured. The samples were degassed at room temperature for 24 h before the measurement. The pore size distributions were also obtained from the isotherms using the Barrett–Joyner–Halenda (BJH) method. Phase formations in aerogels were confirmed using wide-angle X-ray diffraction (WAXD) measurements on a XEUSS SAXS/WAXS system from Xenocs operated at 50 kV and 0.60 mA in the transmission mode using Cu Kα radiation of wavelength 1.54 Å. The two-dimensional patterns were recorded on a Mar 345 image plate system (detector) and the Fit2D software was used for data processing. Variable temperature WAXD measurements were carried out with the aid of Linkam THMS 600 hot stage connected to the LNP 95 cooling system to understand the phase transformation behavior of various aerogel samples. The samples were heated from room temperature at a rate of 10 °C/min to 230 °C and the X-ray patterns were acquired at 10 °C intervals, after a dwell time of 1 minute at each temperature. Phase transitions were confirmed using an advanced research-grade modulated differential scanning calorimeter (DSC) TA Q2000 under a nitrogen

atmosphere by heating the samples from room temperature up to 300 °C at a rate of 10 °C/min. To confirm the complete drying of aerogels, thermogravimetric analysis (TGA) was carried out under continuous nitrogen flow using TA Q50, a fourth-generation thermogravimetric analyzer. The samples were heated from room temperature to 800 °C at a rate of 10 °C/min. The dielectric constants were measured using a vector network analyzer (Model No. E5071C, ENA series, 300 kHz-20 GHz; Agilent Technologies, Santa Clara, USA) by a waveguide technique in the X band (8.2–12.4 GHz) of the microwave frequency. The samples were annealed at various temperatures in the air atmosphere by keeping in a hot air oven preset at the required temperature (90, 140 or 220 °C) for 1 h and the corresponding phase formations were confirmed using WAXD before the dielectric measurements. For the X band, samples used were of the dimension 22.86 × 10.8 mm. The thermal conductivity (λ) of aerogels was measured with TCi thermal conductivity analyzer (C-Thermo Technologies Ltd., Canada) using the transient plane method. The samples with thickness not less than 10 mm were used and five measurements were done for each sample, the average value of which is taken as the final thermal conductivity. The normal incident sound absorption coefficient of all the samples was obtained using a Brüel & Kjær impedance tube, type 4206 (Denmark). Cylindrical samples with a diameter of 29 mm and thickness of 12 mm were used for measurements in the frequency band from 300 to 6400 Hz via the two-microphone method.

2.4. Results and Discussion

2.4.1. Hierarchical Porous Aerogels of sPS (δ_e and ε_e)

The ability of sPS to form co-crystalline phases has been exploited to prepare two forms of crystalline nanoporous aerogels by the supercritical carbon dioxide drying method.[12, 28, 30, 31, 33] In our previous work, the δ_e aerogel was prepared from δ gel using xylene as the solvent by the freeze-drying method.[29] In the present work, ε_e aerogel was

prepared by the freeze-drying method as described in the Experimental Section. Unlike in the case of δ gel, acrylonitrile was used as a non-solvent for the preparation of ε gel along with chloroform as solvent. On cooling the polymer solutions to room temperature, thermoreversible gelation takes place, which was very quick in the case of ε gel as the phase separation here is induced not just by temperature, but also by a non-solvent. A systematic solvent exchange strategy was adopted to transform the δ and ε organogels to hydrogels. This step is crucial as it allows to circumvent the structural deformations occurring during the freeze-drying of gels and makes the entire processing route eco-friendly by allowing the recovery of organic solvents and making them available for reuse. As optimized from our previous work,[29] the polymer concentration in solution was kept at 3 wt% and the duration of steps like gel aging, solvent exchange, freezing, drying, etc. was controlled to derive aerogels of varying porosity (84 to 97 %). We could achieve hierarchical porous sPS aerogels with porosity as high as 97 % and there was only negligible shrinkage to the gel structure upon drying, as shown in Figure 2.1a. Solvent exchange with ethanol followed by water was crucial in achieving the higher porosity and retaining the shape and size of the aerogels as same as that of the gels before freeze-drying. Figure 2.1b depicts the ultralow density of the ε aerogel with 97 % porosity and it can bear a load of almost 1000 times its weight without structural disintegration (Figure 2.1c). The δ_e aerogel with similar porosity has sufficient strength to bear the load of 1500 times to its original weight as reported in our previous work.[29] The X-ray diffraction profiles in Figure 2.1d confirm the successful formation of crystalline nanoporous sPS aerogels. The reflections at $2\theta = 8.4°, 10.1°, 14.1°, 16.9°, 18.7°,$ and $20.7°$ and $2\theta = 6.9°,$ $8.1°, 13.9°, 16.4°,$ and $20.6°$ correspond to δ_e and ε_e forms of sPS, respectively.[30, 56] As evident from the X-ray diffraction profiles, high purity crystalline δ_e and ε_e aerogels (without the traces of other crystalline forms) were achieved in this study by the freeze-

drying method. The diffuse scattering observed at low 2θ ($< 4°$) in Figure 2.1d indicates the presence of microporosity (< 2 nm) in both δ_e and ε_e forms of sPS. Gowd et al. reported such diffuse scattering in the X-ray pattern of the δ_e form due to the presence of crystalline porosity and it decreased significantly upon heating when the structure transformed to the γ form.[42] It is also worth mentioning here that such diffuse scattering was not observed in the X-ray diffraction patterns of the gel state of δ and ε forms of sPS. The mechanical properties of δ_e and ε_e aerogels with porosity ~ 97% were investigated by compression experiments and the corresponding stress-strain diagrams are provided in Figure 2.1e. Both aerogels exhibited an irreversible buckling behavior and were converted to dense solids at higher loads. Even at 75% strain, no fracturing of the aerogels was observed. However, the compressive modulus calculated from the slope of the linear elastic region of the stress-strain curve for ε_e aerogel was lower (~ 0.08 MPa) than that of the δ_e aerogel (~ 0.38 MPa). The difference in the compressive modulus is mainly due to the difference in the microstructure and morphology of these aerogels, which will be discussed in the later section.
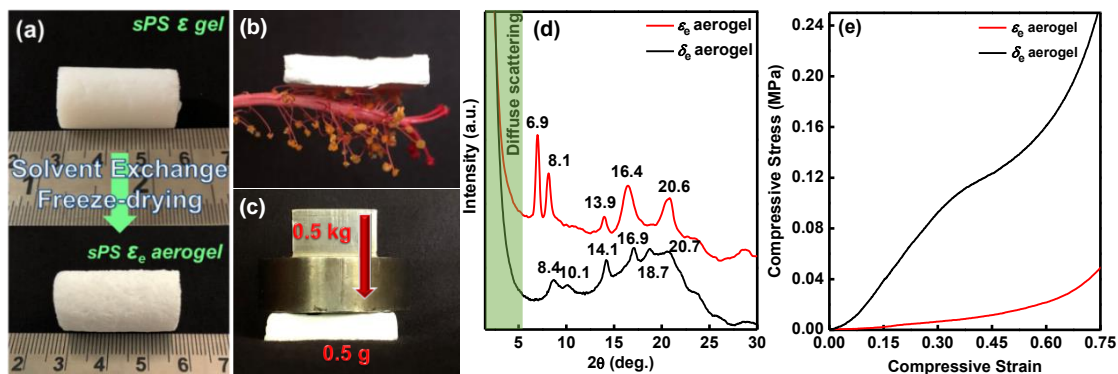
Figure 2.1. Photographs of (a) ε gel and corresponding aerogel obtained by freeze-drying process, (b) nanoporous ε aerogel resting on the stamen of a flower, (c) ε aerogel holding 1000 times its original weight, (d) WAXD patterns and (e) the stress-strain plots of δ_e and ε_e aerogels measured at room temperature.

SEM images in Figure 2.2 compare the surface morphology of δ_e and ε_e aerogels. The macroporous structure of both these aerogels exhibits flake-like morphologies, but the flake sizes are quite small in the ε_e aerogel. The magnified SEM images (Figures 2.2b and 2.2d) show the mesoporous structure where a significant difference in morphology is observed between the δ_e and ε_e forms of sPS aerogels. The microstructure of ε_e aerogel reveals a mixed morphology of fibers and lamellar structures unlike the δ_e aerogel with interconnected fibrillar network morphology. The lamellar structures are having sizes approximately in the range of 0.5 – 1 μm whereas the fiber diameters will be a few tens of nanometres. The morphology of the freeze-dried ε_e aerogel is comparable with the morphology of the reported ε_e aerogel prepared from the supercritical drying process albeit the slight changes in the dimensions of the lamellar structures.[30] The difference in morphology between the δ_e and ε_e aerogels can be attributed to the difference in polymer-solvent interactions, the presence of non-solvent in the case of ε gel, the rate of solvent crystal sublimation during freeze-drying, etc. The BET surface areas obtained from nitrogen adsorption-desorption isotherms for δ_e and ε_e aerogels are 301 m^2 g^{-1} and 227 m^2 g^{-1}, respectively. The micrometer-sized lamellar structures in ε_e aerogel lower its overall surface area when compared with the all fibrous network structure of the δ_e aerogel. Both the samples exhibit typical type IV adsorption isotherms confirming the mesoporous nature of the sPS aerogels (Figure 2.2e). The distribution of pore diameters is broad covering all the mesopores and some of the macropores as shown in the pore size distribution curves in Figure 2.2f. In the 20-50 nm range, ε_e aerogel has the highest pore volume indicating the presence of the higher fraction of mesopores. Also, the peak of the distribution curve comes in the mesoporous range for ε_e aerogel whereas it is beyond 50 nm in the case of δ_e aerogel. X-ray diffraction, SEM and BET surface area measurements

revealed the presence of macro, meso and microporous structures in both δ_e and ε_e aerogels.
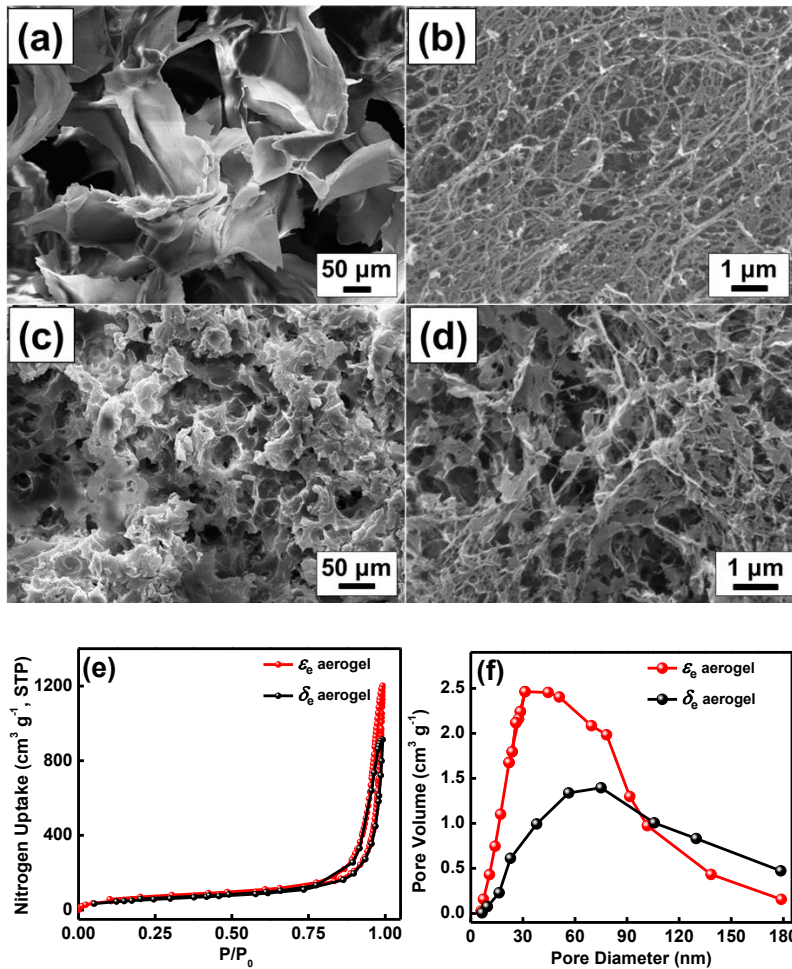
Figure 2.2. *SEM images of (a & b) δ_e and (c & d) ε_e aerogels at different magnifications. (e) N_2 adsorption-desorption isotherms and (f) pore size distribution of δ_e and ε_e aerogels.*

2.4.2. Crystalline Transitions of δ_e and ε_e Aerogels of sPS upon Heating

Thermal-induced crystalline transitions of the δ_e form are investigated extensively in the literature using unoriented film, powder and uniaxially oriented samples.[41, 42, 45, 46, 49, 57] On the other hand, only one study appeared on thermal-induced crystalline transitions of the ε_e form using thermally annealed unoriented films.[45] Further, this study did not focus on the high-temperature transitions of the ε_e form. In that study, the ε_e form was prepared using the previously known procedure, i.e., chloroform sorption and

desorption in the γ form films and this procedure always leads to the formation of the ε_e form with the traces of δ_e and/or γ form. In the present investigation, we have systematically compared the thermal-induced crystalline transitions of δ_e and ε_e aerogels (high purity crystalline forms) using temperature-dependent measurements of WAXD and DSC. Figure 2.3 shows the temperature-dependent WAXD patterns of δ_e and ε_e aerogels in the temperature range of 30 – 230 °C and the patterns were recorded at 10 °C intervals. The temperature-dependent WAXD patterns of δ_e aerogel are shown in Figure 2.3a and changes in the integrated intensities of representative crystalline reflection of each crystalline form at $2\theta = 8.4°$ (δ_e), 9.8° (*intermediate phase*), 9.3° (γ), 6.2° (β) and 6.7° (α) were evaluated by deconvolution and plotted against the temperature as shown in Figure 2.3b. The crystalline reflections corresponding to the δ_e form disappeared completely in the temperature range of 70-90 °C. In consistent with the literature,[41, 42, 45, 57] the δ_e form aerogel transiently transformed into the "*intermediate helical phase*" in the temperature range of 80-110 °C. On further heating, the intermediate phase transformed to the γ form. It was speculated that the crystalline cavities present in the δ_e form were responsible for this unusual formation of the intermediate form as it was not observed in the δ co-crystalline form.[41] It is worth mentioning here that the strong diffuse scattering observed at low 2θ ($< 4°$) disappeared completely once the structure transformed from the δ_e form to γ form (indicated with an arrow mark in Figure 2.3a). This observation further confirms the disappearance of the crystalline porosity (microporosity) during the crystalline transition from δ_e to γ form. On further heating, the γ form transformed to the mixture of α and β forms above 180 °C. In literature, it was shown that the γ form transformed exclusively into the kinetically favorable α form in the case of the powder samples.[46] Gowd et al. reported the β crystal formation along with α crystals for the thick δ-form film (co-crystals) and proposed that the residual solvent molecules residing in the

amorphous regions of the δ or γ form films triggered the formation of the β form.[47] However, when the same group used the uniaxially oriented δ_e samples with no residual solvents, again minor fraction of the β form was observed along with the α form at a higher temperature (> 180 °C).[41] In the present study, as evident from the TGA thermogram (Figure 2.3c), the presence of residual solvent is almost nil both in the δ_e and ε_e aerogels of sPS. As discussed above, in the case of δ_e aerogels, at a higher temperature, fractions of thermodynamically stable β form is observed along with the α form. The reason for the appearance of the β form will be discussed in the forthcoming section.

The temperature-dependent WAXD patterns of the ε_e aerogel and the temperature dependence of the integrated intensities of the reflections at $2\theta = 6.9°$ (ε_e), 9.3° (γ), and 6.7° (α) evaluated from the WAXD patterns are shown in Figure 2.3d and 2.3e. Unlike the δ_e form, the transition from ε_e aerogel did not show the intermediate helical phase on heating. A direct transition from the ε_e to γ form is observed and these two crystalline forms coexist in the temperature range of 100 – 120 °C, which is consistent with the results obtained by Rizzo et al. for nanoporous ε-form films.[45] It is worth adding here that though the channel-shaped cavities are present in the ε_e form, the transition from ε_e to γ form occurred smoothly without the formation of intermediate helical phase as observed in the case of the δ_e form. Similar to the δ_e form, in this case also the strong diffuse scattering at lower 2θ disappeared completely when the ε_e form is fully transformed to the γ form (Figure 2.3d) indicating the disappearance of channel-shaped cavities during the transition. At the higher temperatures, the γ form transformed exclusively into the α form (180 – 200 °C). No trace of the β form is observed as in the case of the δ_e aerogel. These results suggest that crystalline transitions occurred differently on heating the nanoporous crystalline forms (δ_e and ε_e) of sPS. Based on the present study, we may say that the thermodynamically stable β form resulted at the higher temperatures in the δ_e aerogel

could be from the energy changes associated with the formation of the intermediate helical phase. The isolated cavities present in the crystal structure of the δ_e form plays a major role in the formation of the intermediate helical phase during the transition from δ_e to γ form and also the thermodynamically stable β form at the higher temperature.
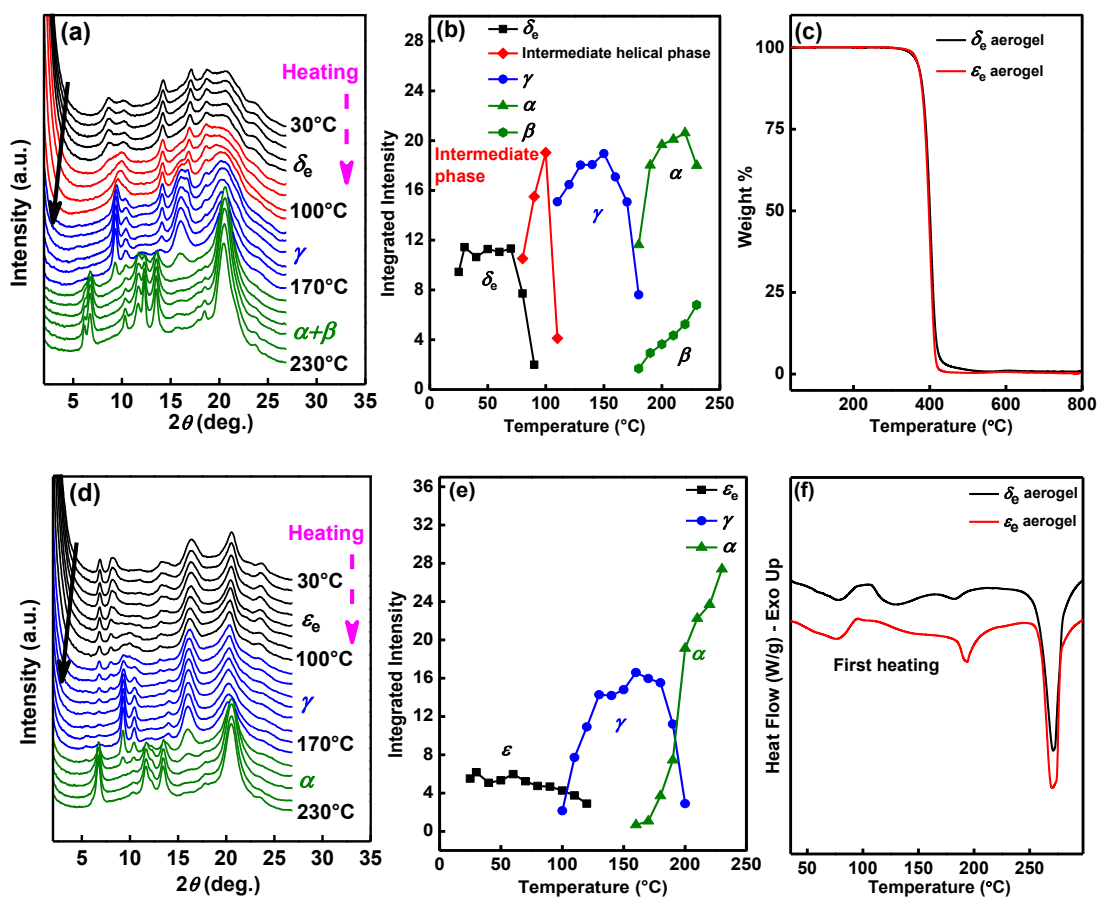
Figure 2.3. *(a) Temperature-dependent WAXD patterns of δ_e aerogel and (b) corresponding changes in the integrated intensities of representative crystalline reflections of each crystalline form at $2\theta = 8.4°$ (δ_e), $9.8°$ (intermediate helical phase), $9.3°$ (γ), $6.2°$ (β) and $6.7°$ (α) during heating, (c) TGA thermograms of δ_e and ε_e aerogels, (d and e) temperature-dependent WAXD patterns of ε_e aerogel and corresponding changes in the integrated intensities of representative crystalline reflections of each crystalline form at $2\theta = 6.9°$ (ε_e), $9.3°$ (γ), and $6.7°$ (α) during heating and (f) DSC thermograms of δ_e and ε_e aerogels in the heating process.*

Figure 2.3f shows the DSC thermograms of δ_e and ε_e aerogels in the heating process at 10 °C/min. Based on the temperature-dependent WAXD results, the endotherm followed by the exotherm in the temperature range of 80 - 120 °C can be assigned to the δ_e to intermediate helical phase to γ form transition in the case of heating of the δ_e aerogel and ε_e to γ form transition in the case of heating of the ε_e aerogel. At a higher temperature, both δ_e and ε_e aerogels show an endothermic peak in the temperature range of 170 – 200 °C corresponding to the γ to $\alpha(\beta)$ or γ to α form transitions. The endothermic peak observed at around 270 °C is due to the melting of the $\alpha(\beta)$ or α form of sPS.

2.4.3. Dielectric Properties of δ_e and ε_e Aerogels of sPS

Dielectric properties of the prepared aerogels were investigated using a microwave transmission waveguide technique. The reliability of this method was proven in our previous work by fitting the measured dielectric constants of sPS aerogels to some of the theoretical models.[29] Because of their microstructure and high porosity, aerogels are inherently low dielectric constant materials. In 1993, Hrubesh et al. reported a dielectric constant less than 1.03 for silica aerogels with 99% porosity which turned out to be the lowest value ever reported for bulk solid material.[58] We measured the dielectric constants of δ_e and ε_e aerogels in the microwave frequency range 8–12 GHz (X-band) of the electromagnetic spectra and obtained consistent values in the entire frequency range. Figure 2.4a shows the measured dielectric constants of crystalline nanoporous sPS aerogels with ~97 % porosity. δ_e aerogel has a dielectric constant of 1.02 ± 0.02 whereas the ε counterpart shows a value of 1.03 ± 0.02. Further, we have prepared a series of samples of both types with varying porosity and measured their dielectric constants. The dielectric constant increased roughly from 1.02 to 1.2 for δ_e aerogel as the porosity decreased from 97 % to 84 % (Figure 2.4b) while the ε_e aerogel also exhibited a similar

trend (Figure 2.4c). This means that by tuning the bulk density/porosity of the aerogels, the dielectric constant values were easily tuned. It has been shown that the dielectric constant varies linearly with aerogel density using silica, polyimide, and polyamide aerogels.[5, 58, 59] Density of aerogels is inversely proportional to their porosity and therefore, as a general rule, we could say that dielectric constant *vs* porosity showcases a linear relationship. This was proved using δ_e and ε_e aerogels as shown in the insets of Figures 2.4b and 2.4c, respectively. An inverse linear variation of dielectric constant against porosity at all X-band frequencies is observed for both δ_e and ε_e aerogels, i.e., the lower the porosity, the higher the dielectric constant. Thus, by tailoring the morphology and porosity of sPS aerogels, their applicability in the field of microelectronics can be widened.
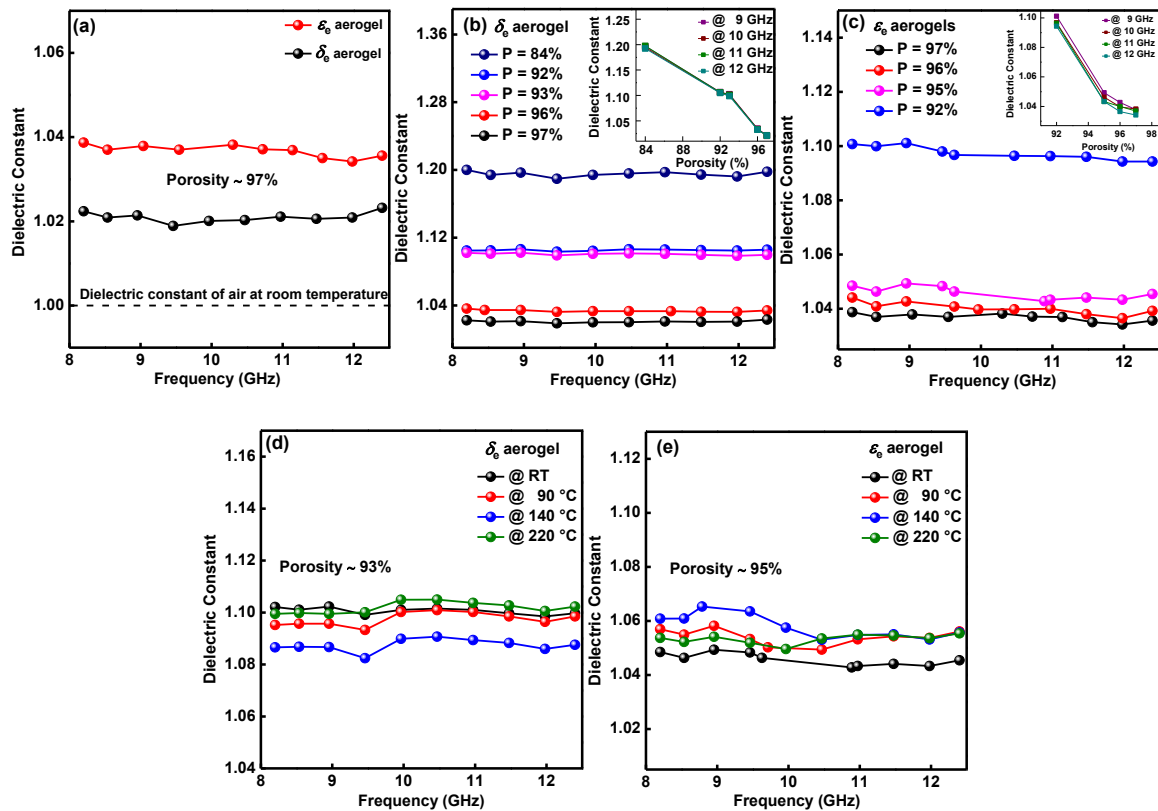
Figure 2.4. *Dielectric constants of various samples in the X-band of the microwave frequency region. (a) Comparison of the dielectric constants of δ_e and ε_e aerogels having porosity = 97%, (b & c) dielectric constants of various δ_e and ε_e aerogels having different*

porosities and the variation of dielectric constant as a function of porosity is shown in the insets of (b) and (c) at different frequencies, and (d & e) the effect of annealing temperature on the dielectric constants of δ_e and ε_e aerogels.

As discussed in the preceding section, both δ_e and ε_e aerogels undergo crystalline transitions upon heating. Various aerogels with different crystalline forms were obtained by annealing the δ_e and ε_e aerogels for 1 h at three different temperatures, namely, 90, 140 and 220 °C. Annealing at these temperatures resulted in the aerogels with intermediate helical phase (in the case of δ_e aerogel), γ and $\alpha(\beta)/\alpha$ crystalline phases. Above 100 °C, the micropores within the crystal lattice are erased and the structure is reorganized to the γ form. In this study, the dielectric constants of various crystalline forms are compared. As the dielectric constant of sPS aerogel depends heavily on its overall porosity, measurement of the dielectric constant of aerogels with crystalline nanoporosity will reveal the influence of microporosity. It has to be noted that by annealing the samples at the higher temperatures, some of the meso as well as the macropores are getting collapsed along with the micropores. Therefore, it is not correct to correlate the dielectric constants of the samples at ambient conditions and after annealing, as the total porosity of the starting samples will be reduced significantly upon annealing. Instead, to probe the role of polymer chain packing (crystalline forms) on the dielectric constant, we have annealed the samples at the above-mentioned temperatures in such a way that the overall porosity of the final samples remains the same by choosing aerogels of varying porosity as the starting material. We have taken δ_e aerogels with starting porosities 94, 95 and 97 % and annealed them at 90, 140 and 220 °C, respectively. After the annealing process, porosity of all the three samples was reduced to ~93 % as the extent of shrinkage to the samples increases with the increase in annealing temperature. Figure 2.4d shows the dielectric constants of δ_e aerogel at room temperature and after annealing at 90, 140 and 220 °C. All

the samples are nearly 93 % porous but differ in their crystal structure. However, the values obtained for these samples were more or less the same, within the limits of experimental error. The lattice packing of polymer chains does not seem to have a visible effect on the eventual dielectric behavior of the sPS aerogel samples. A similar study was carried out using ε_e aerogels, where the total porosity is 95% and similar results were obtained as shown in Figure 2.4e.

2.4.4. Thermal Conductivity and Acoustic Properties of δ_e and ε_e Aerogels

sPS aerogels can be excellent thermal insulation materials because of their highly porous network structure. Thermal transport in aerogels takes place mainly through three mechanisms: solid conduction, gaseous conduction and radiative transmission. The summation of these three components brings about the total thermal conductivity (λ) of the aerogel. As reported earlier, the λ of bulk sPS lies in the range of 0.2-0.3 Wm^{-1}K^{-1}.[51] On conversion to aerogel, the λ of sPS reduced drastically and the values obtained for δ_e and ε_e aerogels (porosity ~95 %) are 0.044 and 0.043 Wm^{-1}K^{-1}, respectively. The obvious reason for massive reduction in λ of aerogel is that it is mostly air and the λ of air is 0.02 Wm^{-1}K^{-1}.[60] On increasing the porosity of the samples, we could attain further diminution in the thermal conductivity of aerogels, for example, 0.041 Wm^{-1}K^{-1} is the value obtained for δ_e aerogel with porosity ~96 %. The thermal conductivity of expanded polystyrene boards demonstrated by Mıhlayanlar et al. is of the order of 0.04 Wm^{-1}K^{-1}.[61] Similar to the dielectric studies, we did a systematic analysis of aerogels with varying porosity to understand the relation that porosity possesses with thermal conductivity. From Figure 2.5a, it is clear that as the porosity decreases, thermal conduction through the δ_e aerogel increases and this relation is monotonic. A similar trend can be expected in the case of ε_e aerogel also. When considering the thermal transport mechanism, solid conduction through the polymer backbone appears to be the major contributor to heat conduction.

Since sPS aerogels are predominantly mesoporous, i.e., pore sizes are less than 50 nm, a strong Knudsen effect will be induced in the system. As the majority of the pores are smaller in size than the mean free path of the gas molecules in free space (~70 nm), the gas molecules undergo collisions with the pore walls before their interactive scattering, resulting in the lowering of gaseous conduction.[7] This explains why the thermal conductivity is slightly lower in the ε_e aerogel than the δ_e aerogel of the same porosity. The solid conduction of a particular material is its intrinsic property. However, as the morphology suggests, sPS aerogel is composed of weakly connected polymer fibrils and these weak connections between the nanofibers reduce the heat transfer through the polymer backbone, eventually resulting in lower total thermal conductivity.[53] Figure 2.5b compares the thermal conductivity of sPS aerogels with some of the polymer-based aerogels reported in literature prepared by freeze-drying method and sPS aerogels investigated here showed comparable or even lesser values.[62-66] The neat polyimide aerogels prepared by Fan et al. exhibited a higher thermal conductivity (0.052 $Wm^{-1}K^{-1}$) than the sPS aerogels.[62] The ultra-low and easily tuneable thermal conductivity of crystalline nanoporous sPS aerogels opens up a wider application prospect to these materials as thermal insulators in the fields of building insulation, cryogenic flasks and packaging.

At times, thermal insulating aerogels can have excellent sound absorption ability also which is a direct consequence of their highly porous structure. The normal incident sound absorption coefficients, i.e., the ratio of absorbed sound intensity in the material to the incident sound intensity, of δ_e and ε_e aerogels at various frequencies (300-6400 Hz) are shown in Figure 2.5c along with the values obtained for the commercial sound insulators such as expanded polystyrene (EPS), polyurethane (PU) foam and expanded polyethylene (EPE). All the samples used for measurements are cylindrical with 12 mm

thickness. The absorption coefficients of all the samples were low initially but improved gradually with the increase in frequency. sPS aerogels showed better absorption ability than commercial materials even at the lower frequencies. EPS has a maximum absorption of 92 % at around 4000 Hz. However, it showed very low absorption values (<20 %) up to 2500 Hz. On the contrary, the ε_e aerogel absorbed more than 80 % of the incident sound waves beyond 1800 Hz consistently with an obvious peak of 97 % between 2300-3000 Hz. In the same frequency range, the values obtained for EPS and EPE are less than 30 % and 60 %, respectively. All these commercial insulators are predominantly macroporous in nature. The δ_e aerogel showed similar results to the ε_e aerogel, but with slightly lower absorption ability. The peak maximum was 92 % for δ_e aerogel in the frequency range 2600-2800 Hz. The excellent acoustic performance of nanoporous crystalline sPS aerogels can be attributed to their highly mesoporous structure. As the sound waves enter a highly porous structure like sPS aerogel, multiple scattering phenomena and the increased vibration of the pore walls result in the effective attenuation of sound waves. The tortuosity of wave propagation caused by channel twists and turns and the nanosized pores result in enhanced friction and air viscosity consumption, thereby improving the sound absorption performance.[6, 67] As mentioned earlier, δ_e aerogel has a lower sound absorption capability than the ε_e aerogel and this could be attributed to the difference in their morphologies. The mesopores morphology of ε_e aerogel provides more area on the pore walls for the sound waves to get scattered. As a result, the magnitude of sound scattering and therefore, the vibration of pore walls will be more in ε_e aerogel, resulting in better sound absorption performance. sPS aerogels can be good alternatives to the traditional acoustic insulators because of their superior sound absorption ability over a broad range of frequencies.
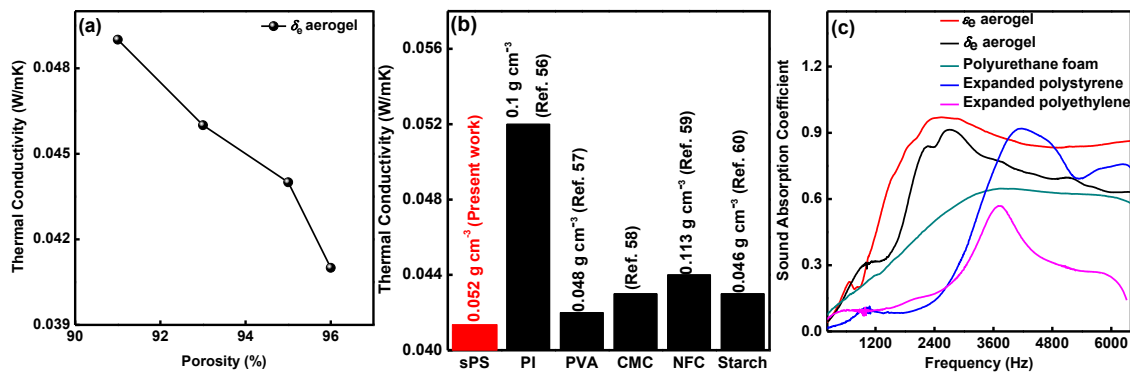
Figure 2.5. *(a) The plot of thermal conductivity of δ_e aerogel as a function of porosity, (b) comparison of the thermal conductivity obtained in the present work with those of reported aerogels prepared by freeze-drying (the density of the sample and reference numbers are provided near the data point) and (c) normal incident sound absorption coefficients of δ_e and ε_e aerogels measured in the frequency range 300-6400 Hz and compared with other commercially available sound insulation materials like EPS, PU foam and EPE.*

2.4.5. Oil/Organic Solvent-Water Separation using δ_e and ε_e Aerogels

The water contact angle (WCA) measurements were carried out on sPS aerogels to study their surface wettability and the values obtained for δ_e and ε_e aerogels with 96% porosity are 139 ± 2° and 132.7 ± 2°, respectively. The images of water droplets on the surface of δ_e and ε_e aerogels are respectively shown in Figure 2.6a and 2.6b. The water droplets remained stable on the aerogel surface without reduction in the WCA over a long period of time. This indicates the highly hydrophobic nature of the prepared aerogels which is attributed to the inherent hydrophobicity of sPS and the surface roughness of aerogels created by the different levels of porosity.[32] When these aerogels were immersed in water using an external force, no water absorption was observed and the moment the external forces were removed, the samples rose to the surface. This property of sPS aerogels could well be utilized for the oil/organic solvent-water separation process. Figure

2.6c displays the selective absorption of dichloromethane stained with iodine from under the water using δ_e aerogel. The solvent droplets are readily absorbed by the aerogel within a few seconds, indicating its high oleophilicity. In Figure 2.6d, hexane colored with iodine is floating on the surface of the water and has been completely removed using δ_e aerogel. Similarly, pump oil and petrol floating on the surface of water were selectively recovered using sPS aerogels with great efficiency. Thus, the combination of high hydrophobicity and oleophilicity makes sure that δ_e and ε_e aerogels are superior oil/organic solvent absorbers. Guerra and coworkers showed high sorption capacity of organic solvents even from very dilute aqueous solutions using crystalline-nanoporous sPS aerogels.[28, 30, 68] To regenerate the δ_e and ε_e aerogels for further absorption process, the oil/solvent-filled aerogels were washed with ethanol and dried in an oven at 60 °C for 60 min. After the washing process, oils/organic solvents can be separated from ethanol by suitable procedures.
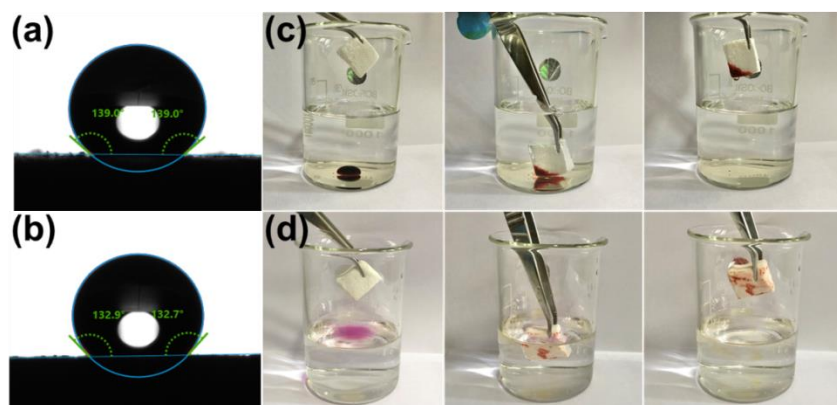
Figure 2.6. *Water contact angles for (a) δ_e and (b) ε_e aerogels. The removal process of (c) dichloromethane and (d) hexane from water using the δ_e aerogel.*

2.5. Conclusions

In summary, we have developed sPS aerogels with isolated (δ_e) and channel-shaped (ε_e) crystalline nanocavities by a facile and feasible freeze-drying technique. The gel solvents were exchanged with green solvents such as ethanol and water, which makes the

entire process eco-friendly. δ_e and ε_e aerogels with porosity as high as 97 % were obtained and we were able to tune the porosity of aerogels by the careful control of the preparation steps. The intricate polymorphic changes occurring in these aerogels were studied using variable temperature WAXD, which revealed some of the fundamental aspects of sPS phase transitions. The dielectric measurements carried out on the aerogels demonstrated the linear relationship between the dielectric constant and porosity. Ultralow values for dielectric constant (1.02 $\pm$ 0.02) and low thermal conductivity (~0.04 Wm^{-1}K^{-1}) were obtained for both types of sPS aerogels. Also, high sound absorption coefficients were obtained, particularly for ε_e aerogel (~0.97) which is having a higher fraction of mesopores. The surface wettability of aerogels was estimated using WCA measurements (~139°) and their highly hydrophobic and oleophilic nature could be utilized for the oil-water separation process. Crystalline-nanoporous aerogels of sPS thus proved to be multifunctional aerogels with prospected applications in microelectronics, thermal/acoustic insulation and oil/solvent spill cleanup.

2.6. References

1. Kistler, S. S. Coherent Expanded Aerogels and Jellies. *Nature* **1931,** 127 (3211), 741-741.
2. Teo, N.; Gu, Z.; Jana, S. C. Polyimide-based aerogel foams, via emulsion-templating. *Polymer* **2018,** 157, 95-102.
3. Randall, J. P.; Meador, M. A. B.; Jana, S. C. Tailoring Mechanical Properties of Aerogels for Aerospace Applications. *ACS Appl. Mater. Interfaces* **2011,** 3 (3), 613-626.
4. Wang, X.; Pan, Y.; Liu, X.; Liu, H.; Li, N.; Liu, C.; Schubert, D. W.; Shen, C. Facile Fabrication of Superhydrophobic and Eco-Friendly Poly(lactic acid) Foam for Oil–Water Separation via Skin Peeling. *ACS Appl. Mater. Interfaces* **2019,** 11 (15), 14362-14367.
5. Meador, M. A. B.; Wright, S.; Sandberg, A.; Nguyen, B. N.; Van Keuls, F. W.; Mueller, C. H.; Rodríguez-Solís, R.; Miranda, F. A. Low Dielectric Polyimide Aerogels As Substrates for Lightweight Patch Antennas. *ACS Appl. Mater. Interfaces* **2012,** 4 (11), 6346-6353.
6. He, C.; Huang, J.; Li, S.; Meng, K.; Zhang, L.; Chen, Z.; Lai, Y. Mechanically Resistant and Sustainable Cellulose-Based Composite Aerogels with Excellent Flame Retardant, Sound-Absorption, and Superantiwetting Ability for Advanced Engineering Materials. *ACS Sustain. Chem. Eng.*, **2018,** 6 (1), 927-936.

7. Li, M.; Qin, Z.; Cui, Y.; Yang, C.; Deng, C.; Wang, Y.; Kang, J. S.; Xia, H.; Hu, Y. Ultralight and Flexible Monolithic Polymer Aerogel with Extraordinary Thermal Insulation by A Facile Ambient Process. *Adv. Mater. Interfaces*, **2019,** 6 (13), 1900314.

8. Illera, D.; Mesa, J.; Gomez, H.; Maury, H. Cellulose Aerogels for Thermal Insulation in Buildings: Trends and Challenges. *Coatings* **2018,** 8 (10), 345.

9. Zhao, S.; Malfait, W. J.; Guerrero-Alburquerque, N.; Koebel, M. M.; Nyström, G. Biopolymer Aerogels and Foams: Chemistry, Properties, and Applications. *Angew. Chem. Int. Ed.* **2018,** 57 (26), 7580-7608.

10. De France, K. J.; Hoare, T.; Cranston, E. D. Review of Hydrogels and Aerogels Containing Nanocellulose. *Chem. Mater.* **2017,** 29 (11), 4609-4631.

11. Asim, N.; Badiei, M.; Alghoul, M. A.; Mohammad, M.; Fudholi, A.; Akhtaruzzaman, M.; Amin, N.; Sopian, K. Biomass and Industrial Wastes as Resource Materials for Aerogel Preparation: Opportunities, Challenges, and Research Directions. *Ind. Eng. Chem. Res.* **2019,** 58 (38), 17621-17645.

12. Daniel, C.; Alfano, D.; Venditto, V.; Cardea, S.; Reverchon, E.; Larobina, D.; Mensitieri, G.; Guerra, G. Aerogels with a Microporous Crystalline Host Phase. *Adv. Mater.* **2005,** 17 (12), 1515-1518.

13. Daniel, C.; Dammer, C.; Guenet, J.-M. On the definition of thermoreversible gels: the case of syndiotactic polystyrene. *Polymer* **1994,** 35 (19), 4243-4246.

14. Daniel, C.; Menelle, A.; Brulet, A.; Guenet, J.-M. Thermoreversible gelation of syndiotactic polystyrene in toluene and chloroform. *Polymer* **1997,** 38 (16), 4193-4199.

15. Daniel, C.; Alfano, D.; Guerra, G.; Musto, P. Physical Gelation of Syndiotactic Polystyrene in the Presence of Large Molar Volume Solvents Induced by Volatile Guests of Clathrate Phases. *Macromolecules* **2003,** 36 (5), 1713-1716.

16. Gowd, E. B.; Tashiro, K.; Ramesh, C. Structural phase transitions of syndiotactic polystyrene. *Prog. Polym. Sci.* **2009,** 34 (3), 280-315.

17. Mochizuki, J.; Sano, T.; Tokami, T.; Itagaki, H. Decisive properties of solvent able to form gels with syndiotactic polystyrene. *Polymer* **2015,** 67, 118-127.

18. Itagaki, H.; Tokami, T.; Mochizuki, J. A trial to clarify a cause of forming physical gels: Morphology of syndiotactic polystyrene in n-alkylbenzene. *Polymer* **2012,** 53 (23), 5304-5312.

19. Daniel, C.; Zhovner, D.; Guerra, G. Thermal Stability of Nanoporous Crystalline and Amorphous Phases of Poly(2,6-dimethyl-1,4-phenylene) Oxide. *Macromolecules* **2013,** 46 (2), 449-454.

20. Golla, M.; Nagendra, B.; Rizzo, P.; Daniel, C.; Ruiz de Ballesteros, O.; Guerra, G. Polymorphism of Poly(2,6-dimethyl-1,4-phenylene)oxide in Axially Stretched Films. *Macromolecules* **2020,** 53 (6), 2287-2294.

21. Matsuda, H.; Inoue, T.; Okabe, M.; Ukaji, T. Study of Polyolefin Gel in Organic Solvents I. Structure of Isotactic Polypropylene Gel in Organic Solvents. *Polym J.,* **1987,** 19 (3), 323-329.

22. Pogodina, N. V.; Winter, H. H. Polypropylene Crystallization as a Physical Gelation Process. *Macromolecules* **1998,** 31 (23), 8164-8172.

23. Dasgupta, D.; Nandi, A. K. Multiporous Polymeric Materials from Thermoreversible Poly(vinylidene fluoride) Gels. *Macromolecules* **2005,** 38 (15), 6504-6512.

24. Dikshit, A. K.; Nandi, A. K. Thermoreversible Gelation of Poly(vinylidene flouride) in Diethyl Adipate: A Concerted Mechanism. *Macromolecules* **1998,** 31 (25), 8886-8892.

25. Domszy, R. C.; Alamo, R.; Edwards, C. O.; Mandelkern, L. Thermoreversible gelation and crystallization of homopolymers and copolymers. *Macromolecules* **1986,** 19 (2), 310-325.

26. Talley, S. J.; Yuan, X.; Moore, R. B. Thermoreversible Gelation of Poly(ether ether ketone). *ACS Macro Lett* **2017,** 6 (3), 262-266.

27. Talley, S. J.; Vivod, S. L.; Nguyen, B. A.; Meador, M. A. B.; Radulescu, A.; Moore, R. B. Hierarchical Morphology of Poly(ether ether ketone) Aerogels. *ACS Appl. Mater. Interfaces* **2019,** 11 (34), 31508-31519.

28. Daniel, C.; Sannino, D.; Guerra, G. Syndiotactic Polystyrene Aerogels: Adsorption in Amorphous Pores and Absorption in Crystalline Nanocavities. *Chem. Mater.* **2008,** 20 (2), 577-582.

29. Joseph, A. M.; Nagendra, B.; Shaiju, P.; Surendran, K. P.; Gowd, E. B. Aerogels of hierarchically porous syndiotactic polystyrene with a dielectric constant near to air. *J. Mater. Chem. C* **2018,** 6 (2), 360-368.

30. D'Aniello, C.; Daniel, C.; Guerra, G. ε Form Gels and Aerogels of Syndiotactic Polystyrene. *Macromolecules* **2015,** 48 (4), 1187-1193.

31. Figueroa-Gerstenmaier, S.; Daniel, C.; Milano, G.; Vitillo, J. G.; Zavorotynska, O.; Spoto, G.; Guerra, G. Hydrogen Adsorption by δ and ε Crystalline Phases of Syndiotactic Polystyrene Aerogels. *Macromolecules* **2010,** 43 (20), 8594-8601.

32. Wang, X.; Jana, S. C. Tailoring of Morphology and Surface Properties of Syndiotactic Polystyrene Aerogels. *Langmuir* **2013,** 29 (18), 5589-5598.

33. Daniel, C.; Giudice, S.; Guerra, G. Syndiotatic Polystyrene Aerogels with β, γ, and ε Crystalline Phases. *Chem. Mater.* **2009,** 21 (6), 1028-1034.

34. Longo, S.; Vitillo, J. G.; Daniel, C.; Guerra, G. Monolithic Aerogels Based on Poly(2,6-diphenyl-1,4-phenylene oxide) and Syndiotactic Polystyrene. *ACS Appl. Mater. Interfaces* **2013,** 5 (12), 5493-5499.

35. Daniel, C.; Pellegrino, M.; Venditto, V.; Aurucci, S.; Guerra, G. Nanoporous-crystalline poly(2,6-dimethyl-1,4-phenylene)oxide (PPO) aerogels. *Polymer* **2016,** 105, 96-103.

36. Nagendra, B.; Antico, P.; Daniel, C.; Rizzo, P.; Guerra, G. Thermal shrinkage and heat capacity of monolithic polymeric physical aerogels. *Polymer* **2020,** 210, 123073.

37. Petraccone, V.; Ruiz de Ballesteros, O.; Tarallo, O.; Rizzo, P.; Guerra, G. Nanoporous Polymer Crystals with Cavities and Channels. *Chem. Mater.* **2008,** 20 (11), 3663-3668.

38. Woo, E. M.; Sun, Y. S.; Yang, C. P. Polymorphism, thermal behavior, and crystal stability in syndiotactic polystyrene vs. its miscible blends. *Prog. Polym. Sci.* **2001,** 26 (6), 945-983.

39. Immirzi, A.; de Candia, F.; Iannelli, P.; Zambelli, A.; Vittoria, V. Solvent-induced polymorphism in syndiotactic polystyrene. *Makromol. Chem. Rapid Comm.*, **1988,** 9 (11), 761-764.

40. Chatani, Y.; Shimane, Y.; Inoue, Y.; Inagaki, T.; Ishioka, T.; Ijitsu, T.; Yukinari, T. Structural study of syndiotactic polystyrene: 1. Polymorphism. *Polymer* **1992,** 33 (3), 488-492.

41. Gowd, E. B.; Shibayama, N.; Tashiro, K. Structural Changes in Thermally Induced Phase Transitions of Uniaxially Oriented δe Form of Syndiotactic Polystyrene Investigated by Temperature-Dependent Measurements of X-ray Fiber Diagrams and Polarized Infrared Spectra. *Macromolecules* **2006,** 39 (24), 8412-8418.

42. Gowd, E. B.; Shibayama, N.; Tashiro, K. Structural Correlation between Crystal Lattice and Lamellar Morphology in the Phase Transitions of Uniaxially Oriented Syndiotactic Polystyrene (δ and δe Forms) As Revealed by Simultaneous

Measurements of Wide-Angle and Small-Angle X-ray Scatterings. *Macromolecules* **2008,** 41 (7), 2541-2547.

43. Gowd, E. B.; Shibayama, N.; Tashiro, K. Structural Changes during Thermally Induced Phase Transitions Observed for Uniaxially Oriented δ Form of Syndiotactic Polystyrene. *Macromolecules* **2007,** 40 (17), 6291-6295.

44. Shaiju, P.; Bhoje Gowd, E. Factors controlling the structure of syndiotactic polystyrene upon the guest exchange and guest extraction processes. *Polymer* **2015,** 56, 581-589.

45. Rizzo, P.; D'Aniello, C.; De Girolamo Del Mauro, A.; Guerra, G. Thermal Transitions of ε Crystalline Phases of Syndiotactic Polystyrene. *Macromolecules* **2007,** 40 (26), 9470-9474.

46. Gowd, E. B.; Nair, S. S.; Ramesh, C. Crystalline Transitions of the Clathrate (δ) Form of Syndiotactic Polystyrene during Heating: Studies Using High-Temperature X-ray Diffraction. *Macromolecules* **2002,** 35 (22), 8509-8514.

47. Gowd, E. B.; Tashiro, K. Effect of Solvent Molecules on Phase Transition Phenomena of Syndiotactic Polystyrene. *Macromolecules* **2007,** 40 (15), 5366-5371.

48. Gowd, E. B.; Tashiro, K.; Ramesh, C. Role of Solvent Molecules as a Trigger for the Crystal Phase Transition of Syndiotactic Polystyrene/Solvent Complex. *Macromolecules* **2008,** 41 (24), 9814-9818.

49. Gowd, E. B.; Nair, S. S.; Ramesh, C.; Tashiro, K. Studies on the Clathrate (δ) Form of Syndiotactic Polystyrene Crystallized by Different Solvents Using Fourier Transform Infrared Spectroscopy. *Macromolecules* **2003,** 36 (19), 7388-7397.

50. Kim, S. J.; Chase, G.; Jana, S. C. Polymer aerogels for efficient removal of airborne nanoparticles. *Sep. Purif. Technol.* **2015,** 156, 803-808.

51. Rossinsky, E.; Müller-Plathe, F. Anisotropy of the thermal conductivity in a crystalline polymer: Reverse nonequilibrium molecular dynamics simulation of the δ phase of syndiotactic polystyrene. *J. Chem. Phys.* **2009,** 130 (13), 134905.

52. Rizvi, A.; Chu, R. K. M.; Park, C. B. Scalable Fabrication of Thermally Insulating Mechanically Resilient Hierarchically Porous Polymer Foams. *ACS Appl. Mater. Interfaces* **2018,** 10 (44), 38410-38417.

53. Samitsu, S. Thermally Stable Mesoporous Poly(ether sulfone) Monoliths with Nanofiber Network Structures. *Macromolecules* **2018,** 51 (1), 151-160.

54. Guo, Y.; Ruan, K.; Shi, X.; Yang, X.; Gu, J. Factors affecting thermal conductivities of the polymers and polymer composites: A review. *Compos Sci Technol.* **2020,** 193, 108134.

55. Gu, J.; Ruan, K. Breaking Through Bottlenecks for Thermally Conductive Polymer Composites: A Perspective for Intrinsic Thermal Conductivity, Interfacial Thermal Resistance and Theoretics. *Nano-Micro Lett.* **2021,** 13 (1), 110.

56. De Rosa, C.; Guerra, G.; Petraccone, V.; Pirozzi, B. Crystal Structure of the Emptied Clathrate Form (δe Form) of Syndiotactic Polystyrene. *Macromolecules* **1997,** 30 (14), 4147-4152.

57. Manfredi, C.; De Rosa, C.; Guerra, G.; Rapacciuolo, M.; Auriemma, F.; Corradini, P. Structural changes induced by thermal treatments on emptied and filled clathrates of syndiotactic polystyrene. *Macromol. Chem. Phys.* **1995,** 196 (9), 2795-2808.

58. Hrubesh, L. W.; Keene, L. E.; Latorre, V. R. Dielectric properties of aerogels. *J. Mater. Res.* **2011,** 8 (7), 1736-1741.

59. Williams, J. C.; Meador, M. A. B.; McCorkle, L.; Mueller, C.; Wilmoth, N. Synthesis and properties of step-growth polyamide aerogels cross-linked with triacid chlorides. *Chem. Mater.* **2014,** 26 (14), 4163-4171.

60. Laby, T. H. The thermal conductivity of air. *Proceedings of the Royal Society of London. Series A, Containing Papers of a Mathematical and Physical Character* **1934,** 144 (853), 494-495.
61. Mıhlayanlar, E.; Dilmaç, Ş.; Güner, A. Analysis of the effect of production process parameters and density of expanded polystyrene insulation boards on mechanical properties and thermal conductivity. *Mater. Des.* **2008,** 29 (2), 344-352.
62. Fan, W.; Zhang, X.; Zhang, Y.; Zhang, Y.; Liu, T. Lightweight, strong, and super-thermal insulating polyimide composite aerogels under high temperature. *Compos Sci Technol.* **2019,** 173, 47-52.
63. Madyan, O. A.; Fan, M. Hydrophobic Clay Aerogel Composites through the Implantation of Environmentally Friendly Water-Repellent Agents. *Macromolecules* **2018,** 51 (24), 10113-10120.
64. Ge, X.; Shan, Y.; Wu, L.; Mu, X.; Peng, H.; Jiang, Y. High-strength and morphology-controlled aerogel based on carboxymethyl cellulose and graphene oxide. *Carbohydr. Polym.* **2018,** 197, 277-283.
65. Fan, J.; Ifuku, S.; Wang, M.; Uetani, K.; Liang, H.; Yu, H.; Song, Y.; Li, X.; Qi, J.; Zheng, Y.; Wang, H.; Shen, J.; Zhang, X.; Li, Q.; Liu, S.; Liu, Y.; Wang, Q.; Li, J.; Lu, P.; Fan, Z.; Chen, W. Robust Nanofibrillated Cellulose Hydro/Aerogels from Benign Solution/Solvent Exchange Treatment. *ACS Sustain. Chem. Eng.* **2018,** 6 (5), 6624-6634.
66. Wang, Y.; Wu, K.; Xiao, M.; Riffat, S. B.; Su, Y.; Jiang, F. Thermal conductivity, structure and mechanical properties of konjac glucomannan/starch based aerogel strengthened by wheat straw. *Carbohydr. Polym.* **2018,** 197, 284-291.
67. Oh, J.-H.; Kim, J.; Lee, H.; Kang, Y.; Oh, I.-K. Directionally Antagonistic Graphene Oxide-Polyurethane Hybrid Aerogel as a Sound Absorber. *ACS Appl. Mater. Interfaces* **2018,** 10 (26), 22650-22660.
68. Daniel, C.; Antico, P.; Guerra, G. Etched Fibers of Syndiotactic Polystyrene with Nanoporous-Crystalline Phases. *Macromolecules* **2018,** 51 (15), 6138-6148.

Thermoreversible Gels of Poly(ʟ-lactide)/Poly(ᴅ-lactide) Blends: A Facile Route to Prepare Blend α-Form and Stereocomplex Aerogels
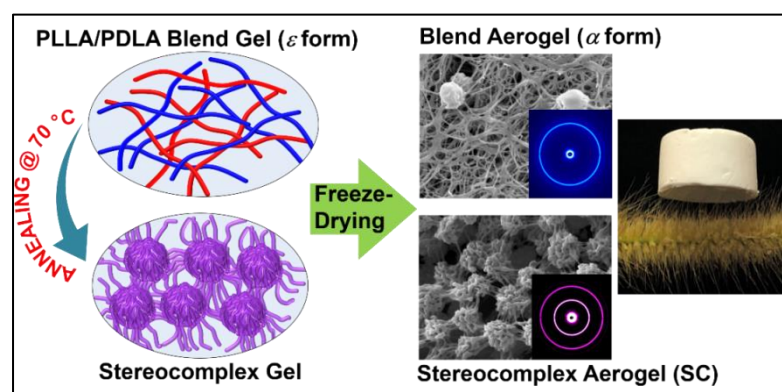
This chapter has been adopted from the following publication

Vipin G. Krishnan, N. M. Praveena, R. B. Amal Raj, Kiran Mohan and E. Bhoje Gowd*

3.1. Abstract

The demand for biodegradable polymer-based aerogels with superior comprehensive properties has escalated in various fields of application, such as packaging, tissue engineering, thermal insulation, acoustic insulation, and environmental remediation. In this work, we report a facile strategy for enhancing the thermal and mechanical properties of polylactide (PLA) aerogels by the stereocomplex (SC) formation between the opposite enantiomers. Thermoreversible gelation of poly(L-lactide) (PLLA)/poly(D-lactide) (PDLA) blend in crystal complex forming solvent and the subsequent thermal annealing of the gel resulted in crystalline pure SC gel, which upon solvent exchange with water and freeze-drying, furnished robust SC aerogel. It was found that the SC content could be tuned by varying the annealing temperature of the blend gel and we could prepare blend aerogels with pure α crystalline form and a mixture of α and SC. Crystalline pure blend α aerogel showed fibrillar morphology, whereas SC aerogel exhibited unique interwoven ball-like microstructures interconnected by PLLA and PDLA chains. The structural evolution during SC formation at the molecular level and the micrometer length scale instigated better properties in the PLA aerogels. When compared with the homopolymer aerogels, the crystalline pure SC aerogel showed enhanced melting temperature of 227 ± 2 °C (50 °C higher), better thermal stability (onset of degradation was delayed by ~ 40 °C), enhanced mechanical strength (compression modulus of 3.3 MPa) and better sound absorption ability. The biodegradability of PLA and the superior properties induced by stereocomplexation make these aerogels potential candidates in applications such as tissue engineering scaffolds, packaging, acoustic insulation, etc.

3.2. Introduction

Nowadays, the entire globe is looking for sustainable alternatives to petroleum-based polymers for various applications. The scenario is no different in the case of lightweight materials also. Aerogels based on biodegradable polymers are going to be the future materials due to their comprehensive mechanical properties, easy processability, facile tunability and environment-friendliness.[1-3] In this chapter, we have switched from fossil-based non-degradable polymers to biopolymers, poly(L-lactide) (PLLA) and poly(D-lactide) (PDLA). These polymers are versatile and commercially available and their aerogels show great potential in different applications, from scaffolds for tissue regeneration to biodegradable packaging.[4-8] Stereocomplexation has been an efficient strategy for enhancing polylactide (PLA) properties, either in bulk or in aerogels/foams.[7, 9-25] Blending the enantiomeric PLAs with the opposite enantiomer can introduce stereocomplex (SC) crystallites, resulting in enhanced crystallinity, thermal properties and mechanical properties.[7, 9-26] The SC formation in PLA mainly depends upon the molecular weights of the homopolymers. Low molecular weight polymers (below 20000 Da) readily favor the SC formation.[14, 20, 21, 27] However, homopolymer crystallization dominates over the SC formation for PLLA/PDLA blends with high molecular weight polymers (above 20000 Da).[14, 20, 21, 28] Several strategies have been developed for the exclusive SC formation in the high molecular weight PLLA/PDLA blends. It was reported that the content of SC is sensitive to several factors, such as chain entanglements, chain diffusion, chain mobility, optical purity, and mixing level of PLLA/PDLA.[11, 15, 20, 23, 29-33] In the conventional route, SC formation was achieved by melt blending and subsequent annealing of the blend at temperatures near the melting temperature of homopolymers.[34, 35] However, no attempts were made to prepare the

exclusive SC aerogels as this procedure involves gel formation and subsequent solvent extraction.

Like many other semicrystalline polymers, PLLA and PDLA also form thermoreversible gels through crystallization, where the small crystallites constitute the physical cross-links (junction zones) of the three-dimensional polymer networks.[36-43] In polymers such as syndiotactic polystyrene (sPS) and poly(phenylene oxide) (PPO), the gelation solvent can form crystal complexes with polymers, i.e., the polymer accommodates solvent molecules within its crystal lattice.[36, 38, 41, 44-46] Similar to sPS and PPO, polylactides (PLLA and PDLA) are also known to form crystal complexes (ε-form) in certain solvents like N, N-dimethylformamide (DMF), tetrahydrofuran (THF), cyclopentanone (CPO), etc.[15, 47-51] PLLA has been demonstrated to form ε gel readily on cooling the polymer solution in DMF to below 0 °C. Matsuda et al. reported that the gelation of PLLA was induced by the solvents that form crystal complexes (ε crystals), and no such gel formation was observed in the solvents that cannot form PLLA crystal complexes.[40] These thermoreversible gels undergo a phase transition upon heating to form stable α-form gels at moderate temperatures. Even though much work has not been done on PDLA crystalline complexes, the same behavior was reported for PDLA in DMF.[15] ε gels of PLLA or PDLA could be converted to aerogels by extracting the gel solvent using techniques like supercritical drying or freeze-drying. However, the direct removal of organic solvents using these methods is tricky due to the high critical temperatures/pressures or low freezing points. Therefore, solvent exchange strategies should be adopted to facilitate the easy removal of gel solvents.[52, 53] Matsuda et al. showed that DMF in PLLA ε gel is readily exchangeable with water without the disintegration of the gel network and in the resultant gel, ε crystals transformed to α

crystals bereft of any morphological changes.[40] However, there are no reports on homopolymer aerogels obtained by this method.

Though there is some understanding of the gel formation of homopolymers, the blending of PLLA and PDLA in crystal complex forming solvents for the preparation of aerogels has never been explored. Recent reports on SC PLA aerogel used 1, 4-dioxane as the solvent for blending the enantiomers of PLA.[7, 54] The blend solution was frozen and then freeze-dried to obtain the aerogels. It has to be noted that 1, 4-dioxane does not induce typical thermoreversible gelation of PLA; hence, the resultant aerogels suffer from poor crystallinity. Praveena et al. tried the gel formation of PLLA/PDLA blends in DMF in the quest of SC crystallization and found that PLLA and PDLA chains in the blend gel crystallized independently into the corresponding crystal complexes (ε-form) rather than into the SC.[15] Although the SC formation was well studied in bulk, many questions are left unanswered in understanding the SC formation in gels and aerogels. For example, is it possible to obtain pure SC gel without homopolymer crystals by blending PLLA and PDLA? Is it possible to convert the SC gel to SC aerogel without structural reorganization during solvent extraction? What happens to the structure of the blend gel in a hierarchical length scale on solvent extraction? So far, no one has attempted to answer the above questions, as gel formation and solvent exchange resulted in the structural change of PLAs.

In this chapter, we propose a simple strategy for the preparation of SC aerogels with crystalline purity by blending PLLA and PDLA in DMF. The PLLA/PDLA blend gel on solvent exchange with water resulted in the α-form gel, which upon freeze-drying furnished α-form aerogel. In order to instigate the chain diffusion and the alternate packing of the opposite enantiomeric chains, the blend ε gel was thermally annealed at 70 °C. As a result, SC gel (without homocrystals) was obtained, which was then converted to

aerogel by solvent exchange and freeze-drying. The degree of crystallinity was enhanced and unique morphologies were generated when the opposite enantiomeric chains co-crystallized into the SC. These hierarchical structural changes resulted in the enhancement of the thermal, mechanical and surface properties of the aerogel.

3.3. Experimental Section

3.3.1. Materials

PLLA ($M_w \sim 101$ kg/mol, Đ ~ 1.8) and PDLA ($M_w \sim 124$ kg/mol, Đ ~ 1.37) were purchased from Sigma-Aldrich. The solvent N, N-dimethylformamide (DMF) [purity ≥99.9%] was supplied by Merck and used as received.

3.3.2. Preparation of Homopolymer Gels and Aerogels

10 wt% solution of PLLA or PDLA in DMF was prepared by heating the solvent at 120 °C. The solution was cooled to below 0 °C by keeping it in the freezer. Thermoreversible gelation occurred immediately and the resulted gel was aged at the same temperature for 48 h. Then, DMF in the gel was exchanged with water by immersing the gel fully in water. This water was replaced with fresh water 4-5 times over a period of 30 h in order to ensure the complete exchange. The hydrogel thus obtained was first frozen at -40 °C and then freeze-dried for 24 h to obtain homopolymer aerogel with an overall porosity of 90 %.

3.3.3. Preparation of PLLA/PDLA Blend Gels and Aerogels

Equal quantities of PLLA and PDLA were used to separately prepare 10 wt% solutions in DMF. The PLLA and PDLA solutions were then mixed thoroughly and the mixed solution was cooled to below 0 °C in the freezer to obtain PLLA/PDLA (1:1) blend gel. This gel was aged at the same temperature for 48 h before further use.

In order to prepare blend α-form aerogel, the above gel was solvent exchanged with water as described earlier and then freeze-dried.

In order to prepare SC aerogel, the above gel was first subjected to thermal annealing at 70 °C. For this, an oil bath was pre-heated to 70 °C using a hot plate and the vial containing the gel was immersed entirely in the oil for 5-10 minutes. Then, the gel was cooled back to the RT and aged in the freezer (< 0 °C) for 12 h. This was followed by solvent exchange and freeze-drying as before to obtain a complete SC aerogel. Following the same procedure, except for a change in the annealing temperature to 50 °C, will result in a (α + SC) aerogel.

3.3.4. Characterization

The porosity of different aerogel samples was determined from the density values using the following equation

$$P = 100 \left[1 - \frac{\rho_{ap}}{\rho_{pol}} \right] \tag{1}$$

where ρ_{ap} is the mass/volume ratio (apparent density) of the prepared aerogel; volume is determined theoretically from the dimensions of the samples and ρ_{pol} is the density of the bulk polymer. XEUSS SAXS/WAXS system from Xenocs operated at 50 kV and 0.60 mA in the transmission mode using Cu Kα radiation of wavelength 1.54 Å was used for WAXD measurements. The two-dimensional patterns were recorded on a Mar 345 image plate system (detector) and the Fit2D software was used for data processing. Variable temperature WAXD measurements were carried out with the aid of Linkam THMS 600 hot stage connected to the LNP 95 cooling system. Infrared spectra of the aerogel samples were collected using a PerkinElmer Series FT-IR spectrum-2 at a resolution of 4 cm^{-1} over the wavenumber range of 4000–400 cm^{-1} in the attenuated total reflectance (ATR) mode. DSC measurements were performed using an advanced research-grade modulated

differential scanning calorimeter TA Q2000 under a nitrogen atmosphere was used for the measurements. The heating rate adopted was 10 °C/min. TGA was carried out under continuous nitrogen flow using TA Q50, a fourth-generation thermogravimetric analyzer. The surface morphologies of various aerogels were probed using a Zeiss EVO 18 cryo-SEM operated at an accelerating voltage of 12 kV. A JEOL 2010 transmission electron microscope operating at 300 kV was used to examine the morphology of the xerogels. The gels were dispersed in DMF, drop casted on a carbon-coated copper grid and naturally dried under dust free atmosphere. An automated DSA30 Drop Shape Analyzer (KRŰSS, Germany) was used for the measurement of WCA. From the nitrogen adsorption-desorption isotherm (Gemini 2375, Micromeritics, Norcross, USA), the BET surface area of the aerogels was measured. The samples were degassed at room temperature for 24 h before the measurement. The pore size distributions were also obtained from the isotherms using the Barrett–Joyner–Halenda (BJH) method. A universal testing machine (Hounsfield, H5KS UTM, Redhill, UK) with a crosshead speed of 1.3 mm min^{-1} was used for the compressive strength analysis of the aerogels. Cylindrical samples with diameter to height ratio of approximately 1.5 : 1 were used for these measurements. The normal incident sound absorption coefficient of all of the samples was obtained using a Brüel & Kjær impedance tube, type 4206 (Denmark) via two microphone method. Cylindrical samples with a diameter of 29 mm and thickness of 12 mm were used for the measurements.

3.4. Results and Discussion

The PLLA/PDLA (1:1) blend gel was prepared by homogeneously mixing the equimolar PLLA and PDLA solutions prepared in DMF and cooling the mixed solution to below 0 °C. Similarly, homopolymer gels were also prepared. The total polymer concentration in the solution was 10 wt % in all the cases. The blend gel, similar to the

PLLA and PDLA gels, crystallized into the ε-form with PLLA and PDLA chains adopting 10_7 helical conformation and accommodating DMF molecules within the orthorhombic lattice ($2\theta = 9.8°$ (111), 11.9° (200), 14.1° (020), 15.7° (121/114), 18.5° (123), 19.5° (223), 20.8° (116) and 23.8° (117)).[47] These gels were quite stable for a long duration even at room temperature, as evident from the wide-angle X-ray diffraction (WAXD) patterns in Figure 3.1a. The gel solvent (DMF) of the blend as well as the homopolymer ε gels was exchanged with water (with a higher freezing temperature (0 °C) than DMF (-61 °C)) before the freeze-drying process to ease the solvent removal and obtain aerogels with negligible size reduction. However, solvent exchange resulted in a phase transition from ε-to-α form through a local disorder in the helical conformation within the crystal lattice following the solvent desorption from the crystal lattice to the amorphous region. The WAXD patterns of the PDLA, PLLA and PLLA/PDLA blend gels after the solvent exchange (Figure 3.1b (A-C)) show characteristic reflections of the α-form ($2\theta = 16.7°$ (200/110) and 19.1° (203)).[55] Note that PLLA/PDLA ratio in the blends is 1:1 throughout the entire work. The α crystalline form of PLA is stable and therefore, solvent extraction from the gels resulted in α-form aerogels, as shown in Figure 3.1c (A-C). The degree of crystallinity of the obtained PLLA, PDLA and PLLA/PDLA α aerogels was 51 ± 2 %, 49 ± 2% and 47 ± 2 %, respectively.
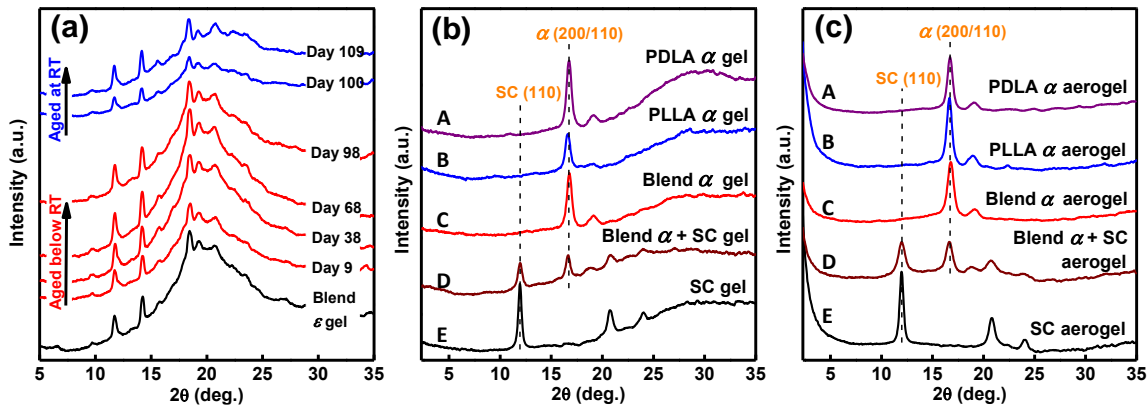
Figure 3.1. WAXD patterns of (a) PLLA/PDLA blend ε gel obtained on successive days after the initial preparation showing the stability of the prepared gel, (b) various gels after the solvent exchange with water, and (c) aerogels (gels after freeze-drying).

Variable temperature WAXD studies of the PLLA/PDLA blend ε gel (Figure 3.2a) show that on heating the gel, the ε form transformed to the α-form around 45 °C (this is an irreversible transition) and simultaneously, some of the disordered PLLA and PDLA chains reorganized to form SC crystals. Further heating resulted in the melting of α crystals (destabilization) and the formation of highly stable SC gel by chain reorganization. It has to be noted that the contents of the α and SC crystals remain the same after annealing the blend gel just above the ε to α transition temperature (50 °C) for 250 min (Figure 3.2b). These experiments suggested that annealing the blend gel at 70 °C is crucial because the α crystals are quite stable below this temperature. Based on the above observations, we planned two experiments. In the first experiment, we annealed the blend ε gel just above the ε to α transition temperature (50 °C) for 5 min, cooled it back to room temperature and then aged it at < 0 °C for 12 h. The WAXD pattern (Figure 3.2c) of the resultant gel shows new reflections at 2θ = 11.9° (110), 20.8° (300/030) and 24.0° (220) along with the characteristic reflections of the α-form. The new peaks corresponding to the SC crystals and this mixed α + SC structure prevailed even after the

solvent exchange (Figure 3.1b (D)). At ~50 °C, as discussed earlier, the solvent molecules from the crystal lattice of the ε form are ejected to the amorphous phase and some of the disordered PLLA and PDLA chains come close to each other due to the activated mobility. As a consequence, the ε crystals reorganize to form α crystals and a fraction of the disordered chains reorganize into SC. The same crystal structure was retained in the aerogel, as shown in Figure 3.1c (D). In the second experiment, thermal annealing of the blend ε gel was carried out at around 70 °C. At this temperature, the whole of PLLA and PDLA α crystals (formed at 50 °C) melted and the polymer chains achieved enough mobility and diffusion ability to discover opposite enantiomeric chains for the reorganization into SC crystals (3_1 helical conformation) (Figure 3.2c).[16] SC form shows the highest stability among all the crystalline forms of PLA and therefore, the SC gel formed by the above experiment retained its crystal structure even after the solvent exchange (Figure 3.1b (E)) and solvent removal (Figure 3.1c (E)). Thus, we prepared pure SC crystalline PLA aerogels by thermally annealing the PLLA/PDLA blend ε gel at ~70 °C for a short duration (10 min) followed by solvent exchange with water and freeze-drying. It has to be noted that thermal annealing of the blend ε gel did not affect the gel stability and no dimensional changes were observed after the annealing process. Freeze-drying resulted in only negligible shrinkage (~3 %) and all the aerogels prepared in this study had a total porosity of ~90 %. SC aerogel exhibited the highest degree of crystallinity of 54 ± 2 %.
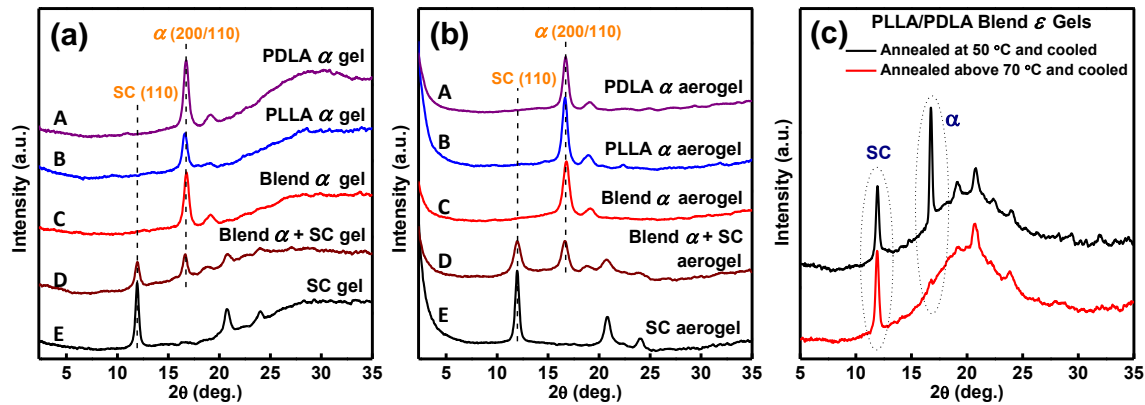
Figure 3.2. (a) Temperature dependent WAXD patterns of PLLA/PDLA blend ε gel during the heating process. (b) Time-variable WAXD patterns of PLLA/PDLA blend ε-gel during isothermal annealing at 50 °C.

The successful formation of aerogels with various crystalline forms was further confirmed by Fourier transform infrared (FTIR) analysis. The IR spectral region between 880 and 980 cm^{-1} corresponds to the r(CH3) + ν(C-COO) vibrational modes, which are sensitive to the chain packing mode of PLA.[56, 57] Similarly, another IR region, 1280-1330 cm^{-1} corresponding to the δ$_s$(CH3) + δ(CH) + ν(C-O-C) vibrations were also found to be helpful in distinguishing between different structural forms of PLAs.[51, 58] Figures 3.3a and 3.3b show explicit spectral differences between the α-form (blend and homopolymers) aerogels and the SC aerogel. The latter exhibits a peak at 908 cm^{-1}, which is absent in all the α-form aerogels. The 921 cm^{-1} band is the characteristic band of the α-form[16, 19, 57] and it was absent in the SC aerogel (Figure 3.3a). In the other spectral region (1280-1330 cm^{-1}) also, the peak positions were quite different for SC (1306 and 1318 cm^{-1}) and α-form (1293 and 1305 cm^{-1}) aerogels, as shown in Figure 3.3b. These observations substantiate the results obtained from the WAXD studies and confirm the crystal structure of all the aerogels prepared in this study. Figure 3.3c shows the carbonyl stretching region of various aerogels. Homopolymer and blend α-form aerogels showed identical carbonyl stretching frequencies (1757 cm^{-1}), whereas, in SC aerogel, there is a shift in the

stretching peak towards the lower wavenumber (1747 cm^{-1}), which is attributed to the conformational change (from 10_7 to 3_1) of PLA chains and the strong interactions between the PLLA and PDLA chains. As expected, the α + SC aerogel exhibited two stretching frequencies in the intermediate region between 1757 and 1747 cm^{-1}, corresponding to the α and SC forms of PLA.
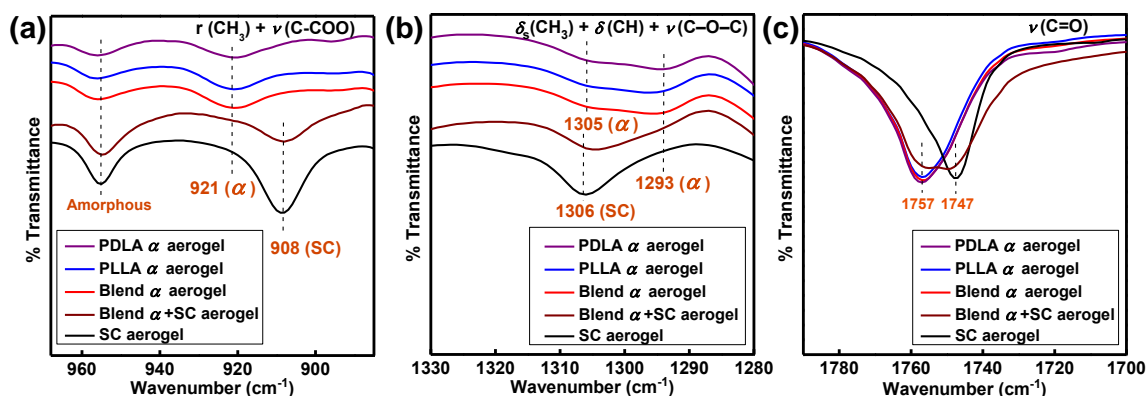
Figure 3.3. FTIR spectra of various aerogels in the regions of (a) 880-980 cm^{-1}, (b) 1280-1330 cm^{-1} and (c) 1700-1800 cm^{-1}.

The homopolymer aerogels melted around 176 ± 2 °C, as shown in the differential scanning calorimetry (DSC) thermograms (Figure 3.4a (A-B)). The SC aerogel exhibited a higher melting temperature (227 ± 2 °C), and no homopolymer melting was observed in this case (Figure 3.4a (E)), which is absolute proof of the crystal purity of the prepared SC aerogel. However, in the blend α-form aerogel, endotherms corresponding to the melting of both α and SC crystals were observed in the DSC. This is because, just after melting all the α crystals, the disordered PLLA and PDLA chains in the blend aerogel attain sufficient mobility to form SC crystals.[17, 20] Pan and co-workers reported that the entanglements degree in freeze-dried samples play a crucial role in SC crystallization.[32] We speculate here that the chain entanglements in aerogels are responsible for the reorganization of molten chains into SC just above the melting of α crystals, which is

different from the bulk samples.[18, 20]   The endotherm (α crystal melting) followed by a small exotherm in Figure 3.4a (C) is characteristic of such polymer chain reorganization and crystal to crystal transition.[18, 59] It has to be noted that in the case of α + SC aerogel, no such exotherm following the first endotherm was observed (Figure 3.4a (D)) due to the low contents of the α crystals in the starting sample. The thermal stability of the aerogels was also enhanced upon SC formation, as shown in Figure 3.3b. The temperature at 50 % weight loss ($T_{50\%}$) for PLLA, PDLA, blend α-form, α + SC and SC aerogels are 316, 322, 329, 337 and 343 °C, respectively. In the case of PLLA/PDLA blend aerogels, the pure crystalline forms (α-form and SC) exhibited better thermal stability than the assorted (α + SC) form.
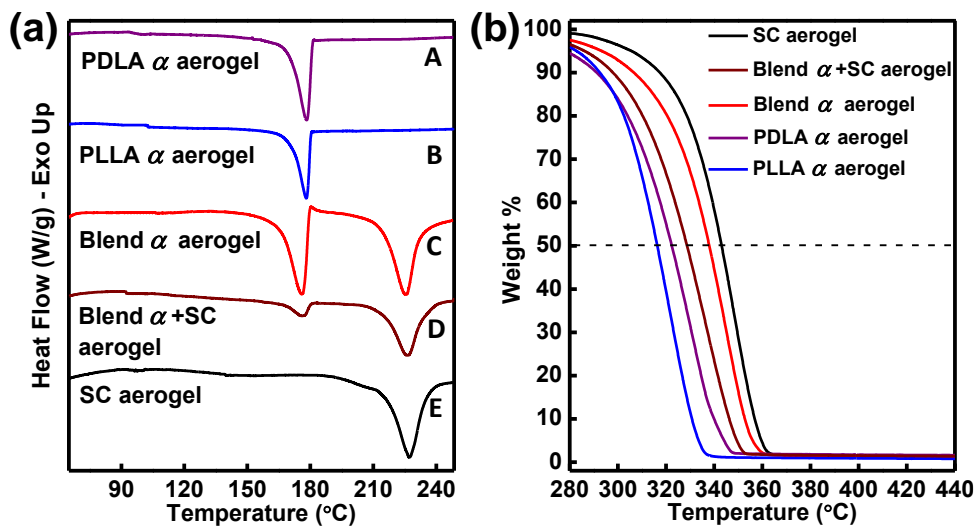
Figure 3.4. *(a) DSC first heating curves and (b) TGA thermograms of various aerogels at a heating rate of 10 °C/min.*

PLLA and PDLA aerogels displayed typical interconnected fibrillar network morphologies, as shown in the scanning electron microscopy (SEM) images (Figures 3.5a and 3.5b). Transmission electron microscopy (TEM) image of PLLA xerogel (gel which is dried under ambient conditions) also shows similar morphology (Figure 3.5c). Whereas, in the blend α-form aerogel, some of the polymer fibers agglomerated into

dense spherical bundles (Figure 3.5d and 3.5f) and these globular species displayed a randomly scattered distribution on the fibrillar network, as given in Figure 3.5e. However, in this case, the microstructure is more of the homo-polymer structure, except for the agglomerated species. It has to be noted that the spherical bundles are more in the TEM image (Figure 3.5f) due to the ambient drying conditions compared to the aerogels prepared by the freeze-drying method (Figure 3.5d). On the other hand, SC aerogel exhibited a unique morphology that is different from the homopolymer and blend (α-form) aerogels. As seen in Figures 3.5g, 3.5h and 3.5i, most of the polymer fibrils wrapped together into globular structures (nodular morphology) of micrometer dimensions upon SC formation and the individual spheres were connected to each other by the short polymer fibers. For this to happen, during the thermal annealing of the blend gel, the PLLA and PDLA fibres have to unwind first to individual polymer chains and then, the PLLA and PDLA chains have to come together at the molecular level. Unlike the blend α-form aerogel, the spherical structures in this case possess a certain level of porosity owing to the loose winding of the polymer fibrils. Therefore, at the micrometer length scale, SC formation resulted in a major reorganization of the morphology from interconnected fibrillar structures to interconnected globular networks (nodular morphology). Such a difference in the microstructure is responsible for the enhancement of the aerogel thermal properties. The observed morphologies of homopolymer and SC aerogels are different from that reported for PLA foams/aerogels.[60-64]

Figure 3.5. *SEM images (magnification × 25000) of (a) PDLA and (b) PLLA aerogels. (c) TEM image of PLLA xerogel. SEM images of blend α-form aerogel magnified (d) 25000 time and (e) 2000 times. (f) TEM image of blend α-form xerogel. SEM images of SC aerogel magnified (g) 25000 time and (h) 2000 times. (i) TEM image of SC xerogel.*

Several other properties were also elevated in SC aerogel due to their unique morphological features, such as surface and mechanical properties. For example, the water contact angle (WCA) measured for SC aerogel was $149.0 \pm 1°$. WCA is a measure of the surface wettability of the aerogels. Since PLAs are inherently hydrophobic in nature, PLLA aerogel exhibited a very high WCA of $141.6 \pm 1°$. Whereas, with the change in the surface morphology, more surface roughness was induced on the SC aerogel when compared to the PLLA aerogel, making it nearly superhydrophobic (Figure 3.6a). Similarly, the Brunauer–Emmett–Teller (BET) surface area was enhanced and a narrow pore size distribution was obtained for SC aerogel when compared to the

homopolymer aerogels. Figure 3.6b shows the nitrogen adsorption-desorption isotherms and pore size distribution curves of PLLA and SC aerogels. Unlike PLLA aerogel, SC aerogel shows a typical Type IV adsorption isotherm with a hysteresis loop (Figure 3.6b), characteristic of a mesoporous solid.[65] The pore size distribution in Figure 3.6c also validates the highly mesoporous structure of SC aerogel and the curve peaks around 12 nm. In PLLA aerogel, the pore size distribution is broad and pore diameters above 50 nm dominate. Thus, it is appropriate to mention that the morphological switch has brought a shift from less mesoporous to highly mesoporous structures in PLA aerogels. The BET surface area was also enhanced in SC aerogel (~ 132 $m^2 g^{-1}$) on comparison with that of PLLA aerogel (~ 113 $m^2 g^{-1}$).
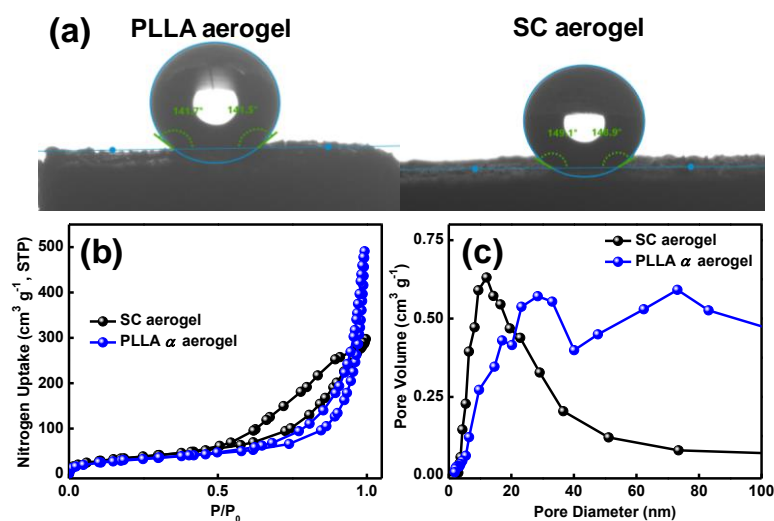
Figure 3.6. *(a) Images of water droplets on the PLLA and SC aerogel surfaces and their contact angles. (b) N_2 adsorption-desorption isotherms and (c) pore size distributions of PLLA and SC aerogels.*

Mechanical strength is of paramount importance for aerogels from the application point of view. PLA homopolymer aerogels are lagging behind and constant efforts have been put through to improve the mechanical properties of these aerogels.[7] The crystallinity of PLLA and SC aerogels prepared in this study are almost the same (52 ± 2

%). However, there is a marked difference in the compression strength between these two aerogels, as shown in Figure 3.7a. The enlarged portion of Figure 3.7a (Figure 3.7b) shows the linear elastic region of the compressive stress-strain curve, the slope of which gives Young's modulus. All the aerogels used for the compression test have an overall porosity close to 90 %. The compression moduli were calculated to be 2.0, 1.8 and 3.3 MPa for PLLA, blend α-form and SC aerogels, respectively. The slight agglomeration of polymer fibrils in the blend α-form aerogel resulted in the lowering of modulus when compared to the homopolymer aerogels. However, the complete transformation of the blend into SC has furnished almost double the compression modulus. Even though PLLA and PDLA aerogels have interconnected fibrillar networks, these networks are not strong enough to withstand higher loads. Whereas in the SC aerogel, the winding of polymer fibrils into globular structures resulted in a muscular monolith. In addition, these spheres were connected to the neighboring spheres not by a single strand but by multiple polymer strands, hence making the interconnections quite strong. Thus, we could obtain PLA aerogels with superior load-bearing properties without compromising the high porosity by allowing the opposite enantiomeric polymer chains to interact and form SC crystals (interconnected globular network). Figure 3.7c shows SC aerogel being balanced on top of caterpillar grass; this indicates the ultra-lightweightness (density $\sim$ 0.09 g cm^{-3}) of the prepared aerogel.

The morphology switch has not just enhanced the mechanical properties of the aerogel, but also improved its sound absorption ability. As demonstrated in our previous study on sPS aerogels, the differences in the pore structure, pore volume and surface area can have significant effects on the sound insulation of aerogels.[52] The ratio of absorbed sound intensity in the material to the incident sound intensity is known as normal incident sound absorption coefficient of a particular material. Figure 3.7d is the plot of sound

absorption coefficient of PLLA and SC aerogels at various frequencies (300−3000 Hz); for comparison, the data obtained for a commercial sound insulator (polyurethane (PU) foam) is also provided. Below 3000 Hz, the SC aerogel exhibited multi-fold enhancement in the sound absorption than the PLLA aerogel and the absorption coefficients are way better than the PU foam. In the frequency range 1800-2000 Hz, absorption coefficients as high as 0.85 were obtained for SC aerogel. The excellence in the acoustic insulation performance of SC aerogel is attributed to its largely mesoporous structure. Sound waves get scattered multiple times inside the porous structure resulting in the vibration of the pore walls. Also, the enhanced friction causes air viscosity consumption. In both these situations, the sound energy will be converted as heat within the material, resulting in a reduction of the sound pressure. As the market is looking for sustainable alternatives to the age-old sound insulation materials, these aerogels with superior comprehensive properties can be excellent candidates.
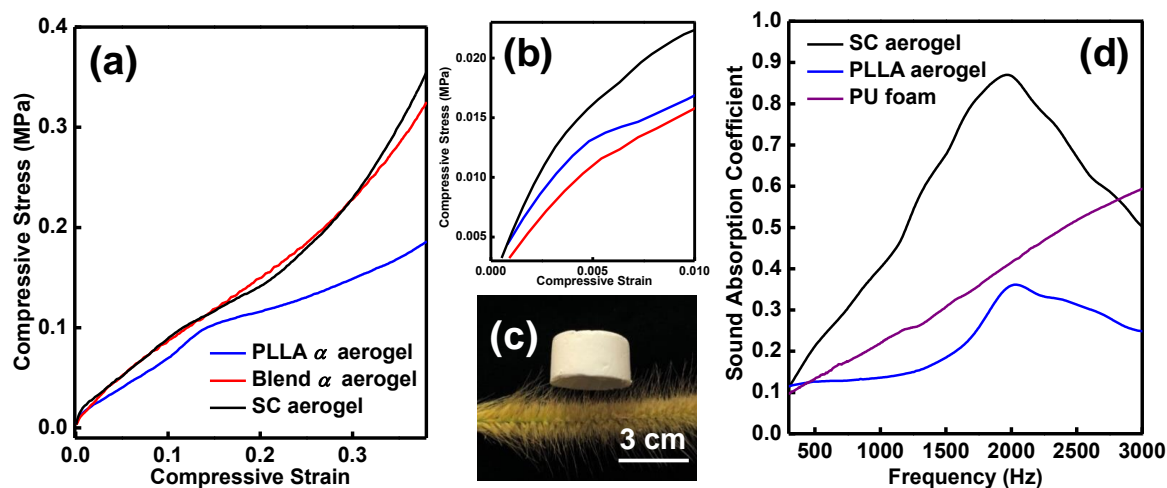
Figure 3.7. (a) Stress-strain plots of various aerogels under compression and (b) the magnified linear elastic region. (c) Photographic image of SC aerogel on top of caterpillar grass. (d) Normal incident sound absorption coefficients of SC and PLLA aerogels measured in the frequency range of 300−3000 Hz.

Based on the results obtained, we have clarified the development of hierarchical structures in PLLA/PDLA blend aerogels (Figure 3.8). Though the homopolymer gels crystallized into the ε form, upon the aerogel preparation, the structure is transformed to the α-form and higher-ordered structures show interconnected fibrillar networks in aerogels (Figure 3.8a-b). The PLLA/PDLA blend in DMF also crystallized into the ε-form on thermoreversible gelation. The blend ε-form gel transformed to the α-form upon solvent exchange and the corresponding α-form aerogel showed an interdigitated fibrillar network with dense agglomerates at random positions (Figure 3.8c). Here, the interdigitating occurs between the fibrils of opposite enantiomeric chains, as there is only a local disorder of the helical chains during the ε-to-α transition. But, when the blend ε-form gel was annealed at 70 °C, the polymer chains attain enough diffusion ability to find opposite enantiomeric chains for the alternate packing into SC crystals. The higher-ordered structure in SC aerogel shows an interconnected network of globular structures, which is completely different from the blend α-form microstructure. In order to form such morphology, the enantiomeric polymer fibrils have to unwind to individual chains first. Only then, the PLLA chains can twine with PDLA chains to form interwoven ball-like microstructures, as shown in Figure 3.8d. The untangled polymer strands form connections between the individual spheres to form a network structure. Thus, it is appropriate to mention that thermal stimulus has not only induced chain mobility and diffusion at the molecular level, but also instigated prodigious microstructural reorganization resulting in perfect SC formation in PLLA/PDLA blend gels and aerogels.
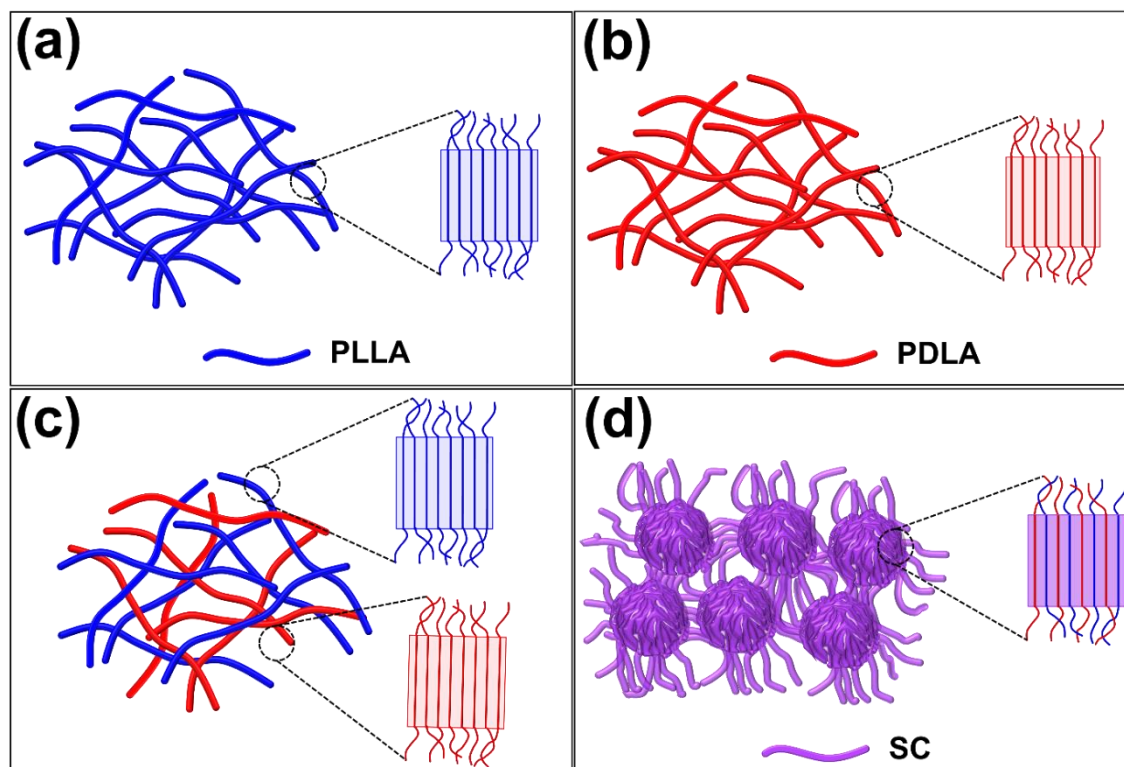
Figure 3.8. Schematic diagram showing the hierarchical structures of various aerogels; (a) PLLA α aerogel, (b) PDLA α aerogel, (c) blend α aerogel and (d) blend SC aerogel.

3.5. Conclusions

In summary, using the thermoreversible gelation approach, we reported the formation of crystalline pure SC gels and aerogels of PLA. The crystal complex forming solvent was used for the PLLA/PDLA blend gel formation. In the initial blend gel, the homopolymers crystallized independently into the corresponding crystal complexes (ε-form) rather than co-crystallizing into the SC. When the gel solvent was exchanged with water and freeze-dried, a blend α-form aerogel was obtained. Thermal treatment of the blend gel resulted in crystalline phase transitions; ε-to-α transition occurred around 50 °C due to the solvent desorption from the crystal lattice to the amorphous region and the subsequent reorganization of the helical chains occurred through a disordered state. At a higher annealing temperature of blend gel (at 70 °C), polymer chains acquired enough energy to diffuse through the system and found the opposite chains for the alternate

packing. As a result, gel with a complete SC crystal structure was obtained, resulting in

SC aerogel upon solvent exchange and freeze-drying. The transitions at the molecular

level were accompanied by hierarchical structural changes and microstructural evolution.

The interconnected fibrillar morphology in the α-form aerogels was converted to unique

interwoven globular network morphology upon the SC formation. These transitions, both

at the molecular level and at the micrometer length scale, resulted in noteworthy

enhancement of the aerogel thermal, mechanical and acoustic properties.

3.6. References

1. Zhao, S.; Malfait, W. J.; Guerrero-Alburquerque, N.; Koebel, M. M.; Nyström, G. Biopolymer Aerogels and Foams: Chemistry, Properties, and Applications. *Angew. Chem. Int. Ed.* **2018**, *57*, 7580-7608.
2. Ahankari, S.; Paliwal, P.; Subhedar, A.; Kargarzadeh, H. Recent Developments in Nanocellulose-Based Aerogels in Thermal Applications: A Review. *ACS Nano* **2021**, *15*, 3849-3874.
3. Takeshita, S.; Zhao, S.; Malfait, W. J.; Koebel, M. M. Chemistry of Chitosan Aerogels: Three-Dimensional Pore Control for Tailored Applications. *Angew. Chem. Int. Ed.* **2021**, *60*, 9828-9851.
4. Reverchon, E.; Pisanti, P.; Cardea, S. Nanostructured PLLA−Hydroxyapatite Scaffolds Produced by a Supercritical Assisted Technique. *Ind. Eng. Chem. Res.* **2009**, *48*, 5310-5316.
5. Salerno, A.; Fernández-Gutiérrez, M.; San Román del Barrio, J.; Pascual, C. D. Macroporous and Nanometre Scale Fibrous PLA and PLA-HA Composite Scaffolds Fabricated by a Bio Safe Strategy. *RSC Adv.* **2014**, *4*, 61491-61502.
6. Mader, M.; Jérôme, V.; Freitag, R.; Agarwal, S.; Greiner, A. Ultraporous, Compressible, Wettable Polylactide/Polycaprolactone Sponges for Tissue Engineering. *Biomacromolecules* **2018**, *19*, 1663-1673.
7. Chen, P.; Bai, D.; Tang, H.; Liu, H.; Wang, J.; Gao, G.; Li, L. Polylactide Aerogel with Excellent Comprehensive Performances Imparted by Stereocomplex Crystallization for Efficient Oil-Water Separation. *Polymer* **2022**, *255*, 125128.
8. Aragón-Gutierrez, A.; Arrieta, M. P.; López-González, M.; Fernández-García, M.; López, D. Hybrid Biocomposites Based on Poly(Lactic Acid) and Silica Aerogel for Food Packaging Applications. *Materials* **2020**, *13*, 4910.
9. Ikada, Y.; Jamshidi, K.; Tsuji, H.; Hyon, S. H. Stereocomplex Formation between Enantiomeric Poly(Lactides). *Macromolecules* **1987**, *20*, 904-906.
10. Okihara, T.; Tsuji, M.; Kawaguchi, A.; Katayama, K.-I.; Tsuji, H.; Hyon, S.-H.; Ikada, Y. Crystal Structure of Stereocomplex of Poly(L-Lactide) and Poly(D-Lactide). *J. Macromol. Sci. Phys* **1991**, *30*, 119-140.
11. Brochu, S.; Prud'homme, R. E.; Barakat, I.; Jerome, R. Stereocomplexation and Morphology of Polylactides. *Macromolecules* **1995**, *28*, 5230-5239.

12. Brizzolara, D.; Cantow, H.-J.; Diederichs, K.; Keller, E.; Domb, A. J. Mechanism of the Stereocomplex Formation between Enantiomeric Poly(Lactide)S. *Macromolecules* **1996**, *29*, 191-197.

13. Cartier, L.; Okihara, T.; Lotz, B. Triangular Polymer Single Crystals: Stereocomplexes, Twins, and Frustrated Structures. *Macromolecules* **1997**, *30*, 6313-6322.

14. Tsuji, H. Poly(Lactide) Stereocomplexes: Formation, Structure, Properties, Degradation, and Applications. *Macromol. Biosci.* **2005**, *5*, 569-597.

15. Praveena, N. M.; Virat, G.; Krishnan, V. G.; Gowd, E. B. Stereocomplex Formation and Hierarchical Structural Changes During Heating of Supramolecular Gels Obtained by Polylactide Racemic Blends. *Polymer* **2022**, *241*, 124530.

16. Zhang, J.; Sato, H.; Tsuji, H.; Noda, I.; Ozaki, Y. Infrared Spectroscopic Study of $CH_3 \cdots OC$ Interaction During Poly(L-Lactide)/Poly(D-Lactide) Stereocomplex Formation. *Macromolecules* **2005**, *38*, 1822-1828.

17. Zhang, J.; Tashiro, K.; Tsuji, H.; Domb, A. J. Investigation of Phase Transitional Behavior of Poly(L-Lactide)/Poly(D-Lactide) Blend Used to Prepare the Highly-Oriented Stereocomplex. *Macromolecules* **2007**, *40*, 1049-1054.

18. Fujita, M.; Sawayanagi, T.; Abe, H.; Tanaka, T.; Iwata, T.; Ito, K.; Fujisawa, T.; Maeda, M. Stereocomplex Formation through Reorganization of Poly(L-Lactic Acid) and Poly(D-Lactic Acid) Crystals. *Macromolecules* **2008**, *41*, 2852-2858.

19. Pan, P.; Yang, J.; Shan, G.; Bao, Y.; Weng, Z.; Cao, A.; Yazawa, K.; Inoue, Y. Temperature-Variable FTIR and Solid-State ^{13}C NMR Investigations on Crystalline Structure and Molecular Dynamics of Polymorphic Poly(L-Lactide) and Poly(L-Lactide)/Poly(D-Lactide) Stereocomplex. *Macromolecules* **2012**, *45*, 189-197.

20. Pan, P.; Han, L.; Bao, J.; Xie, Q.; Shan, G.; Bao, Y. Competitive Stereocomplexation, Homocrystallization, and Polymorphic Crystalline Transition in Poly(L-Lactic Acid)/Poly(D-Lactic Acid) Racemic Blends: Molecular Weight Effects. *J. Phys. Chem. B* **2015**, *119*, 6462-6470.

21. Tsuji, H. Poly(Lactic Acid) Stereocomplexes: A Decade of Progress. *Adv. Drug Deliv. Rev.* **2016**, *107*, 97-135.

22. Li, Z.; Tan, B. H.; Lin, T.; He, C. Recent Advances in Stereocomplexation of Enantiomeric Pla-Based Copolymers and Applications. *Prog. Polym. Sci.* **2016**, *62*, 22-72.

23. Zhou, D.; Xu, M.; Li, J.; Tan, R.; Ma, Z.; Dong, X.-H. Effect of Chain Length on Polymer Stereocomplexation: A Quantitative Study. *Macromolecules* **2021**, *54*, 4827-4833.

24. Zhou, W.; Wang, K.; Wang, S.; Yuan, S.; Chen, W.; Konishi, T.; Miyoshi, T. Stoichiometry and Packing Structure of Poly(Lactic Acid) Stereocomplex as Revealed by Solid-State NMR and 13^c Isotope Labeling. *ACS Macro Lett* **2018**, *7*, 667-671.

25. Tashiro, K.; Kouno, N.; Wang, H.; Tsuji, H. Crystal Structure of Poly(Lactic Acid) Stereocomplex: Random Packing Model of PDLA and PLLA Chains as Studied by X-Ray Diffraction Analysis. *Macromolecules* **2017**, *50*, 8048-8065.

26. Chen, W.; Wang, S.; Zhang, W.; Ke, Y.; Hong, Y.-l.; Miyoshi, T. Molecular Structural Basis for Stereocomplex Formation of Polylactide Enantiomers in Dilute Solution. *ACS Macro Lett* **2015**, *4*, 1264-1267.

27. Tsuji, H.; Ikada, Y. Stereocomplex Formation between Enantiomeric Poly(Lactic Acids). 9. Stereocomplexation from the Melt. *Macromolecules* **1993**, *26*, 6918-6926.

28. Xie, Q.; Bao, J.; Shan, G.; Bao, Y.; Pan, P. Fractional Crystallization Kinetics and Formation of Metastable B-Form Homocrystals in Poly(L-Lactic Acid)/Poly(D-Lactic

Acid) Racemic Blends Induced by Precedingly Formed Stereocomplexes. *Macromolecules* **2019**, *52*, 4655-4665.

29. Tsuji, H.; Horii, F.; Hyon, S. H.; Ikada, Y. Stereocomplex Formation between Enantiomeric Poly(Lactic Acid)s. 2. Stereocomplex Formation in Concentrated Solutions. *Macromolecules* **1991**, *24*, 2719-2724.

30. Liu, J.; Qi, X.; Feng, Q.; Lan, Q. Suppression of Phase Separation for Exclusive Stereocomplex Crystallization of a High-Molecular-Weight Racemic Poly(L-Lactide)/Poly(D-Lactide) Blend from the Glassy State. *Macromolecules* **2020**, *53*, 3493-3503.

31. Brzeziński, M.; Biela, T. Supramolecular Polylactides by the Cooperative Interaction of the End Groups and Stereocomplexation. *Macromolecules* **2015**, *48*, 2994-3004.

32. Sun, C.; Zheng, Y.; Xu, S.; Ni, L.; Li, X.; Shan, G.; Bao, Y.; Pan, P. Role of Chain Entanglements in the Stereocomplex Crystallization between Poly(Lactic Acid) Enantiomers. *ACS Macro Lett* **2021**, *10*, 1023-1028.

33. Bao, R.-Y.; Yang, W.; Wei, X.-F.; Xie, B.-H.; Yang, M.-B. Enhanced Formation of Stereocomplex Crystallites of High Molecular Weight Poly(L-Lactide)/Poly(D-Lactide) Blends from Melt by Using Poly(Ethylene Glycol). *ACS Sustain. Chem. Eng.* **2014**, *2*, 2301-2309.

34. Bao, R.-Y.; Yang, W.; Jiang, W.-R.; Liu, Z.-Y.; Xie, B.-H.; Yang, M.-B.; Fu, Q. Stereocomplex Formation of High-Molecular-Weight Polylactide: A Low Temperature Approach. *Polymer* **2012**, *53*, 5449-5454.

35. Tsuji, H.; Hyon, S. H.; Ikada, Y. Stereocomplex Formation between Enantiomeric Poly(Lactic Acid)s. 4. Differential Scanning Calorimetric Studies on Precipitates from Mixed Solutions of Poly(D-Lactic Acid) and Poly(L-Lactic Acid). *Macromolecules* **1991**, *24*, 5657-5662.

36. Daniel, C.; Dammer, C.; Guenet, J.-M. On the Definition of Thermoreversible Gels: The Case of Syndiotactic Polystyrene. *Polymer* **1994**, *35*, 4243-4246.

37. Guenet, J. Thermoreversible Gelation of Polymers and Biopolymers, Academic Press 1992.

38. Daniel, C.; Menelle, A.; Brulet, A.; Guenet, J.-M. Thermoreversible Gelation of Syndiotactic Polystyrene in Toluene and Chloroform. *Polymer* **1997**, *38*, 4193-4199.

39. Talley, S. J.; Yuan, X.; Moore, R. B. Thermoreversible Gelation of Poly(Ether Ether Ketone). *ACS Macro Lett* **2017**, *6*, 262-266.

40. Matsuda, Y.; Fukatsu, A.; Wang, Y.; Miyamoto, K.; Mays, J. W.; Tasaka, S. Fabrication and Characterization of Poly(L-Lactic Acid) Gels Induced by Fibrous Complex Crystallization with Solvents. *Polymer* **2014**, *55*, 4369-4378.

41. Gowd, E. B.; Tashiro, K.; Ramesh, C. Structural Phase Transitions of Syndiotactic Polystyrene. *Prog. Polym. Sci.* **2009**, *34*, 280-315.

42. Kobayashi, M.; Nakaoki, T.; Ishihara, N. Molecular Conformation in Glasses and Gels of Syndiotactic and Isotactic Polystyrenes. *Macromolecules* **1990**, *23*, 78-83.

43. Daniel, C.; Deluca, M. D.; Guenet, J. M.; Brûlet, A.; Menelle, A. Thermoreversible Gelation of Syndiotactic Polystyrene in Benzene. *Polymer* **1996**, *37*, 1273-1280.

44. Daniel, C.; Longo, S.; Fasano, G.; Vitillo, J. G.; Guerra, G. Nanoporous Crystalline Phases of Poly(2,6-Dimethyl-1,4-Phenylene)Oxide. *Chem. Mater.* **2011**, *23*, 3195-3200.

45. Daniel, C.; Pellegrino, M.; Venditto, V.; Aurucci, S.; Guerra, G. Nanoporous-Crystalline Poly(2,6-Dimethyl-1,4-Phenylene)Oxide (PPO) Aerogels. *Polymer* **2016**, *105*, 96-103.

46. Immirzi, A.; de Candia, F.; Iannelli, P.; Zambelli, A.; Vittoria, V. Solvent-Induced Polymorphism in Syndiotactic Polystyrene. *Macromol. Rapid Commun.* **1988**, *9*, 761-764.

47. Marubayashi, H.; Asai, S.; Sumita, M. Complex Crystal Formation of Poly(L-Lactide) with Solvent Molecules. *Macromolecules* **2012**, *45*, 1384-1397.

48. Marubayashi, H.; Asai, S.; Sumita, M. Guest-Induced Crystal-to-Crystal Transitions of Poly(L-Lactide) Complexes. *J. Phys. Chem. B* **2013**, *117*, 385-397.

49. Rizzo, P.; Ianniello, G.; Venditto, V.; Tarallo, O.; Guerra, G. Poly(L-Lactic Acid): Uniplanar Orientation in Cocrystalline Films and Structure of the Cocrystalline Form with Cyclopentanone. *Macromolecules* **2015**, *48*, 7513-7520.

50. Shaiju, P.; Murthy, N. S.; Gowd, E. B. Molecular, Crystalline, and Lamellar Length-Scale Changes in the Poly(L-Lactide) (PLLA) During Cyclopentanone (CPO) Desorption in PLLA/CPO Cocrystals. *Macromolecules* **2016**, *49*, 224-233.

51. Praveena, N. M.; Shaiju, P.; Raj, R. B. A.; Gowd, E. B. Infrared Bands to Distinguish Amorphous, Meso and Crystalline Phases of Poly(Lactide)s: Crystallization and Phase Transition Pathways of Amorphous, Meso and Co-Crystal Phases of Poly(L-Lactide) in the Heating Process. *Polymer* **2022**, *240*, 124495.

52. Krishnan, V. G.; Joseph, A. M.; Kuzhichalil Peethambharan, S.; Gowd, E. B. Nanoporous Crystalline Aerogels of Syndiotactic Polystyrene: Polymorphism, Dielectric, Thermal, and Acoustic Properties. *Macromolecules* **2021**, *54*, 10605-10615.

53. Joseph, A. M.; Nagendra, B.; Shaiju, P.; Surendran, K. P.; Gowd, E. B. Aerogels of Hierarchically Porous Syndiotactic Polystyrene with a Dielectric Constant near to Air. *J. Mater. Chem. C* **2018**, *6*, 360-368.

54. Liu, X.; Zhang, M.; Hou, Y.; Pan, Y.; Liu, C.; Shen, C. Hierarchically Superhydrophobic Stereocomplex Poly (Lactic Acid) Aerogel for Daytime Radiative Cooling. *Adv. Funct. Mater.* **2022**, *32*, 2207414.

55. Sasaki, S.; Asakura, T. Helix Distortion and Crystal Structure of the α-Form of Poly(L-Lactide). *Macromolecules* **2003**, *36*, 8385-8390.

56. Kang, S.; Hsu, S. L.; Stidham, H. D.; Smith, P. B.; Leugers, M. A.; Yang, X. A Spectroscopic Analysis of Poly(Lactic Acid) Structure. *Macromolecules* **2001**, *34*, 4542-4548.

57. Zhang, J.; Duan, Y.; Sato, H.; Tsuji, H.; Noda, I.; Yan, S.; Ozaki, Y. Crystal Modifications and Thermal Behavior of Poly(L-Lactic Acid) Revealed by Infrared Spectroscopy. *Macromolecules* **2005**, *38*, 8012-8021.

58. Chao, Y.-K.; Praveena, N. M.; Yang, K.-C.; Gowd, E. B.; Ho, R.-M. Crystallization of Polylactides Examined by Vibrational Circular Dichroism of Intra- and Inter-Chain Chiral Interactions. *Soft Matter* **2022**, *18*, 2722-2725.

59. Gowd, E. B.; Shibayama, N.; Tashiro, K. Structural Changes in Thermally Induced Phase Transitions of Uniaxially Oriented δ_e Form of Syndiotactic Polystyrene Investigated by Temperature-Dependent Measurements of X-Ray Fiber Diagrams and Polarized Infrared Spectra. *Macromolecules* **2006**, *39*, 8412-8418.

60. Salerno, A.; Domingo, C. Making Microporous Nanometre-Scale Fibrous PLA Aerogels with Clean and Reliable Supercritical CO_2 Based Approaches. *Microporous and Mesoporous Mater* **2014**, *184*, 162-168.

61. Yan, Z.; Liao, X.; He, G.; Li, S.; Guo, F.; Zou, F.; Li, G. Green and High-Expansion PLLA/PDLA Foams with Excellent Thermal Insulation and Enhanced Compressive Properties. *Ind. Eng. Chem. Res.* **2020**, *59*, 19244-19251.

62. Wang, X.; Pan, Y.; Liu, X.; Liu, H.; Li, N.; Liu, C.; Schubert, D. W.; Shen, C. Facile Fabrication of Superhydrophobic and Eco-Friendly Poly(Lactic Acid) Foam for Oil–

Water Separation Via Skin Peeling. *ACS Appl. Mater. Interfaces* **2019**, *11*, 14362-14367.

63. Kanno, T.; Uyama, H. Unique Leafy Morphology of Poly(Lactic Acid) Monoliths Controlled Via Novel Phase Separation Technology. *RSC Adv.* **2017**, *7*, 33726-33732.

64. Wang, L.; Lee, R. E.; Wang, G.; Chu, R. K. M.; Zhao, J.; Park, C. B. Use of Stereocomplex Crystallites for Fully-Biobased Microcellular Low-Density Poly(Lactic Acid) Foams for Green Packaging. *Chem. Eng. J.* **2017**, *327*, 1151-1162.

65. Barton, T. J.; Bull, L. M.; Klemperer, W. G.; Loy, D. A.; McEnaney, B.; Misono, M.; Monson, P. A.; Pez, G.; Scherer, G. W.; Vartuli, J. C.; Yaghi, O.M. Tailored Porous Materials. *Chem. Mater.* **1999**, *11*, 2633-2656.

Flame Retardant Polylactide Aerogels by Incorporating Multi-Element Moieties into the Polymer Gels during the Solvent Exchange Process
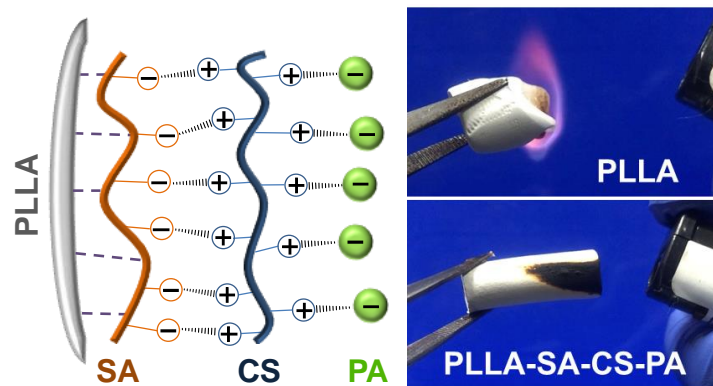
4.1. Abstract

The growing demand for aerogels based on biodegradable polymers in the construction field, structural applications and packaging can be encountered only by overcoming their inherent limitation of high flammability. Owing to their biodegradability, biocompatibility and good mechanical properties, polylactide (PLA) aerogels present extensive application prospects. However, the high flammability and melt-dripping phenomenon of PLA hold back these materials from the market. Though several strategies are available in the literature for improving the flame retardancy of PLA in its bulk form, there are barely any such reports on PLA aerogels. Therefore, it is high time to innovate and introduce novel and sustainable approaches for the enhancement of flame retardancy of PLA aerogels. Herein, utilizing the electrostatic interactions, biobased ionic molecules (sodium alginate (SA), chitosan (CS) and phytic acid (PA)) were deposited on poly(L-lactide) (PLLA) skeleton in the gel state through a solvent exchange cum layer-by-layer assembly approach using water as the exchange/assembly media. Freeze-drying of the hydrogels modified with SA, CS and PA furnished highly flame retardant PLLA aerogels. The new strategy does not involve complex chemical reactions, toxic flame retardants, or harmful solvents and can be used for the modification of aerogels of other polymers. The modified aerogels developed in this study exhibited self-extinguishment of flame, the highest limiting oxygen index of any porous PLA (~ 32 %), and a tremendous reduction in flammability parameters such as heat release rate, heat release capacity, etc.

4.2. Introduction

Aerogels based on polylactide (PLA) meet sustainability goals set for lightweight materials due to their excellent biodegradability and low toxic nature. In the previous chapter, we could enhance the thermal and mechanical properties of PLA aerogels by stereocomplex formation. PLA aerogels with superior properties are highly attractive for biomedical (tissue engineering scaffolds) and packaging applications. Apart from these, PLA aerogels possess huge potential in the construction field as thermal and acoustic insulators. However, the high flammability and melt-dripping behavior of PLA pose a serious threat that limits its application in such emerging fields.[1,2] Therefore, to expand the practical usage of PLA aerogels for various industrial applications, flame retardancy is of utmost importance. Traditionally, halogenated flame retardants have been employed for polymeric systems; but their adverse impact on the environment and human health prompted researchers to look for alternatives. To take advantage of the biodegradability of PLA, it is obvious that the flame retardants should not introduce much of non-biodegradable components in the final material.[3] Hence, bio-based flame retardants have attracted research interest, particularly for PLA.[4-8]

In recent times, intumescent flame retardants (IFR) based on biomass derived molecules such as chitosan (CS), phytic acid (PA), alginate, etc. have become popular for enhancing the flame retardancy of bulk PLA.[9-11] CS is an environment friendly biodegradable cationic polysaccharide with multiple hydroxyl groups, PA is a bio sourced phosphorus-rich anionic molecule and alginate is a natural anionic polysaccharide (linear copolymer). All these biobased materials are readily water soluble.[12-14] Therefore, electrostatic interactions between these differently charged molecules can be exploited to assemble them layer-by-layer (LbL) on top of materials to modify their surfaces in an organic solvent-free system.[15] Such LbL assemblies have been successful in generating

core-shell structured flame retardants for PLA. For example, Xiong et al. fabricated core-shell flame retardants using ammonium polyphosphate (APP) as the core.[9] Cationic CS and anionic PA were alternately deposited on negatively charged APP core via LbL assembly in water. The addition of APP-CS-PA core-shell particles to PLA enhanced its flame retardancy as well as toughness. Zhang et al. employed a similar strategy to prepare core-shell bio-based flame retardant for PLA, where, instead of PA, they used alginate.[10] They could achieve an LOI value of ~30.6 % for the PLA composite with three layers of the CS-alginate shell. However, all these reports have been on bulk PLA, not on PLA aerogels. LbL coating has been successfully used for improving the flame retardancy PU foams because of their high flexibility and structural stability.[16-18] However, that is not the case with thermoplastic polymer aerogels, which involves gel formation prior to the solvent extraction, and mostly, the flame retardants have to be incorporated into the system before the gelation. Also, it has to be made sure that the incorporation of flame retardants does not affect the intrinsic porous structure of the aerogels.

Recently, Kang et al. introduced a novel method to integrate biobased molecules into the semicrystalline polymer aerogels.[19] They prepared organogels of poly(3-hydroxybutyrate) (PHB) by non-solvent induced phase separation method and these gels were solvent exchanged with aqueous solution of CS. They could successfully load CS into the PHB hydrogels and prepare PHB/CS composite aerogels by freeze-drying. Inspired by this approach, solvent exchange process and the LbL assembly method were integrated to incorporate flame retardants into the PLA gels and aerogels. In our previous chapter, we have already demonstrated the success of solvent exchange of PLA thermoreversible gels with water and the subsequent freeze-drying to obtain highly porous aerogels.[20]

In this chapter, we devised a novel and green strategy to fabricate flame retardant poly(L-lactide) (PLLA) aerogels without the use of halogenated or inorganic flame retardants. Herein, we employed solvent exchange method to incorporate biobased ionic molecules into the 3D framework of PLLA gels prepared by thermally induced phase separation (TIPS) method. The selected molecules (CS, PA and sodium alginate (SA)) combine P and N rich moieties and provide multiple hydroxyl groups with high charring efficiency. By exploiting the electrostatic interactions between them, these guest molecules were alternately deposited one over the other (in different sequential orders) on the PLLA framework in the gel state. The as-prepared hydrogels were freeze-dried to obtain aerogels with excellent flame retardant properties. PLLA aerogels prepared with different sequential deposition of SA, CS and PA were tested for flammability. The PLLA-SA-CS-PA aerogels showed the best result with limiting oxygen index (LOI) value as high as 32.0 % (as compared to 18.5 % of neat PLLA aerogel), which is the highest value obtained for any PLA aerogel/foam. The modified aerogels also exhibited self-extinguishment of flame. The new protocol adopted in this work is a generalized one, which can be applied for the flame retardant modification of not just the PLA gels, but also the thermoreversible gels of other polymers.

4.3. Experimental Section

4.3.1. Materials

PLLA ($M_w \sim 260$ kg/mol, Đ ~ 1.5), chitosan (low molecular weight, degree of deacetylation $\geq 75\%$), sodium alginate, and phytic acid solution (50 % (w/w) in H_2O) were purchased from Sigma-Aldrich Co. and used without further purification. The gel solvent, N, N-dimethylformamide (DMF) [purity $\geq 99.9\%$] and glacial acetic acid were

supplied by Merck and used as received. Deionized (DI) water was used for the solvent exchange process.

4.3.2. Preparation of Flame Retardant Aerogels

6 wt% PLLA solution was prepared by dissolving 0.3 g of PLLA in 5 mL of DMF by heating at 120 °C. The solution was then transferred to 10 mL plastic syringe and cooled below 0 °C. The obtained PLLA thermoreversible gel was aged at the same temperature for 24 h before the solvent exchange process was carried out.

For the solvent exchange, 2 wt% aqueous solutions of SA, CS and PA were prepared independently. PLLA gel made from 5 mL solution was first immersed in 100 mL of SA (anionic) solution. After 12 h, the gel was taken out and washed with water to remove the excess SA solution from the gel surface. In the next step, the gel was kept immersed in 100 mL of CS (cationic) solution for 12 h. Since we used an anionic solution in the first step, the second immersion should be in a cationic solution in order to induce electrostatic interaction. Again, washing was done and the gel was subjected to the third step of solvent exchange. 100 mL of PA (anionic) solution was used this time. After 12 h, the final washing was done, and we obtained an LbL-coated PLLA hydrogel. According to the order of LbL coating, this sample is named as PLLA-SA-CS-PA gel. Similarly, PLLA-PA-CS-SA, PLLA-CS-SA-CS, and PLLA-CS-PA-CS gels were also prepared by altering the order of the solution for solvent exchange. For comparison, PLLA gel exchanged with pure water was also prepared.

The PLLA hydrogels (modified and unmodified) obtained after the solvent exchange were frozen at -40 °C and then freeze-dried for 24 h to obtain the corresponding aerogels.

4.3.3. Characterization

Densities of aerogel samples were calculated theoretically from their mass/volume ratio. Using a scanning electron microscope (Zeiss EVO 18 cryo-SEM operating at an accelerating voltage of 15 kV), the morphology of various aerogels was examined. FTIR analysis was performed using a PerkinElmer Series FT-IR Spectrum Two machine at a resolution of 4 cm^{-1} and 32 scans in the wavenumber range of 4000-400 cm^{-1} to confirm the aerogel modification. Water contact angle (WCA) measurements performed using an automated DSA30 Drop Shape Analyzer, KRŰSS, Germany further confirmed the surface modification of aerogels. Elemental analysis of the aerogels was carried out with energy dispersive spectroscope (EDS) attached to the SEM. Structural stability of the aerogels after the modification process was confirmed from wide-angle X-ray diffraction patterns acquired using XEUSS SAXS/WAXS system from Xenocs operated at 50 kV and 0.60 mA in the transmission mode using Cu Kα radiation (λ = 1.54 Å). Mar 345 image plate system detected the 2D-patterns and the Fit2D software was used for data processing. Thermal degradation behavior of the aerogels before and after the flame retardant treatment was monitored using a thermogravimetric analyzer (TGA) TA Q50. The samples were heated from room temperature to 800 °C at a rate of 10 °C/min under nitrogen atmosphere.

The flammability properties of the aerogels were analyzed by horizontal burning tests, limiting oxygen index (LOI) measurements and microscale combustion calorimetry (MCC). A Critical Oxygen Index Apparatus (as per ASTM D2863-08, ISO 4589) from Spectrum Automation and Controls coupled with Servomex Servoflex MiniMP (United Kingdom), a high-performance oxygen gas analyzer, was employed for the LOI measurements. For MCC (MCC-1 (FTT)) test, milligrams of the aerogel samples were heated to 700 °C at a heating rate of 1 °C/s in a stream of nitrogen (80 cm^3/min). The

resulting volatile anaerobic thermal degradation products are mixed with 80 cm^3/min carrying gas (nitrogen of 80 mL/min; oxygen of 20 mL/min) and subsequently burned at 900 °C in a combustion furnace.

4.4. Results and Discussion

PLLA is known to form thermoreversible gels in solvents such as DMF, THF, cyclopentanone, etc. by TIPS.[21-23] However, there are barely any reports on the aerogels of PLLA prepared from such thermoreversible gels, which may be due to the difficulty in extracting organic solvents from the PLLA gels without the structural disintegration. Nowadays, freeze-drying has become a popular method for solvent extraction from polymer gels, particularly due to the introduction of the solvent exchange process. With solvent exchange, organic solvents from the gels can be easily replaced with water, and the resulting hydrogels can be converted into aerogels by freeze-drying without much difficulty. In the previous chapter, we successfully employed solvent exchange and freeze-drying methods to fabricate PLLA, PDLA and SC aerogels. Herein, we have used a modified solvent exchange technique to prepare flame retardant PLLA aerogels. As described in the experimental part, PLLA/DMF gels were prepared initially. Instead of water, aqueous solutions of CS, SA, or PA were used as solvent exchange media. CS contains numerous primary amino groups, which are polarisable in aqueous acidic medium and render cationic nature to CS. SA is anionic due to the carboxylate and hydroxyl groups present; so is PA because of its multiple phosphate groups.

By changing the order in which different molecules are assembled on PLLA, i.e., by changing the order of solvent exchange, different samples were prepared. Figure 4.1 illustrates the LbL assembly in PLLA-SA-CS-PA gel achieved by the modified solvent exchange method. Here, the electrostatic/ionic interactions between the oppositely charged molecules play the major role of holding them one over the other. In other words,

ionic interactions stabilize the LbL assembly by providing enough interaction strength between the guest molecules. However, PLLA does not possess sites for ionic bonding. Therefore, the interaction between PLLA and the first layer molecule (SA in the case of PLLA-SA-CS-PA) is brought about by hydrogen bonding, as shown in Figure 4.1. Different aerogel samples were prepared in this study and the corresponding densities are provided in Table 4.1. After the modification process, the densities of all the aerogels increased, which is a direct evidence of the successful incorporation of biobased molecules into the PLLA gel during the solvent exchange. It has to be noted that there was slight volume shrinkage to the PLLA gels during the solvent exchange, and the extent of shrinkage increased with each immersion step. This is attributed to the osmotic pressure of the exchange media and the resultant capillary forces.[19] However, there was no shrinkage to the hydrogels during the freeze-drying, which is a clear indication of the fact that the 3D solid framework of the gels did not lose the mechanical strength even after the modification. Among the prepared aerogels, PLLA-SA-CS-PA aerogel exhibited the highest density, i.e., greater fractions of guest molecules got loaded into the PLLA-SA-CS-PA gel during the solvent exchange. The key to the effective incorporation of guest molecules into the PLLA gel is the interaction between PLLA and the first layer (SA in this case). In all other samples, either CS or PA interacts with PLLA. Looking at the densities, we have to infer that the hydrogen bonding interactions between PLLA and SA are much more effective than that between PLLA and CS/PA in the gels. As the PLLA-CS or PLLA-PA interactions are weaker, less amounts of CS or PA are getting integrated into the PLLA structure, allowing lesser electrostatic interaction sites for the subsequent molecular assembly.
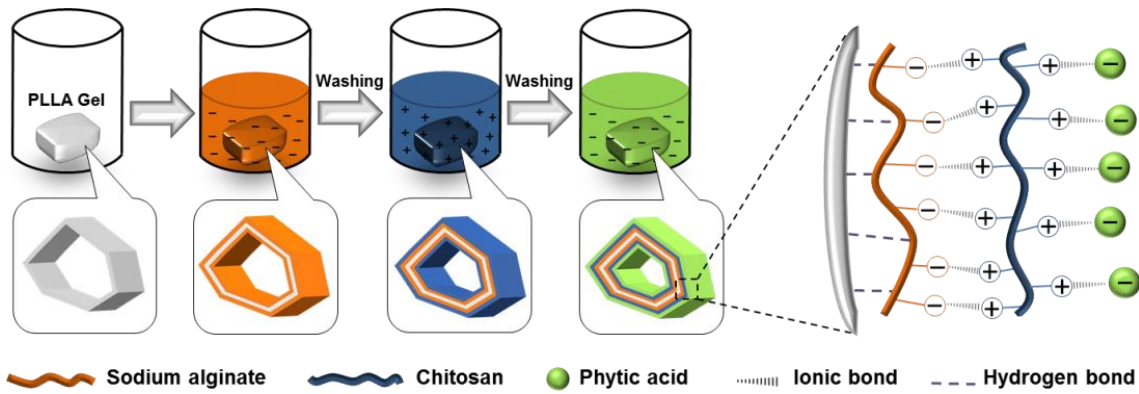
Figure 4.1. Schematic illustration of LbL assembly of SA, CS, and PA onto the PLLA thermoreversible gel brought about by modified solvent exchange method (the possible interactions between various molecules are also shown).

Table 4.1. Density and water contact angle of various aerogels prepared in this study.

Samples	Density (g cm^{-3})	Water Contact Angle (°)
PLLA	0.08	130 ± 2
PLLA-CS-PA-CS	0.10	108 ± 2
PLLA-CS-SA-CS	0.09	123 ± 2
PLLA-PA-CS-SA	0.09	106 ± 2
PLLA-SA-CS-PA	0.13	99 ± 2

The morphologies of neat and modified PLLA aerogels are shown in the SEM images (Figure 4.2) and the corresponding insets show their photographic images. Figure 4.2a shows the typical interconnected fibrillar network morphology of neat PLLA aerogel. Such morphology is retained in PLLA aerogels even after the incorporation of guest molecules (Figure 4.2(b-e)). The fibers were smooth in the neat PLLA aerogel, whereas, the fiber surface developed a certain level of roughness after the modification. As shown in Figure 4.2e, the fibers became increasingly dense and the fiber thickness was maximum in the PLLA-SA-CS-PA aerogel. This further confirms the excellent PLLA-SA interactions and the successful LbL assembly of SA-CS-PA in PLLA aerogel. With the

introduction of hydrophilic moieties (SA, CS and PA) into the hydrophobic PLLA substrate (WCA ~ 132 ± 2°), however, the WCA of the aerogels got diminished (Table 4.1). PLLA-SA-CS-PA aerogel showed the lowest WCA among the prepared aerogels but was still hydrophobic in nature. The reduction in the hydrophobicity of PLLA aerogels is yet another evidence for effective LbL coatings.
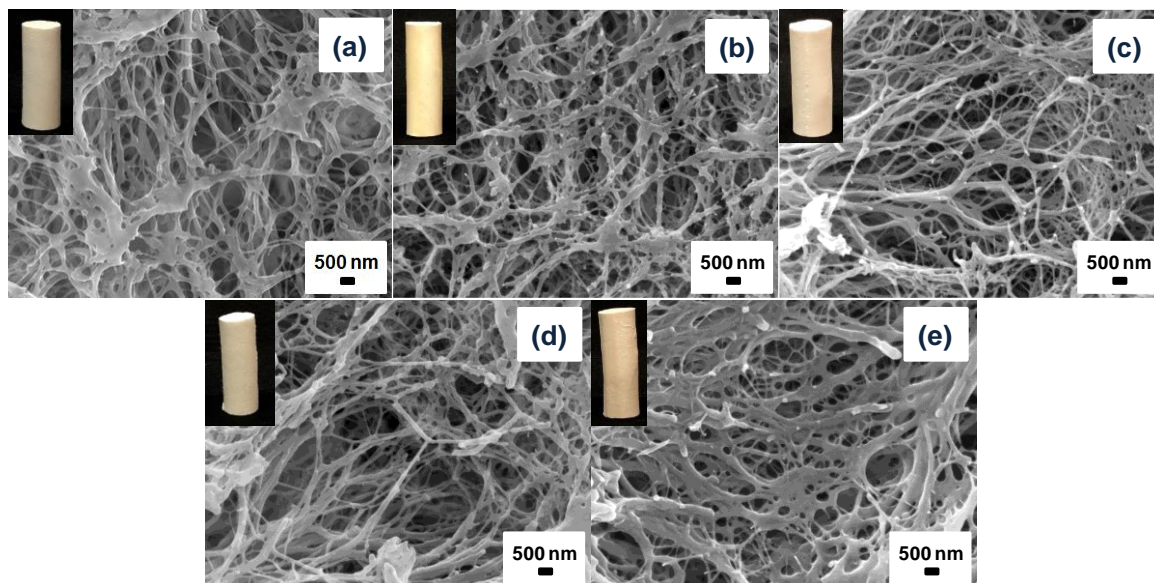
Figure 4.2. *SEM images of various aerogel samples. (a) PLLA, (b) PLLA-CS-PA-CS, (c) PLLA-CS-SA-CS, (d) PLLA-PA-CS-SA, and (e) PLLA-SA-CS-PA aerogels. Corresponding insets show the photographic images of the aerogels.*

In order to probe the elemental composition, energy dispersive spectroscopy (EDS) analysis of the aerogels was carried out. Figure 4.3 shows the ED spectra of neat PLLA and PLLA-SA-CS-PA aerogels and the corresponding data are given in the inset tables. Neat PLLA aerogel shows the characteristic bands of C and O only. Whereas, PLLA-SA-CS-PA aerogel exhibited bands corresponding to P and N, in addition to C and O bands. P and N contents were fairly high after the modification process, which can be really advantageous for flame retardancy.
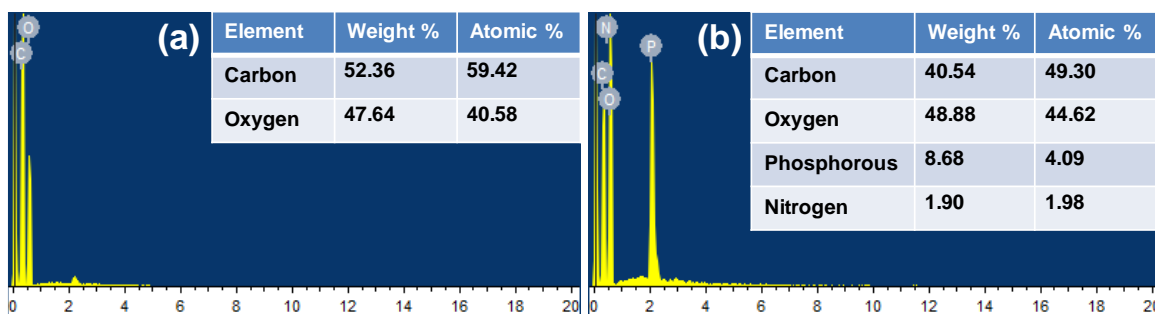
Figure 4.3. *EDS spectra of (a) PLLA and (b) PLLA-SA-CS-PA aerogels.*

The neat PLLA aerogel and the modified aerogels exhibited almost similar WAXD patterns with diffraction peaks only corresponding to PLLA crystal planes, as shown in Figure 4.4a. This is an indirect evidence for the homogeneous and uniform coating of guest molecules on the PLLA structure. Uneven coating or agglomeration of any of the ionic molecules would have resulted in other WAXD peaks corresponding to CS/SA/PA. The carbonyl stretching region in the FTIR spectra (Figure 4.4b) of the aerogels provides enough evidence for the effective hydrogen bonding interaction between PLLA and the first layer molecule. The absorption band corresponding to the C=O stretching lies at 1758 cm^{-1} in the case of neat PLLA aerogel. Whereas, after the LbL assembly, there is a red shift in the C=O stretching frequency in all the aerogels. This is particularly prominent in PLLA-SA-CS-PA aerogel, where the frequency shifted to 1755 cm^{-1}. The current observation validates our previous hypothesis that PLLA and SA possess strong interactive forces between them. As seen in Figure 4.4c, there is a new peak at 1650 cm^{-1} in the PLLA-SA-CS-PA aerogel, which corresponds to the carboxylate of SA and amide I of CS. Also, the peak at 489 cm^{-1} is characteristic of O-P-O bending. All these absorption bands provide further proof for the effective LbL assembly on the PLLA matrix.
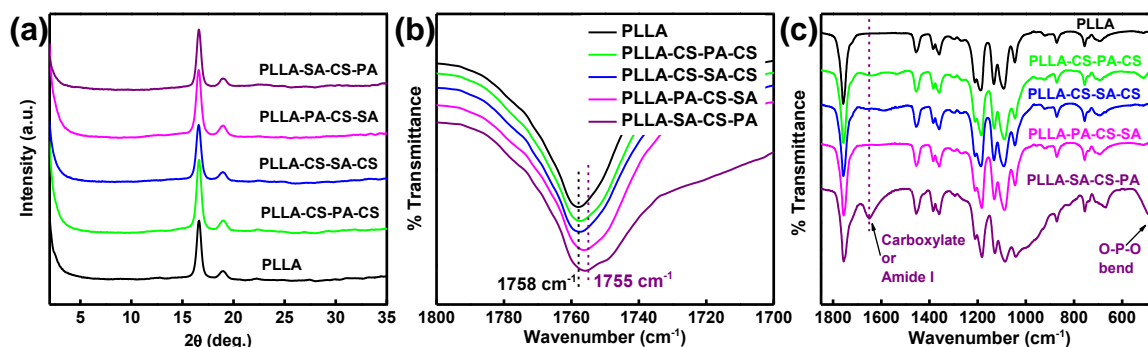
Figure 4.4. *(a) WAXD patterns of various aerogels. FTIR spectra of various aerogels in the (b) carbonyl frequency range, and (c) range of 400-1800 cm⁻¹.*

Thermal properties of all the aerogels were studied using TGA in the nitrogen atmosphere and the results are summarized in Table 4.2. The onset of degradation of neat PLLA aerogel is ~280 °C and it decomposes completely in a single step, as shown in Figure 4.5a. However, the modified aerogels undergo multistep degradation process, due to the different degradation behavior of their constituent components (Figure 4.5b). The initial weight loss below 100 °C corresponds to the removal of moisture absorbed by the incorporated hydrophilic molecules. Since PLLA-SA-CS-PA aerogel has a higher fraction of guest molecules loaded, it showed almost 10 % moisture loss. In PLLA-CS-SA-CS and PLLA-PA-CS-SA aerogels, CS catalyzed the early degradation of PLLA, which resulted in the significant reduction of their thermal stability ($T_{50\%}$). Char residues were also very low. But in the case of PLLA-SA-CS-PA aerogel, the PLLA backbone decomposition was slightly delayed. Good thermal stability (similar to neat PLLA aerogel) and high char yield were obtained for PLLA-SA-CS-PA aerogel; the latter is highly beneficial for flame retardancy.
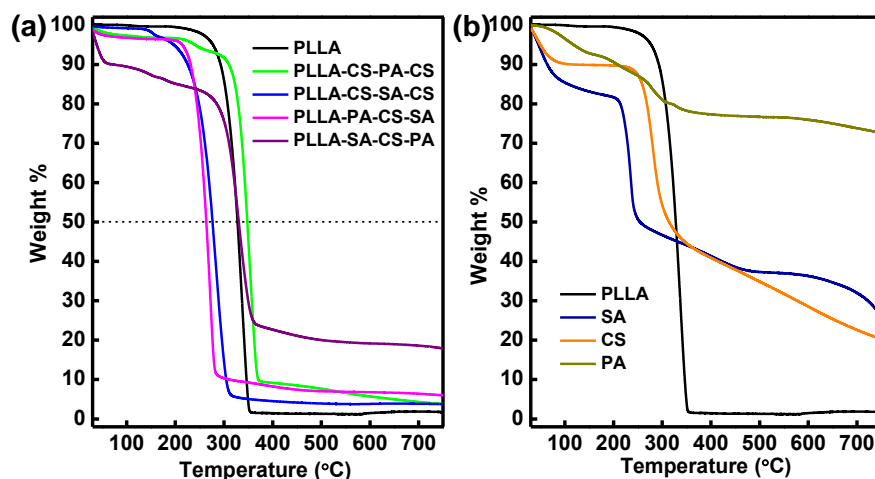
Figure 4.5. *TGA thermograms of (a) all the aerogels prepared in this study and (b) bulk PLLA, SA, CS and PA.*

Table 4.2. *Thermal properties of aerogels quantified from TGA.*

Samples	$T_{10\%}$ (°C)	$T_{50\%}$ (°C)	T_{max} (°C)	Residue (%)
PLLA	293	327	354	1
PLLA-CS-PA-CS	310	347	373	4
PLLA-CS-SA-CS	226	276	315	4
PLLA-PA-CS-SA	232	264	288	6
PLLA-SA-CS-PA	80	331	456	19

LOI measurements were performed for the preliminary understanding of the flammability characteristics of various aerogel samples. LOI is the minimum concentration of oxygen in the atmosphere that is required to sustain the combustion of a sample after ignition[24] and the LOI test results are provided in Table 4.3. Neat PLLA aerogel is highly flammable with LOI value of 18.8 ± 0.2 %. The solvent exchange induced LbL assembly of biobased molecules on PLLA has definitely modified the flammability properties of PLLA aerogels. The LOI values of PLLA aerogels increased after the modification process. As expected from the char residues, PLLA-SA-CS-PA aerogel recorded the highest value among all the aerogels. LOI as high as 32.6 ± 0.6 % was obtained, which is the highest value ever reported for a PLA based aerogel/foam. The

horizontal burning tests conducted on the aerogels are in good agreement with the LOI results. On exposure to a butane flame, neat PLLA aerogel caught fire immediately and burned vigorously with dripping of flammable particles, even after the removal of flame source (Figure 4.7a). But, the modified aerogels formed carbonaceous char layers at once on the point of contact of the flame. The carbonaceous char layer was particularly highly intense for PLLA-SA-CS-PA aerogel and the flame self-extinguished within no time (Figure 4.6a). The char layer formed acts as a protective layer by isolating the underlying PLLA from the flame and preventing the heat transfer, thus resulting in excellent flame retardancy. The strong interaction between PLLA and SA and the effective LbL assembly of SA, CS, and PA (induced by the electrostatic interactions) resulted in the high loading of P and N rich moieties in the PLLA-SA-CS-PA aerogel. CS and SA with polysaccharide rings and enormous hydroxyl groups act as char agents in the flame retardancy mechanism. The phosphate groups of PA enhance the carbonization capability of CS and SA and further reinforce the protective char layer. It is this synergy between SA, CS and PA which imparts anti-fire properties to the PLLA aerogel.

For the quantitative estimation of the flammability characteristics of the aerogels, MCC analysis was carried out. The important parameters obtained from this method are the heat release rate (HRR) and total heat release (THR), and their estimation is based on oxygen consumption during the burning process. HRR is the prime property to be considered in this context, since the rate at which heat is released by a material during burning can significantly contribute to the fire growth and its spreading.[25] Other parameters such as heat release capacity (HRC), peak heat release rate (PHRR), and time to peak heat release rate (TTPHRR) can also be obtained, which are listed in Table 4.3. Figure 4.6b shows the HRR curves of neat and modified PLLA aerogels as a function of temperature. As seen, the neat PLLA aerogel has a sharp HRR curve with a peak value of

472 W/g. In the case of modified aerogels, PHRR values reduced drastically and the HRR curves broadened. The best results were obtained for PLLA-SA-CS-PA aerogel; tremendous reduction in PHRR from 472 to 132 W/g, HRC from 492 to 144 J/gK, and THR from 18.4 to 6.6 kJ/g was observed, which is in good agreement with the LOI and UL94 test results. Thus, it has been proved that the strategy adopted in this work renders PLLA aerogels with excellent flame retardancy. This concept is not limited to just PLLA thermoreversible gels; it can also be applied to various other semicrystalline polymers for their flame retardant modification, provided they form thermoreversible gels in organic solvents.

Table 4.3. *Flammability parameters of aerogels estimated from LOI and MCC tests.*

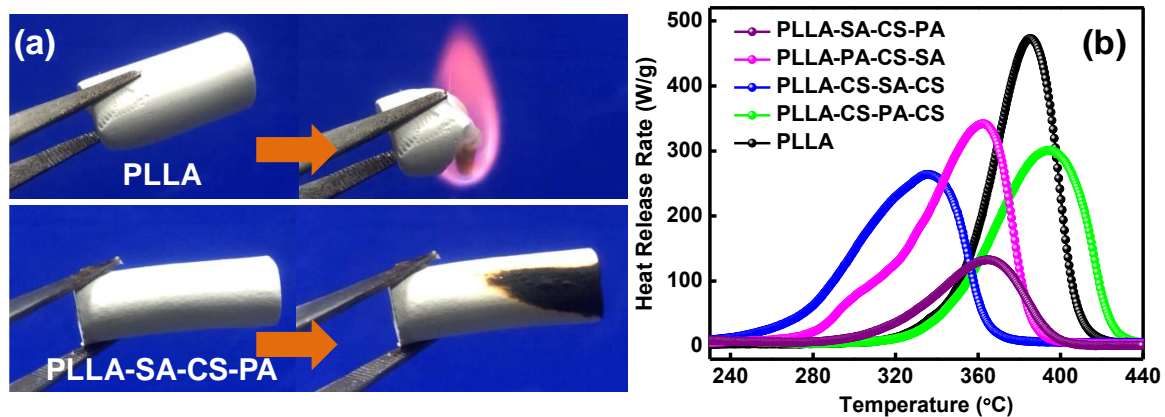| Samples	LOI (%)	PHRR (W/g)	TTPHRR (s)	THR (kJ/g)	HRC (J/gK)
PLLA	18.8 ± 0.2	472	366	18.4	492
PLLA-CS-PA-CS	24.0 ± 0.3	301	359	14.5	337
PLLA-CS-SA-CS	21.4 ± 0.4	264	321	15.6	306
PLLA-PA-CS-SA	23.4 ± 0.2	341	328	17.8	415
PLLA-SA-CS-PA	32.6 ± 0.6	132	328	6.6	144

Figure 4.6. *(a) Photographs showing the burning behavior of neat PLLA and PLLA-SA-CS-PA aerogels during the horizontal burning tests. (b) HRR curves of the aerogels as a function of temperature obtained from MCC tests.*

4.5. Conclusions

In summary, we developed a sustainable and novel strategy for the flame retardant modification of PLLA aerogels using biobased molecules by integrating solvent exchange and LbL assembly methods in one place. PLLA thermoreversible gels were solvent exchanged with aqueous solutions of SA, CS and PA step by step in different sequential orders and the resultant hydrogels were freeze-dried to obtain flame retardant aerogels. Here, the hydrogen bonding between PLLA and the guest molecules and the ionic interactions between the guest molecules play a crucial role in obtaining stable LbL coating. The biobased molecules got evenly coated over the fibrillar structures of the aerogels and high loadings were obtained. The guest molecules were rich in N and P and acted as char forming flame retardants to furnish excellent anti-fire properties to the aerogels. The PLLA-SA-CS-PA aerogel showed the highest flame retardancy with LOI as high as ~ 32 % and HRR as low as 132 W/g. These aerogels could self-extinguish the flame in less than a second. The whole process can be visualized as a general protocol for the modification of aerogels of semicrystalline polymers which are capable of forming thermoreversible gels in organic solvents. Therefore, it is possible to enhance the flame retardancy of PDLA, SC, PHB and even sPS aerogels using this method.

4.6. References

1. Zhao, X.; Guerrero, F. R.; Llorca, J.; Wang, D.-Y. New superefficiently flame-retardant bioplastic poly (lactic acid): flammability, thermal decomposition behavior, and tensile properties. *ACS Sustainable Chemistry & Engineering* **2016**, *4*, 202-209.
2. Zhang, S.; Jin, X.; Gu, X.; Chen, C.; Li, H.; Zhang, Z.; Sun, J. The preparation of fully bio-based flame retardant poly (lactic acid) composites containing casein. *Journal of Applied Polymer Science* **2018**, *135*, 46599.
3. Song, Y. P.; Wang, D. Y.; Wang, X. L.; Lin, L.; Wang, Y. Z. A method for simultaneously improving the flame retardancy and toughness of PLA. *Polymers for advanced technologies* **2011**, *22*, 2295-2301.
4. Xiao, L.; Mai, Y.; He, F.; Yu, L.; Zhang, L.; Tang, H.; Yang, G. Bio-based green composites with high performance from poly (lactic acid) and surface-modified microcrystalline cellulose. *Journal of Materials Chemistry* **2012**, *22*, 15732-15739.

5. Zhang, T.; Yan, H.; Shen, L.; Fang, Z.; Zhang, X.; Wang, J.; Zhang, B. Chitosan/phytic acid polyelectrolyte complex: a green and renewable intumescent flame retardant system for ethylene–vinyl acetate copolymer. *Industrial & Engineering Chemistry Research* **2014**, *53*, 19199-19207.

6. Rosely, C. S.; Joseph, A. M.; Leuteritz, A.; Gowd, E. B. Phytic acid modified boron nitride nanosheets as sustainable multifunctional nanofillers for enhanced properties of poly (l-lactide). *ACS Sustainable Chemistry & Engineering* **2020**, *8*, 1868-1878.

7. Lazar, S. T.; Kolibaba, T. J.; Grunlan, J. C. Flame-retardant surface treatments. *Nature Reviews Materials* **2020**, *5*, 259-275.

8. Wang, M.; Yin, G.-Z.; Yang, Y.; Fu, W.; Palencia, J. L. D.; Zhao, J.; Wang, N.; Jiang, Y.; Wang, D.-Y. Bio-based flame retardants to polymers: A review. *Advanced Industrial and Engineering Polymer Research* **2022**.

9. Xiong, Z.; Zhang, Y.; Du, X.; Song, P.; Fang, Z. Green and scalable fabrication of core–shell biobased flame retardants for reducing flammability of polylactic acid. *ACS Sustainable Chemistry & Engineering* **2019**, *7*, 8954-8963.

10. Zhang, Y.; Xiong, Z.; Ge, H.; Ni, L.; Zhang, T.; Huo, S.; Song, P.; Fang, Z. Core–shell bioderived flame retardants based on chitosan/alginate coated ammonia polyphosphate for enhancing flame retardancy of polylactic acid. *ACS Sustainable Chemistry & Engineering* **2020**, *8*, 6402-6412.

11. Chen, C.; Gu, X.; Jin, X.; Sun, J.; Zhang, S. The effect of chitosan on the flammability and thermal stability of polylactic acid/ammonium polyphosphate biocomposites. *Carbohydrate Polymers* **2017**, *157*, 1586-1593.

12. Xiao, Y.; Zheng, Y.; Wang, X.; Chen, Z.; Xu, Z. Preparation of a chitosan-based flame-retardant synergist and its application in flame-retardant polypropylene. *Journal of Applied Polymer Science* **2014**, *131*.

13. Krishnan, V. G.; Rosely, C. S.; Leuteritz, A.; Gowd, E. B. High-Strength, Flexible, Hydrophobic, Sound-Absorbing, and Flame-Retardant Poly (vinyl alcohol)/Polyelectrolyte Complex Aerogels. *ACS Applied Polymer Materials* **2022**, *4*, 5113-5124.

14. Lee, K. Y.; Mooney, D. J. Alginate: properties and biomedical applications. *Progress in polymer science* **2012**, *37*, 106-126.

15. Iler, R. Multilayers of colloidal particles. *Journal of colloid and interface science* **1966**, *21*, 569-594.

16. Kim, Y. S.; Harris, R.; Davis, R. Innovative approach to rapid growth of highly clay-filled coatings on porous polyurethane foam. *ACS Macro Letters* **2012**, *1*, 820-824.

17. Kim, Y. S.; Li, Y.-C.; Pitts, W. M.; Werrel, M.; Davis, R. D. Rapid growing clay coatings to reduce the fire threat of furniture. *ACS applied materials & interfaces* **2014**, *6*, 2146-2152.

18. Hai, Y.; Wang, C.; Jiang, S.; Liu, X. Layer-by-Layer assembly of aerogel and alginate toward self-extinguishing flexible polyurethane foam. *Industrial & Engineering Chemistry Research* **2019**, *59*, 475-483.

19. Kang, J.; Yun, S. I. Chitosan-reinforced PHB hydrogel and aerogel monoliths fabricated by phase separation with the solvent-exchange method. *Carbohydrate Polymers* **2022**, *284*, 119184.

20. Krishnan, V. G.; Praveena, N.; Raj, R. A.; Mohan, K.; Gowd, E. B. Thermoreversible Gels of Poly (l-lactide)/Poly (d-lactide) Blends: A Facile Route to Prepare Blend α-Form and Stereocomplex Aerogels. *ACS Applied Polymer Materials* **2023**.

21. Matsuda, Y.; Fukatsu, A.; Tasaka, S. Solvent exchange and gelation mechanism of poly (l-lactic acid) gel formed by complex crystallization with solvents. *Chemistry Letters* **2013**, *42*, 1046-1047.

22. Matsuda, Y.; Fukatsu, A.; Wang, Y.; Miyamoto, K.; Mays, J. W.; Tasaka, S. Fabrication and characterization of poly (l-lactic acid) gels induced by fibrous complex crystallization with solvents. *Polymer* **2014**, *55*, 4369-4378.

23. Matsuda, Y.; Miyamoto, K.; Ashizawa, H.; Fukui, T.; Tasaka, S. Elevation of flow temperature of poly (l-lactic acid) gel by controlling its morphology and crystal form. *Polymer Bulletin* **2017**, *74*, 4361-4370.

24. Benzarti, K.; Colin, X.: Understanding the durability of advanced fibre-reinforced polymer (FRP) composites for structural applications. In *Advanced Fibre-Reinforced Polymer (FRP) Composites for Structural Applications*; Elsevier, 2013; pp 361-439.

25. Mouritz, A.; Mathys, Z.; Gibson, A. Heat release of polymer composites in fire. *Composites Part A: Applied science and manufacturing* **2006**, *37*, 1040-1054.

High Strength, Flexible, Hydrophobic, Sound Absorbing and Flame Retardant Polyvinyl Alcohol/Polyelectrolyte Complex Aerogels
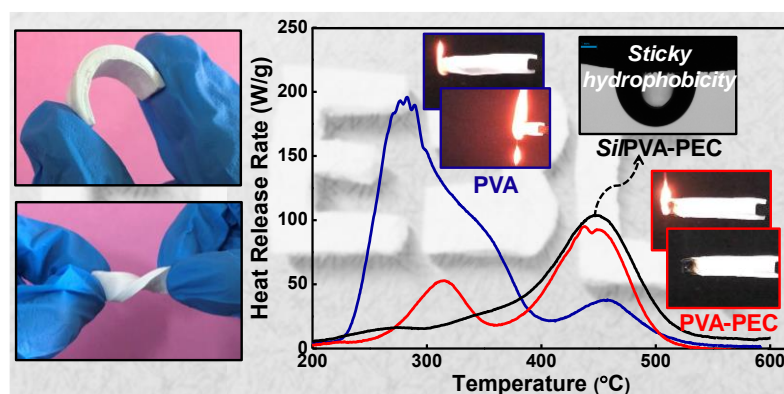
5.1. Abstract

The demand for sustainable materials has risen enormously in many applications due to the enhanced global awareness of environmental safety and protection. When it comes to structural and functional materials, tough and mechanically robust lightweight materials derived from renewable resources and/or by environmentally benign processes seem to be the way forward. Biodegradable aerogels with flexibility and high strength are attractive for construction, acoustic and thermal insulation, but are seriously plagued by their flammability. Improving the flame retardancy of these aerogels has been a hot topic of research and inorganic fillers and layered materials have been widely used for this purpose. However, the poor interfacial compatibility of these fillers has affected the processability and mechanical properties of the aerogels and reduced their overall performance. In this study, we have used a completely organic and sustainable polyelectrolyte complex (PEC) as filler for fabricating mechanically strong, sound absorbing and flame retardant polyvinyl alcohol (PVA) aerogels with the aid of an environmentally-friendly freeze-drying method. The non-covalent interactions between the polymer and filler ensured excellent compatibility as well as interfacial adhesion of the filler, and we could achieve a perfect balance between the density and mechanical properties of the aerogels. The prepared aerogels exhibited flexibility, good sound absorption ability in the mid-frequency range and excellent flame-retardancy (LOI ~ 28 %) with self-extinguishing behavior. A simple silane modification endowed sticky hydrophobicity to the aerogels and further enhanced their anti-fire properties. These sustainable multifunctional aerogels could find a plethora of applications in real life, particularly in buildings and structures as fire-safety materials and sound insulators.

5.2. Introduction

Biodegradable/biopolymer-based aerogels have growing demand in various fields of application such as thermal and acoustic insulation,[1-9] electronics,[10-14] etc., thanks to their superior mechanical properties over conventional inorganic aerogels and sustainability. Polyvinyl alcohol (PVA) is another commercially important and successful polymer, which is a formidable candidate for the preparation of aerogels owing to its low cost, high solubility in water and good mechanical properties. Its biodegradable, biocompatible and non-toxic nature makes it an even more versatile polymer. Environmentally-benign aerogels based on PVA have been developed in recent times using freeze-drying technology.[15-17] However, similar to many other organic polymers, the limiting factors of pristine PVA are the high flammability (LOI ~19.8 %) and super-hydrophilicity induced by its organic skeleton composed of plenty of hydroxyl groups, and this restricts the feasibility of PVA in many practical applications.

Extensive research has been done in improving the flame retardant properties of PVA aerogels, especially by incorporating inorganic fillers like clay, ammonium polyphosphate (APP), etc., into the polymer matrix to fabricate organic/inorganic composite aerogels.[17-20] Schiraldi and co-workers have developed a series of additives for PVA aerogels to improve flame retardant and other properties.[21-24] For example, APP modified with piperazine was used as an intumescent flame retardant in the PVA-montmorillonite aerogel system to demonstrate the improved flame retardancy.[25] The same group introduced another approach towards the development of flame retardant aerogels by growing a conformal silica coating onto the PVA aerogel. Further, they did a fluorocarbon silane treatment, which furnished durable superhydrophobic aerogels.[26] The synergistic effect of two-dimensional layered nanomaterials such as α-zirconium phosphate, MXene and boron nitride nanosheets with APP was well utilized to enhance

the fire safety of PVA aerogels.[27-29] However, the poor interfacial compatibility of inorganic additives often leads to poor mechanical properties and durability. In addition, high loadings of inorganic additives to achieve the satisfactory flame retardancy of PVA can negatively affect aerogel formation. Due to these reasons, reactive flame retardants attracted the attention of researchers as they preserve the mechanical properties of polymer aerogels and afford satisfactory flame retardancy. Shang et al. fabricated flame retardant PVA aerogels with high mechanical and dimensional stability without the aid of any inorganic species by chemical cross-linking with melamine-formaldehyde.[30] But the potential toxicity of melamine and formaldehyde can cause danger to humans as well as the environment. Therefore, alternative materials or methods are vital for the preparation of sustainable and eco-friendly PVA-based aerogels with enhanced overall properties.

Recently, there have been reports on polyelectrolyte complexes (PECs) as flame retardant additives for polymers and their composites.[31-35] PECs are a family of multicomponent polymeric materials formed by the ionic interactions between oppositely charged polyions. Usually, water-soluble polycations and/or polyanions have been utilized for the synthesis of PECs without the aid of cross-linking agents or catalysts.[36-38] At the industrial scale, PECs are used as flocculants for wastewater treatment, dewatering agents in papermaking, additives in detergents and cosmetics, and binders in the pharmaceutical industry.[36, 37] Zhang et al. demonstrated the applicability of PEC on ethylene-vinyl acetate copolymer as a green intumescent flame retardant.[31] A water-soluble poly(allylamine)-polyphosphate PEC that can extinguish flame was coated onto polyester-cotton fabric by Grunlan and co-workers, and the resultant coating was wash durable.[39] In another work, flame-retardant epoxy resins were prepared using poly(diallyldimethylammonium) and polyphosphate PEC.[40] However, to the best of our

knowledge, PECs have never been applied to polymeric aerogel systems, albeit their huge potential to boost aerogel properties.

In this chapter, we fabricated PVA based aerogels that are strong, flame retardant, hydrophobic, flexible and sound-absorbing. Herein, we have blended biosourced PECs into the PVA matrix to prepare a fully organic flame retardant polymer aerogel. PEC is synthesized from chitosan (CS), a cationic biopolymer and phytic acid (PA), a phosphorus-rich anionic molecule obtained from bioresources. Abundant hydroxyl groups in PVA enable a strong interfacial adhesion of PECs through hydrogen bonding. Furthermore, the addition of PEC did not alter the low-density behavior of aerogels. The hybrid aerogels' microstructure, compression properties, thermal stability, and acoustic properties were characterized and compared with neat PVA aerogel. The highly hydrophilic aerogels are further converted into hydrophobic (water contact angle over 136°) using a commercial silane by a simple chemical vapor deposition (CVD). Before and after the hydrophobic modification, the aerogels were characterized for flammability using UL94, LOI and microscale combustion calorimetry (MCC), and the possible flame retardant mechanism was discussed. The aerogels prepared in this study can find applications as structural materials for buildings and as acoustic insulators.

5.3. Experimental Section

5.3.1. Materials

PVA (M_w ~ 89000-98000, 99% hydrolyzed), chitosan (low molecular weight, degree of deacetylation ≥ 75%), phytic acid sodium salt hydrate (from rice) and methyltrichlorosilane (99%) were purchased from Sigma-Aldrich Co. and used without further purification. Hydrochloric acid and citric acid (CA) were obtained from Rankem Chemicals and Merck India, respectively. Potassium carbonate (K_2CO_3) was provided by

Avra Synthesis Pvt. Ltd. Deionised (DI) water was used in the entire experimental process.

5.3.2. Preparation of PEC

PEC was prepared by slightly modifying a reported procedure.[31] Initially, 2 wt% solution of CS was prepared by dissolving 4.07 g of CS powder in 200 mL of DI water with the aid of 3 mL of 5M hydrochloric acid (HCl). The dissolution was done by stirring at room temperature for 2 h and the pH of the resultant CS solution was 1.2. Subsequently, excess PA solution (4 wt%) was also prepared in 200 mL of DI water by dissolving 8.3 g of phytic acid sodium salt hydrate at room temperature by mechanical stirring. The pH of the PA solution was adjusted to 1.5 using 5M HCl. Then, this solution was added dropwise to the CS solution with vigorous stirring to yield a white precipitate. After complete precipitation, the solution was stirred overnight and the precipitate was allowed to settle down. The white precipitate was then collected by filtration and washed several times with DI water before drying in the hot air oven first, followed by vacuum drying at 60 °C for 24 h. The dried precipitate, which was yellowish in color, was ground to a fine powder and stored in a vacuum desiccator for further use.

5.3.3. Preparation of PVA-PEC Aerogels

5 wt% PVA solutions were used for the preparation of PVA-based aerogels. In a typical preparation procedure, 1 g of PVA powder was dissolved in 15 mL of DI water by mechanical stirring at 90 °C for 2 h. The required amount of powder PEC was taken in a separate container with 5 mL of DI water and sonicated for 30 min. The PEC dispersion was added to the PVA solution with constant stirring, and subsequently, 0.2 g of CA was added to the PVA-PEC mixture. The stirring was continued for 2 h at 90 °C. Then, the homogeneous solution was transferred to a plastic mold and immediately frozen in a

liquid nitrogen bath. The frozen sample was subjected to freeze-drying to obtain the required aerogel. The sample was named as PVA-*x*PEC, where *x* stands for the weight % of PEC with respect to the total solid content of the sample. Composite aerogels containing 5, 10, 20 and 30 % of PEC were prepared and stored in a vacuum desiccator at room temperature for further use. A control sample was also prepared following the above procedure, without the addition of PEC (neat PVA aerogel) for the purpose of comparison.

5.3.4. Hydrophobic Surface Modification of PVA-PEC Aerogels

A chemical vapor deposition (CVD) technique was employed to modify the aerogel surfaces.[41] Briefly, a saturated solution of K_2CO_3 was kept open inside a desiccator for 12 h to absorb the moisture and maintain a constant relative humidity. Later, another open vial with 1 mL of methyltrichlorosilane was introduced into the desiccator along with the aerogel samples. The desiccator was sealed and kept in the hot air oven at 50 °C for 24 h, when silanization occurred. The silanized aerogels were then placed in a vacuum oven at 50 °C for 24 h to remove the residual silane and HCl and stored in a vacuum desiccator for further characterization. The surface-modified samples were named as *Sil*PVA-*x*PEC.

5.3.5. Characterization

The apparent density of various aerogel samples was determined theoretically from their mass/volume ratio. The elemental composition of powder PEC and monolithic aerogels was obtained using PHI 5000 Versa Probe-II Focus X-ray photoelectron spectroscope (XPS) (purchased from ULVAC-PHI Inc., USA) equipped with microfocused (200 μm, 15 kV) monochromatic Al−Kα X-ray source (hν = 1486.6 eV). Fourier transform infrared (FTIR) analysis was performed using a PerkinElmer Series

FT-IR Spectrum Two machine at a resolution of 4 cm^{-1} and 32 scans in the wavenumber range of 4000-400 cm^{-1}. Wide-angle X-ray diffraction (WAXD) patterns of the aerogels were acquired using XEUSS SAXS/WAXS system from Xenocs operated at 50 kV and 0.60 mA in the transmission mode using Cu Kα radiation (λ = 1.54 Å). Mar 345 image plate system detected the 2D-patterns and the Fit2D software was used for data processing. Differential scanning calorimetry (DSC) measurements were conducted with an advanced research-grade modulated differential scanning calorimeter TA Q2000 under nitrogen gas flow. The samples were heated from room temperature to 250 °C at a rate of 10 °C/min and then cooled back to room temperature at the same rate. Compression tests were carried out on cylindrical aerogel samples (2:1 diameter to height ratio) in order to evaluate their mechanical performance. Universal Testing Machine (Hounsfield, H5KS UTM, Redhill, UK) with a crosshead speed of 1.5 mm/min was used for the same. Thermal stability and thermal degradation behavior of all the PVA-based aerogels were monitored using a thermogravimetric analyzer (TGA) TA Q50. The samples were heated from room temperature to 600 °C at a rate of 10 °C/min under nitrogen atmosphere. The acoustic performance of the prepared aerogels was evaluated by measuring the normal incident sound absorption coefficients using a Brüel & Kjær impedance tube, type 4206 (Denmark). Cylindrical samples with a diameter ~29 mm and thickness ~15 mm were measured in the frequency band from 300 to 6400 Hz via the two-microphone method. In order to study the wetting behavior of the aerogels before and after the silane treatment, water contact angles (WCA) of the samples were measured at room temperature using an automated DSA30 Drop Shape Analyzer, KRŰSS, Germany. For the preliminary analysis of the flammability properties of the aerogels, horizontal burning tests were conducted under laboratory conditions using a Bunsen burner with a butane flame. LOI was measured for the aerogels using a Critical Oxygen Index Apparatus (as per ASTM

D2863-08, ISO 4589) from Spectrum Automation and Controls coupled with Servomex Servoflex MiniMP (United Kingdom), a high-performance oxygen gas analyzer. The microscale combustion calorimetry (MCC) (MCC-1 (FTT)) was performed for the further analysis of the flame retardant properties of the aerogels. Milligrams of the sample were heated to 700 °C at a heating rate of 1 °C/s in a stream of nitrogen (80 cm^3/min). The resulting volatile anaerobic thermal degradation products are mixed with 80 cm^3/min carrying gas (nitrogen of 80 mL/min; oxygen of 20 mL/min) and subsequently burned at 900 °C in a combustion furnace.

5.4. Results and Discussion

5.4.1. Fully Organic Flame Retardant Fillers

Popular halogen-based fillers in flame retardancy are being abandoned across the globe for the adverse environmental impacts they have generated in recent times. Clays and many other inorganic materials have been successfully employed as eco-friendly alternatives to halogenated anti-fire fillers.[4, 18, 20, 27] However, a completely organic filler material has not gained much attention, particularly for aerogels, probably due to their lower efficiency than their inorganic counterparts. Herein, the electrostatic and hydrogen bonding interactions between CS and PA have been utilized to prepare a green water insoluble additive, with the ultimate aim of fabricating polymer aerogels with enhanced properties. CS with abundance of polarizable primary amino groups can effectively interact with the phosphate groups of PA to form stable complexes. These complexes can be considered as polyelectrolyte complexes and the schematic illustration of their formation is given in Figure 5.1a. Briefly, to the freshly prepared aqueous acidic CS solution, excess of PA sodium salt hydrate solution in water was added and immediate precipitation occurred, as shown in Figure 5.1b. The as-obtained white precipitate was

filtered, washed, vacuum dried and ground to obtain a fine powder with pale yellow color

(Figure 5.1b) and the PA/CS weight ratio in this complex is approximately 0.86:1.
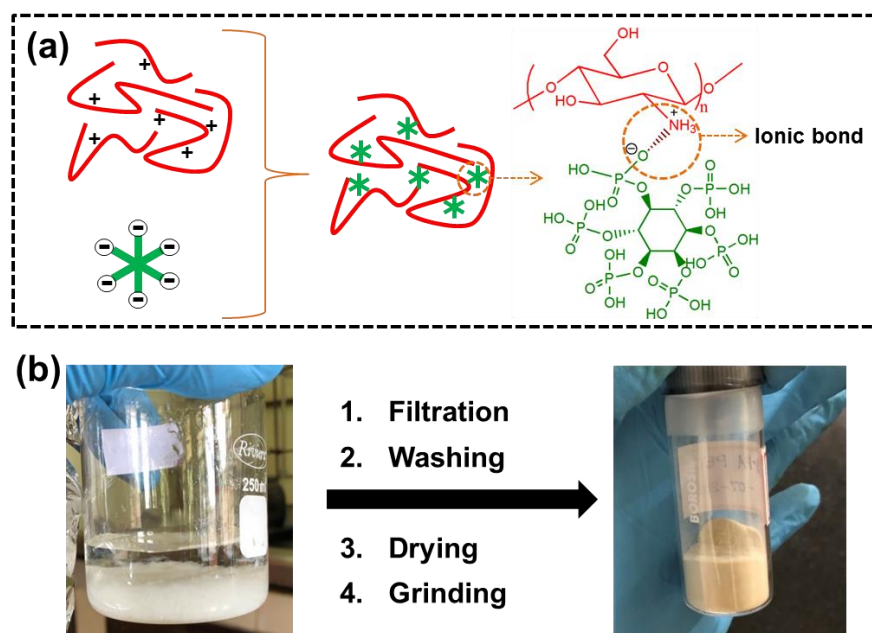
Figure 5.1. (a) Schematic illustration of the formation of PEC from CS and PA. (b) Photographic images showing the precipitated (white) PEC and the PEC powder (pale yellow) after the filtration, washing, drying and grinding processes.

The prepared PEC consists of carbon, oxygen, nitrogen and phosphorus elements, whose approximate elemental composition was obtained from X-ray photoelectron spectroscopy (XPS), as shown in the survey spectrum in Figure 5.2a. The percentages of C, O, N and P elements in the PEC are approximately 48.4, 42.5, 4.9 and 4.2, respectively. The successful ionic complexation reaction between CS and PA is confirmed using FTIR analysis and the corresponding spectra are given in Figure 5.2b. CS shows characteristic absorption bands approximately at 1650 (C=O stretching (amide I)), 1589 (N-H bending of primary amine) and 1560 (N-H bending (amide II)) cm^{-1} and PA has peaks at 1645 (O-P-O stretching) and 1185 (P=O stretching) cm^{-1}. However, in PEC, a new band appeared in place of the N-H bending peak at 1530 cm^{-1}, which is ascribed to the protonated NH$_2$ group (NH$_3^+$) of CS in the presence of acid. Similarly, the

band at 1042 cm^{-1} in PEC corresponds to the stretching mode of $(PO_3)^{2-}$. Thus, the oppositely charged functional groups can easily interact via ionic bonds in the organic complex. Further confirmation of the interactions is obtained from high-resolution XPS spectra and WAXD patterns given in Figures 5.2c and 5.2d, respectively. The bonds corresponding to each peak in the XPS high-resolution C1s, O1s, N1s and P2p spectra of PEC are well labelled in Figure 5.2c. The N1s spectrum was deconvoluted into two peaks: 397.8 and 399.8 eV, corresponding to C-N and NH_3^+ bonds, respectively. Also, the deconvolution of P2p spectrum shows peaks corresponding to P=O and P-O/$(PO_3)^{2-}$ bonds at 129.6 and 131.9 eV, respectively. The WAXD patterns (Figure 5.2d) show an amorphous structure for PA with a broad peak between 15 - 35° and a semicrystalline structure for CS with a sharp diffraction peak around 20°. The intensity of the crystalline peak of CS reduced significantly in the PEC, which indicates the reduction in the degree of crystallinity. Such a situation has arisen because of the interaction of PA with CS, which resulted in the breakage of intramolecular hydrogen bonding interactions between NH_2 and OH groups of CS.[31]

Figure 5.2e shows the TGA thermograms of CS, PA and PEC under a nitrogen atmosphere. The weight loss below 100 °C is due to the removal of the absorbed water. PEC undergoes early degradation, about 60 °C earlier than CS and this phenomenon in PEC is catalyzed by PA. Similarly, the maximum degradation temperature is also lower in the case of PEC. However, the thermal degradation of PEC yields significantly higher char residue than CS. At 600 °C, the residual char yield for CS is 32 wt%, whereas it is 49 wt% for the PEC. The carbonization of CS got enhanced in the presence of PA, which is advantageous when it comes to fire safety applications. Integrating a carbon-nitrogen source like CS and a phosphorus-rich PA into a complex material could effectively function as flame retardant additives for polymers.
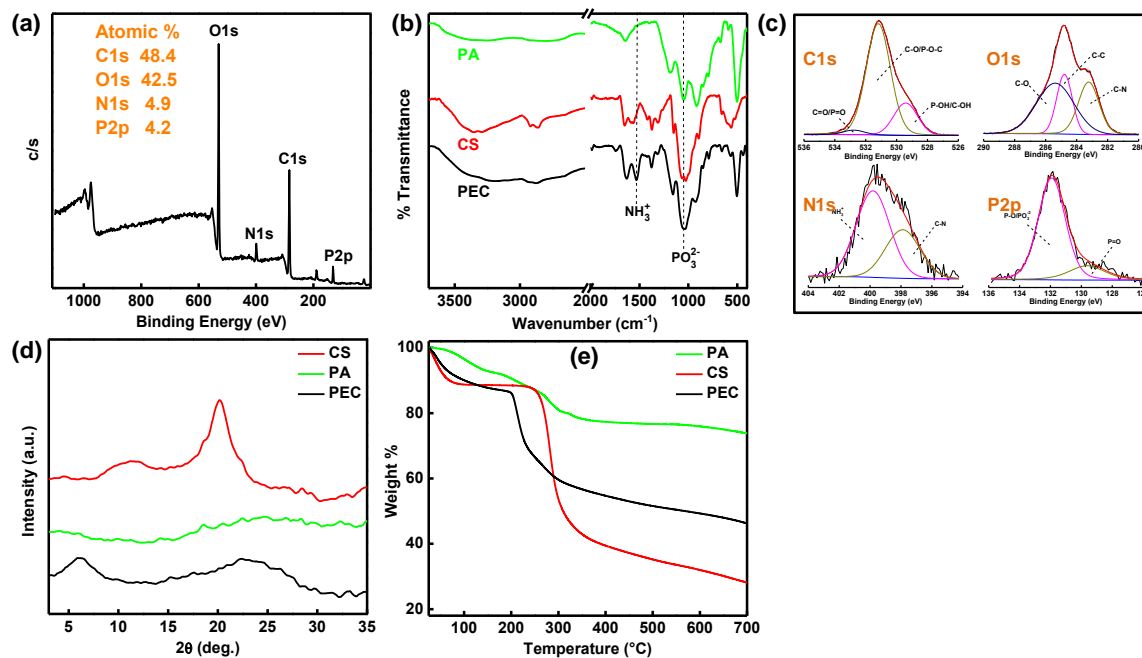
Figure 5.2. *(a) XPS survey spectrum of PEC (inset shows the atomic % of various elements of PEC). (b) FTIR spectra of PA, CS and PEC. (c) XPS high-resolution C1s, O1s, N1s and P2p spectra of the PEC. The bonds corresponding to each peak are labelled here. (d) WAXD patterns obtained for CS, PA and PEC. (e) TGA thermograms under nitrogen atmosphere of PA, CS and PEC.*

5.4.2. PEC Incorporated Polymer Aerogels

As mentioned in the Experimental Section, PVA aerogels were prepared with different weight loadings of PEC, i.e., 5, 10, 20 and 30 wt% and a neat PVA aerogel (without the addition of PEC) was also prepared for comparison. PVA is biodegradable by nature and the entire synthesis (of both PEC and aerogel) was carried out in the water as the only medium, making the whole process and the end-product environmentally-friendly. The availability of plenty of reactive hydroxyl groups across the PVA surface allows for the esterification between PVA and CA to form crosslinks between the polymer chains.[42] Sometimes, CA can react with the hydroxyl groups of PEC to form crosslinks between PVA and PEC, but the probability of such an interaction is minimum.

However, strong hydrogen bonding interactions are possible between PVA and PEC in the water medium. The PVA-PEC hydrogels stabilized by both covalent as well as non-covalent interactions were freeze-dried to remove the solvent and Figure 5.3 illustrates the entire scheme of aerogel formation.
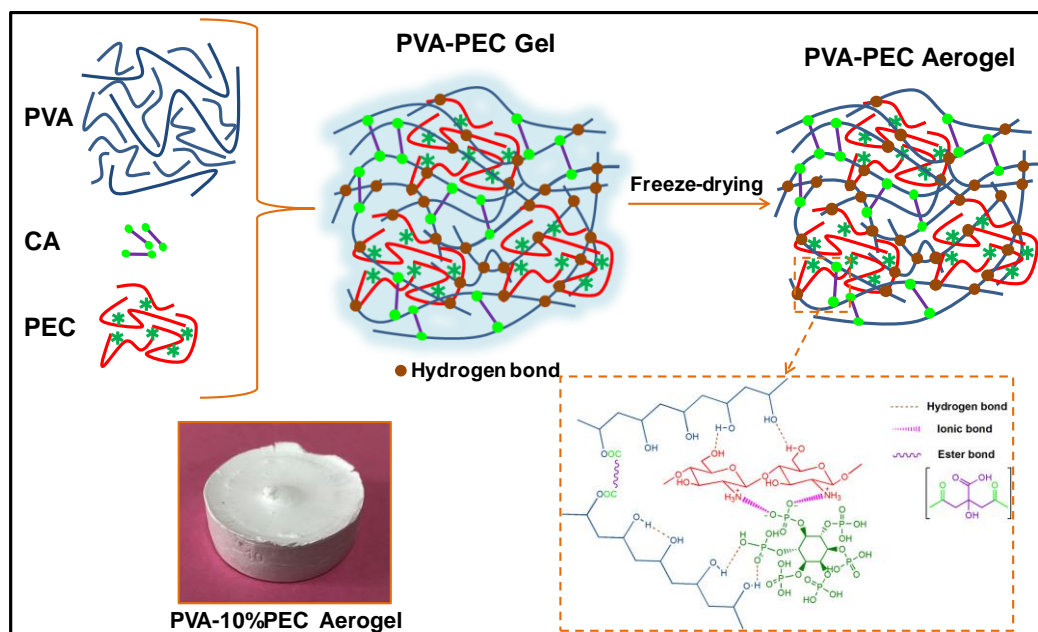
Figure 5.3. *Schematic illustration of the formation of PVA-PEC aerogels along with the photographic image of PVA-10%PEC aerogel.*

The successful incorporation of PEC into the PVA matrix was further confirmed from the XPS survey spectrum, as shown in Figure 5.4a. The approximate elemental composition of neat PVA and PVA-30%PEC aerogels are C – 62.2 % & O – 37.8 % and C – 51.3 %, O – 44.3 %, N – 3.4 % & P – 1.0 %, respectively. Figure 5.4b shows the high-resolution C1s spectra of PVA-30%PEC and neat PVA aerogels. The intensity of the C-C band decreased and that of the C-O band increased in the PVA-30%PEC aerogel when compared with neat PVA aerogel. The addition of PEC to the polymer matrix brought more oxygen containing moieties to the system and therefore, the oxygen content in the PVA-PEC aerogel increased. Also, the peaks shifted to lower binding energies, i.e., from 284.6 to 283.3 eV for the C-C bond and 286.1 to 284.8 eV for the C-O bond

indicating the reduction in bond strengths, which is evidence for PVA-PEC interactions.

A similar observation was made in the case of high-resolution O1s spectra also (Figure

5.4c). PEC dispersion in the aerogel is so excellent that clear peaks were obtained for

PVA-30%PEC aerogel in the high-resolution N1s and P2p spectra (Figure 5.4d). WAXD

patterns in Figure 5.4e further exemplify the compatibility between PVA and PEC. The

X-ray diffraction peak corresponding to the PEC at lower 2θ (~ 5°) is not visible in the

WAXD patterns of PVA-PEC aerogels till 20 wt% loading. However, at 30 wt% PEC

loading, the lower angle peak (~ 5°) started to come up in the aerogel, which is an

indication of the aggregation of PEC. Hence, we can conclude that even at high loadings

of PEC, excellent miscibility between PVA and PEC was achieved.
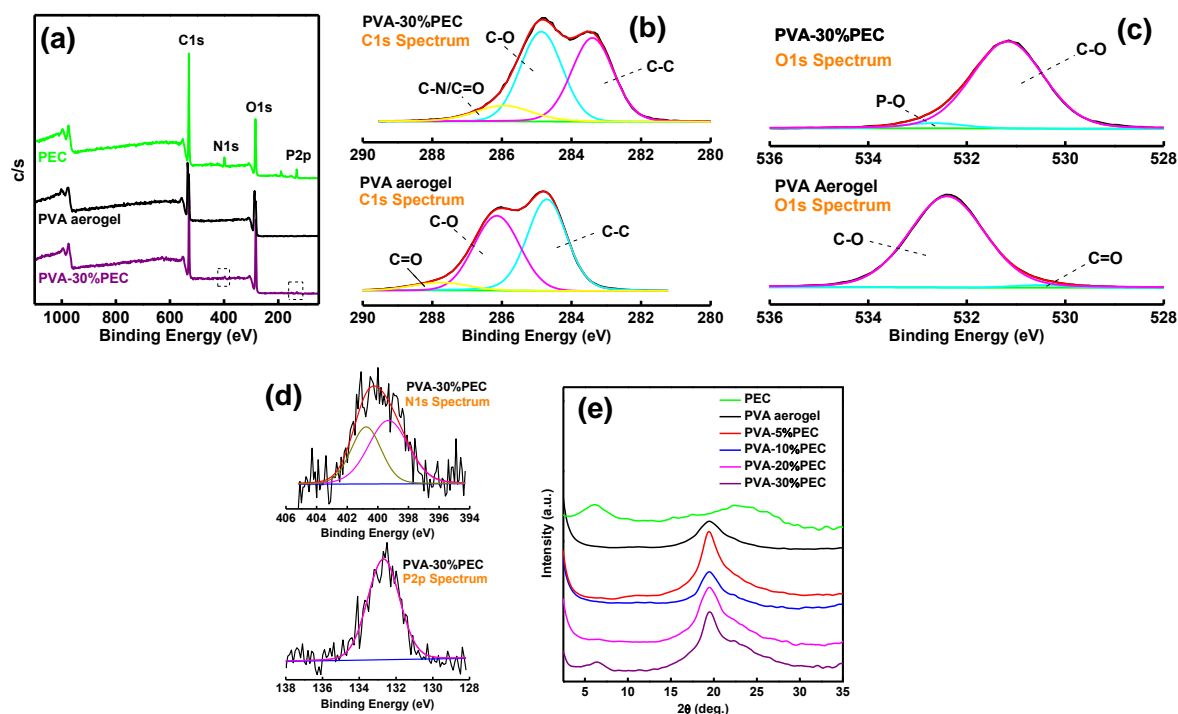
Figure 5.4. *XPS (a) survey spectra, (b) high-resolution C1s spectra, (c) high-resolution*

O1s spectra and (d) high-resolution N1s and P2p spectra of PEC, PVA aerogel and PVA-

30%PEC aerogels. (e) WAXD patterns of PEC, pure PVA aerogel and PVA-PEC

aerogels.

FTIR spectra of neat PVA and PVA-20%PEC aerogels have been compared in Figures 5.5a and 5.5b. The peak at 1716 cm^{-1} confirms the successful esterification between PVA and CA as this peak can be assigned to the carbonyl of –COO– group.[42] The intensity of the 1716 cm^{-1} peak is low in the PVA-PEC aerogel due to the presence of other reactive organic moieties, which further confirms the abovementioned point. There are possibilities for the reactive amino groups in CS to form amide linkages with CA, but the intense peak at 1540 cm^{-1} in PVA-20%PEC aerogel corresponding to the NH$_3^+$ group ensures that such a linkage is not present in the PVA-PEC system. The peak at 1032 cm^{-1} corresponding to the (PO$_3$)$^{2-}$ stretching confirms the ionic complexation between CS and PA even in the PVA-PEC aerogel. The IR absorption band at 1635 cm^{-1} is a combination of carbonyl (Amide I) and O–P–O stretching vibrations of PEC and hence, is absent in PVA aerogel. The –C–O stretching peak (1091 cm^{-1}) of PVA has been shifted to a lower wavenumber, i.e., 1065 cm^{-1} in PVA-PEC aerogel, which may be due to the hydrogen bonds formed between the free hydroxyl groups of PVA and PEC.
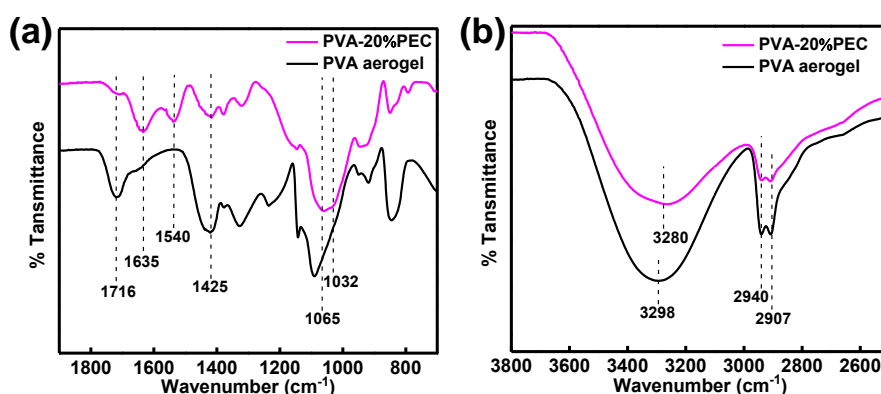
Figure 5.5. *FTIR spectra of PVA and PVA-20%PEC aerogels in the range of (a) 700-1900 cm^{-1} and (b) 2500–3800 cm^{-1}.*

In Figure 5.5b, the PVA aerogel shows a single broad absorption band at around 3298 cm^{-1} and this peak is assigned to the hydroxyl stretching vibration. Whereas in the case of PVA-20%PEC, this peak has shifted to 3280 cm^{-1} pertaining to the enhanced

hydrogen bonding interaction between PVA and PEC. The decrease in the intensity of –

CH_2 asymmetric (2940 cm^{-1}) and symmetric (2907 cm^{-1}) stretching vibrations in PVA-

PEC aerogel also confirms the successful incorporation of PEC into the PVA matrix.

Figures 5.6a & 5.6b show the DSC first heating and cooling curves, respectively, of neat

PVA and PVA-PEC aerogels with different PEC loadings. In the first heating curves, the

broad endotherms around 80 °C are due to the evaporation of moisture absorbed by the

samples. The melting temperatures were more or less the same (~ 230 °C) for all the

samples. But it is worth mentioning here that, during cooling from the melt, neat PVA

aerogel undergoes crystallization at around 210 °C and such melt crystallizations were

absent in all other samples (PVA-PEC aerogels). With the addition of PEC to the PVA

matrix, PVA chains are unable to reorganize into crystallites due to the strong interactions

induced by the PEC. This observation also indicates the fact that crosslinking interactions

(covalent and non-covalent) are persisting within the PVA-PEC aerogels.
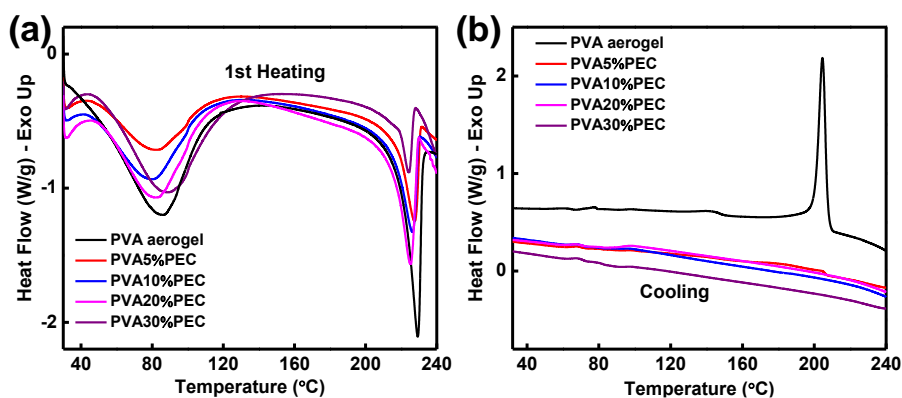
Figure 5.6. *DSC thermograms (a) first heating and (b) cooling curves of PVA aerogel and PVA-PEC aerogels with different PEC loadings.*

Aerogels were prepared using 5 wt% PVA solutions and the PEC loading was

calculated with respect to the dry weight of the polymer. All the aerogel samples

exhibited relatively low density ranging from 0.055 to 0.069 g/cm^3. The density of neat

PVA aerogel was 0.055 g/cm^3 and the addition of PEC resulted in only a slight increase

in density; for 20 wt% PEC loading, the density is ~0.06 g/cm^3. This indicates the lightweight nature of the prepared aerogels. Interestingly, these aerogels were highly flexible and could be made in or cut into any shape (Figure 5.7a). However, during compression experiments, these aerogels exhibited an irreversible buckling behavior and were converted to dense solids without any disintegration of the samples, similar to syndiotactic polystyrene aerogels.[9, 43] Figure 5.7b gives the compressive stress-strain curves for neat PVA and PVA-PEC aerogels and their deformation behavior is similar to that of a typical honey-comb like open-cell foam.[30] The compressive moduli of the samples were calculated from the slope of the linear elastic region of the stress-strain curves and are tabulated in Table 5.1. As observed in Figure 5.7b, the compressive strength of PVA aerogels is enhanced with the incorporation of PEC. The compression modulus increased to 1.55 MPa in PVA-20%PEC aerogel as compared to 0.45 MPa of neat PVA aerogel. This is mainly attributed to the strong interaction as well as the excellent miscibility between PVA and PEC in the aerogel system. However, on further increasing the PEC content (30 %), the compression modulus dropped down to 0.67 MPa, which may be due to the structural instability induced by the agglomeration of PEC particles, as indicated earlier in the WAXD pattern of PVA-30%PEC aerogel (Figure 5.4e). At 30 % PEC loading, the PVA concentration is not enough to uniformly bind the PEC particles within the matrix, which resulted in the agglomeration. Higher loadings of inorganic additives such as clay, silica, etc., can sometimes better enhance the compression strength of PVA-based aerogels, but at the expense of the low-density nature.[22, 26, 44] In this work, we could obtain an excellent balance between the density and mechanical strength of aerogels, which is not so easy to attain.
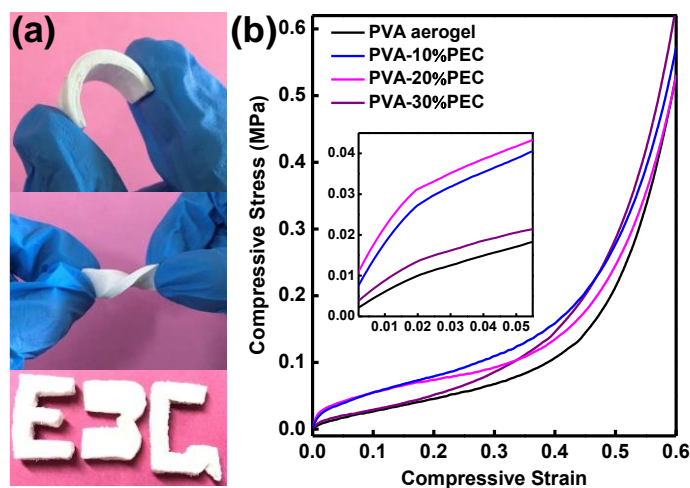
Figure 5.7. (a) Photographs showing the flexible nature of PVA-PEC aerogels and PVA-PEC aerogel prepared in the shape of alphabets. (b) Compressive stress-strain curves of PVA and PVA-PEC aerogels.

The surface morphologies of PVA and PVA-PEC aerogels with different PEC concentrations are shown in Figure 5.8. Figures 5.8a, 5.8b, 5.8c and 5.8d corresponds to PVA aerogel, PVA-10%PEC, PVA-20%PEC and PVA-30%PEC, respectively. The SEM images revealed that all the aerogels have a layered structure that accompanied the ice crystal growth direction. With the incorporation of PEC, the distance between the PVA layers has changed slightly and as shown in the magnified images, the pore size and distribution were also modified. The ice template method allows the polymer chains as well as the fillers to concentrate at the grain boundaries of the ice crystals[26] and therefore, the morphology remained more or less similar in all the samples and it could be assumed that PECs remain on the PVA layers. The neat PVA aerogel is extremely hydrophilic, thanks to the chemical structure of PVA with enormous surface OH functional groups and we could not measure the water contact angle (WCA) as the water droplets were not stable on the surface. Upon contact with the surface, the droplets were immediately absorbed by the PVA aerogel. Whereas, when PEC was introduced into the system, the

WCA of the aerogels improved slightly, as shown in the insets of Figure 5.8. The WCA values obtained for aerogels with 5, 10, 20 and 30 % PEC loadings were 27.2, 26.9, 29.4 and 27.1° (± 1.5°), respectively. This might be due to the reduction in the number of free surface hydroxyl groups on PVA-PEC aerogels in comparison with pure PVA aerogel because of the extensive hydrogen bonding interactions. All these aerogels are highly moisture sensitive and can absorb moisture from the surroundings. Therefore, the aerogels were stored in a desiccator for further characterization.
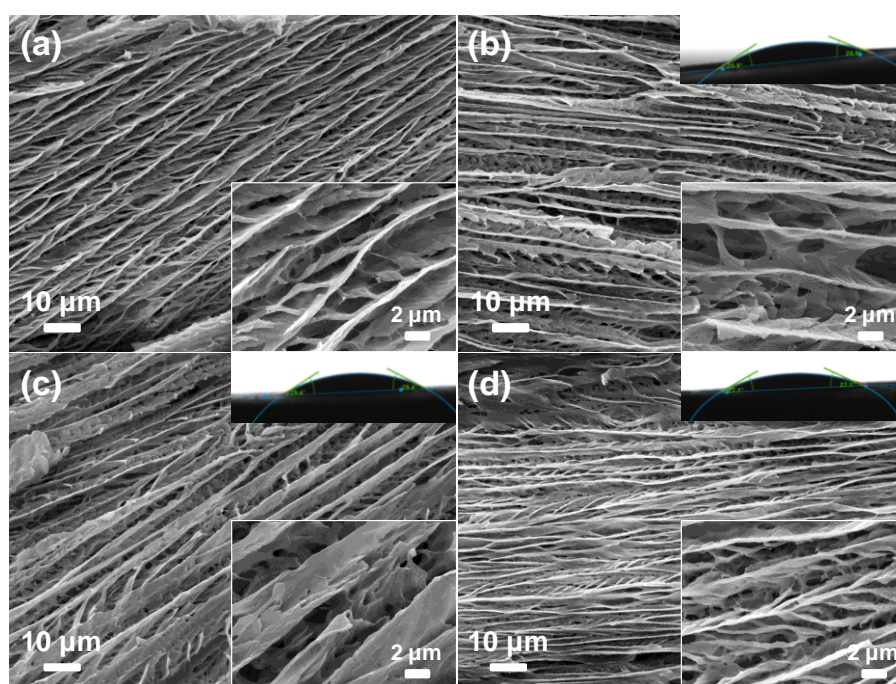
Figure 5.8. *SEM images of various aerogel samples. (a) PVA, (b) PVA-10%PEC, (c) PVA-20%PEC and (d) PVA-30%PEC aerogels. Corresponding insets show the magnified SEM images and images of the water droplets on the aerogel surfaces and their contact angles.*

The thermal degradation behavior and the thermal stability of PVA-PEC aerogels were investigated in nitrogen atmosphere using TGA and the results are given in Figure 5.9a and Table 5.1. $T_{10\%}$, $T_{50\%}$ and T_{max} are the temperatures at which 10 %, 50 % and

maximum weight loss occur, respectively. In all the samples, almost 10 % of the weight was lost below 100 °C due to the removal of the absorbed moisture, which indicates the moisture sensitivity of the prepared aerogels. Apart from the initial water loss, the degradation of neat PVA aerogel occurs in two stages, as shown by the two weight loss steps. The first step is the decomposition of the hydroxyl groups of PVA, which occurs in a temperature range of 220-350 °C. The polymer backbone decomposition takes place at the later stage, beyond 350 °C. However, in the case of PVA-PEC aerogels, PEC catalyzed the early degradation of PVA. The weight loss starting at ~ 200 °C in PVA-PEC aerogels is a combination of PEC decomposition and the PVA dehydroxylation catalyzed by the phosphorus containing moieties from PEC. After the incorporation of PEC, the thermal stability of the aerogels enhanced significantly, as evident from the $T_{50\%}$ values. $T_{50\%}$ increased from 281 °C for neat PVA aerogel to 348, 330, 331 and 381 °C for PVA-5%PEC, PVA-10%PEC, PVA-20%PEC and PVA-30%PEC aerogels, respectively, i.e., nearly 100 °C enhancement upon addition of 30% PEC. The char residue also increased with the increase in PEC content, from 4 % (neat PVA aerogel) to 33 % (PVA-30%PEC aerogel). This indicates the better char forming ability of PVA-PEC aerogels when compared with neat PVA aerogel at higher temperatures. Thus, we can conclude that the introduction of PEC (rich in N, P and C elements) into the PVA matrix can substantially enhance the thermal stability of the aerogels and induce greater carbonaceous char residues, which may act as a protective layer during the combustion of the aerogels.

The porous structure of PVA-based aerogels renders good sound absorption capability to them. In Figure 5.9b, the normal incident sound absorption coefficients of various aerogel samples are plotted as a function of frequency and all the samples exhibited good absorption coefficients in the mid-frequency range. Neat PVA aerogel

absorbed more than 80 % of the incident sound waves consistently between 2400-3100 Hz with a maximum of 94 % at around 2700 Hz. The incorporation of PEC did not alter the general absorption characteristic of the PVA aerogel, though slight differences are observable in the case of PVA-20%PEC and PVA-30%PEC aerogels. In PVA-30%PEC aerogel, the maximum absorption shifted slightly to the higher frequency side (3000-3500 Hz), whereas it shifted to lower frequencies for PVA-20%PEC aerogel. The curve of PVA-10%PEC aerogel is almost superimposed with that of neat PVA aerogel. The similarity in the morphology of neat PVA and PEC incorporated PVA aerogels (due to the ice templating) contributes to the similar trend in their sound absorption. The efficient absorption of sound waves in the mid-frequency range by these highly porous monoliths can be attributed to the tortuosity in the sound propagation path and multiple internal reflections at the cell walls generated by the highly porous network structure, which effectively attenuate the sound waves.[5, 6, 45]
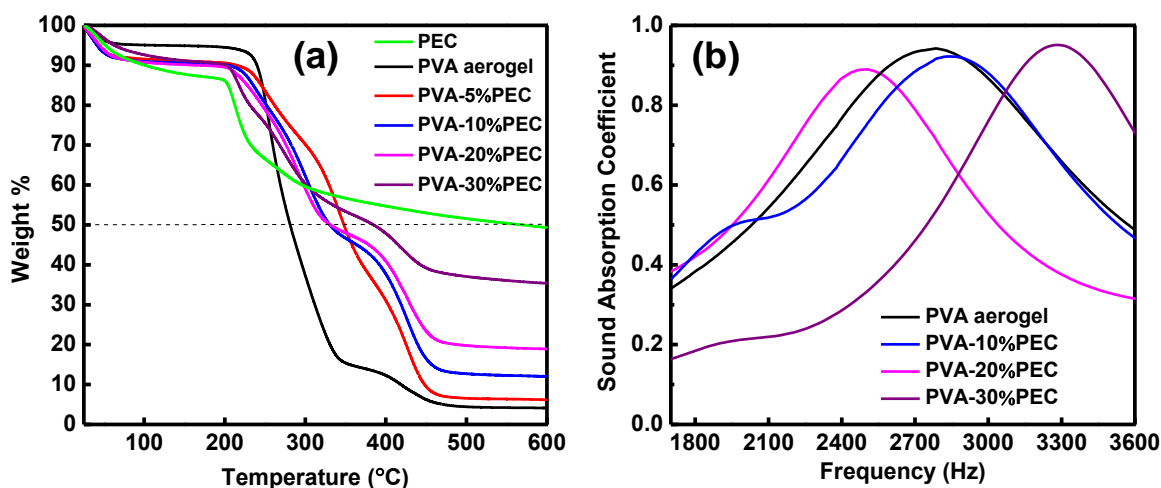
Figure 5.9. *(a) TGA thermograms of PVA and PVA-PEC aerogels obtained at a heating rate of 10 °C/min. (b) Normal incident sound absorption coefficients of PVA and PVA-PEC aerogels in the frequency range of 1700-3600 Hz.*

Table 5.1. *Mechanical and thermal properties of various aerogels prepared in this study.*

Samples	Density (g cm^{-3})	Compression Modulus (MPa)	$T_{10\%}$ (°C)	$T_{50\%}$ (°C)	T_{max} (°C)	Residue (%)
PVA aerogel	0.055	0.45	241	281	465	4
PVA-10%PEC	0.057	1.24	204	330	452	11
PVA-20%PEC	0.060	1.55	166	331	456	18
PVA-30%PEC	0.069	0.67	201	384	450	33

5.4.3. Combustion Behavior

Horizontal burning tests and limiting oxygen index (LOI) measurements were carried out for the preliminary estimation of the flame retardant behavior of the prepared aerogels. The results of LOI test are provided in Table 5.2. Figure 5.10 shows the results of the horizontal burning tests conducted on each sample. The LOI value obtained for neat PVA aerogel was ~ 19.6 % and it increased with the increase in PEC content in PVA-PEC aerogels; the maximum value obtained is ~ 28 % at 30% PEC loading. As shown in Figure 5.10, PVA aerogel readily catches fire (within 2 s) and continues to burn vigorously even after removing the flame source. In addition, it shows dripping of particles which are further inflammable and the 8 cm long sample completely burned down within 140 s leaving behind a black residue. PEC has definitely modified the flammability behavior of PVA aerogels. PVA-10%PEC aerogel took 12 s to catch fire on ignition with a butane flame and it was able to self-extinguish the fire in 100 s. Half of the sample was burned before the fire extinguishment and no melt dripping was observed. Flame retardancy of the aerogels got better and better with the increase of PEC content. The time taken to ignition for PVA-20%PEC aerogel was 15 s and the flame got extinguished itself in 15 s. The best result was obtained for PVA-30%PEC aerogel, for which the time to ignition was 32 s and the time to extinguish was 10 s. Hardly any

sample got burned, i.e., the sample remained intact and intense charring occurred at the point of contact with the flame, as shown in Figure 5.10.
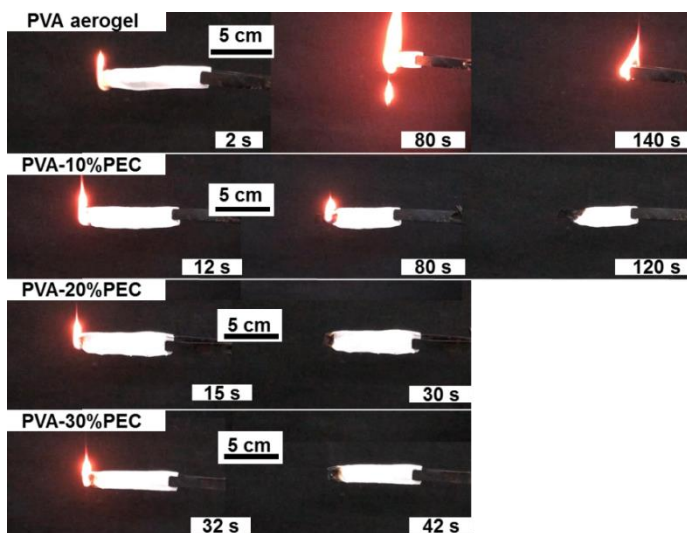
Figure 5.10. Photographs showing the burning behavior of PVA and PVA-PEC aerogels during the horizontal burning tests conducted using a butane flame. The images at different time during the burning process show the excellent flame retardant and self-extinguishing behavior of PVA-PEC aerogels.

For the quantitative estimation of the flammability characteristics of the aerogels, microscale combustion calorimetry (MCC) was used and the results are listed in Table 5.2. Figure 5.11 differentiates between the HRR curves of neat PVA and PVA-PEC aerogels, where HRR is plotted as a function of temperature. For neat PVA aerogel, the HRR value increases sharply after 200 °C and reaches its peak (195 W/g) at around 280 °C. Between 400-500 °C, another small peak was obtained, which indicates the multi-step thermal degradation of PVA aerogel. However, in PVA-PEC aerogels, there was a slight shift in the HRR curves towards the high-temperature side, which may be due to the enhanced thermal stability of PEC incorporated PVA aerogels. Also, the HRR values were significantly reduced in the PVA-PEC aerogels, particularly in the temperature range of 250-360 °C in comparison with the neat PVA aerogel. From 195 W/g of PVA

aerogel, the PHRR drastically decreased to 95 W/g for PVA-20%PEC, which is a clear indicator of the enhanced flame retardant properties after the addition of PEC to the PVA matrix. During the burning of PVA aerogel, plenty of hydrocarbon volatiles are released into the flame at the initial stage of degradation, i.e., during the decomposition of hydroxyl groups, which results in the generation of lots of heat.[46] But in the case of PVA-PEC aerogels, due to the action of PEC, flammable volatiles are least produced during the first stage (250-360 °C) of decomposition. This resulted in the lowering of the HRR of PVA-PEC aerogels initially. However, the peak values of HRR curves for PVA-PEC aerogels were obtained between 400-500 °C, which manifests the fact that maximum flammability and flashover potential of PVA-PEC aerogels were reached in the second step of degradation. Therefore, the TTPHRR values were increased from 270 s in PVA aerogels to 402, 416 and 423 s in PVA-10%PEC, PVA-20%PEC and PVA-30%PEC aerogels, respectively. The carbonaceous layer formed during the initial degradation step acts as a barrier to prevent the underlying material from burning. Thus, we can conclude that the results from MCC measurements support the results obtained by LOI measurements and horizontal burning tests (UL 94) and the PVA aerogels attained excellent flame retardancy in the presence of PEC.

Table 5.2. *Flame retardant parameters estimated from LOI and MCC tests and water contact angles of the aerogel samples prepared in this study.*

Sample	LOI (%)	PHRR (W/g)	TTPHRR (s)	THR (kJ/g)	HRC (J/gK)	WCA (°)
PVA aerogel	19.6 ± 0.3	195	270	19.67	295	---
PVA-10%PEC	22.1 ± 0.3	121	402	15.47	199	26.9 ± 1.5
PVA-20%PEC	25.6 ± 0.3	95	416	11.20	145	29.4 ± 1.5
PVA-30%PEC	27.9 ± 0.7	116	423	13.60	207	27.1 ± 1.5
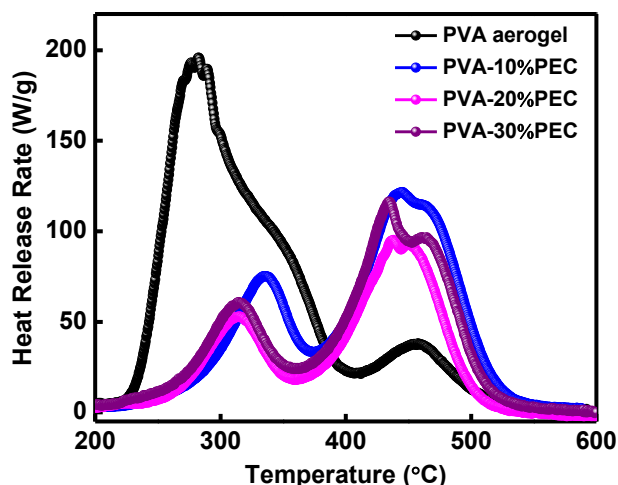
Figure 5.11. *Heat release rate versus temperature curves for PVA and PVA-PEC aerogels obtained by MCC test.*

5.4.4. Hydrophobic Surface Modification of Aerogels and Their Performance Comparison

The moisture sensitivity as well as the highly hydrophilic nature of PVA-based aerogels, is a hurdle for their practical usage. By engineering the surface chemistry of materials, hydrophobic or even superhydrophobic surfaces could be obtained. Following this concept, we performed a simple surface silanization using methyltrichlorosilane by thermal chemical vapor deposition (CVD) on the aerogels. After the silanization reaction in the presence of water, a hydrophobic silicone coating was formed over the aerogel surface.[41] CVD using silane is a well-known strategy for making hydrophobic surfaces.[16, 41, 47] Although methyltrichlorosilane was used for surface modification, no chlorine elements were introduced onto the surface modified aerogels. On coating the aerogels using hydrophobic methyl groups, as we have done here, the WCA enhanced significantly, as given in Table 5.3. All the aerogel samples became highly hydrophobic and the maximum value of WCA, i.e., 136.4 ± 1.5° was obtained for PVA-30%PEC aerogel, as shown in Figure 5.12a. Hereafter, the silane-modified aerogels will be denoted with *Sil* in front, for example, silanized PVA-30%PEC aerogel is denoted as *Sil*PVA-

30%PEC aerogel. The successful formation of silicone coating over the aerogel surfaces was confirmed using FTIR spectroscopy (Figure 5.12b). The peaks at 1269, 1028 and 775 cm^{-1}, respectively, correspond to C-Si-O, Si-O-C and Si-O-Si bonds. To our surprise, the aerogels after surface modification showed excellent water adhesion properties along with hydrophobicity. The water droplet did not fall down even after turning the aerogel surface upside down and Figure 5.12c demonstrates the water adhesion property of *Sil*PVA-30%PEC aerogel. Water droplet as big as 43 µL could be tightly pinned and suspended upside down from the aerogel surface (Figure 5.12d), which further illustrates the abovementioned property. Such a sticky hydrophobicity could possibly be because of the surface morphology of the coated aerogels, which shows numerous protrusions, micro wrinkles and folds, as shown in Figure 5.12e. As a result, the water droplets cannot directly contact the cellular surface of the aerogels but can penetrate into the pores to some extent and this leads to the Cassie impregnating wetting state.[48, 49] Thus, we can conclude that the micro-roughness of the surface, together with the low surface energy of the silicone coating, leads to the rose petal-like nature in surface modified aerogels. It was also observed that the compression strength measured for the surface-modified PVA-PEC aerogels was more or less the same as that of the unmodified aerogels (Figure 5.12f).

Table 5.3. *Flame retardant parameters estimated from LOI and MCC tests and water contact angles of the aerogel samples after the silane modification.*

Sample	LOI (%)	PHRR (W/g)	TTPHRR (s)	THR (kJ/g)	HRC (J/gK)	WCA (°)
*Sil*PVA aerogel	21.8 ± 0.4	139	361	14.67	205	126.5 ± 1.5
*Sil*PVA-10%PEC	24.6 ± 0.6	139	411	13.60	143	133.1 ± 1.5
*Sil*PVA-20%PEC	26.9 ± 0.4	140	404	12.53	134	134.2 ± 1.5
*Sil*PVA-30%PEC	31.2 ± 0.3	103	415	10.50	100	136.4 ± 1.5
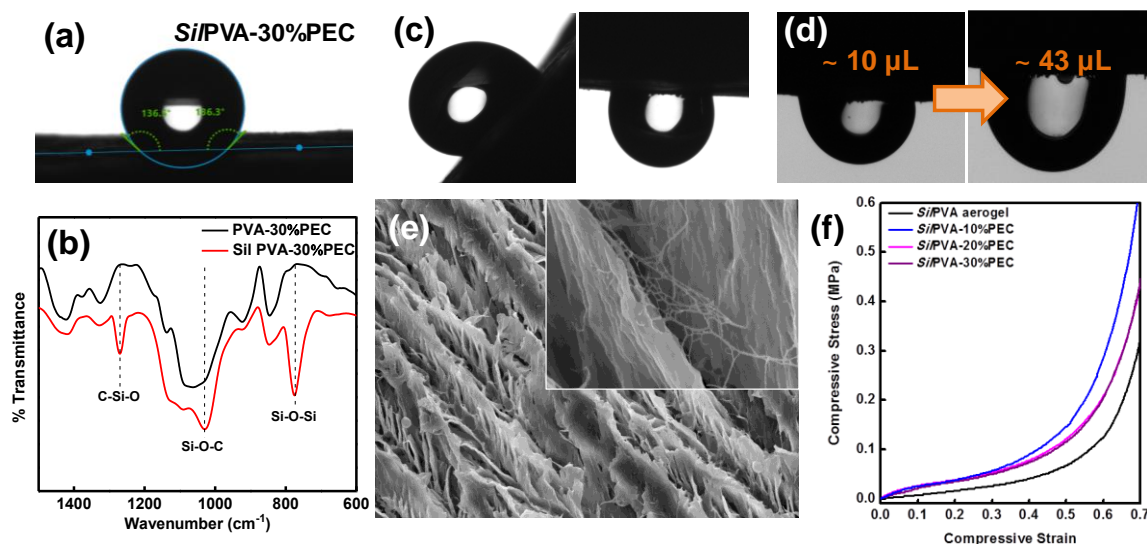
Figure 5.12. *(a) Image showing the WCA of PVA-30%PEC aerogel after the surface silane treatment. The contact angle has increased from ~ 27° to ~ 136°. (b) FTIR spectra of PVA-30%PEC aerogel before and after silane modification. (c) and (d) Photographic images demonstrating the excellent water adhesion property of PVA-PEC aerogels. The water droplet did not fall down even after 360° rotation of the aerogel surface. As much as 43 µL of water can be suspended upside down on the aerogel surface (SilPVA-30%PEC). (e) SEM image of SilPVA-30%PEC (Inset shows the magnified image). Numerous protrusions and wrinkles are clearly visible on the aerogel surface after silane modification. (f) Compressive stress-strain curves of PVA and PVA-PEC aerogels afetr surface modification.*

The surface modification of aerogels had a significant influence on their thermal and flammability properties. TGA thermograms in Figure 5.13a compare the thermal stability of PVA-PEC aerogels before and after the silanization process. The silane-coated aerogels showed better thermal stability than the uncoated ones, as evident from the improved $T_{50\%}$ values. $T_{50\%}$ for PVA-10%PEC and PVA-20%PEC aerogels were 330 and 331 °C, respectively, whereas the same for *Sil*PVA-10%PEC and *Sil*PVA-20%PEC are 402 and 405 °C, respectively. There is a clear cut elevation in the thermal stability,

which could be attributed to the hindrance of PVA backbone decomposition due to the covalent association between PVA and silane.[16, 47] Also, the surface modification of aerogels reduced their moisture sensitivity, as evident from the lower weight loss % below 100 °C for *Sil*PVA-10%PEC and *Sil*PVA-20%PEC aerogels (Figure 5.13a).

Similarly, the anti-fire performance of all the samples has been improved further upon surface modification, as evident from Figure 5.13b, which demonstrates the horizontal burning test of *Sil*PVA-30%PEC aerogel. We could observe that the moment the flame source was removed, the fire got extinguished and a charred layer was formed on the aerogel surface. Complimentary results were obtained for *Sil*PVA-PEC aerogels from the MCC tests. The HRR peak around 300 °C was almost nullified in the case of *Sil*PVA-PEC aerogels as compared to the unmodified aerogels (Figure 5.13c). This is because the silane coating has delayed the decomposition of the organic moieties of the aerogels, resulting in lower heat generation. However, at higher temperatures (400-500 °C), peak HRR values similar to the unmodified aerogels were reached probably because of the degradation of the organics. From Table 5.3, it is clear that the LOI values have increased significantly after the silane coating, even for the neat PVA aerogel. LOI as high as 31.2 % was marked for *Sil*PVA-30%PEC aerogel and the parameters such as PHRR, THR and HRC were very low for the silylated aerogels. Whereas for *Sil*PVA aerogel, i.e., silane-modified PVA aerogel without PEC, LOI and PHRR were 21.8 % and 139 W/g, respectively. Thus, it was proved that the synergistic effect of PEC and the silane coating could not only retard the moisture sensitivity of PVA-based aerogels but also enhance their thermal stability and flame retardancy to a great extent.
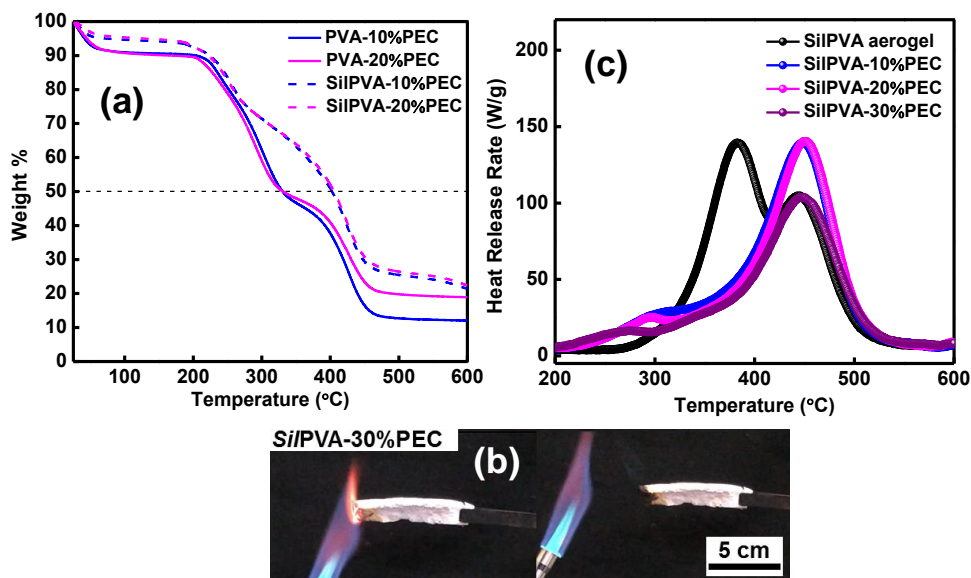
Figure 5.13. *(a) Comparison of TGA thermograms of PVA-PEC aerogels before and after the surface silanization process. (b) Photographs showing the burning behaviour of SilPVA-30%PEC aerogels during the horizontal burning tests. The flame got extinguished as soon as the flame source was removed. (c) Heat release rate versus temperature curves for PVA and PVA-PEC aerogels obtained by MCC test after silanization.*

5.5. Conclusions

In summary, a sustainable organic anti-fire filler prepared from CS and PA by ionic complexation was employed for the fabrication of PVA hybrid aerogels by an environmentally-friendly freeze-drying technique using water as the only medium. Aerogels with different weight loadings of PEC were prepared and their properties were compared with that of neat PVA aerogel. The successful interactions between PVA and PEC and the subsequent excellent miscibility between them resulted in the enhanced mechanical and thermal properties of PVA-PEC aerogels. The aerogels exhibited very low density (~ 0.06 g/cm^3) and high compressive modulus (~ 1.5 MPa) at the same time. The early degradation in PVA-PEC aerogels catalyzed by the PEC resulted in higher char

yields as well as the enhanced thermal stability of aerogels. Depending on the PEC content, the aerogels showed maximum sound absorption (~ 90 %) at different frequency ranges. Burning tests, LOI measurements and MCC analysis together demonstrated the excellent flame retardant behavior of PVA aerogels after the PEC incorporation. The LOI value increased from ~ 19 % to ~ 28 % as the PEC content increased from 0 to 30 % and all the PVA-PEC aerogels exhibited self-extinguishment of flame. The delayed degradation of PVA and the intense char layer formed due to the action of PEC resulted in the improved flame retardancy of aerogels. In order to overcome the hydrophilic nature of the prepared aerogels, surface silane treatment was carried out by a simple CVD method. The surface modified aerogels showed a combination of hydrophobicity (WCA ~ 136°) and water adhesion properties due to the speciality in the surface morphology and their thermal stability and flame retardancy were improved further. The multifunctional properties of the sustainable aerogels prepared in this study indicate that these materials have broad application prospects, particularly as structural and sound insulating materials.

5.6. References

1. Noroozi, M.; Panahi-Sarmad, M.; Abrisham, M.; Amirkiai, A.; Asghari, N.; Golbaten-Mofrad, H.; Karimpour-Motlagh, N.; Goodarzi, V.; Bahramian, A. R.; Zahiri, B. Nanostructure of Aerogels and Their Applications in Thermal Energy Insulation. *ACS Applied Energy Materials* **2019**, *2* (8), 5319-5349.
2. An, L.; Wang, J.; Petit, D.; Armstrong, J. N.; Hanson, K.; Hamilton, J.; Souza, M.; Zhao, D.; Li, C.; Liu, Y. An all-ceramic, anisotropic, and flexible aerogel insulation material. *Nano letters* **2020**, *20* (5), 3828-3835.
3. Li, M.; Qin, Z.; Cui, Y.; Yang, C.; Deng, C.; Wang, Y.; Kang, J. S.; Xia, H.; Hu, Y. Ultralight and Flexible Monolithic Polymer Aerogel with Extraordinary Thermal Insulation by A Facile Ambient Process. *Advanced Materials Interfaces* **2019**, *6* (13), 1900314.
4. Zhu, J.; Xiong, R.; Zhao, F.; Peng, T.; Hu, J.; Xie, L.; Xie, H.; Wang, K.; Jiang, C. Lightweight, High-Strength, and Anisotropic Structure Composite Aerogel Based on Hydroxyapatite Nanocrystal and Chitosan with Thermal Insulation and Flame Retardant Properties. *ACS Sustainable Chemistry & Engineering* **2019**, *8* (1), 71-83.
5. Oh, J.-H.; Kim, J.; Lee, H.; Kang, Y.; Oh, I.-K. Directionally antagonistic graphene oxide-polyurethane hybrid aerogel as a sound absorber. *ACS applied materials & interfaces* **2018**, *10* (26), 22650-22660.

6. He, C.; Huang, J.; Li, S.; Meng, K.; Zhang, L.; Chen, Z.; Lai, Y. Mechanically Resistant and Sustainable Cellulose-Based Composite Aerogels with Excellent Flame Retardant, Sound-Absorption, and Superantiwetting Ability for Advanced Engineering Materials. *ACS Sustainable Chemistry & Engineering* **2018**, *6* (1), 927-936.

7. Takeshita, S.; Yoda, S. Chitosan aerogels: transparent, flexible thermal insulators. *Chemistry of Materials* **2015**, *27* (22), 7569-7572.

8. Si, Y.; Yu, J.; Tang, X.; Ge, J.; Ding, B. Ultralight nanofibre-assembled cellular aerogels with superelasticity and multifunctionality. *Nature communications* **2014**, *5* (1), 1-9.

9. Krishnan, V. G.; Joseph, A. M.; Kuzhichalil Peethambharan, S.; Gowd, E. B. Nanoporous Crystalline Aerogels of Syndiotactic Polystyrene: Polymorphism, Dielectric, Thermal, and Acoustic Properties. *Macromolecules* **2021**, *54*, 10605-10615.

10. Joseph, A. M.; Nagendra, B.; Shaiju, P.; Surendran, K.; Gowd, E. B. Aerogels of hierarchically porous syndiotactic polystyrene with a dielectric constant near to air. *Journal of Materials Chemistry C* **2018**, *6* (2), 360-368.

11. Meador, M. A. B.; Wright, S.; Sandberg, A.; Nguyen, B. N.; Van Keuls, F. W.; Mueller, C. H.; Rodríguez-Solís, R.; Miranda, F. A. Low dielectric polyimide aerogels as substrates for lightweight patch antennas. *ACS applied materials & interfaces* **2012**, *4* (11), 6346-6353.

12. Guo, H.; Dewey, O. S.; McCorkle, L. S.; Meador, M. A. B.; Pasquali, M. Polyimide aerogels as lightweight dielectric insulators for carbon nanotube cables. *ACS Applied Polymer Materials* **2019**, *1* (7), 1680-1688.

13. Pottathara, Y. B.; Tiyyagura, H. R.; Ahmad, Z.; Sadasivuni, K. K. Graphene based aerogels: fundamentals and applications as supercapacitors. *Journal of Energy Storage* **2020**, *30*, 101549.

14. Senokos, E.; Rana, M.; Vila, M.; Fernandez-Cestau, J.; Costa, R. D.; Marcilla, R.; Vilatela, J. J. Transparent and flexible high-power supercapacitors based on carbon nanotube fibre aerogels. *Nanoscale* **2020**, *12* (32), 16980-16986.

15. Guo, W.; Liu, J.; Zhang, P.; Song, L.; Wang, X.; Hu, Y. Multi-functional hydroxyapatite/polyvinyl alcohol composite aerogels with self-cleaning, superior fire resistance and low thermal conductivity. *Composites Science and Technology* **2018**, *158*, 128-136.

16. Zheng, Q.; Cai, Z.; Gong, S. Green synthesis of polyvinyl alcohol (PVA)–cellulose nanofibril (CNF) hybrid aerogels and their use as superabsorbents. *Journal of materials chemistry A* **2014**, *2* (9), 3110-3118.

17. Wang, L.; Sánchez-Soto, M.; Maspoch, M. L. Polymer/clay aerogel composites with flame retardant agents: Mechanical, thermal and fire behavior. In *Materials & Design (1980-2015)*, Vol. 52; 2013; pp 609-614.

18. Shen, P.; Zhao, H.-B.; Huang, W.; Chen, H.-B. Poly (vinyl alcohol)/clay aerogel composites with enhanced flame retardancy. *RSC advances* **2016**, *6* (111), 109809-109814.

19. Shang, K.; Ye, D.-D.; Kang, A.-H.; Wang, Y.-T.; Liao, W.; Xu, S.; Wang, Y.-Z. Robust and fire retardant borate-crosslinked poly (vinyl alcohol)/montmorillonite aerogel via melt-crosslink. *Polymer* **2017**, *131*, 111-119.

20. Simón-Herrero, C.; Gómez, L.; Romero, A.; Valverde, J. L.; Sanchez-Silva, L. Nanoclay-based PVA aerogels: synthesis and characterization. *Industrial & Engineering Chemistry Research* **2018**, *57* (18), 6218-6225.

21. Chen, H.-B.; Liu, B.; Huang, W.; Wang, J.-S.; Zeng, G.; Wu, W.-H.; Schiraldi, D. A. Fabrication and properties of irradiation-cross-linked poly (vinyl alcohol)/clay aerogel composites. *ACS applied materials & interfaces* **2014**, *6* (18), 16227-16236.

22. Chen, H.-B.; Wang, Y.-Z.; Schiraldi, D. A. Preparation and Flammability of Poly(vinyl alcohol) Composite Aerogels. *ACS Applied Materials & Interfaces* **2014**, *6* (9), 6790-6796.

23. Wang, Y.-T.; Zhao, H.-B.; Degracia, K.; Han, L.-X.; Sun, H.; Sun, M.; Wang, Y.-Z.; Schiraldi, D. A. Green approach to improving the strength and flame retardancy of poly (vinyl alcohol)/clay aerogels: incorporating biobased gelatin. *ACS applied materials & interfaces* **2017**, *9* (48), 42258-42265.

24. Chen, H.-B.; Schiraldi, D. A. Flammability of polymer/clay aerogel composites: an overview. *Polymer Reviews* **2019**, *59* (1), 1-24.

25. Wang, Y.-T.; Liao, S.-F.; Shang, K.; Chen, M.-J.; Huang, J.-Q.; Wang, Y.-Z.; Schiraldi, D. A. Efficient approach to improving the flame retardancy of poly (vinyl alcohol)/clay aerogels: incorporating piperazine-modified ammonium polyphosphate. *ACS applied materials & interfaces* **2015**, *7* (3), 1780-1786.

26. Sun, H.; Schiraldi, D. A.; Chen, D.; Wang, D.; Sánchez-Soto, M. Tough polymer aerogels incorporating a conformal inorganic coating for low flammability and durable hydrophobicity. *ACS applied materials & interfaces* **2016**, *8* (20), 13051-13057.

27. Luo, Y.; Xie, D.; Chen, Y.; Han, T.; Chen, R.; Sheng, X.; Mei, Y. Synergistic effect of ammonium polyphosphate and α-zirconium phosphate in flame-retardant poly (vinyl alcohol) aerogels. *Polymer Degradation and Stability* **2019**, *170*, 109019.

28. Sheng, X.; Li, S.; Zhao, Y.; Zhai, D.; Zhang, L.; Lu, X. Synergistic Effects of Two-Dimensional MXene and Ammonium Polyphosphate on Enhancing the Fire Safety of Polyvinyl Alcohol Composite Aerogels. *Polymers* **2019**, *11* (12), 1964.

29. Zhang, Q.; Wang, X.; Tao, X.; Li, Z.; Li, X.; Zhang, Z. Polyvinyl alcohol composite aerogel with remarkable flame retardancy, chemical durability and self-cleaning property. *Composites Communications* **2019**, *15*, 96-102.

30. Shang, K.; Yang, J.-C.; Cao, Z.-J.; Liao, W.; Wang, Y.-Z.; Schiraldi, D. A. Novel polymer aerogel toward high dimensional stability, mechanical property, and fire safety. *ACS Applied Materials & Interfaces* **2017**, *9* (27), 22985-22993.

31. Zhang, T.; Yan, H.; Shen, L.; Fang, Z.; Zhang, X.; Wang, J.; Zhang, B. Chitosan/Phytic Acid Polyelectrolyte Complex: A Green and Renewable Intumescent Flame Retardant System for Ethylene–Vinyl Acetate Copolymer. *Ind. Eng. Chem. Res.* **2014**, *53* (49), 19199-19207.

32. Cai, X.; Chen, H.; Jiang, D.; Pan, M.; Mei, C. The thermal property and flame retardancy of RPC with a polyelectrolyte complex of nanocrystalline cellulose and ammonium polyphosphate. *Journal of Thermal Analysis and Calorimetry* **2018**, *134* (3), 2089-2096.

33. Zhang, Z.; Li, X.; Ma, Z.; Ning, H.; Zhang, D.; Wang, Y. A facile and green strategy to simultaneously enhance the flame retardant and mechanical properties of poly (vinyl alcohol) by introduction of a bio-based polyelectrolyte complex formed by chitosan and phytic acid. *Dalton Transactions* **2020**, *49* (32), 11226-11237.

34. Zhou, Y.; Tawiah, B.; Noor, N.; Zhang, Z.; Sun, J.; Yuen, R. K.; Fei, B. A facile and sustainable approach for simultaneously flame retarded, UV protective and reinforced poly (lactic acid) composites using fully bio-based complexing couples. *Composites Part B: Engineering* **2021**, *215*, 108833.

35. Cheng, X.-W.; Guan, J.-P.; Yang, X.-H.; Tang, R.-C.; Yao, F. A bio-resourced phytic acid/chitosan polyelectrolyte complex for the flame retardant treatment of wool fabric. *Journal of cleaner production* **2019**, *223*, 342-349.

36. Lankalapalli, S.; Kolapalli, V. Polyelectrolyte complexes: A review of their applicability in drug delivery technology. *Indian journal of pharmaceutical sciences* **2009**, *71* (5), 481.

37. Verma, A.; Verma, A. Polyelectrolyte complex-an overview. *International Journal of Pharmaceutical Sciences and Research* **2013**, *4* (5), 1684.

38. Meka, V. S.; Sing, M. K.; Pichika, M. R.; Nali, S. R.; Kolapalli, V. R.; Kesharwani, P. A comprehensive review on polyelectrolyte complexes. *Drug discovery today* **2017**, *22* (11), 1697-1706.

39. Haile, M.; Leistner, M.; Sarwar, O.; Toler, C. M.; Henderson, R.; Grunlan, J. C. A wash-durable polyelectrolyte complex that extinguishes flames on polyester–cotton fabric. *RSC advances* **2016**, *6* (40), 33998-34004.

40. Zhang, L.; Yi, D.; Hao, J. Poly (diallyldimethylammonium) and polyphosphate polyelectrolyte complex as flame retardant for char-forming epoxy resins. *Journal of Fire Sciences* **2020**, *38* (4), 333-347.

41. Gong, X.; Wang, Y.; Zeng, H.; Betti, M.; Chen, L. Highly porous, hydrophobic, and compressible cellulose nanocrystals/poly (vinyl alcohol) aerogels as recyclable absorbents for oil–water separation. *ACS Sustainable Chemistry & Engineering* **2019**, *7* (13), 11118-11128.

42. Chen, J.; Han, S.; Huang, M.; Li, J.; Zhou, M.; He, J. Green crosslinked nanofibers membrane based on CS/PVA combined with polybasic organic acid for tympanic membrane repair. *International Journal of Polymeric Materials and Polymeric Biomaterials* **2022**, *71* (4), 291-301.

43. Wang, X.; Jana, S. C. Synergistic hybrid organic–inorganic aerogels. *ACS applied materials & interfaces* **2013**, *5* (13), 6423-6429.

44. Wang, L.; Sanchez-Soto, M.; Maspoch, M. L. Polymer/clay aerogel composites with flame retardant agents: Mechanical, thermal and fire behavior. *Materials & Design (1980-2015)* **2013**, *52*, 609-614.

45. Rapisarda, M.; Malfense Fierro, G.-P.; Meo, M. Ultralight graphene oxide/polyvinyl alcohol aerogel for broadband and tuneable acoustic properties. *Scientific reports* **2021**, *11* (1), 1-10.

46. Mouritz, A. Durability of composites exposed to elevated temperature and fire. In *Durability of composites for civil structural applications*, Elsevier, 2007; pp 98-125.

47. Javadi, A.; Zheng, Q.; Payen, F.; Javadi, A.; Altin, Y.; Cai, Z.; Sabo, R.; Gong, S. Polyvinyl alcohol-cellulose nanofibrils-graphene oxide hybrid organic aerogels. *ACS applied materials & interfaces* **2013**, *5* (13), 5969-5975.

48. Feng, L.; Zhang, Y.; Xi, J.; Zhu, Y.; Wang, N.; Xia, F.; Jiang, L. Petal effect: a superhydrophobic state with high adhesive force. *Langmuir* **2008**, *24* (8), 4114-4119.

49. Hu, H.; Zhao, Z.; Wan, W.; Gogotsi, Y.; Qiu, J. Polymer/graphene hybrid aerogel with high compressibility, conductivity, and "sticky" superhydrophobicity. *ACS applied materials & interfaces* **2014**, *6* (5), 3242-3249.

Chapter 6

Overall Summary and Future Perspectives

6.1. Overall Summary

The interest in polymer-based aerogels has surged in the last few years, thanks to their unique properties, multi-functions and superior mechanical properties. These are significant materials from the viewpoints of both science and industry, as they combine low cost, robustness, durability and easy processing of polymers with extraordinary aerogel properties and are expected to replace the conventional lightweight materials from the market in the coming days. The overall concept of the thesis is to develop mechanically robust and thermally stable thermoplastic polymer aerogels with multifunctional properties using an environment-friendly freeze-drying technique. Polymer aerogels can be prepared either from chemical gels, where the polymer chains form covalently crosslinked networks, or from physical gels, where crystallization or non-covalent interactions act as crosslinked points to form a three-dimensional network structure. Our focus was on the physical gelation of polymers, particularly the thermoreversible gelation based on polymer crystallization for the preparation of aerogels. Enhancement of the flame-retardant properties of polymer aerogels was another challenge addressed in the present thesis.

The first chapter provided a brief introduction to aerogels and their importance. Polymer-based aerogels and their advantages over conventional aerogels were specifically highlighted. Various gelation mechanisms in polymers, gel drying techniques and the significance of solvent exchange in aerogel preparation were elaborately discussed. Flammability test methods and flame-retardant mechanisms of polymeric systems, and finally, the application prospects of polymer-based aerogels were briefed.

In the second chapter, we studied the influence of structure and morphology on the thermal, mechanical, dielectric and acoustic properties of sPS aerogels. For this, we prepared two nanoporous crystalline forms of sPS aerogels, namely δ and ε forms (δ_e and

ε_e), from their respective gels. We found that by tuning the crystal structure of sPS, the morphology and pore structure of aerogels could be tuned. The δ_e and ε_e aerogels prepared in this study exhibited hierarchical porosity with ordered microporosity (<2 nm) and disordered meso and macroporosities (>2 nm). Using variable temperature WAXD, we investigated the phase transition behavior of these aerogels. We further found that aerogels with different crystalline forms have different values for dielectric constant, thermal conductivity and sound absorption coefficients. As a whole, we succeeded in developing hierarchically porous crystalline nanoporous sPS aerogels with ultralow dielectric constant (1.02 ± 0.02), thermal conductivity as low as 0.04 W m^{-1} K^{-1}, and high sound absorption coefficient (close to 1). Moreover, these aerogels exhibited excellent oleophilicity, which was demonstrated in oil/organic solvent separation experiments.

In the third chapter, we selected the commercially successful biodegradable polymer PLA for the fabrication of aerogels with high thermal stability. Similar to the previous work, the crystal structure and chain conformation of the polymer played a crucial role in determining the PLA aerogel properties. Herein, we reported a temperature-assisted method for forming SC gel by blending enantiomeric PLLA and PDLA in a crystal complex forming solvent. Fast thermoreversible gelation of PLLA/PDLA blend solution occurred on cooling the solution to below 0 °C. Thermal annealing of the PLLA/PDLA blend gel at 70 °C furnished crystalline pure SC gel. The SC gel was solvent exchanged with water and freeze-dried to obtain SC aerogel with enhanced thermal and mechanical properties. SC content of the gel was tuned by varying the annealing temperature of the gel and we were able to prepare blend aerogels with pure α crystalline form and a mixture of α and SC. Crystalline pure blend α aerogel showed fibrillar morphology, whereas SC aerogel exhibited unique interwoven ball-like microstructures interconnected by PLLA and PDLA chains. When compared with the

homopolymer aerogels, the SC aerogel showed an enhanced melting temperature of 227 ± 2 °C (50 °C higher), better thermal stability (onset of degradation was delayed by ~ 40 °C), improved mechanical strength (compression modulus of 3.3 MPa) and better sound absorption ability. The structural evolution during SC formation at the molecular level and the micrometer length scale was found to be responsible for the enhanced aerogel properties.

The fourth chapter focused on improving the flame retardancy of PLA aerogels. We formulated a novel strategy for incorporating ionic polymers/molecules into the thermoreversible gels of PLLA during the solvent exchange process and the subsequent removal of solvents by freeze-drying to obtain flame retardant aerogels. Here, we made use of the ionic interactions between the guest molecules to layer-by-layer deposit SA, CS and PA on PLLA. Aerogels with different sequences of deposition were prepared and the flammability properties were investigated. We have modified the solvent exchange process to introduce N and P-rich moieties with excellent char-forming capability into the system. The PLLA aerogel with SA-CS-PA sequential deposition showed the best results with a LOI value of ~32.0 % (as compared to 18.5 % of neat PLLA aerogel) and self-extinguishment of flame. The same protocol can be used for the improvement of flame retardancy of other polymer-based aerogels as well, including the PDLA and SC aerogels.

In the last working chapter, we developed a completely organic and sustainable flame retardant filler for PVA aerogels. The filler developed is a PEC made from CS and PA. Ice templating followed by freeze-drying of PVA-PEC solutions in water resulted in mechanically strong and flexible PVA aerogels. Noncovalent interactions ensured the interfacial adhesion of PEC and therefore, excellent compatibility between PVA and PEC. We could achieve excellent flame retardancy (LOI ~28%) with self-extinguishing behavior for PVA aerogels without compromising the mechanical strength, flexibility,

low density and good sound absorption ability. Surface silane modification of the prepared aerogels endowed sticky hydrophobicity to them and further enhanced their anti-fire properties.

6.2. Future Perspectives

The present thesis supplied new insights into the polymer-based aerogels and provides an excellent scope for further works in the future, as discussed below:

- The thesis revealed that the crystal structure of polymer influences the morphology, and ultimately, the properties of aerogels, using some of the commercially important semicrystalline polymers. The studies can be extended to other polymers as well, particularly, PHB, which is an upcoming sustainable polymer of commercial relevance.

- sPS aerogels with crystalline nanoporosity have proven to be ideal materials for acoustic insulation. Therefore, the large-scale preparation of these aerogels can be tried, which is quite possible with supercritical CO_2 drying.

- SC aerogel prepared in the present thesis proves to be an excellent material with enhanced thermal and mechanical properties. All the other properties (thermal transport, dielectric, piezoelectric, EMI shielding, etc.) of SC aerogels can be examined to further widen its application prospects.

- The flame retardant modification based on solvent exchange and LbL assembly can be attempted on various polymers such as PDLA, SC, PHB, sPS, PPO, nylons and so on, and its efficiency in improving the flame retardancy of these aerogels can be documented.

ABSTRACT

Name of the Student: *Vipin G. Krishnan*	Registration No: *10CC17A39011*
Faculty of Study: *Chemical Sciences*	Year of Submission: *2023*
CSIR Lab: *CSIR-National Institute for Interdisciplinary Science & Technology (CSIR-NIIST), TVM, Kerala*	Name of the Supervisor: *Dr. E. Bhoje Gowd*
Title of the thesis: *Semicrystalline Polymer-based Aerogels: Structure, Morphology and Multifunctional Properties*	

The present thesis focuses on the development of mechanically robust and thermally stable aerogels with multifunctional properties using commercially important thermoplastic polymers. The first two working chapters deal with the structure-morphology-property relationship in semi-crystalline polymer aerogels. In Chapter 2, hierarchically porous crystalline nanoporous syndiotactic polystyrene aerogels with different crystal forms are prepared and their multifunctional properties are compared. In the second working chapter, stereocomplex formation between opposite enantiomeric polylactides in the gel state is explored for the preparation of mechanically robust and thermally stable sustainable aerogels. In the last two working chapters, efforts are made to enhance the flame-retardancy of biodegradable polymer aerogels without the use of halogenated or inorganic fillers. The third working chapter introduces a novel approach of incorporating ionic polymers/molecules into the thermoreversible gels during the solvent exchange process to fabricate flame-retardant polylactide aerogels. In Chapter 5, a sustainable polyelectrolyte complex developed from chitosan and phytic acid is used as flame-retardant filler for polyvinyl alcohol aerogels. Overall summary and the future perspectives of the research work are described in Chapter 6.

LIST OF PUBLICATIONS

Emanating from thesis work

1. Nanoporous Crystalline Aerogels of Syndiotactic Polystyrene: Polymorphism, Dielectric, Thermal, and Acoustic Properties; **Vipin G. Krishnan**, Angel Mary Joseph, Surendran K. P. and E. Bhoje Gowd*, *Macromolecules*, 2021, 54, 22, 10605–10615.

2. High-Strength, Flexible, Hydrophobic, Sound-Absorbing, and Flame-Retardant Poly(vinyl alcohol)/ Polyelectrolyte Complex Aerogels; **Vipin G. Krishnan**, C. V. Sijla Rosely, Andreas Leuteritz and E. Bhoje Gowd*, *ACS Applied Polymer Materials*, 2022, 4, 7, 5113–5124.

3. Thermoreversible Gels of Poly(ʟ-lactide)/Poly(ᴅ-lactide) Blends: A Facile Route to Prepare Blend α-Form and Stereocomplex Aerogels; **Vipin G. Krishnan**, N. M. Praveena, Amal Raj R. B., Kiran Mohan and E. Bhoje Gowd*, *ACS Applied Polymer Materials*, 2023, 5, 2, 1556–1564.

4. Flame Retardant Polylactide Aerogels by Incorporating Multi-Element Moieties into the Polymer Gels during the Solvent Exchange Process; **Vipin G. Krishnan**, Sruthi Suresh and E. Bhoje Gowd* (Manuscript under preparation).

Not related to thesis work

1. Stereocomplex Formation and Hierarchical Structural Changes During Heating of Supramolecular Gels Obtained by Polylactide Racemic Blends; N.M. Praveena, G. Virat, **Vipin G. Krishnan** and E. Bhoje Gowd*, *Polymer*, 2022, 241, 124530.

2. Liquid Phase Exfoliated Nanosheets as Multifunctional Fillers to Semicrystalline Polymers; Sruthi Suresh, **Vipin G. Krishnan**, Ashitha George, Baku Nagendra, C. V. Sijla Rosely and E. Bhoje Gowd*, *Journal of Macromolecular Science, Part A*, 2022, 59, 4, 257-270.

3. Lightweight, Mechanically Robust and Flame Retardant PVDF-MXene Aerogels for High-Efficiency Electromagnetic Interference Shielding; Sruthi Suresh, **Vipin G. Krishnan**, Surendran K. P. and E. Bhoje Gowd* (Manuscript under preparation).

4. Temperature Induced Structural Changes in Poly(3-hydroxybutyric acid) Aerogels; N. S. Akhila, **Vipin G. Krishnan**, Jefin P. Thomas and E. Bhoje Gowd* (Manuscript under preparation).

LIST OF CONFERENCE PRESENTATIONS

1. **Vipin G. Krishnan**, N. M. Praveena, Amal Raj R. B. and E. Bhoje Gowd, Thermoreversible Gels of Poly(L-lactide)/Poly(D-lactide) Blends: A Facile Route to Prepare Blend α-Form and Stereocomplex Aerogels, SPSI MACRO 2022 - International Conference on Science and Technology of Polymers and Advanced Materials through Innovation, Entrepreneurship and Industry held on November 2-4, 2022 at Pune, India (**Best Poster Presentation Award**).

2. **Vipin G. Krishnan**, N. M. Praveena, Amal Raj R. B. and E. Bhoje Gowd, Co-crystalline Thermoreversible Gels of Poly(L-lactide)/Poly(D-lactide) Blends: A Facile Route to Prepare Blend α-Form and Stereocomplex Aerogels, 3rd International Conference on Crystal Engineering: From Molecule to Crystal (CE:FMC2022) held on 31 August- 02 September, 2022 at Pahalgam, Kashmir, India (**Best Poster Presentation Award**).

3. **Vipin G. Krishnan**, N. M. Praveena, Amal Raj R. B. and E. Bhoje Gowd, Stereocomplex Gels and Aerogels of Polylactic Acid, International Conference on Chemistry and Applications of Soft Materials (CASM 2022), held on July 25-27, 2022 at CSIR-National Institute for Interdisciplinary Science and Technology, Thiruvananthapuram (Poster presentation).

4. **Vipin G. Krishnan**, Angel Mary Joseph, Surendran K. P. and E. Bhoje Gowd, Nanoporous Crystalline Aerogels of Syndiotactic Polystyrene: Polymorphism, Dielectric, Thermal and Acoustic Insulation Properties, MRSI International Symposium on Advanced Materials (ISAM-2021), held on March 26-27, 2021 through MS Teams online platform (**Best Oral Presentation Award**).

5. **Vipin G. Krishnan**, Angel Mary Joseph, Surendran K. P. and E. Bhoje Gowd, Ultra-Low Dielectric Constant Aerogels of Syndiotactic Polystyrene with Nanoporous Channels (ε) and Cavities (δ), Second International Conference on Advanced

Materials and Technology (ICMAT-20), held on January 16-18, 2020 at JSS Science and Technology University, Mysuru, India (Oral presentation).

6. **Vipin G. Krishnan**, Angel Mary Joseph, Surendran K. P. and E. Bhoje Gowd, Ultra-Low Dielectric Constant Aerogels of Syndiotactic Polystyrene with Nanoporous Channels (ε) and Cavities (δ), International Conference on Functional Materials (ICFM 2020), held on January 6-8, 2020 at Materials Science Centre, Indian Institute of Technology Kharagpur (Poster presentation).

7. **Vipin G. Krishnan**, Angel Mary Joseph, G. Virat, Surendran K. P. and E. Bhoje Gowd, Ultra-Low Dielectric Constant Aerogels of Syndiotactic Polystyrene with Nanoporous Channels (ε) and Cavities (δ), International Conference on Polymer Science and Technology (SPSI-MACRO-2018), held on December 19-22, 2018 at Indian Institute of Science Education and Research (IISER) Pune (Poster presentation).

Nanoporous Crystalline Aerogels of Syndiotactic Polystyrene: Polymorphism, Dielectric, Thermal, and Acoustic Properties[†]

Vipin G. Krishnan, Angel Mary Joseph, Surendran Kuzhichalil Peethambharan, and E. Bhoje Gowd*

Read Online

ACCESS | Metrics & More | Article Recommendations | SI Supporting Information

ABSTRACT: Hierarchically porous crystalline nanoporous aerogels of syndiotactic polystyrene (sPS) received much attention because of their unique nanoporous structures along with meso- and macroporosity. Depending on the difference in the packing of polymer chains within the crystal lattice, sPS has two nanoporous crystalline forms, namely, δ and ε forms (δ_e and ε_e). In this study, we have prepared high-purity nanoporous δ and ε forms of sPS aerogels from their respective gels using a solvent exchange strategy with green solvents, followed by an environmentally friendly freeze-drying technique. Using these highly porous aerogels, the phase transition behavior of sPS at higher temperatures was investigated. The δ_e form showed a complex phase transition behavior on heating, and at a higher temperature, the γ form (obtained through an intermediate helical phase) transformed into a mixture of α and β forms. On the other hand, the ε_e form transformed directly into the γ form, and on further heating, the γ form transformed exclusively into the α form. The dielectric, thermal, and acoustic properties of crystalline-nanoporous aerogels were promising with an ultralow dielectric constant (1.02 ± 0.02), thermal conductivity (λ) as low as 0.04 W m^{-1} K^{-1}, and a high sound absorption coefficient (close to 1). Moreover, these aerogels exhibited excellent oleophilicity, which was demonstrated in oil/organic solvent separation experiments. These multifunctional aerogels of sPS can, therefore, find a multitude of applications, especially in thermal and acoustic insulation and molecular sorption of oil/organic solvents.
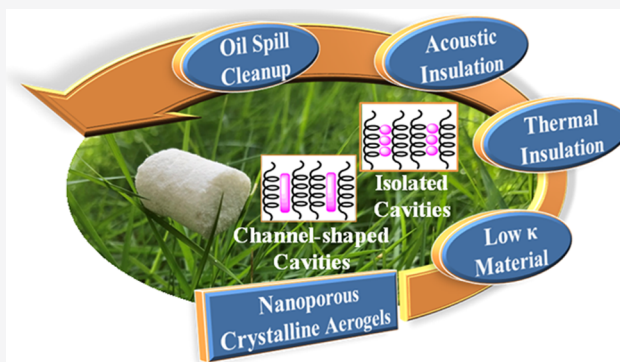
INTRODUCTION

Aerogel monoliths based on polymers are trending nowadays in diverse fields of application, such as thermal insulation, packaging, acoustic insulation, oil spill cleanup, sorbents of volatile organic compounds, antennas and electronics, etc., mainly because of their ability to surpass the drawbacks of traditional inorganic aerogels, which are highly fragile and brittle.[1−11] Semicrystalline polymers like syndiotactic polystyrene (sPS),[12−18] poly(2,6-dimethyl-1,4-phenylene) oxide (PPO),[19,20] isotactic polypropylene,[21,22] poly(vinylidene fluoride),[23,24] polyethylene,[25] poly(ether ether ketone),[26,27] etc. are capable of forming thermoreversible gels in various solvents where the junction zones of the gel network are made up of polymer crystalline phases, which provide the required robustness to the system. Among them, sPS and PPO received remarkable attention due to their ability to form physical aerogels with crystalline nanoporosity.[12,28−37]

Guerra and co-workers reported a physically bonded aerogel of sPS using the δ form gel by supercritical carbon dioxide (CO$_2$) extraction, and it is the first example of a nanoporous crystalline aerogel of sPS.[12] Similar to the δ aerogel, ε form sPS aerogels also possess empty spaces within the crystal lattices, and both these phases exhibit a helical trans-trans-gauche-gauche (T$_2$G$_2$) polymer chain conformation with the nanocavities being isolated in the monoclinic δ form and channel-shaped in the

orthorhombic ε form, parallel to the chain axes.[12,30,31] Such cavities have a diameter of less than 2 nm, which together with the typical disordered amorphous mesopores (2−50 nm) and macropores (greater than 50 nm) of the aerogels render hierarchical porosity to the δ and ε sPS aerogels.[29] The polymorphism of sPS is even more complex with additional crystalline phases α and β having a planar zigzag all-trans (T$_4$) chain conformation and γ with closely packed helical T$_2$G$_2$ chains.[16,38−44] Most of the reported literature on sPS aerogels focuses on the δ form aerogel, probably due to the complex procedures involved in the making of the ε aerogel. Daniel and co-workers formulated a strategy to produce the ε aerogel in its finest crystalline purity.[30] ε aerogels prepared from the γ form aerogels by chloroform sorption/desorption, the previously known method, presented traces of the γ and/or δ form.[31,33,37] The pure ε phase obtained in aerogels could be effectively
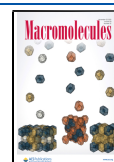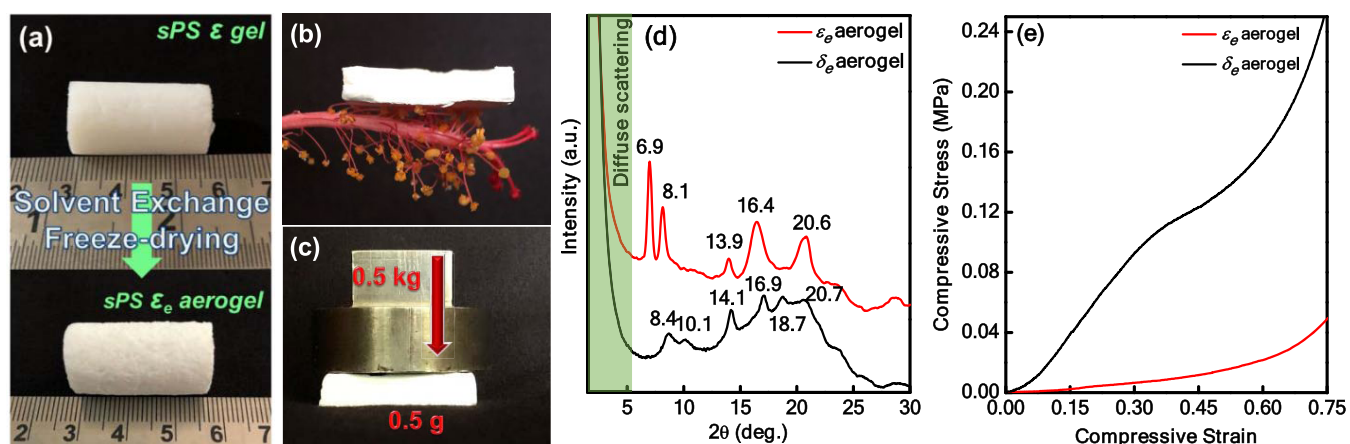
Figure 1. Photographs of (a) ε gel and the corresponding aerogel obtained by a freeze-drying process; (b) nanoporous ε aerogel resting on the stamen of a flower; (c) ε_e aerogel holding 1000 times its original weight; and (d) WAXD patterns and (e) stress−strain plots of δ_e and ε_e aerogels measured at room temperature.

utilized to unravel the intricate polymorphism of sPS by the systematic investigation of the structural transitions.

Rizzo et al. investigated the thermal transition behavior of the ε crystalline phase of sPS using thin films and compared it with the δ form.[45] Unlike the δ form, the nanoporous ε form transformed directly into the γ form on heating above 100 °C without passing through the intermediate phase (disordered helical phase). Although high-temperature transitions were reported in the case of nanoporous δ form, no reports are available on the crystalline transitions at a higher temperature using the ε form. For example, Gowd et al. reported that the γ form transformed into a mixture of α and β forms for the thick δ form film or uniaxially oriented sample (cocrystal), while a completely dried thin film (or powder) transformed exclusively into the kinetically stable α phase.[41,42,46−49] They have reported that the residual solvents in the amorphous phase of δ or γ form triggered the β crystal formation.[47] On the other hand, when the uniaxially oriented nanoporous δ form was used, the γ form transformed into a mixture of α and β forms at higher temperatures even though no solvent residues were there in the amorphous phase of the γ form.[41,42] The origin of the formation of the β form at higher temperatures is unclear when the nanoporous δ form was used as a starting material. As aerogels are fully dried and no residual solvents are present, these are the right candidates to understand the phase transition behavior. In this paper, a detailed investigation was carried out on the phase transition behavior of both nanoporous δ and ε phases using aerogels.

sPS aerogels are deployed in molecular sorption, namely, volatile organic compounds absorption, adsorption of H_2, and trapping of airborne nanoparticles, mainly due to the nanosized pores possessed by them.[28,31,50] Nanoporous crystalline polymer aerogels, however, have never been exploited for their low dielectric constant and thermal and acoustic insulation. The first attempt in that direction was brought off by Joseph et al., who demonstrated the ultralow dielectric constant of sPS δ type aerogels (1.03 ± 0.02), which is the lowest value ever reported for any polymer aerogel.[29] Rossinsky et al. investigated the thermal conductivity of the crystalline δ phase of sPS in the bulk, and the average value was found out to be 0.2−0.3 W m^{-1} K^{-1}.[51] Thermal conductivity increased with the increase in material density, which is the general trend. However, there are no reports on the thermal insulation behavior of sPS aerogels, to the

best of our knowledge. The micro-/mesopores in aerogels can induce a Knudsen effect, which lowers the gaseous conductivity as compared to commercial thermal insulators, such as expanded polystyrene, which are macroporous in nature. Also, the conduction through the condensed phase (solid conduction) will be lower in micro-/mesoporous aerogels than in dense (nonporous) matrix materials as the three-dimensional network structure in aerogels is composed of weakly connected nanofibers.[52−55] These features of sPS aerogels, therefore, could not only reduce the heat conduction through them but also influence their sound absorption characteristics. He et al. have shown that the high porosity and small pore size of cellulose-based aerogels resulted in their excellent sound insulation performance.[6] The hydrophobic nature of sPS presents an added advantage to its aerogels in terms of water repellence, and this could be extended to the selective absorption of oil/organic solvents (oleophilicity) from a water mixture. Amid other excellent thermally insulating materials or acoustic insulators, sPS aerogels thus stand out as they could combine a whole lot of properties within a single system, which is explored in the second part of the paper.

Herein, we proposed a sustainable method for the preparation of nanoporous ε and δ forms of sPS aerogels using freeze-drying as the solvent extraction technique. The organic solvents used for the preparation of gels were recovered completely after the solvent exchange process with green solvents (water and ethanol). Processes like the aging of gel, solvent exchange, freezing, etc. were carefully controlled to obtain samples with different porosities; the highest attained porosity was 97%. By the controlled heating of aerogels, the phase transition behavior of nanoporous sPS δ and ε forms was investigated using wide-angle X-ray diffraction (WAXD) and differential scanning calorimetry (DSC). The nanoporous crystalline aerogels of sPS proved to be multifaceted materials with spectacularly low values for dielectric constant (1.02 ± 0.02) and thermal conductivity (∼0.04 W m^{-1} K^{-1}), excellent acoustic insulation performance with sound absorption coefficients as high as 0.97 in the midfrequency range and superior oil/organic solvent absorption ability. These multifunctional properties of sPS aerogels permit them to be potential alternatives to conventional materials in the fields of microelectronics, thermal management, acoustic insulation, and oil/solvent spill cleanup.
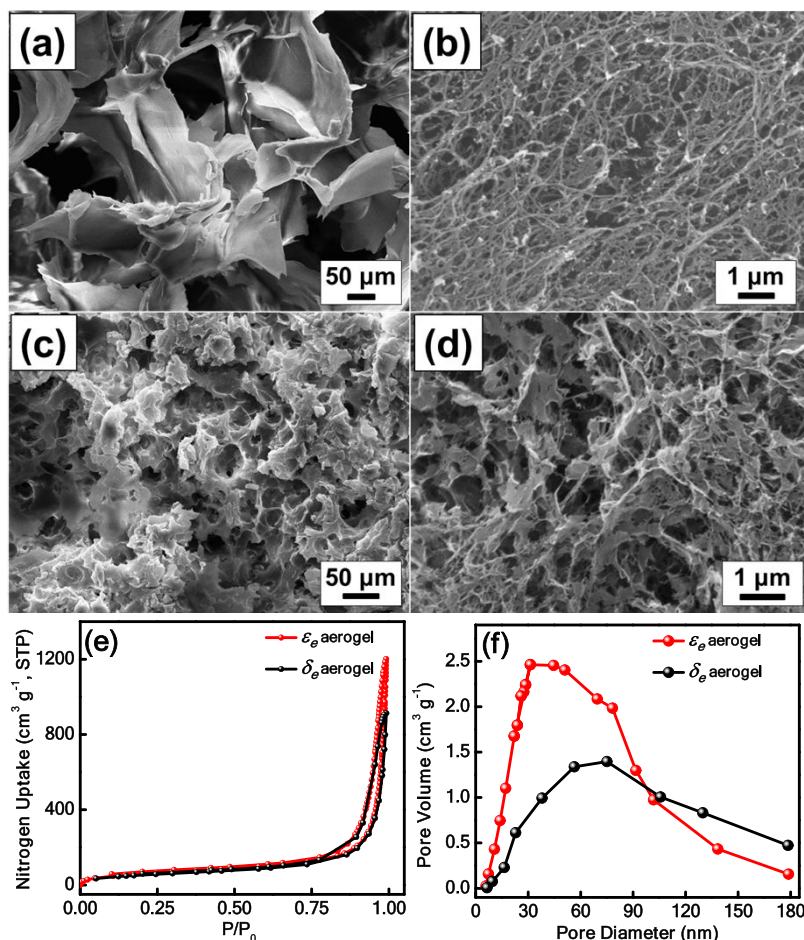
Figure 2. SEM images of (a and b) δ_e and (c and d) ε_e aerogels at different magnifications. (e) N$_2$ adsorption−desorption isotherms and (f) pore-size distribution of δ_e and ε_e aerogels.

RESULTS AND DISCUSSION

Hierarchical Porous Aerogels of sPS (δ_e and ε_e). The ability of sPS to form cocrystalline phases has been exploited to prepare two forms of crystalline nanoporous aerogels by the supercritical carbon dioxide drying method.[12,28,30,31,33] In our previous work, the δ_e aerogel was prepared from the δ gel using xylene as the solvent by the freeze-drying method.[29] In the present work, the ε_e aerogel was prepared by the freeze-drying method, as described in the Experimental Section. Unlike in the case of the δ gel, acrylonitrile was used as a nonsolvent for the preparation of the ε gel along with chloroform as the solvent. On cooling the polymer solutions to room temperature, thermoreversible gelation takes place, which is very quick in the case of the ε gel as the phase separation here is induced not just by temperature but also by a nonsolvent. A systematic solvent exchange strategy was adopted to transform the δ and ε organogels into hydrogels. This step is crucial as it allows to circumvent the structural deformations occurring during the freeze-drying of gels and makes the entire processing route eco-friendly by allowing the recovery of organic solvents and making them available for reuse. As optimized from our previous work,[29] the polymer concentration in solution was kept at 3 wt % and the duration of steps like gel aging, solvent exchange, freezing, drying, etc. was controlled to derive aerogels of varying porosities (84−97%). We could achieve hierarchical porous sPS aerogels with the porosity as high as 97%, and there was only negligible shrinkage to the gel structure upon drying, as shown in

Figure 1a. Solvent exchange with ethanol followed by water was crucial in achieving the high porosity and retaining the shape and size of the aerogels as same as that of the gels before freeze-drying. Figure 1b depicts the ultralow density of the ε aerogel with 97% porosity, and it can bear a load of almost 1000 times its weight without structural disintegration (Figure 1c). The δ_e aerogel with a similar porosity has sufficient strength to bear a load of 1500 times its original weight as reported in our previous work.[29] The X-ray diffraction profiles in Figure 1d confirm the successful formation of crystalline nanoporous sPS aerogels. The reflections at $2\theta = 8.4, 10.1, 14.1, 16.9, 18.7$, and $20.7°$ and $2\theta = 6.9, 8.1, 13.9, 16.4$, and $20.6°$ correspond to δ_e and ε_e forms of sPS, respectively.[30,56] As evident from the X-ray diffraction profiles, high-purity crystalline δ_e and ε_e aerogels (without the traces of other crystalline forms) were achieved in this study by the freeze-drying method. The diffuse scattering observed at low 2θ ($<4°$) in Figure 1d indicates the presence of microporosity (<2 nm) in both δ_e and ε_e forms of sPS. Gowd et al. reported such diffuse scattering in the X-ray pattern of the δ_e form due to the presence of crystalline porosity, and it decreased significantly upon heating when the structure transformed into the γ form.[42] It is also worth mentioning here that such diffuse scattering was not observed in the X-ray diffraction patterns of the gel state of δ and ε forms of sPS. The mechanical properties of δ_e and ε_e aerogels with a porosity of ~97% were investigated by compression experiments and the corresponding stress−strain diagrams are provided in Figure 1e. Both aerogels exhibited an
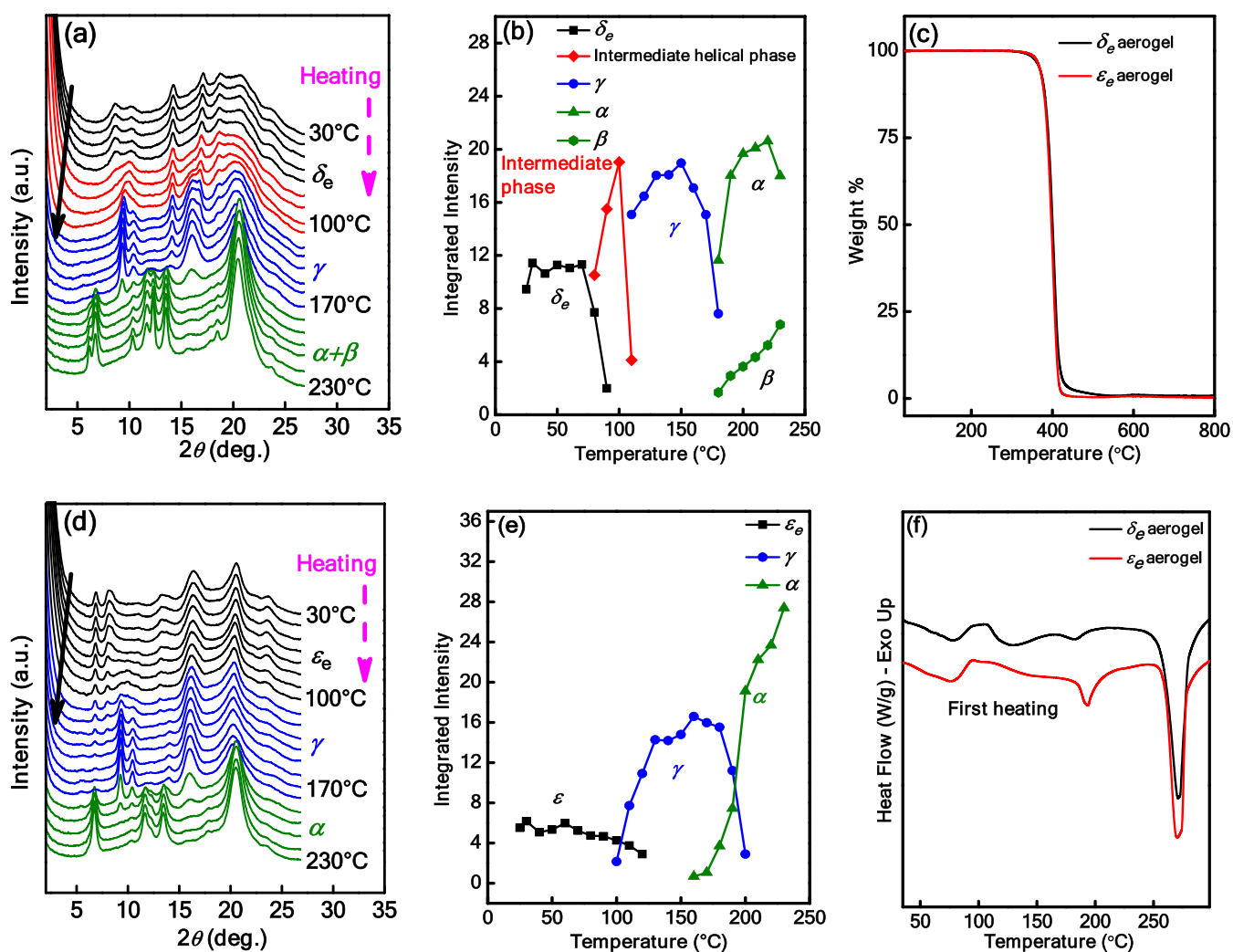
Figure 3. (a) Temperature-dependent WAXD patterns of the δ_e aerogel and (b) corresponding changes in the integrated intensities of representative crystalline reflections of each crystalline form at $2\theta = 8.4°$ (δ_e), $9.8°$ (*intermediate helical phase*), $9.3°$ (γ), $6.2°$ (β), and $6.7°$ (α) during heating. (c) TGA thermograms of δ_e and ε_e aerogels. (d and e) Temperature-dependent WAXD patterns of the ε_e aerogel and the corresponding changes in the integrated intensities of representative crystalline reflections of each crystalline form at $2\theta = 6.9°$ (ε_e), $9.3°$ (γ), and $6.7°$ (α) during heating and (f) DSC thermograms of δ_e and ε_e aerogels in the heating process.

irreversible buckling behavior and were converted to dense solids at higher loads. Even at 75% strain, no fracturing of the aerogels was observed. However, the compressive modulus calculated from the slope of the linear elastic region of the stress−strain curve for the ε_e aerogel was lower (~0.08 MPa) than that of the δ_e aerogel (~0.38 MPa). The difference in the compressive modulus is mainly due to the difference in the microstructure and morphology of these aerogels, which will be discussed in the later section.

A comparison of the SEM images is made in Figure 2 with respect to the surface morphology of δ_e and ε_e aerogels. The macroporous structure of both these aerogels exhibits flakelike morphologies, but the flake sizes are quite small in the ε_e aerogel. The magnified SEM images (Figure 2b,d) show the mesoporous structure where a significant difference in morphology is observed between the δ_e and ε_e forms of sPS aerogels. The microstructure of the ε_e aerogel reveals a mixed morphology of fibers and lamellar structures, unlike the δ_e aerogel with an interconnected fibrillar network morphology. The lamellar structures exhibit sizes approximately in the range of 0.5−1 μm, whereas the fiber diameters will be a few tens of nanometers.

The morphology of the freeze-dried ε_e aerogel is comparable to the morphology of the reported ε_e aerogel prepared from the supercritical drying process, albeit the slight changes in dimensions of the lamellar structures.[30] The difference in the morphology between δ_e and ε_e aerogels can be attributed to the difference in polymer−solvent interactions, the presence of a nonsolvent in the case of the ε gel, the rate of solvent crystal sublimation during freeze-drying, etc. The BET surface areas obtained from nitrogen adsorption−desorption isotherms for δ_e and ε_e aerogels are 301 and 227 m^2 g^{-1}, respectively. The micrometer-sized lamellar structures in the ε_e aerogel lower its overall surface area when compared with the all fibrous network structure of the δ_e aerogel. Both samples exhibit typical type IV adsorption isotherms, confirming the mesoporous nature of the sPS aerogels (Figure 2e). The distribution of pore diameters is broad, covering all of the mesopores and some of the macropores, as shown in the pore-size distribution curves in Figure 2f. In the 20−50 nm range, the ε_e aerogel has the highest pore volume, indicating the presence of a higher fraction of mesopores. Also, the peak of the distribution curve comes in the mesoporous range for the ε_e aerogel, whereas it is beyond 50 nm
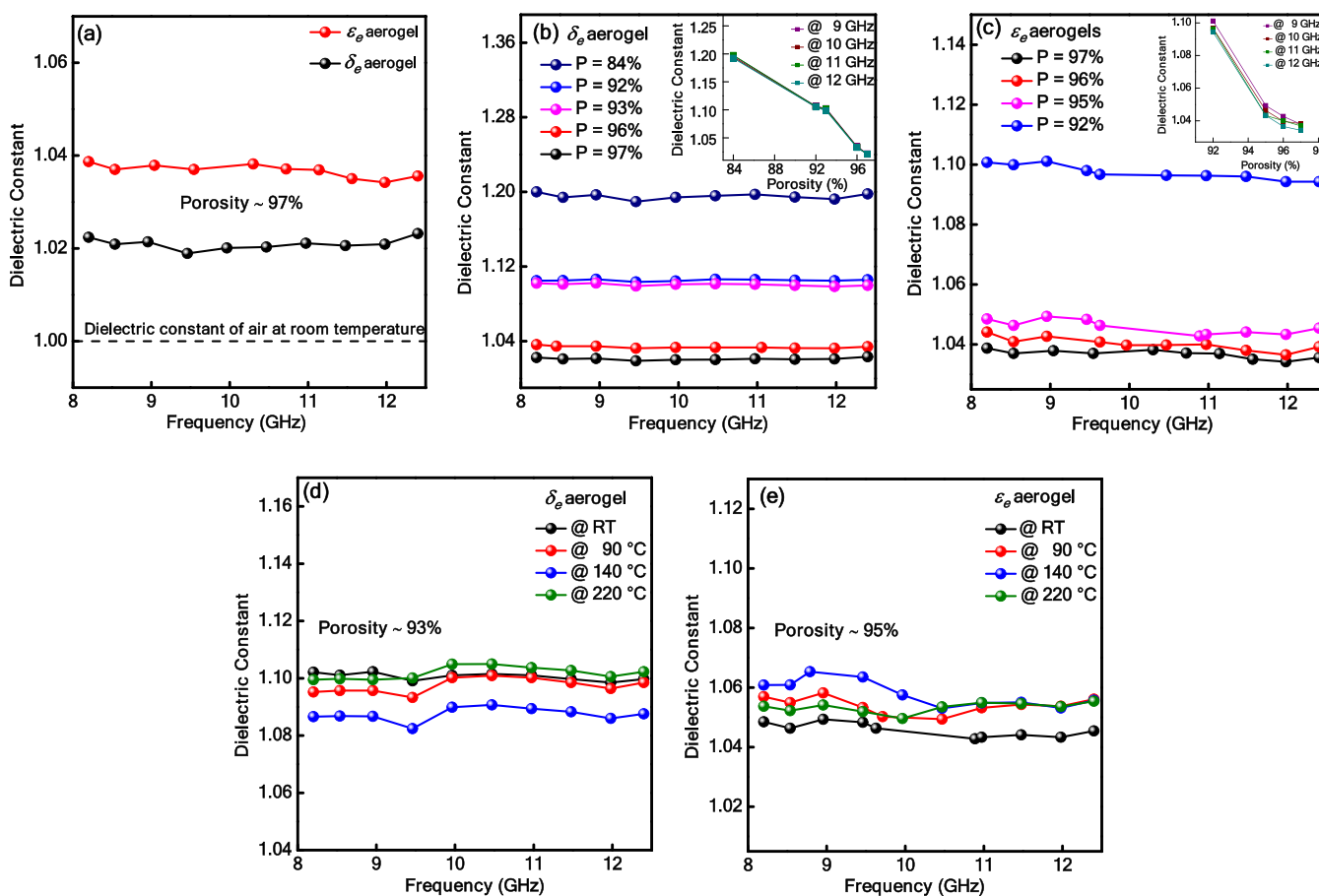
Figure 4. Dielectric constants of various samples in the X-band of the microwave frequency region. (a) Comparison of the dielectric constants of δ_e and ε_e aerogels having porosity = 97%; (b and c) dielectric constants of various δ_e and ε_e aerogels having different porosities, and the variation of dielectric constant as a function of porosity is shown in the insets of (b) and (c) at different frequencies; and (d and e) effect of annealing temperature on the dielectric constants of δ_e and ε_e aerogels.

in the case of the δ_e aerogel. X-ray diffraction, SEM, and BET surface area measurements revealed the presence of macro-, meso-, and microporous structures in both δ_e and ε_e aerogels.

Crystalline Transitions of δ_e and ε_e Aerogels of sPS upon Heating. Thermally induced crystalline transitions of the δ_e form are investigated extensively in the literature using an unoriented film, powder, and uniaxially oriented samples.[41,42,45,46,49,57] On the other hand, only one study appeared on thermally induced crystalline transitions of the ε_e form using thermally annealed unoriented films.[45] Further, this study did not focus on the high-temperature transitions of the ε_e form. In that study, the ε_e form was prepared using the previously known procedure, i.e., chloroform sorption and desorption in the γ form films, and this procedure always leads to the formation of the ε_e form with traces of the δ_e and/or γ form. In the present investigation, we have systematically compared the thermally induced crystalline transitions of δ_e and ε_e aerogels (high-purity crystalline forms) using temperature-dependent measurements of WAXD and DSC. Figure 3 shows the temperature-dependent WAXD patterns of δ_e and ε_e aerogels in the temperature range of 30−230 °C, and the patterns were recorded at 10 °C intervals. The temperature-dependent WAXD patterns of the δ_e aerogel are shown in Figure 3a, and changes in the integrated intensities of the representative crystalline reflection of each crystalline form at 2θ = 8.4° (δ_e), 9.8° (*intermediate phase*), 9.3° (γ), 6.2° (β), and 6.7° (α) were evaluated by deconvolution and plotted against the temperature, as shown in Figure 3b. The crystalline

reflections corresponding to the δ_e form disappeared completely in the temperature range of 70−90 °C. In accordance with the literature,[41,42,45,57] the δ_e form aerogel transiently transformed into the "*intermediate helical phase*" in the temperature range of 80−110 °C. On further heating, the intermediate phase transformed into the γ form. It was speculated that the crystalline cavities present in the δ_e form were responsible for this unusual formation of the intermediate form as it was not observed in the δ cocrystalline form.[41] It is worth mentioning here that the strong diffuse scattering observed at low 2θ (<4°) disappeared completely once the structure transformed from the δ_e form into the γ form (indicated with an arrow mark in Figure 3a). This observation further confirms the disappearance of the crystalline porosity (microporosity) during the crystalline transition from the δ_e to the γ form. On further heating, the γ form transformed into a mixture of α and β forms above 180 °C. In the literature, it was shown that the γ form transformed exclusively into the kinetically favorable α form in the case of the powder samples.[46] Gowd et al. reported the β crystal formation along with α crystals for the thick δ-form film (cocrystals) and proposed that the residual solvent molecules residing in the amorphous regions of the δ or γ form films triggered the formation of the β form.[47] However, when the same group used the uniaxially oriented δ_e samples with no residual solvents, again a minor fraction of the β form was observed along with the α form at a higher temperature (>180 °C).[41] In the present study, as evident from the TGA thermogram (Figure 3c), the

presence of a residual solvent is almost nil both in δ_e and ε_e aerogels of sPS. As discussed above, in the case of δ_e aerogels, at a higher temperature, fractions of thermodynamically stable β form are observed along with the α form. The reason for the appearance of the β form will be discussed in the forthcoming section.

The temperature-dependent WAXD patterns of the ε_e aerogel and the temperature dependence of the integrated intensities of the reflections at $2\theta = 6.9°$ (ε_e), $9.3°$ (γ), and $6.7°$ (α) evaluated from the WAXD patterns are shown in Figure 3d,e. Unlike the δ_e form, the transition from the ε_e aerogel did not show the intermediate helical phase on heating. A direct transition from the ε_e to γ form is observed, and these two crystalline forms coexist in the temperature range of 100–120 °C, which is consistent with the results obtained by Rizzo et al. for nanoporous ε-form films.[45] It is worth adding here that although the channel-shaped cavities are present in the ε_e form, the transition from the ε_e to γ form occurred smoothly without the formation of the intermediate helical phase as observed in the case of the δ_e form. Similar to the δ_e form, in this case also the strong diffuse scattering at lower 2θ disappeared completely when the ε_e form is fully transformed into the γ form (Figure 3d), indicating the disappearance of channel-shaped cavities during the transition. At higher temperatures, the γ form transformed exclusively into the α form (180–200 °C). No trace of the β form is observed as in the case of the δ_e aerogel. These results suggest that crystalline transitions occurred differently on heating the nanoporous crystalline forms (δ_e and ε_e) of sPS. Based on the present study, we may say that the thermodynamically stable β form achieved at the higher temperatures in the δ_e aerogel could be from the energy changes associated with the formation of the intermediate helical phase. The isolated cavities present in the crystal structure of the δ_e form plays a major role in the formation of the intermediate helical phase during the transition from the δ_e to the γ form and also the thermodynamically stable β form at the higher temperature.

Figure 3f shows the DSC thermograms of δ_e and ε_e aerogels in the heating process at 10 °C/min. Based on the temperature-dependent WAXD results, the endotherm followed by the exotherm in the temperature range of 80–120 °C can be assigned to the δ_e to intermediate helical phase to γ form transition in the case of heating of the δ_e aerogel and the ε_e to γ form transition in the case of heating of the ε_e aerogel. At a higher temperature, both δ_e and ε_e aerogels show an endothermic peak in the temperature range of 170–200 °C corresponding to the γ to $\alpha(\beta)$ or γ to α form transitions. The endothermic peak observed at around 270 °C is due to the melting of the $\alpha(\beta)$ or α form of sPS.

Dielectric Properties of δ_e and ε_e Aerogels of sPS. Dielectric properties of the prepared aerogels were investigated using a microwave transmission waveguide technique. The reliability of this method was proven in our previous work by fitting the measured dielectric constants of sPS aerogels to some of the theoretical models.[29] Because of their microstructure and high porosity, aerogels are inherently low dielectric constant materials. In 1993, Hrubesh et al. reported a dielectric constant less than 1.03 for silica aerogels with 99% porosity, which turned out to be the lowest value ever reported for a bulk solid material.[58] We measured the dielectric constants of δ_e and ε_e aerogels in the microwave frequency range of 8–12 GHz (X-band) of the electromagnetic spectra and obtained consistent values in the entire frequency range. Figure 4a shows the measured dielectric constants of crystalline nanoporous sPS

aerogels with ~97% porosity. The δ_e aerogel has a dielectric constant of 1.02 ± 0.02, whereas the ε counterpart shows a value of 1.03 ± 0.02. Further, we have prepared a series of samples of both types with varying porosities and measured their dielectric constants. The dielectric constant increased roughly from 1.02 to 1.2 for the δ_e aerogel as the porosity decreased from 97 to 84% (Figure 4b), and the ε_e aerogel also exhibited a similar trend (Figure 4c). This means that by tuning the bulk density/porosity of the aerogels, the dielectric constant values could be easily tuned. It has been shown that the dielectric constant varies linearly with aerogel density using silica, polyimide, and polyamide aerogels.[5,58,59] Density of aerogels is inversely proportional to their porosity, and therefore, as a general rule, we could say that dielectric constant vs porosity showcases a linear relationship. This was proved using δ_e and ε_e aerogels, as shown in the insets of Figure 4b,c, respectively. An inverse linear variation of the dielectric constant against porosity at all X-band frequencies is observed for both δ_e and ε_e aerogels, i.e., the lower the porosity, the higher the dielectric constant. Thus, by tailoring the morphology and porosity of sPS aerogels, their applicability in the field of microelectronics can be widened.

As discussed in the preceding section, both δ_e and ε_e aerogels undergo crystalline transitions upon heating. Various aerogels with different crystalline forms were obtained by annealing the δ_e and ε_e aerogels for 1 h at three different temperatures, namely, 90, 140, and 220 °C. Annealing at these temperatures resulted in aerogels with the intermediate helical phase (in the case of the δ_e aerogel), γ, and $\alpha(\beta)/\alpha$ crystalline phases. Above 100 °C, the micropores within the crystal lattice are erased and the structure is reorganized to the γ form. In this study, the dielectric constants of various crystalline forms are compared. As the dielectric constant of an sPS aerogel depends heavily on its overall porosity, measurement of the dielectric constant of aerogels with crystalline nanoporosity will reveal the influence of microporosity. It has to be noted that by annealing the samples at higher temperatures, some of the meso- as well as the macropores are getting collapsed along with the micropores. Therefore, it is not correct to correlate the dielectric constants of the samples at ambient conditions and after annealing, as the total porosity of the starting samples will be reduced significantly upon annealing. Instead, to probe the effect of polymer chain packing (crystalline forms) on the dielectric constant, we have annealed the samples at the abovementioned temperatures in such a way that the overall porosity of the final samples remains the same by choosing aerogels of varying porosities as the starting material. We have taken δ_e aerogels with starting porosities of 94, 95, and 97% and annealed them at 90, 140, and 220 °C, respectively. After the annealing process, the porosity of all the three samples was reduced to ~93% as the extent of shrinkage to the samples increases with the increase in the annealing temperature. Figure 4d shows the dielectric constants of the δ_e aerogel at room temperature and after annealing at 90, 140, and 220 °C. All of the samples are nearly 93% porous but differ in their crystal structure. However, the values obtained for these samples were more or less the same, within the limits of experimental error. The lattice packing of polymer chains does not seem to have a visible effect on the eventual dielectric behavior of the sPS aerogel samples. A similar study was carried out using ε_e aerogels, where the total porosity was 95% and similar results were obtained, as shown in Figure 4e.

Thermal Conductivity and Acoustic Properties of δ_e and ε_e Aerogels. sPS aerogels can be excellent thermal insulation materials because of their highly porous network
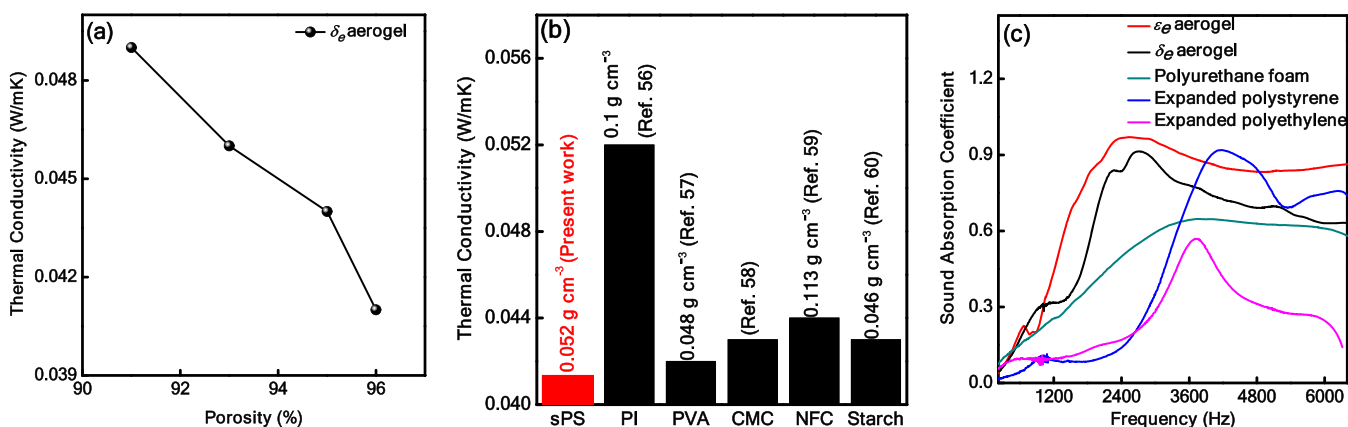
Figure 5. (a) Plot of thermal conductivity of the δ_e aerogel as a function of porosity; (b) comparison of the thermal conductivity obtained in the present work with those of reported aerogels prepared by freeze-drying (the density of the sample and reference numbers are provided near the data point); and (c) normal incident sound absorption coefficients of δ_e and ε_e aerogels measured in the frequency range of 300−6400 Hz and compared with other commercially available sound insulation materials like EPS, PU foam, and EPE.

structure. Thermal transport in aerogels takes place mainly through three mechanisms: solid conduction, gaseous conduction, and radiative transmission. The summation of these three components brings about the total thermal conductivity (λ) of the aerogel. As reported earlier, the λ of bulk sPS lies in the range of 0.2−0.3 W m^{-1} K^{-1}.[51] On conversion to an aerogel, the λ of sPS reduces drastically and the values obtained for δ_e and ε_e aerogels (porosity ~95%) are 0.044 and 0.043 W m^{-1} K^{-1}, respectively. The obvious reason for the massive reduction in λ of the aerogel is because it is mostly air, and the λ of air is 0.02 W m^{-1} K^{-1}.[60] On increasing the porosity of the samples, we could attain further diminution in the thermal conductivity of aerogels, for example, 0.041 W m^{-1} K^{-1} is the value obtained for the δ_e aerogel with a porosity of ~96%. The thermal conductivity of expanded polystyrene boards demonstrated by Mıhlayanlar et al. is of the order of 0.04 W m^{-1} K^{-1}.[61] Similar to the dielectric studies, we did a systematic analysis of aerogels with varying porosities to understand the relation of porosity with thermal conductivity. From Figure 5a, it is clear that as the porosity decreases, thermal conduction through the δ_e aerogel increases, and this relation is monotonic. A similar trend can be expected in the case of the ε_e aerogel also. When considering the thermal transport mechanism, solid conduction through the polymer backbone appears to be the major contributor to heat conduction. Since sPS aerogels are predominantly mesoporous, i.e., pore sizes are less than 50 nm, a strong Knudsen effect will be induced in the system. As the majority of the pores are smaller in size than the mean free path of the gas molecules in free space (~70 nm), the gas molecules undergo collisions with the pore walls before their interactive scattering, resulting in the lowering of gaseous conduction.[7] This explains why the thermal conductivity is slightly lower in the ε_e aerogel than the δ_e aerogel of the same porosity. The solid conduction of a particular material is its intrinsic property. However, as the morphology suggests, the sPS aerogel is composed of weakly connected polymer fibrils, and these weak connections between the nanofibers reduce the heat transfer through the polymer backbone, eventually resulting in lower total thermal conductivity.[53] Figure 5b compares the thermal conductivity of sPS aerogels with some of the polymer-based aerogels reported in the literature prepared by the freeze-drying method, and sPS aerogels investigated here showed comparable or even lesser values.[62−66] The neat polyimide aerogels prepared by Fan et al.

exhibited a higher thermal conductivity (0.052 W m^{-1} K^{-1}) than the sPS aerogels.[62] The ultralow and easily tunable thermal conductivity of crystalline nanoporous sPS aerogels opens up a wider application prospect to these materials as thermal insulators in the fields of building insulation, cryogenic flasks, and packaging.

At times, thermal insulating aerogels can have excellent sound absorption ability also, which is a direct consequence of their highly porous structure. The normal incident sound absorption coefficients, i.e., the ratio of absorbed sound intensity in the material to the incident sound intensity, of δ_e and ε_e aerogels at various frequencies (300−6400 Hz) are shown in Figure 5c along with the values obtained for the commercial sound insulators such as expanded polystyrene (EPS), polyurethane (PU) foam, and expanded polyethylene (EPE). All of the samples used for measurements were cylindrical with 12 mm thickness. The absorption coefficients of all of the samples were low initially but improved gradually with the increase in frequency. sPS aerogels showed better absorption ability than commercial materials even at the lower frequencies. EPS has a maximum absorption of 92% at around 4000 Hz. However, it showed very low absorption values (<20%) up to 2500 Hz. On the contrary, the ε_e aerogel absorbed more than 80% of the incident sound waves beyond 1800 Hz consistently with an obvious peak of 97% between 2300 and 3000 Hz. In the same frequency range, the values obtained for EPS and EPE are less than 30 and 60%, respectively. All these commercial insulators are predominantly macroporous in nature. The δ_e aerogel showed results similar to the ε_e aerogel but with slightly lower absorption ability. The peak maximum was 92% for the δ_e aerogel in the frequency range of 2600−2800 Hz. The excellent acoustic performance of nanoporous crystalline sPS aerogels can be attributed to their highly mesoporous structure. As the sound waves enter a highly porous structure like a sPS aerogel, multiple scattering phenomena and the increased vibration of the pore walls result in the effective attenuation of sound waves. The tortuosity of wave propagation caused by channel twists and turns and the nanosized pores result in enhanced friction and air viscosity consumption, thereby improving the sound absorption performance.[6,67] As mentioned earlier, the δ_e aerogel has a lower sound absorption capability than the ε_e aerogel, and this could be attributed to the difference in their morphologies. The mesoporous morphology of the ε_e aerogel provides more area on
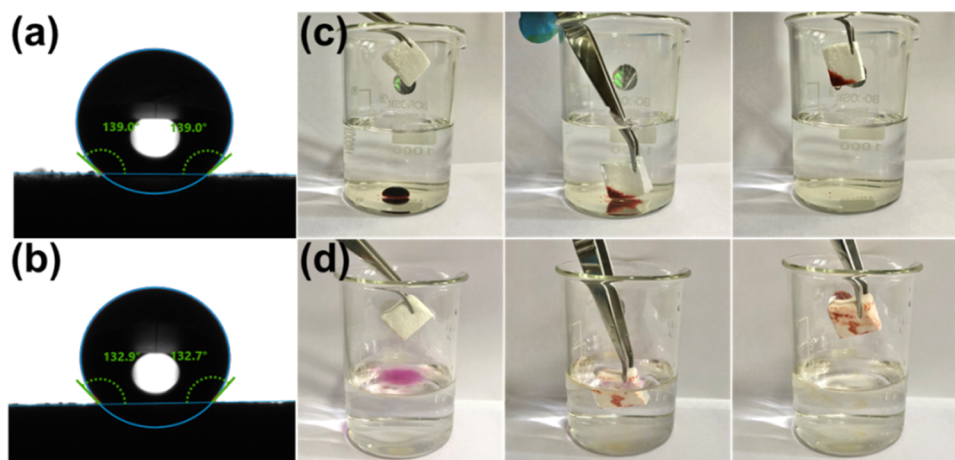
Figure 6. Water contact angles for (a) δ_e and (b) ε_e aerogels. The removal process of (c) dichloromethane and (d) hexane from water using the δ_e aerogel.

the pore walls for the sound waves to get scattered. As a result, the magnitude of sound scattering and, therefore, the vibration of pore walls will be more in the ε_e aerogel, resulting in better sound absorption performance. sPS aerogels can be good alternatives to the traditional acoustic insulators because of their superior sound absorption ability over a broad range of frequencies.

Oil/Organic Solvent−Water Separation using δ_e and ε_e Aerogels. The water contact angle (WCA) measurements were carried out on sPS aerogels to study their surface wettability, and the values obtained for δ_e and ε_e aerogels with 96% porosity were 139 ± 2 and 132.7 ± 2°, respectively. The images of water droplets on the surface of δ_e and ε_e aerogels are, respectively, shown in Figure 6a,b. The water droplets remained stable on the aerogel surface without reduction in the WCA over a long period of time. This indicates the highly hydrophobic nature of the prepared aerogels, which is attributed to the inherent hydrophobicity of sPS and the surface roughness of aerogels created by the different levels of porosity.[32] When these aerogels were immersed in water using an external force, no water absorption was observed, and the moment the external forces were removed, the samples rose to the surface. This property of sPS aerogels could well be utilized for the oil/organic solvent−water separation process. Figure 6c and Movie S1 display the selective absorption of dichloromethane stained with iodine from under the water using the δ_e aerogel. The solvent droplets are readily absorbed by the aerogel within a few seconds, indicating its high oleophilicity. Figure 6d shows hexane colored with iodine floating on the surface of the water and being completely removed using the δ_e aerogel. Similarly, pump oil and petrol floating on the surface of water were selectively recovered using sPS aerogels with great efficiency (Movies S2 and S3). Thus, the combination of high hydrophobicity and oleophilicity makes sure that δ_e and ε_e aerogels are superior oil/organic solvent absorbers. Guerra and co-workers showed a high sorption capacity of organic solvents even from very dilute aqueous solutions using crystalline nanoporous sPS aerogels.[28,30,68] To regenerate the δ_e and ε_e aerogels for further absorption process, the oil/solvent-filled aerogels were washed with ethanol and dried in an oven at 60 °C for 60 min. After the washing process, oils/organic solvents can be separated from ethanol by suitable procedures.

CONCLUSIONS

In summary, we have developed sPS aerogels with isolated (δ_e) and channel-shaped (ε_e) crystalline nanocavities by a facile and feasible freeze-drying technique. The gel solvents were exchanged with green solvents such as ethanol and water, which makes the entire process eco-friendly. δ_e and ε_e aerogels with porosity as high as 97% were obtained, and we were able to tune the porosity of aerogels by the careful control of the preparation steps. The intricate polymorphic changes occurring in these aerogels were studied using variable temperature WAXD, which revealed some of the fundamental aspects of sPS phase transitions. The dielectric measurements carried out on the aerogels demonstrated the linear relationship between the dielectric constant and porosity. Ultralow values for dielectric constant (1.02 ± 0.02) and low thermal conductivity (∼0.04 W m^{-1} K^{-1}) were obtained for both types of sPS aerogels. Also, high sound absorption coefficients were obtained, particularly for the ε_e aerogel (∼0.97), which has a higher fraction of mesopores. The surface wettability of aerogels was estimated using WCA measurements (∼139°), and their highly hydrophobic and oleophilic nature could be utilized for the oil−water separation process. Crystalline nanoporous aerogels of sPS thus proved to be multifunctional aerogels with prospected applications in microelectronics, thermal/acoustic insulation, and oil/solvent spill cleanup.

EXPERIMENTAL SECTION

Materials. sPS (M_w: 272 000 and Đ: 2.28) used in this study was kindly supplied by Idemitsu Petrochemical Co., Ltd. (Japan). The solvent used for δ gel preparation was a mixture of isomers of xylene, purchased from Merck, India. Chloroform (Sigma-Aldrich Co.) and acrylonitrile (TCI Co., Ltd.) were used for the preparation of the ε gel. The polymer and all of the above solvents were used as received. The solvent exchange was done using ethanol (S.D. Fine Chemicals) and distilled water.

Preparation of the δ Form Aerogel of sPS. The δ form sPS aerogel was prepared according to our previous report.[29] Briefly, sPS pellets were dissolved in xylene by heating above 140 °C (boiling point of xylene). After complete dissolution of the polymer, the solution with a polymer concentration of 3 wt % was transferred to plastic molds and cooled down to room temperature at a rate of 1.5 °C/min, where gelation occurred. The as-obtained gels were aged at room temperature for 3 h, and the solvent was exchanged systematically by immersing the gel in different solvents and solvent mixtures. In the first step, the organogels were fully immersed in ethanol to exchange the pre-existing

xylene, and then, the solvents were removed by decantation. In the second step, the gels were repeatedly washed with a mixture of ethanol/distilled water. Initially, ethanol content was kept high in the solvent mixture (ethanol/distilled water (75/25 v/v)) and then the gels were washed by changing the compositions of ethanol/distilled water mixture, where the water content was slowly increased. In the final step, the gels were immersed exclusively in water for 1 h to obtain hydrogels. The entire solvent exchange process was carried out for 12 h. The as-obtained hydrogels were transferred to an ultralow temperature (ULT) freezer (at −60 °C) and frozen for 12 h and then lyophilized. Rotary evaporation of the solvent mixtures obtained after the solvent exchange process was carried out to separate and recover xylene.

Preparation of the ε Form Aerogel of sPS. The freeze-drying technique was used to prepare the ε form of sPS aerogels with the aid of a systematic solvent exchange procedure. To prepare the ε gel of sPS, a combination of chloroform (solvent) and acrylonitrile (nonsolvent) was used. sPS pellets were first dissolved completely in chloroform in a tightly sealed setup by heating above the boiling point of chloroform (60 °C). Then, a slightly hot mixture of chloroform and acrylonitrile (volume ratio 1:2) was slowly added to the polymer solution with stirring. The final solution was immediately transferred to plastic molds and cooled down to room temperature at a rate of 1.5 °C/min. The ε gel thus obtained was aged for 2 h at room temperature and subjected to solvent exchange as earlier. This was followed by freezing of hydrogel at −60 °C for 12 h in a ULT freezer and freeze-drying to obtain the ε form of sPS aerogels with 100% crystalline purity. In the final solution, the polymer concentration was 3 wt % and the volume ratio of chloroform to acrylonitrile was 1:1. Similar to the above case, a rotary evaporator was used for the recovery of solvents (chloroform and acrylonitrile). We prepared both δ_e and ε_e aerogel samples with different shapes and dimensions for various characterizations, the largest being 5 cm × 5 cm × 2 cm in dimension.

Characterization. The total porosity of different sPS aerogel samples was determined from the density values using the following equation

$$P = 100 \left[1 - \frac{\rho_{ap}}{\rho_{pol}} \right]$$

(1)

where ρ_{ap} is the mass/volume ratio (apparent density) of the prepared aerogel (volume is determined theoretically from the dimensions of the samples) and ρ_{pol} is the density of the bulk polymer. A universal testing machine (Hounsfield, H5KS UTM, Redhill, U.K.) with a crosshead speed of 1.0 mm min^{-1} was used for the compressive strength analysis of the aerogels and cylindrical samples with a diameter-to-height ratio of approximately 1:1 were used for the measurements. Scanning electron microscopy was employed to examine the morphologies of various samples and the measurements were performed using a Zeiss EVO 18 cryo-SEM operating at an accelerating voltage of 15 kV. The water contact angle of the samples was measured at room temperature using an automated DSA30 Drop Shape Analyzer, KRÜSS, Germany. The measurements were carried out at different regions on the same aerogel as well as on the same region of the aerogel over a period of 15 min. From the nitrogen adsorption−desorption isotherm (Gemini 2375, Micromeritics, Norcross), the Brunauer−Emmett−Teller (BET) surface area of the porous aerogels was measured. The samples were degassed at room temperature for 24 h before the measurement. The pore-size distributions were also obtained from the isotherms using the Barrett−Joyner−Halenda (BJH) method. Phase formations in aerogels were confirmed using wide-angle X-ray diffraction (WAXD) measurements on a XEUSS SAXS/WAXS system from Xenocs operated at 50 kV and 0.60 mA in the transmission mode using Cu Kα radiation of wavelength 1.54 Å. The two-dimensional patterns were recorded on a Mar 345 image plate system (detector), and the Fit2D software was used for data processing. Variable temperature WAXD measurements were carried out with the aid of a Linkam THMS 600 hot stage connected to the LNP 95 cooling system to understand the phase transformation behavior of various aerogel samples. The samples were heated from room temperature at a rate of 10 °C/min to 230 °C and the X-ray patterns were acquired at 10 °C intervals, after a dwell time of 11

min at each temperature. Phase transitions were confirmed using an advanced research-grade modulated differential scanning calorimeter (DSC) TA Q2000 under a nitrogen atmosphere by heating the samples from room temperature up to 300 °C at a rate of 10 °C/min. To confirm the complete drying of aerogels, thermogravimetric analysis (TGA) was carried out under continuous nitrogen flow using TA Q50, a fourth-generation thermogravimetric analyzer. The samples were heated from room temperature to 800 °C at a rate of 10 °C/min. The dielectric constants were measured using a vector network analyzer (Model No. E5071C, ENA series, 300 kHz-20 GHz; Agilent Technologies, Santa Clara) by a waveguide technique in the X-band (8.2−12.4 GHz) of the microwave frequency. The samples were annealed at various temperatures by keeping them in a vacuum oven for 1 h at a required preset temperature, and the corresponding phase formations were confirmed using WAXD before the dielectric measurements. For the X-band, samples used were of the dimension 22.86 × 10.8 mm^2. The thermal conductivity (λ) of aerogels was measured with a TCi thermal conductivity analyzer (C-Thermo Technologies Ltd., Canada) using the transient plane method. The samples with thickness not less than 10 mm were used, and five measurements were done for each sample, the average value of which was taken as the final thermal conductivity. The normal incident sound absorption coefficient of all of the samples was obtained using a Brüel & Kjær impedance tube, type 4206 (Denmark). Cylindrical samples with a diameter of 29 mm and thickness of 12 mm were used for measurements in the frequency band from 300 to 6400 Hz via the two-microphone method.

■ ASSOCIATED CONTENT

ⓈI Supporting Information

The Supporting Information is available free of charge at https://pubs.acs.org/doi/10.1021/acs.macromol.1c01555.

Movies: Selective absorption of solvent, pump oil, and petrol from water using aerogels (MOV)

(MOV)

(MOV)

■ AUTHOR INFORMATION

Corresponding Author

E. Bhoje Gowd − *Materials Science and Technology Division CSIR-National Institute for Interdisciplinary Science and Technology, Trivandrum 695019 Kerala, India; Academy of Scientific and Innovative Research (AcSIR), Ghaziabad 201002, India;* ⓞ orcid.org/0000-0002-2878-5845; Phone: +91-471-2515474; Email: bhojegowd@niist.res.in; Fax: +91-471-2491712

Authors

Vipin G. Krishnan − *Materials Science and Technology Division CSIR-National Institute for Interdisciplinary Science and Technology, Trivandrum 695019 Kerala, India; Academy of Scientific and Innovative Research (AcSIR), Ghaziabad 201002, India*

Angel Mary Joseph − *Materials Science and Technology Division CSIR-National Institute for Interdisciplinary Science and Technology, Trivandrum 695019 Kerala, India*

Surendran Kuzhichalil Peethambharan − *Materials Science and Technology Division CSIR-National Institute for Interdisciplinary Science and Technology, Trivandrum 695019 Kerala, India; Academy of Scientific and Innovative Research (AcSIR), Ghaziabad 201002, India;* ⓞ orcid.org/0000-0001-5269-1489

Complete contact information is available at:
https://pubs.acs.org/10.1021/acs.macromol.1c01555

DEDICATION

[†]Dedicated to Dr. Swaminathan Sivaram on the occasion of his 75th birthday.

REFERENCES

(1) Kistler, S. S. Coherent Expanded Aerogels and Jellies. *Nature* **1931**, *127*, 741.

(2) Teo, N.; Gu, Z.; Jana, S. C. Polyimide-based aerogel foams, via emulsion-templating. *Polymer* **2018**, *157*, 95−102.

(3) Randall, J. P.; Meador, M. A. B.; Jana, S. C. Tailoring Mechanical Properties of Aerogels for Aerospace Applications. *ACS Appl. Mater. Interfaces* **2011**, *3*, 613−626.

(4) Wang, X.; Pan, Y.; Liu, X.; Liu, H.; Li, N.; Liu, C.; Schubert, D. W.; Shen, C. Facile Fabrication of Superhydrophobic and Eco-Friendly Poly(lactic acid) Foam for Oil−Water Separation via Skin Peeling. *ACS Appl. Mater. Interfaces* **2019**, *11*, 14362−14367.

(5) Meador, M. A. B.; Wright, S.; Sandberg, A.; Nguyen, B. N.; Van Keuls, F. W.; Mueller, C. H.; Rodríguez-Solís, R.; Miranda, F. A. Low Dielectric Polyimide Aerogels As Substrates for Lightweight Patch Antennas. *ACS Appl. Mater. Interfaces* **2012**, *4*, 6346−6353.

(6) He, C.; Huang, J.; Li, S.; Meng, K.; Zhang, L.; Chen, Z.; Lai, Y. Mechanically Resistant and Sustainable Cellulose-Based Composite Aerogels with Excellent Flame Retardant, Sound-Absorption, and Superantiwetting Ability for Advanced Engineering Materials. *ACS Sustainable Chem. Eng.* **2018**, *6*, 927−936.

(7) Li, M.; Qin, Z.; Cui, Y.; Yang, C.; Deng, C.; Wang, Y.; Kang, J. S.; Xia, H.; Hu, Y. Ultralight and Flexible Monolithic Polymer Aerogel with Extraordinary Thermal Insulation by A Facile Ambient Process. *Adv. Mater. Interfaces* **2019**, *6*, No. 1900314.

(8) Illera, D.; Mesa, J.; Gomez, H.; Maury, H. Cellulose Aerogels for Thermal Insulation in Buildings: Trends and Challenges. *Coatings* **2018**, *8*, No. 345.

(9) Zhao, S.; Malfait, W. J.; Guerrero-Alburquerque, N.; Koebel, M. M.; Nyström, G. Biopolymer Aerogels and Foams: Chemistry, Properties, and Applications. *Angew. Chem., Int. Ed.* **2018**, *57*, 7580−7608.

(10) De France, K. J.; Hoare, T.; Cranston, E. D. Review of Hydrogels and Aerogels Containing Nanocellulose. *Chem. Mater.* **2017**, *29*, 4609−4631.

(11) Asim, N.; Badiei, M.; Alghoul, M. A.; Mohammad, M.; Fudholi, A.; Akhtaruzzaman, M.; Amin, N.; Sopian, K. Biomass and Industrial Wastes as Resource Materials for Aerogel Preparation: Opportunities, Challenges, and Research Directions. *Ind. Eng. Chem. Res.* **2019**, *58*, 17621−17645.

(12) Daniel, C.; Alfano, D.; Venditto, V.; Cardea, S.; Reverchon, E.; Larobina, D.; Mensitieri, G.; Guerra, G. Aerogels with a Microporous Crystalline Host Phase. *Adv. Mater.* **2005**, *17*, 1515−1518.

(13) Daniel, C.; Dammer, C.; Guenet, J.-M. On the definition of thermoreversible gels: the case of syndiotactic polystyrene. *Polymer* **1994**, *35*, 4243−4246.

(14) Daniel, C.; Menelle, A.; Brulet, A.; Guenet, J.-M. Thermoreversible gelation of syndiotactic polystyrene in toluene and chloroform. *Polymer* **1997**, *38*, 4193−4199.

(15) Daniel, C.; Alfano, D.; Guerra, G.; Musto, P. Physical Gelation of Syndiotactic Polystyrene in the Presence of Large Molar Volume Solvents Induced by Volatile Guests of Clathrate Phases. *Macromolecules* **2003**, *36*, 1713−1716.

(16) Gowd, E. B.; Tashiro, K.; Ramesh, C. Structural phase transitions of syndiotactic polystyrene. *Prog. Polym. Sci.* **2009**, *34*, 280−315.

(17) Mochizuki, J.; Sano, T.; Tokami, T.; Itagaki, H. Decisive properties of solvent able to form gels with syndiotactic polystyrene. *Polymer* **2015**, *67*, 118−127.

(18) Itagaki, H.; Tokami, T.; Mochizuki, J. A trial to clarify a cause of forming physical gels: Morphology of syndiotactic polystyrene in n-alkylbenzene. *Polymer* **2012**, *53*, 5304−5312.

(19) Daniel, C.; Zhovner, D.; Guerra, G. Thermal Stability of Nanoporous Crystalline and Amorphous Phases of Poly(2,6-dimethyl-1,4-phenylene) Oxide. *Macromolecules* **2013**, *46*, 449−454.

(20) Golla, M.; Nagendra, B.; Rizzo, P.; Daniel, C.; Ruiz de Ballesteros, O.; Guerra, G. Polymorphism of Poly(2,6-dimethyl-1,4-phenylene)oxide in Axially Stretched Films. *Macromolecules* **2020**, *53*, 2287−2294.

(21) Matsuda, H.; Inoue, T.; Okabe, M.; Ukaji, T. Study of Polyolefin Gel in Organic Solvents I. Structure of Isotactic Polypropylene Gel in Organic Solvents. *Polym J.* **1987**, *19*, 323−329.

(22) Pogodina, N. V.; Winter, H. H. Polypropylene Crystallization as a Physical Gelation Process. *Macromolecules* **1998**, *31*, 8164−8172.

(23) Dasgupta, D.; Nandi, A. K. Multiporous Polymeric Materials from Thermoreversible Poly(vinylidene fluoride) Gels. *Macromolecules* **2005**, *38*, 6504−6512.

(24) Dikshit, A. K.; Nandi, A. K. Thermoreversible Gelation of Poly(vinylidene flouride) in Diethyl Adipate: A Concerted Mechanism. *Macromolecules* **1998**, *31*, 8886−8892.

(25) Domszy, R. C.; Alamo, R.; Edwards, C. O.; Mandelkern, L. Thermoreversible gelation and crystallization of homopolymers and copolymers. *Macromolecules* **1986**, *19*, 310−325.

(26) Talley, S. J.; Yuan, X.; Moore, R. B. Thermoreversible Gelation of Poly(ether ether ketone). *ACS Macro Lett* **2017**, *6*, 262−266.

(27) Talley, S. J.; Vivod, S. L.; Nguyen, B. A.; Meador, M. A. B.; Radulescu, A.; Moore, R. B. Hierarchical Morphology of Poly(ether ether ketone) Aerogels. *ACS Appl. Mater. Interfaces* **2019**, *11*, 31508−31519.

(28) Daniel, C.; Sannino, D.; Guerra, G. Syndiotactic Polystyrene Aerogels: Adsorption in Amorphous Pores and Absorption in Crystalline Nanocavities. *Chem. Mater.* **2008**, *20*, 577−582.

(29) Joseph, A. M.; Nagendra, B.; Shaiju, P.; Surendran, K. P.; Gowd, E. B. Aerogels of hierarchically porous syndiotactic polystyrene with a dielectric constant near to air. *J. Mater. Chem. C* **2018**, *6*, 360−368.

(30) D'Aniello, C.; Daniel, C.; Guerra, G. ε Form Gels and Aerogels of Syndiotactic Polystyrene. *Macromolecules* **2015**, *48*, 1187−1193.

(31) Figueroa-Gerstenmaier, S.; Daniel, C.; Milano, G.; Vitillo, J. G.; Zavorotynska, O.; Spoto, G.; Guerra, G. Hydrogen Adsorption by δ and ε Crystalline Phases of Syndiotactic Polystyrene Aerogels. *Macromolecules* **2010**, *43*, 8594−8601.

(32) Wang, X.; Jana, S. C. Tailoring of Morphology and Surface Properties of Syndiotactic Polystyrene Aerogels. *Langmuir* **2013**, *29*, 5589−5598.

(33) Daniel, C.; Giudice, S.; Guerra, G. Syndiotatic Polystyrene Aerogels with β, γ, and ε Crystalline Phases. *Chem. Mater.* **2009**, *21*, 1028−1034.

(34) Longo, S.; Vitillo, J. G.; Daniel, C.; Guerra, G. Monolithic Aerogels Based on Poly(2,6-diphenyl-1,4-phenylene oxide) and Syndiotactic Polystyrene. *ACS Appl. Mater. Interfaces* **2013**, *5*, 5493−5499.

(35) Daniel, C.; Pellegrino, M.; Venditto, V.; Aurucci, S.; Guerra, G. Nanoporous-crystalline poly(2,6-dimethyl-1,4-phenylene)oxide (PPO) aerogels. *Polymer* **2016**, *105*, 96−103.

(36) Nagendra, B.; Antico, P.; Daniel, C.; Rizzo, P.; Guerra, G. Thermal shrinkage and heat capacity of monolithic polymeric physical aerogels. *Polymer* **2020**, *210*, No. 123073.

(37) Petraccone, V.; Ruiz de Ballesteros, O.; Tarallo, O.; Rizzo, P.; Guerra, G. Nanoporous Polymer Crystals with Cavities and Channels. *Chem. Mater.* **2008**, *20*, 3663−3668.

(38) Woo, E. M.; Sun, Y. S.; Yang, C. P. Polymorphism, thermal behavior, and crystal stability in syndiotactic polystyrene vs. its miscible blends. *Prog. Polym. Sci.* **2001**, *26*, 945−983.

(39) Immirzi, A.; de Candia, F.; Iannelli, P.; Zambelli, A.; Vittoria, V. Solvent-induced polymorphism in syndiotactic polystyrene. *Makromol. Chem. Rapid Comm.* **1988**, *9*, 761−764.

(40) Chatani, Y.; Shimane, Y.; Inoue, Y.; Inagaki, T.; Ishioka, T.; Ijitsu, T.; Yukinari, T. Structural study of syndiotactic polystyrene: 1. Polymorphism. *Polymer* **1992**, *33*, 488−492.

(41) Gowd, E. B.; Shibayama, N.; Tashiro, K. Structural Changes in Thermally Induced Phase Transitions of Uniaxially Oriented δe Form of Syndiotactic Polystyrene Investigated by Temperature-Dependent Measurements of X-ray Fiber Diagrams and Polarized Infrared Spectra. *Macromolecules* **2006**, *39*, 8412−8418.

(42) Gowd, E. B.; Shibayama, N.; Tashiro, K. Structural Correlation between Crystal Lattice and Lamellar Morphology in the Phase Transitions of Uniaxially Oriented Syndiotactic Polystyrene (δ and δe Forms) As Revealed by Simultaneous Measurements of Wide-Angle and Small-Angle X-ray Scatterings. *Macromolecules* **2008**, *41*, 2541−2547.

(43) Gowd, E. B.; Shibayama, N.; Tashiro, K. Structural Changes during Thermally Induced Phase Transitions Observed for Uniaxially Oriented δ Form of Syndiotactic Polystyrene. *Macromolecules* **2007**, *40*, 6291−6295.

(44) Shaiju, P.; Bhoje Gowd, E. Factors controlling the structure of syndiotactic polystyrene upon the guest exchange and guest extraction processes. *Polymer* **2015**, *56*, 581−589.

(45) Rizzo, P.; D'Aniello, C.; De Girolamo Del Mauro, A.; Guerra, G. Thermal Transitions of ε Crystalline Phases of Syndiotactic Polystyrene. *Macromolecules* **2007**, *40*, 9470−9474.

(46) Gowd, E. B.; Nair, S. S.; Ramesh, C. Crystalline Transitions of the Clathrate (δ) Form of Syndiotactic Polystyrene during Heating: Studies Using High-Temperature X-ray Diffraction. *Macromolecules* **2002**, *35*, 8509−8514.

(47) Gowd, E. B.; Tashiro, K. Effect of Solvent Molecules on Phase Transition Phenomena of Syndiotactic Polystyrene. *Macromolecules* **2007**, *40*, 5366−5371.

(48) Gowd, E. B.; Tashiro, K.; Ramesh, C. Role of Solvent Molecules as a Trigger for the Crystal Phase Transition of Syndiotactic Polystyrene/Solvent Complex. *Macromolecules* **2008**, *41*, 9814−9818.

(49) Gowd, E. B.; Nair, S. S.; Ramesh, C.; Tashiro, K. Studies on the Clathrate (δ) Form of Syndiotactic Polystyrene Crystallized by Different Solvents Using Fourier Transform Infrared Spectroscopy. *Macromolecules* **2003**, *36*, 7388−7397.

(50) Kim, S. J.; Chase, G.; Jana, S. C. Polymer aerogels for efficient removal of airborne nanoparticles. *Sep. Purif. Technol.* **2015**, *156*, 803−808.

(51) Rossinsky, E.; Müller-Plathe, F. Anisotropy of the thermal conductivity in a crystalline polymer: Reverse nonequilibrium molecular dynamics simulation of the δ phase of syndiotactic polystyrene. *J. Chem. Phys.* **2009**, *130*, No. 134905.

(52) Rizvi, A.; Chu, R. K. M.; Park, C. B. Scalable Fabrication of Thermally Insulating Mechanically Resilient Hierarchically Porous Polymer Foams. *ACS Appl. Mater. Interfaces* **2018**, *10*, 38410−38417.

(53) Samitsu, S. Thermally Stable Mesoporous Poly(ether sulfone) Monoliths with Nanofiber Network Structures. *Macromolecules* **2018**, *51*, 151−160.

(54) Guo, Y.; Ruan, K.; Shi, X.; Yang, X.; Gu, J. Factors affecting thermal conductivities of the polymers and polymer composites: A review. *Compos Sci Technol.* **2020**, *193*, No. 108134.

(55) Gu, J.; Ruan, K. Breaking Through Bottlenecks for Thermally Conductive Polymer Composites: A Perspective for Intrinsic Thermal Conductivity, Interfacial Thermal Resistance and Theoretics. *Nano-Micro Lett.* **2021**, *13*, No. 110.

(56) De Rosa, C.; Guerra, G.; Petraccone, V.; Pirozzi, B. Crystal Structure of the Emptied Clathrate Form (δe Form) of Syndiotactic Polystyrene. *Macromolecules* **1997**, *30*, 4147−4152.

(57) Manfredi, C.; De Rosa, C.; Guerra, G.; Rapacciuolo, M.; Auriemma, F.; Corradini, P. Structural changes induced by thermal treatments on emptied and filled clathrates of syndiotactic polystyrene. *Macromol. Chem. Phys.* **1995**, *196*, 2795−2808.

(58) Hrubesh, L. W.; Keene, L. E.; Latorre, V. R. Dielectric properties of aerogels. *J. Mater. Res.* **2011**, *8*, 1736−1741.

(59) Williams, J. C.; Meador, M. A. B.; McCorkle, L.; Mueller, C.; Wilmoth, N. Synthesis and properties of step-growth polyamide aerogels cross-linked with triacid chlorides. *Chem. Mater.* **2014**, *26*, 4163−4171.

(60) Laby, T. H. The thermal conductivity of air. *Proceedings of the Royal Society of London. Series A, Containing Papers of a Mathematical and Physical Character* **1934**, *144*, 494−495.

(61) Mıhlayanlar, E.; Dilmaç, Ş.; Güner, A. Analysis of the effect of production process parameters and density of expanded polystyrene insulation boards on mechanical properties and thermal conductivity. *Mater. Des.* **2008**, *29*, 344−352.

(62) Fan, W.; Zhang, X.; Zhang, Y.; Zhang, Y.; Liu, T. Lightweight, strong, and super-thermal insulating polyimide composite aerogels under high temperature. *Compos Sci Technol.* **2019**, *173*, 47−52.

(63) Madyan, O. A.; Fan, M. Hydrophobic Clay Aerogel Composites through the Implantation of Environmentally Friendly Water-Repellent Agents. *Macromolecules* **2018**, *51*, 10113−10120.

(64) Ge, X.; Shan, Y.; Wu, L.; Mu, X.; Peng, H.; Jiang, Y. High-strength and morphology-controlled aerogel based on carboxymethyl cellulose and graphene oxide. *Carbohydr. Polym.* **2018**, *197*, 277−283.

(65) Fan, J.; Ifuku, S.; Wang, M.; Uetani, K.; Liang, H.; Yu, H.; Song, Y.; Li, X.; Qi, J.; Zheng, Y.; Wang, H.; Shen, J.; Zhang, X.; Li, Q.; Liu, S.; Liu, Y.; Wang, Q.; Li, J.; Lu, P.; Fan, Z.; Chen, W. Robust Nanofibrillated Cellulose Hydro/Aerogels from Benign Solution/Solvent Exchange Treatment. *ACS Sustainable Chem. Eng.* **2018**, *6*, 6624−6634.

(66) Wang, Y.; Wu, K.; Xiao, M.; Riffat, S. B.; Su, Y.; Jiang, F. Thermal conductivity, structure and mechanical properties of konjac gluco-mannan/starch based aerogel strengthened by wheat straw. *Carbohydr. Polym.* **2018**, *197*, 284−291.

(67) Oh, J.-H.; Kim, J.; Lee, H.; Kang, Y.; Oh, I.-K. Directionally Antagonistic Graphene Oxide-Polyurethane Hybrid Aerogel as a Sound Absorber. *ACS Appl. Mater. Interfaces* **2018**, *10*, 22650−22660.

(68) Daniel, C.; Antico, P.; Guerra, G. Etched Fibers of Syndiotactic Polystyrene with Nanoporous-Crystalline Phases. *Macromolecules* **2018**, *51*, 6138−6148.

High-Strength, Flexible, Hydrophobic, Sound-Absorbing, and Flame-Retardant Poly(vinyl alcohol)/Polyelectrolyte Complex Aerogels

Vipin G. Krishnan, C. V. Sijla Rosely, Andreas Leuteritz, and E. Bhoje Gowd*

ACCESS | Metrics & More | Article Recommendations | SI Supporting Information

ABSTRACT: Biodegradable aerogels with flexibility and high strength are attractive for construction, and acoustic and thermal insulation but are seriously plagued by their flammability. Improving the flame retardancy of these aerogels has been a hot topic of research and inorganic fillers, and layered materials have been widely used for this purpose. However, the poor interfacial compatibility of these fillers has affected the processability and mechanical properties of the aerogels and reduced their overall performance. In this study, we have used a completely organic and sustainable polyelectrolyte complex (PEC) as a filler for fabricating mechanically strong, sound-absorbing, and flame-retardant poly-(vinyl alcohol) (PVA) aerogels with the aid of an environmentally friendly freeze-drying method. The noncovalent interactions between the polymer and filler ensured excellent compatibility as well as interfacial adhesion of the filler, and we could achieve a perfect balance between the density and mechanical properties of the aerogels. The prepared aerogels exhibited flexibility, good sound absorption ability in the mid-frequency range, and excellent flame retardancy (LOI ~28%) with self-extinguishing behavior. A simple silane modification endowed sticky hydrophobicity to the aerogels and further enhanced their antifire properties. These sustainable multifunctional aerogels could find a plethora of applications in real life, particularly in buildings and structures as fire safety materials and sound insulators.

KEYWORDS: polymer aerogels, poly(vinyl alcohol), polyelectrolyte complex, flame retardant, hydrophobic, sound absorption
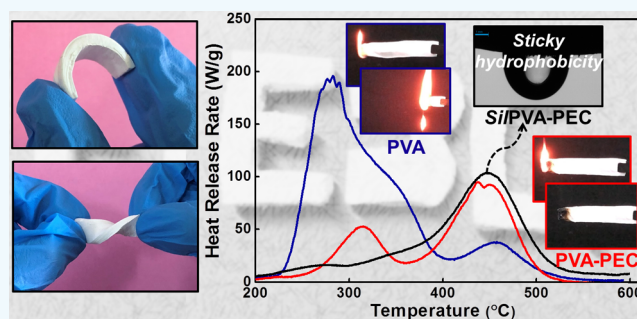
■ INTRODUCTION

The demand for sustainable materials has risen enormously in many applications due to the enhanced global awareness of environmental safety and protection. When it comes to structural and functional materials, tough and mechanically robust lightweight materials derived from renewable resources and/or by environmentally benign processes seem to be the way forward. Being an outstanding class of lightweight materials, aerogels, first reported by Kistler,[1,2] are the go-to materials for the future as they possess properties like extremely low densities, high porosities, high surface-to-volume ratios, low thermal conductivities, low dielectric constants, low sonic velocities, etc.[3] These unique traits qualify them as thermal and acoustic insulators,[4−12] low dielectric substrates,[13−17] supercapacitor materials,[18−20] etc. Polymer-based, particularly biodegradable/biopolymer-based aerogels, are trending nowadays, thanks to their superior mechanical properties over conventional inorganic aerogels and sustainability. Many environmentally benign aerogels based on poly(vinyl alcohol) (PVA),[21−23] poly(lactic acid),[24,25] cellulose,[26−28] chitosan,[7,10,28] starch,[28,29] etc. have been developed in recent times using the freeze-drying technology. Compared to supercritical CO$_2$ drying, which requires high operating

pressures, freeze drying is a greener, low-cost, and more feasible method for the extraction of solvents from wet gels without the collapse of the gel structure.

PVA is a formidable candidate for the preparation of aerogels owing to its low cost, high solubility in water, and good mechanical properties. Its biodegradable, biocompatible, and nontoxic nature makes it an even more versatile polymer. However, the limiting factors of pristine PVA are the high flammability (limiting oxygen index (LOI) ~19.8%) and superhydrophilicity induced by its organic skeleton composed of plenty of hydroxyl groups, which restrict its feasibility in many practical applications. Extensive research has been done in improving the flame-retardant properties of PVA aerogels, especially by incorporating inorganic fillers like clay, ammonium polyphosphate (APP), etc., into the polymer
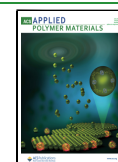
matrix to fabricate organic/inorganic composite aerogels.[23,30−32] Schiraldi and co-workers have developed a series of additives for PVA aerogels to improve flame-retardant and other properties.[33−36] For example, APP modified with piperazine was used as an intumescent flame retardant in the PVA-montmorillonite aerogel system to demonstrate the improved flame retardancy.[37] The same group introduced another approach toward the development of flame-retardant aerogels by growing a conformal silica coating onto the PVA aerogel. Further, they did a fluorocarbon silane treatment, which furnished durable superhydrophobic aerogels.[38] The synergistic effect of two-dimensional layered nanomaterials such as α-zirconium phosphate, MXene, and boron nitride nanosheets with APP was well utilized to enhance the fire safety of PVA aerogels.[39−41] However, the poor interfacial compatibility of inorganic additives often leads to poor mechanical properties and durability. In addition, high loadings of inorganic additives to achieve the satisfactory flame retardancy of PVA can negatively affect aerogel formation. Due to these reasons, reactive flame retardants attracted the attention of researchers as they preserve the mechanical properties of polymer aerogels and afford satisfactory flame retardancy. Shang et al. fabricated flame-retardant PVA aerogels with high mechanical and dimensional stability without the aid of any inorganic species by chemical cross-linking with melamine-formaldehyde.[42] But the potential toxicity of melamine and formaldehyde can cause danger to humans as well as the environment. Therefore, alternative materials or methods are vital for the preparation of sustainable and eco-friendly PVA-based aerogels with enhanced overall properties.

Recently, there have been reports on using polyelectrolyte complexes (PECs) as flame-retardant additives for polymers and their composites.[43−47] PECs are a family of multi-component polymeric materials formed by the ionic interactions between oppositely charged polyions. Usually, water-soluble polycations and/or polyanions have been utilized for the synthesis of PECs without the aid of cross-linking agents or catalysts.[48−50] At the industrial scale, PECs are used as flocculants for wastewater treatment, dewatering agents in papermaking, additives in detergents and cosmetics, and binders in the pharmaceutical industry.[48,49] Zhang et al. demonstrated the applicability of PEC on ethylene-vinyl acetate copolymer as a green intumescent flame retardant.[43] A water-soluble poly(allylamine)-polyphosphate PEC that can extinguish flame was coated onto polyester-cotton fabric by Grunlan and co-workers, and the resultant coating was wash durable.[51] In another work, flame-retardant epoxy resins were prepared using poly(diallyldimethylammonium) and polyphosphate PEC.[52] However, to the best of our knowledge, PECs have never been applied to polymeric aerogel systems, albeit their huge potential to boost aerogel properties.

Inspired by the eco-friendly nature of PECs, we aim to fabricate water-based polymer aerogels that are strong, flame-retardant, hydrophobic, flexible, and sound-absorbing. In the present study, we have blended biosourced PECs into the PVA matrix to prepare a fully organic flame retardant polymer aerogel. PEC is synthesized from chitosan (CS), a cationic biopolymer, and phytic acid (PA), a phosphorus-rich anionic molecule obtained from bioresources. Abundant hydroxyl groups in PVA enable a strong interfacial adhesion of PECs through hydrogen bonding. Furthermore, the addition of PEC did not alter the low-density behavior of aerogels. The hybrid

aerogels' microstructure, compression properties, thermal stability, and acoustic properties were characterized and compared with neat PVA aerogel. The highly hydrophilic aerogels are further converted into hydrophobic (water contact angle over 136°) using a commercial silane by a simple chemical vapor deposition (CVD). Before and after the hydrophobic modification, the aerogels were characterized for flammability using UL94, LOI, and microscale combustion calorimetry (MCC), and the possible flame-retardant mechanism was discussed. The aerogels prepared in this study can find applications as structural materials for buildings and as acoustic insulators.

■ EXPERIMENTAL SECTION

Materials. PVA (M_w ∼89 000 to 98 000, 99% hydrolyzed), chitosan (low molecular weight, degree of deacetylation ≥75%), phytic acid sodium salt hydrate (from rice), and methyltrichlorosilane (99%) were purchased from Sigma-Aldrich Co. and used without further purification. Hydrochloric acid and citric acid were obtained from Rankem Chemicals and Merck India, respectively. Potassium carbonate (K_2CO_3) was provided by Avra Synthesis Pvt. Ltd. Deionized (DI) water was used in the entire experimental process.

Preparation of PEC. PEC was prepared by slightly modifying a reported procedure.[43] Initially, 2 wt % solution of CS was prepared by dissolving 4.07 g of CS powder in 200 mL of DI water with the aid of 3 mL of 5 M hydrochloric acid (HCl). The dissolution was done by stirring at room temperature for 2 h, and the pH of the resultant CS solution was 1.2. Subsequently, excess PA solution (4 wt %) was also prepared in 200 mL of DI water by dissolving 8.3 g of phytic acid sodium salt hydrate at room temperature by mechanical stirring. The pH of the PA solution was adjusted to 1.5 using 5 M HCl. Then, this solution was added dropwise to the CS solution with vigorous stirring to yield a white precipitate. After complete precipitation, the solution was stirred overnight and the precipitate was allowed to settle down. The white precipitate was then collected by filtration and washed several times with DI water before drying in the hot-air oven first, followed by vacuum drying at 60 °C for 24 h. The dried precipitate, which was yellowish in color, was ground to a fine powder and stored in a vacuum desiccator for further use.

Preparation of PVA-PEC Aerogels. PVA solutions (5 wt %) were used for the preparation of PVA-based aerogels. In a typical preparation procedure, 1 g of PVA powder was dissolved in 15 mL of DI water by mechanical stirring at 90 °C for 2 h. The required amount of powder PEC was taken in a separate container with 5 mL of DI water and sonicated for 30 min. The PEC dispersion was added to the PVA solution with constant stirring, and subsequently, 0.2 g of citric acid was added to the PVA-PEC mixture. The stirring was continued for 2 h at 90 °C. Then, the homogeneous solution was transferred to a plastic mold and immediately frozen in a liquid nitrogen bath. The frozen sample was subjected to freeze-drying to obtain the required aerogel. The sample was named as PVA-xPEC, where x stands for the wt % of PEC with respect to the total solid content of the sample. Composite aerogels containing 5, 10, 20, and 30% of PEC were prepared and stored in a vacuum desiccator at room temperature for further use. A control sample was also prepared following the above procedure, without the addition of PEC (neat PVA aerogel) for the purpose of comparison.

Hydrophobic Surface Modification of PVA-PEC Aerogels. A chemical vapor deposition (CVD) technique was employed to modify the aerogel surfaces.[53] Briefly, a saturated solution of K_2CO_3 was kept open inside a desiccator for 12 h to absorb the moisture and maintain a constant relative humidity. Later, another open vial with 1 mL of methyltrichlorosilane was introduced into the desiccator along with the aerogel samples. The desiccator was sealed and kept in the hot-air oven at 50 °C for 24 h when silanization occurred. The silanized aerogels were then placed in a vacuum oven at 50 °C for 24 h to remove the residual silane and HCl and stored in a vacuum desiccator

for further characterization. The surface-modified samples were named as *Sil*PVA-*x*PEC.

Characterization. The apparent density of various aerogel samples was determined theoretically from their mass/volume ratio. The elemental composition of powder PEC and monolithic aerogels was obtained using PHI 5000 Versa Probe-II Focus X-ray photo-electron spectroscope (XPS) (purchased from ULVAC-PHI, Inc.) equipped with microfocused (200 μm, 15 kV) monochromatic Al Kα X-ray source (hν = 1486.6 eV). Fourier transform infrared (FTIR) analysis was performed using a PerkinElmer Series FT-IR Spectrum Two machine at a resolution of 4 cm^{-1} and 32 scans in the wavenumber range of 4000−400 cm^{-1}. Wide-angle X-ray diffraction (WAXD) patterns of the aerogels were acquired using XEUSS SAXS/WAXS system from Xenocs operated at 50 kV and 0.60 mA in the transmission mode using Cu Kα radiation (λ = 1.54 Å). A Mar 345 image plate system detected the 2D patterns and the Fit2D software was used for data processing. Differential scanning calorimetry (DSC) measurements were conducted with an advanced research-grade modulated differential scanning calorimeter TA Q2000 under nitrogen gas flow. The samples were heated from room temperature to 250 °C at a rate of 10 °C/min and then cooled back to room temperature at the same rate. Compression tests were carried out on cylindrical aerogel samples (2:1 diameter-to-height ratio) to evaluate their mechanical performance. Universal Testing Machine (Hounsfield, H5KS UTM, Redhill, U.K.) with a crosshead speed of 1.5 mm/min was used for the same. Thermal stability and thermal degradation behavior of all of the PVA-based aerogels were monitored using a thermogravimetric analyzer (TGA) TA Q50. The samples were heated from room temperature to 600 °C at a rate of 10 °C/min under nitrogen atmosphere. The acoustic performance of the prepared aerogels was evaluated by measuring the normal incident sound absorption coefficients using a Brüel & Kjær impedance tube, type 4206 (Denmark). Cylindrical samples with diameter ∼29 mm and thickness ∼15 mm were measured in the frequency band from 300 to 6400 Hz via the two-microphone method. To study the wetting behavior of the aerogels before and after the silane treatment, water contact angles (WCA) of the samples were measured at room temperature using an automated DSA30 Drop Shape Analyzer, KRÜSS, Germany. For the preliminary analysis of the flammability properties of the aerogels, horizontal burning tests were conducted under laboratory conditions using a Bunsen burner with a butane flame. Limiting oxygen index (LOI), i.e., the lowest concentration of oxygen required to burn a sample, was measured for the aerogels using a critical oxygen index apparatus (as per ASTM D2863-08, ISO 4589) from Spectrum Automation and Controls coupled with Servomex Servoflex MiniMP (United Kingdom), a high-performance oxygen gas analyzer. The microscale combustion calorimetry (MCC) (MCC-1 (FTT)) was performed for the further analysis of the flame retardant properties of the aerogels. Milligrams of the sample were heated to 700 °C at a heating rate of 1 °C/s in a stream of nitrogen (80 cm^3/min). The resulting volatile anaerobic thermal degradation products are mixed with 80 cm^3/min carrying gas (nitrogen of 80 mL/min; oxygen of 20 mL/min) and subsequently burned at 900 °C in a combustion furnace. Various flammability parameters such as HRR (heat release rate; W/g), THR (total heat release; kJ/g), HRC (heat release capacity; J/gK), etc. were measured from this test.

■ RESULTS AND DISCUSSION

Fully Organic Flame-Retardant Fillers. Popular halogen-based fillers in flame retardancy are being abandoned across the globe for the adverse environmental impacts they have generated in recent times. Clays and many other inorganic materials have been successfully employed as eco-friendly alternatives to halogenated antifire fillers.[7,30,32,39] However, a completely organic filler material has not gained much attention, particularly for aerogels, probably due to their lower efficiency than their inorganic counterparts. Herein, noncovalent interactions, particularly the ionic interactions

between a macromolecule and a small molecule have been utilized to prepare a green water-insoluble additive, with the ultimate aim of fabricating polymer aerogels with enhanced properties. The macromolecule selected is CS with a low molecular weight, which has an abundance of polarizable primary amino groups. PA is an anionic molecule rich in phosphate groups and can effectively interact with chitosan to form stable complexes. These complexes can be considered as polyelectrolyte complexes, and the schematic illustration of their formation is given in Figure 1a. Briefly, to the freshly
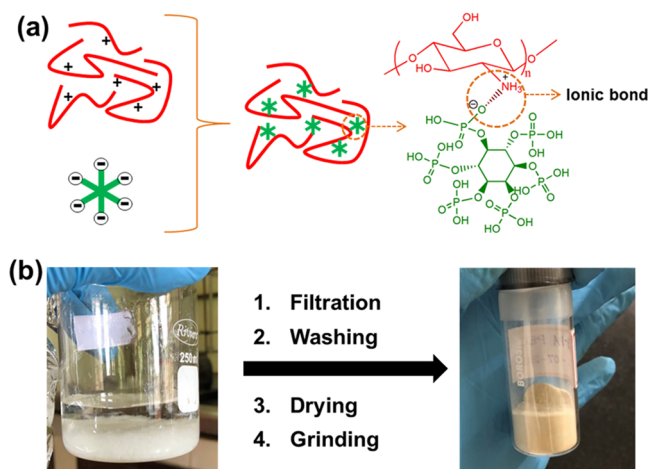

Figure 1. (a) Schematic illustration of the formation of PEC from CS and PA. (b) Photographic images showing the precipitated (white) PEC and the PEC powder (pale yellow) after the filtration, washing, drying, and grinding processes.

prepared aqueous acidic CS solution, excess of PA sodium salt hydrate solution in water was added and immediate precipitation occurred, as shown in Figure 1b. The as-obtained white precipitate was filtered, washed, vacuum-dried, and ground to obtain a fine powder with pale yellow color (Figure 1b) and the PA/CS weight ratio in this complex is ∼0.86:1.

The prepared PEC consists of carbon, oxygen, nitrogen, and phosphorus elements, whose approximate elemental composition was obtained from X-ray photoelectron spectroscopy (XPS), as shown in the survey spectrum in Figure 2a. The percentages of C, O, N, and P elements in the PEC are ∼48.4, 42.5, 4.9, and 4.2, respectively. The successful ionic complexation reaction between CS and PA is confirmed using FTIR analysis, and the corresponding spectra are given in Figure 2b. CS shows characteristic absorption bands approximately at 1650 cm^{-1} (C═O stretching (amide I)), 1589 cm^{-1} (N−H bending of primary amine), and 1560 cm^{-1} (N−H bending (amide II)), and PA has peaks at 1645 cm^{-1} (O−P−O stretching) and 1185 cm^{-1} (P═O stretching). However, in PEC, a new band appeared in place of the N−H bending peak at 1530 cm^{-1}, which is ascribed to the protonated NH$_2$ group (NH$_3^+$) of CS in the presence of acid. Similarly, the band at 1042 cm^{-1} in PEC corresponds to the stretching mode of (PO$_3$)$^{2-}$. Thus, the oppositely charged functional groups can easily interact via ionic bonds in the organic complex. Further confirmation of the interactions is obtained from high-resolution XPS spectra and WAXD patterns given in the Supporting Information (Figures S1 and S2). The bonds corresponding to each peak in the XPS high-resolution C 1s, O 1s, N 1s, and P 2p spectra of PEC are well labeled in Figure S1.
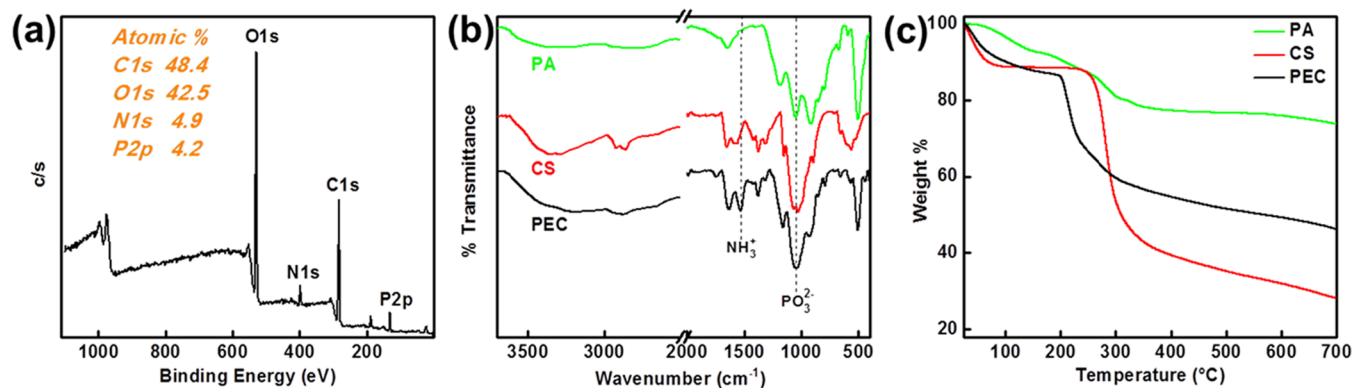
Figure 2. (a) XPS survey spectrum of PEC (the inset shows the atomic % of various elements of PEC). (b) FTIR spectra and (c) TGA thermograms under nitrogen atmosphere of PA, CS, and PEC.
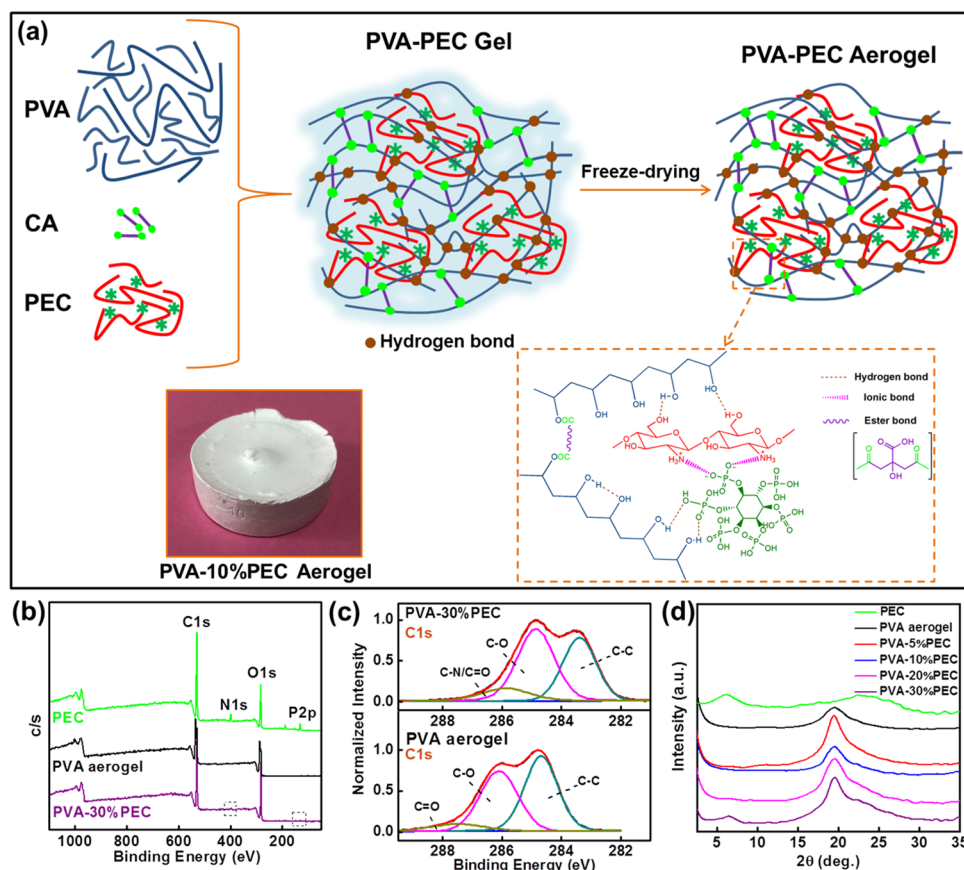

Figure 3. (a) Schematic illustration of the formation of PVA-PEC aerogels along with the photographic image of PVA-10%PEC aerogel. (b) XPS survey spectra; (c) high-resolution C 1s spectra; and (d) WAXD patterns of PEC, pure PVA aerogel, and PVA-PEC aerogels.

The N 1s spectrum was deconvoluted into two peaks: 397.8 and 399.8 eV, corresponding to C−N and NH_3^+ bonds. Also, the deconvolution of the P 2p spectrum shows peaks corresponding to P=O and P−O/$(PO_3)^{2-}$ bonds at 129.6 and 131.9 eV, respectively. The WAXD patterns (Figure S2) show an amorphous structure for PA with a broad peak between 15 and 35° and a semicrystalline structure for CS with a sharp diffraction peak around 20°. The intensity of the crystalline peak of CS reduced significantly in the PEC, which indicates the reduction in the degree of crystallinity. Such a situation has arisen because of the interaction of PA with CS, which resulted in the breakage of intramolecular hydrogen-bonding interactions between NH_2 and OH groups of CS.[43]

Figure 2c shows the TGA thermograms of CS, PA, and PEC under a nitrogen atmosphere. The weight loss below 100 °C is due to the removal of the absorbed water. PEC undergoes early degradation, about 60 °C earlier than CS, and this phenomenon in PEC is catalyzed by PA. Similarly, the maximum degradation temperature is also lower in the case of PEC. However, the thermal degradation of PEC yields significantly higher char residue than CS. At 600 °C, the residual char yield for CS is 32 wt %, whereas it is 49 wt % for the PEC. The carbonization of CS got enhanced in the presence of PA, which is advantageous when it comes to fire safety applications. Integrating a carbon−nitrogen source like
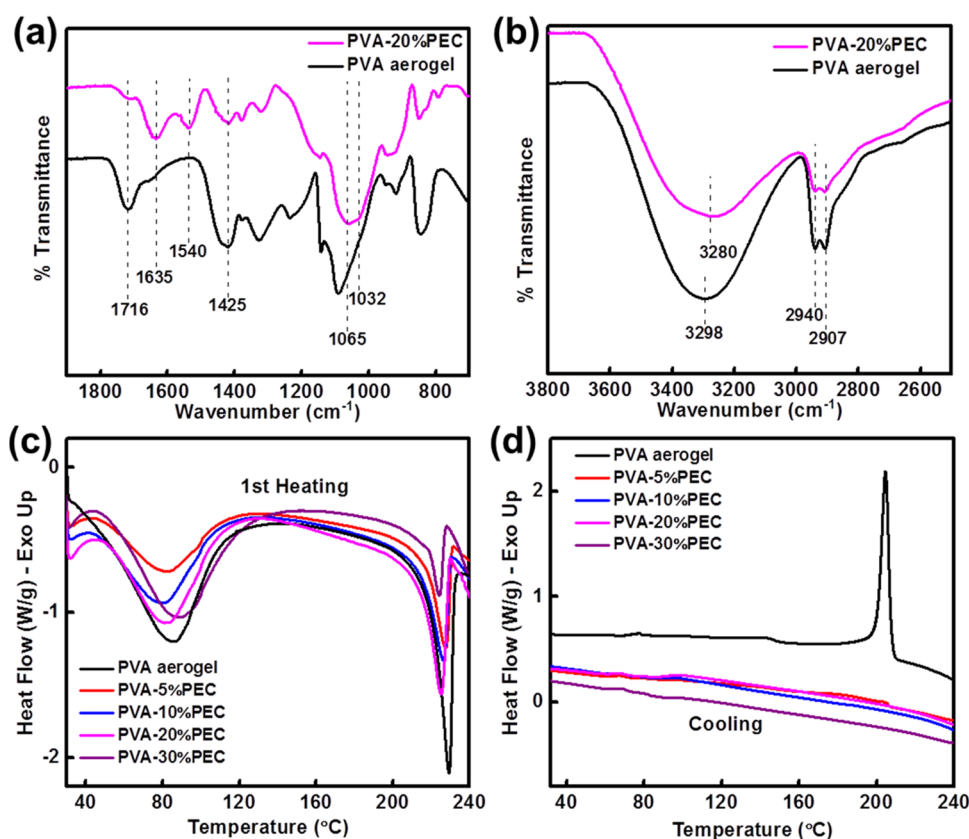
Figure 4. FTIR spectra of PVA and PVA-20%PEC aerogels in the range of (a) 700−1900 cm^{-1} and (b) 2500−3800 cm^{-1}. DSC thermograms (c) first heating and (d) cooling curves of PVA aerogel and PVA-PEC aerogels with different PEC loadings.

CS and a phosphorus-rich PA into a complex material could effectively function as flame-retardant additives for polymers.

PEC-Incorporated Polymer Aerogels. As mentioned in the Experimental Section, PVA aerogels were prepared with different weight loadings of PEC, i.e., 5, 10, 20, and 30 wt %, and a neat PVA aerogel (without the addition of PEC) was also prepared for comparison. PVA is biodegradable by nature and the entire synthesis (of both PEC and aerogel) was carried out in the water as the only medium, making the whole process and the end-product environmentally friendly. The availability of plenty of reactive hydroxyl groups across the PVA surface allows for the esterification between PVA and citric acid to form cross-links between the polymer chains.[54] Sometimes, citric acid can react with the hydroxyl groups of PEC to form cross-links between PVA and PEC, but the probability of such an interaction is minimum. However, strong hydrogen-bonding interactions are possible between PVA and PEC in the water medium. The PVA-PEC hydrogels stabilized by both covalent as well as noncovalent interactions were freeze-dried to remove the solvent, and Figure 3a illustrates the entire scheme of aerogel formation. The successful incorporation of PEC into the PVA matrix was further confirmed from the XPS survey spectrum, as shown in Figure 3b. The approximate elemental composition of neat PVA and PVA-30%PEC aerogels is C—62.2% and O—37.8%, and C—51.3%, O—44.3%, N—3.4%, and P—1.0%, respectively. Figure 3c shows the high-resolution C 1s spectra of PVA-30%PEC and neat PVA aerogels. The intensity of the C−C band decreased, and that of the C−O band increased in the PVA-30%PEC aerogel compared with neat PVA aerogel. The addition of PEC to the polymer matrix brought more oxygen-containing moieties to

the system, and therefore, the oxygen content in the PVA-PEC aerogel increased. Also, the peaks shifted to lower binding energies, i.e., from 284.6 to 283.3 eV for the C−C bond and 286.1 to 284.8 eV for the C−O bond, indicating the reduction in bond strengths, which is evidence for PVA-PEC interactions. A similar observation was made in the case of high-resolution O 1s spectra also (Figure S3a). PEC dispersion in the aerogel is so excellent that clear peaks were obtained for PVA-30%PEC aerogel in the high-resolution N 1s and P 2p spectra (Figure S3b). WAXD patterns in Figure 3d further exemplify the compatibility between PVA and PEC. The X-ray diffraction peak corresponding to the PEC at lower 2θ (~5°) is not visible in the WAXD patterns of PVA-PEC aerogels till 20 wt % loading. However, at 30 wt % PEC loading, the lower angle peak (~5°) started to come up in the aerogel, which is an indication of the aggregation of PEC. Hence, we can conclude that even at high loadings of PEC, excellent miscibility between PVA and PEC was achieved.

FTIR spectra of neat PVA and PVA-20%PEC aerogels are compared in Figure 4a,b. The peak at 1716 cm^{-1} confirms the successful esterification between PVA and citric acid as this peak can be assigned to the carbonyl of the −COO− group.[54] The intensity of the 1716 cm^{-1} peak is low in the PVA-PEC aerogel due to the presence of other reactive organic moieties, which further confirms the above-mentioned point. There are possibilities for the reactive amino groups in CS to form amide linkages with citric acid, but the intense peak at 1540 cm^{-1} in PVA-20%PEC aerogel corresponding to the NH$_3^+$ group ensures that such a linkage is not present in the PVA-PEC system. The peak at 1032 cm^{-1} corresponding to the (PO$_3$)$^{2-}$ stretching confirms the ionic complexation between CS and

Table 1. Mechanical and Thermal Properties of Various Aerogels Prepared in This Study

samples	density (g/cm^3)	compression modulus (MPa)	$T_{10\%}$ (°C)	$T_{50\%}$ (°C)	T_{max} (°C)	residue (%)
PVA aerogel	0.055	0.45	241	281	465	4
PVA-10%PEC	0.057	1.24	204	330	452	11
PVA-20%PEC	0.060	1.55	166	331	456	18
PVA-30%PEC	0.069	0.67	201	384	450	33

PA even in the PVA-PEC aerogel. The IR absorption band at 1635 cm^{-1} is a combination of carbonyl (Amide I) and O−P−O stretching vibrations of PEC and hence is absent in PVA aerogel. The −C−O stretching peak (1091 cm^{-1}) of PVA has been shifted to a lower wavenumber, i.e., 1065 cm^{-1} in PVA-PEC aerogel, which may be due to the hydrogen bonds formed between the free hydroxyl groups of PVA and PEC.

In Figure 4b, the PVA aerogel shows a single broad absorption band at around 3298 cm^{-1} and this peak is assigned to the hydroxyl stretching vibration, whereas in the case of PVA-20%PEC, this peak has shifted to 3280 cm^{-1} pertaining to the enhanced hydrogen-bonding interaction between PVA and PEC. The decrease in the intensity of −CH$_2$ asymmetric (2940 cm^{-1}) and symmetric (2907 cm^{-1}) stretching vibrations in PVA-PEC aerogel also confirms the successful incorporation of PEC into the PVA matrix. Figure 4c,d shows the DSC first heating and cooling curves, respectively, of neat PVA and PVA-PEC aerogels with different PEC loadings. In the first heating curves, the broad endotherms around 80 °C are due to the evaporation of moisture absorbed by the samples. The melting temperatures were more or less the same (∼230 °C) for all of the samples. But it is worth mentioning here that, during cooling from the melt, neat PVA aerogel undergoes crystallization at around 210 °C and such melt crystallizations were absent in all other samples (PVA-PEC aerogels). With the addition of PEC to the PVA matrix, PVA chains are unable to reorganize into crystallites due to the strong interactions induced by the PEC. This observation also indicates the fact that cross-linking interactions (covalent and noncovalent) are persisting within the PVA-PEC aerogels.

Aerogels were prepared using 5 wt % PVA solutions, and the PEC loading was calculated with respect to the dry weight of the polymer. All of the aerogel samples exhibited relatively low density ranging from 0.055 to 0.069 g/cm^3. The density of neat PVA aerogel was 0.055 g/cm^3, and the addition of PEC resulted in only a slight increase in density; for 20 wt % PEC loading, the density is ∼0.06 g/cm^3. This indicates the lightweight nature of the prepared aerogels. Interestingly, these aerogels were highly flexible and could be made in or cut into any shape (Figure S4a). However, during compression experiments, these aerogels exhibited an irreversible buckling behavior and were converted to dense solids without any disintegration of the samples, similar to syndiotactic polystyrene aerogels.[12,55] Figure S4b gives the compressive stress−strain curves for neat PVA and PVA-PEC aerogels, and their deformation behavior is similar to that of a typical honeycomb-like open-cell foam.[42] The compressive moduli of the samples were calculated from the slope of the linear elastic region of the stress−strain curves and are tabulated in Table 1. As observed in Figure S4b, the compressive strength of PVA aerogels is enhanced with the incorporation of PEC. The compression modulus increased to 1.55 MPa in PVA-20%PEC aerogel compared to 0.45 MPa of neat PVA aerogel. This is mainly attributed to the strong interaction as well as the excellent miscibility between PVA and PEC in the aerogel system.

However, on further increasing the PEC content (30%), the compression modulus dropped down to 0.67 MPa, which may be due to the structural instability induced by the agglomeration of PEC particles, as indicated earlier in the WAXD pattern of PVA-30%PEC aerogel (Figure 3d). At 30% PEC loading, the PVA concentration is not enough to uniformly bind the PEC particles within the matrix, which resulted in the agglomeration. Higher loadings of inorganic additives such as clay, silica, etc. can sometimes better enhance the compression strength of PVA-based aerogels, but at the expense of the low-density nature.[34,38,56] In this work, we could obtain an excellent balance between the density and mechanical strength of aerogels, which is not so easy to attain.

The surface morphologies of PVA and PVA-PEC aerogels with different PEC concentrations are shown in Figure S5. The SEM images revealed that all of the aerogels have a layered structure that accompanied the ice crystal growth direction. With the incorporation of PEC, the distance between the PVA layers has changed slightly, and as shown in the magnified images, the pore size and distribution were also modified. The ice template method allows the polymer chains as well as the fillers to concentrate at the grain boundaries of the ice crystals,[38] and therefore, the morphology remained more or less similar in all of the samples, and it could be assumed that PECs remain on the PVA layers. The neat PVA aerogel is extremely hydrophilic, thanks to the chemical structure of PVA with enormous surface OH functional groups, and we could not measure the water contact angle (WCA) as the water droplets were not stable on the surface. Upon contact with the surface, the droplets were immediately absorbed by the PVA aerogel. However, when PEC was introduced into the system, the WCA of the aerogels improved slightly, as shown in Figure S6. The WCA values obtained for aerogels with 5, 10, 20, and 30% PEC loadings were 27.2, 26.9, 29.4, and 27.1° (±1.5°), respectively. This might be due to the reduction in the number of free surface hydroxyl groups on PVA-PEC aerogels in comparison with pure PVA aerogel because of the extensive hydrogen-bonding interactions. All of these aerogels are highly moisture-sensitive and can absorb moisture from the surroundings. Therefore, the aerogels were stored in a desiccator for further characterization.

The thermal degradation behavior and the thermal stability of PVA-PEC aerogels were investigated in nitrogen atmosphere using TGA, and the results are given in Figure 5 and Table 1. $T_{10\%}$, $T_{50\%}$, and T_{max} are the temperatures at which 10%, 50%, and maximum weight loss occur, respectively. In all of the samples, almost 10% of the weight was lost below 100 °C due to the removal of the absorbed moisture, which indicates the moisture sensitivity of the prepared aerogels. Apart from the initial water loss, the degradation of neat PVA aerogel occurs in two stages, as shown by the two weight loss steps. The first step is the decomposition of the hydroxyl groups of PVA, which occurs in a temperature range of 220−350 °C. The polymer backbone decomposition takes place at the later stage, beyond 350 °C. However, in the case of PVA-
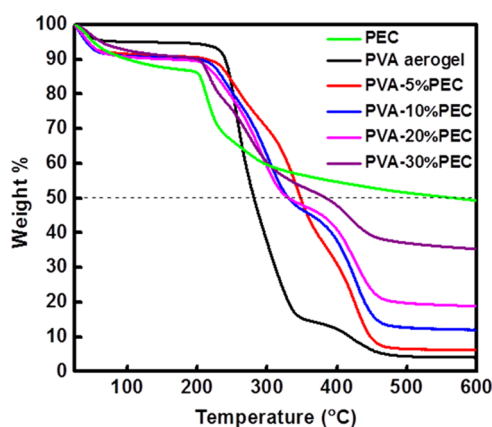
Figure 5. TGA thermograms of PVA and PVA-PEC aerogels obtained at a heating rate of 10 °C/min.

PEC aerogels, PEC catalyzed the early degradation of PVA. The weight loss starting at ∼200 °C in PVA-PEC aerogels is a combination of PEC decomposition and the PVA dehydroxylation catalyzed by the phosphorus-containing moieties from PEC. After the incorporation of PEC, the thermal stability of the aerogels enhanced significantly, as evident from the $T_{50\%}$ values. $T_{50\%}$ increased from 281 °C for neat PVA aerogel to 348, 330, 331, and 381 °C for PVA-5%PEC, PVA-10%PEC, PVA-20%PEC, and PVA-30%PEC aerogels, respectively, i.e., nearly 100 °C enhancement upon addition of 30% PEC. The char residue also increased with the increase in PEC content, from 4% (neat PVA aerogel) to 33% (PVA-30%PEC aerogel). This indicates the better char forming ability of PVA-PEC aerogels compared with neat PVA aerogel at higher temperatures. Thus, we can conclude that the introduction of PEC (rich in N, P, and C elements) into the PVA matrix can substantially enhance the thermal stability of the aerogels and induce greater carbonaceous char residues, which may act as a protective layer during the combustion of the aerogels.

The porous structure of PVA-based aerogels renders good sound absorption capability to them. In Figure 6, the normal incident sound absorption coefficients of various aerogel samples are plotted as a function of frequency and all of the samples exhibited good absorption coefficients in the mid-frequency range. Neat PVA aerogel absorbed more than 80% of the incident sound waves consistently between 2400 and 3100 Hz with a maximum of 94% at around 2700 Hz. The
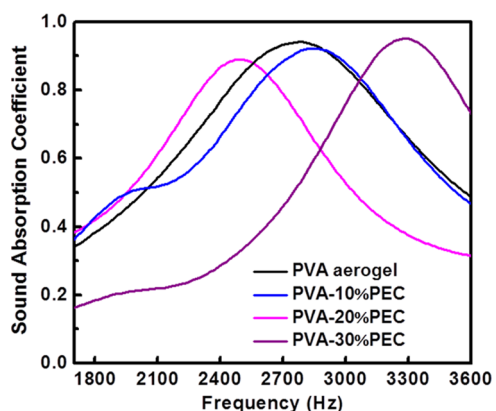

Figure 6. Normal incident sound absorption coefficients of PVA and PVA-PEC aerogels in the frequency range of 1700−3600 Hz.

incorporation of PEC did not alter the general absorption characteristic of the PVA aerogel, though slight differences are observable in the case of PVA-20%PEC and PVA-30%PEC aerogels. In the PVA-30%PEC aerogel, the maximum absorption shifted slightly to the higher-frequency side (3000−3500 Hz), whereas it shifted to lower frequencies for the PVA-20%PEC aerogel. The curve of the PVA-10%PEC aerogel is almost superimposed with that of neat PVA aerogel. The similarity in the morphology of neat PVA and PEC-incorporated PVA aerogels (due to the ice templating) contributes to the similar trend in their sound absorption. The efficient absorption of sound waves in the mid-frequency range by these highly porous monoliths can be attributed to the tortuosity in the sound propagation path and multiple internal reflections at the cell walls generated by the highly porous network structure, which effectively attenuate the sound waves.[8,9,57]

Combustion Behavior. Horizontal burning tests and limiting oxygen index (LOI) measurements were carried out for the preliminary estimation of the flame retardant behavior of the prepared aerogels. LOI is the minimum concentration of oxygen in the atmosphere that is required to sustain the combustion of a sample after ignition[58] and the results of the LOI test are provided in Table 2. Figure 7 shows the results of the horizontal burning tests conducted on each sample. The videos of the burning tests are also provided in the Supporting Information (Movies S1, S2, S3, and S4). The LOI value obtained for neat PVA aerogel was ∼19.6%, and it increased with the increase in PEC content in PVA-PEC aerogels; the maximum value obtained is ∼28% at 30% PEC loading. As shown in Figure 7, PVA aerogel readily catches fire (within 2 s) and continues to burn vigorously even after removing the flame source. In addition, it shows dripping of particles, which are further inflammable, and the 8 cm long sample completely burned down within 140 s leaving behind a black residue. PEC has definitely modified the flammability behavior of PVA aerogels. PVA-10%PEC aerogel took 12 s to catch fire on ignition with a butane flame, and it was able to self-extinguish the fire in 100 s. Half of the sample was burned before the fire extinguishment, and no melt dripping was observed. Flame retardancy of the aerogels got better and better with the increase of PEC content. The time taken to ignition for PVA-20%PEC aerogel was 15 s, and the flame got extinguished itself in 15 s. The best result was obtained for PVA-30%PEC aerogel, for which the time to ignition was 32 s and the time to extinguishment was 10 s. Hardly any sample got burned, i.e., the sample remained intact and intense charring occurred at the point of contact with the flame, as shown in Figure 7.

For the quantitative estimation of the flammability characteristics of the aerogels, microscale combustion calorimetry (MCC) was used. The important parameters obtained from this method are the heat release rate (HRR) and total heat release (THR), and their estimation is based on the oxygen consumption during the burning process. HRR is the prime property to be considered in this context since the rate at which heat is released by a material during burning can significantly contribute to the fire growth and its spreading.[59] Other key parameters such as heat release capacity (HRC), peak heat release rate (PHRR), and time to peak heat release rate (TTPHRR) can also be obtained, which are listed in Table 2. Figure S7a differentiates between the HRR curves of neat PVA and PVA-PEC aerogels, where HRR is plotted as a function of temperature. For neat PVA aerogel, the HRR value

Table 2. Flame-Retardant Parameters Estimated from LOI and MCC Tests and Water Contact Angles of the Aerogel Samples Prepared in This Study

sample	LOI (%)	PHRR (W/g)	TTPHRR (s)	THR (kJ/g)	HRC (J/g K)	WCA (deg)
PVA aerogel	19.6 ± 0.3	195	270	19.67	295	
*Sil*PVA aerogel	21.8 ± 0.4	139	361	14.67	205	126.5 ± 1.5
PVA-10%PEC	22.1 ± 0.3	121	402	15.47	199	26.9 ± 1.5
*Sil*PVA-10%PEC	24.6 ± 0.6	139	411	13.60	143	133.1 ± 1.5
PVA-20%PEC	25.6 ± 0.3	95	416	11.20	145	29.4 ± 1.5
*Sil*PVA-20%PEC	26.9 ± 0.4	140	404	12.53	134	134.2 ± 1.5
PVA-30%PEC	27.9 ± 0.7	116	423	13.60	207	27.1 ± 1.5
*Sil*PVA-30%PEC	31.2 ± 0.3	103	415	10.50	100	136.4 ± 1.5
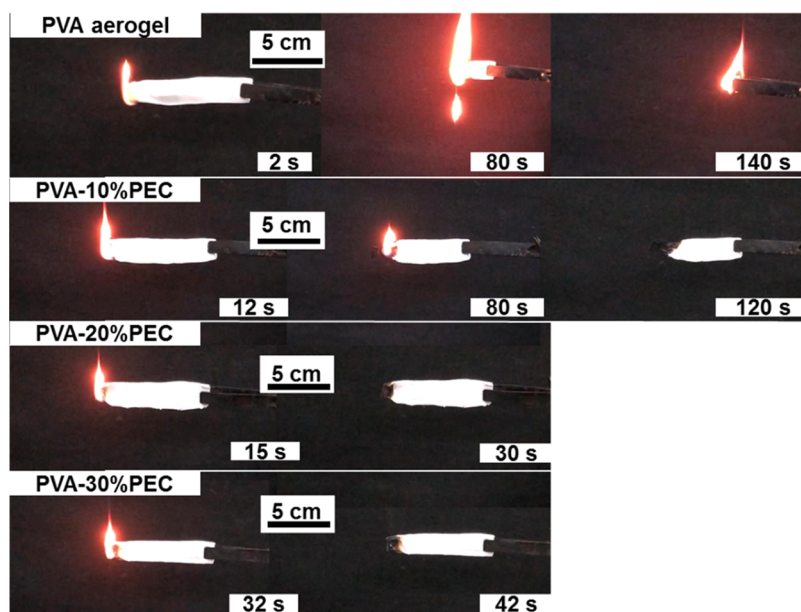
Figure 7. Photographs showing the burning behavior of PVA and PVA-PEC aerogels during the horizontal burning tests conducted using a butane flame. The images at different times during the burning process show the excellent flame retardant and self-extinguishing behavior of PVA-PEC aerogels.

increases sharply after 200 °C and reaches its peak (195 W/g) at around 280 °C. Between 400 and 500 °C, another small peak was obtained, which indicates the multistep thermal degradation of PVA aerogel. However, in PVA-PEC aerogels, there was a slight shift in the HRR curves towards the high-temperature side, which may be due to the enhanced thermal stability of PEC-incorporated PVA aerogels. Also, the HRR values were significantly reduced in the PVA-PEC aerogels, particularly in the temperature range of 250−360 °C in comparison with the neat PVA aerogel. From 195 W/g for PVA aerogel, the PHRR drastically decreased to 95 W/g for PVA-20%PEC, which is a clear indicator of the enhanced flame retardant properties after the addition of PEC to the PVA matrix. During the burning of PVA aerogel, plenty of hydrocarbon volatiles are released into the flame at the initial stage of degradation, i.e., during the decomposition of hydroxyl groups, which results in the generation of a lot of heat.[60] But in the case of PVA-PEC aerogels, due to the action of PEC, flammable volatiles are least produced during the first stage (250−360 °C) of decomposition. This resulted in the lowering of the HRR of PVA-PEC aerogels initially. However, the peak values of HRR curves for PVA-PEC aerogels were obtained between 400 and 500 °C, which manifests the fact that maximum flammability and flashover potential of PVA-PEC aerogels were reached in the second step of degradation.

Therefore, the TTPHRR values were increased from 270 s in PVA aerogels to 402, 416, and 423 s in PVA-10%PEC, PVA-20%PEC, and PVA-30%PEC aerogels, respectively. The carbonaceous layer formed during the initial degradation step acts as a barrier to prevent the underlying material from burning. Thus, we can conclude that the results from MCC measurements support the results obtained by LOI measurements and horizontal burning tests (UL 94) and the PVA aerogels attained excellent flame retardancy in the presence of PEC.

Hydrophobic Surface Modification of Aerogels and Their Performance Comparison. The moisture sensitivity as well as the highly hydrophilic nature of PVA-based aerogels is a hurdle for their practical usage. By engineering the surface chemistry of materials, hydrophobic or even superhydrophobic surfaces could be obtained. Following this concept, we performed a simple surface silanization using methyltrichlorosilane by thermal chemical vapor deposition (CVD) on the aerogels. After the silanization reaction in the presence of water, a hydrophobic silicone coating was formed over the aerogel surface.[53] CVD using silane is a well-known strategy for making hydrophobic surfaces.[22,53,61] Although methyltrichlorosilane was used for surface modification, no chlorine elements were introduced onto the surface-modified aerogels. On coating the aerogels using hydrophobic methyl groups, as we

have done here, the WCA enhanced significantly, as given in Table 2. All of the aerogel samples became highly hydrophobic, and the maximum value of WCA, i.e., 136.4 ± 1.5°, was obtained for PVA-30%PEC aerogel, as shown in Figure 8a.
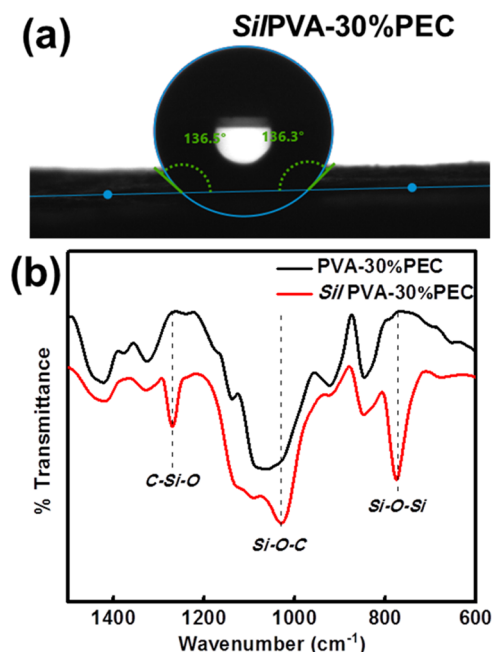

Figure 8. (a) Image showing the WCA of PVA-30%PEC aerogel after the surface silane treatment. The contact angle has increased from ~27 to ~136°. (b) FTIR spectra of PVA-30%PEC aerogel before and after silane modification.

Hereafter, the silane-modified aerogels will be denoted with *Sil* in front, for example, silanized PVA-30%PEC aerogel is denoted as the *Sil*PVA-30%PEC aerogel. The successful formation of silicone coating over the aerogel surfaces was confirmed using FTIR spectroscopy (Figure 8b). The peaks at 1269, 1028, and 775 cm^{-1} correspond to C−Si−O, Si−O−C, and Si−O−Si bonds. To our surprise, the aerogels after surface modification showed excellent water adhesion properties along with hydrophobicity. The water droplet did not fall down even after turning the aerogel surface upside down, and Figure S8a demonstrates the water adhesion property of *Sil*PVA-30%PEC aerogel. Water droplets as big as 43 μL could be tightly pinned and suspended upside down from the aerogel surface (Figure S8b), which further illustrates the above-mentioned property. Such a sticky hydrophobicity could possibly be because of the surface morphology of the coated aerogels, which shows numerous protrusions, micro wrinkles, and folds, as shown in Figure S8c. As a result, the water droplets cannot directly contact the cellular surface of the aerogels but can penetrate the pores to some extent, and this leads to the Cassie impregnating wetting state.[62,63] Thus, we can conclude that the micro-roughness of the surface, together with the low surface energy of the silicone coating, leads to the rose petal-like nature in surface-modified aerogels. It was also observed that the compression strength measured for the surface-modified PVA-PEC aerogels was more or less the same as that of the unmodified aerogels (Figure S4c).

The surface modification of aerogels had a significant influence on their thermal and flammability properties. The TGA thermograms in Figure S9 compare the thermal stability

of PVA-PEC aerogels before and after the silanization process. The silane-coated aerogels showed better thermal stability than the uncoated ones, as evident from the improved $T_{50\%}$ values. $T_{50\%}$ for PVA-10%PEC and PVA-20%PEC aerogels were 330 and 331 °C, respectively, whereas the same for *Sil*PVA-10% PEC and *Sil*PVA-20%PEC are 402 and 405 °C, respectively. There is a clear-cut elevation in the thermal stability, which could be attributed to the hindrance of PVA backbone decomposition due to the covalent association between PVA and silane.[22,61] Also, the surface modification of aerogels reduced their moisture sensitivity, as evident from the lower weight loss % below 100 °C for *Sil*PVA-10%PEC and *Sil*PVA-20%PEC aerogels (Figure S9).

Similarly, the antifire performance of all of the samples has been improved further upon surface modification, as evident from Figure S10, which demonstrates the horizontal burning test of *Sil*PVA-30%PEC aerogel. We could observe that the moment the flame source was removed, the fire got extinguished and a charred layer was formed on the aerogel surface. Complimentary results were obtained for *Sil*PVA-PEC aerogels from the MCC tests. The HRR peak around 300 °C was almost nullified in the case of *Sil*PVA-PEC aerogels compared to the unmodified aerogels (Figure S7b). This is because the silane coating has delayed the decomposition of the organic moieties of the aerogels, resulting in lower heat generation. However, at higher temperatures (400−500 °C), peak HRR values similar to the unmodified aerogels were reached probably because of the degradation of the organics. From Table 2, it is clear that the LOI values have increased significantly after the silane coating, even for the neat PVA aerogel. LOI as high as 31.2% was marked for *Sil*PVA-30%PEC aerogel and the parameters such as PHRR, THR, and HRC were very low for the silylated aerogels. However, for *Sil*PVA aerogel, i.e., silane-modified PVA aerogel without PEC, LOI and PHRR were 21.8% and 139 W/g, respectively. Thus, it was proved that the synergistic effect of PEC and the silane coating could not only retard the moisture sensitivity of PVA-based aerogels but also enhance their thermal stability and flame retardancy to a great extent.

■ CONCLUSIONS

In summary, a sustainable organic antifire filler prepared from CS and PA by ionic complexation was employed for the fabrication of PVA hybrid aerogels by an environmentally friendly freeze-drying technique using water as the only medium. Aerogels with different weight loadings of PEC were prepared, and their properties were compared with that of neat PVA aerogel. The successful interactions between PVA and PEC and the subsequent excellent miscibility between them resulted in the enhanced mechanical and thermal properties of PVA-PEC aerogels. The aerogels exhibited very low density (~0.06 g/cm^3) and high compressive modulus (~1.5 MPa) at the same time. The early degradation in PVA-PEC aerogels catalyzed by the PEC resulted in higher char yields as well as the enhanced thermal stability of aerogels. Depending on the PEC content, the aerogels showed maximum sound absorption (~90%) at different frequency ranges. Burning tests, LOI measurements, and MCC analysis together demonstrated the excellent flame-retardant behavior of PVA aerogels after the PEC incorporation. The LOI value increased from ~19 to ~28% as the PEC content increased from 0 to 30%, and all of the PVA-PEC aerogels exhibited self-extinguishment of flame. The delayed degradation of PVA and

the intense char layer formed due to the action of PEC resulted in the improved flame retardancy of aerogels. To overcome the hydrophilic nature of the prepared aerogels, surface silane treatment was carried out by a simple CVD method. The surface-modified aerogels showed a combination of hydrophobicity (WCA ~136°) and water adhesion properties due to the specialty in the surface morphology, and their thermal stability and flame retardancy were improved further. The multifunctional properties of the sustainable aerogels prepared in this study indicate that these materials have broad application prospects, particularly as structural and sound insulating materials.

ASSOCIATED CONTENT

ⓢ Supporting Information

The Supporting Information is available free of charge at https://pubs.acs.org/doi/10.1021/acsapm.2c00639.

> High-resolution XPS spectra of PEC and aerogels; WAXS patterns of chitosan, phytic acid, and PEC; photographs of aerogels; images of water droplets on aerogels and contact angle measurements; TGA thermograms of aerogels; and photographs showing the burning behavior of *Sil*PVA-30%PEC aerogel (PDF)

> Horizontal burning test conducted on PVA aerogel (Movie S1) (MOV)

> Horizontal burning test conducted on PVA-10%PEC aerogel (Movie S2) (MOV)

> Horizontal burning test conducted on PVA-20%PEC aerogel (Movie S3) (MOV)

> Horizontal burning test conducted on PVA-30%PEC aerogel (Movie S4) (MOV)

AUTHOR INFORMATION

Corresponding Author

E. Bhoje Gowd − *Materials Science and Technology Division, CSIR-National Institute for Interdisciplinary Science and Technology, Trivandrum 695019 Kerala, India; Academy of Scientific and Innovative Research (AcSIR), Ghaziabad 201002, India;* ⓞ orcid.org/0000-0002-2878-5845; Phone: +91-471-2515474; Email: bhojegowd@niist.res.in; Fax: +91-471-2491712

Authors

Vipin G. Krishnan − *Materials Science and Technology Division, CSIR-National Institute for Interdisciplinary Science and Technology, Trivandrum 695019 Kerala, India; Academy of Scientific and Innovative Research (AcSIR), Ghaziabad 201002, India*

C. V. Sijla Rosely − *Materials Science and Technology Division, CSIR-National Institute for Interdisciplinary Science and Technology, Trivandrum 695019 Kerala, India; Academy of Scientific and Innovative Research (AcSIR), Ghaziabad 201002, India*

Andreas Leuteritz − *Leibniz-Institut für Polymerforschung Dresden e.V., D-01069 Dresden, Germany*

Complete contact information is available at:
https://pubs.acs.org/10.1021/acsapm.2c00639

Notes

The authors declare no competing financial interest.

REFERENCES

(1) Kistler, S. S. Coherent Expanded Aerogels and Jellies. *Nature* **1931**, *127*, 741.

(2) Kistler, S. S. Coherent Expanded-Aerogels. *J. Phys. Chem. A* **1932**, *36*, 52−64.

(3) Pierre, A. C.; Pajonk, G. M. Chemistry of Aerogels and Their Applications. *Chem. Rev.* **2002**, *102*, 4243−4266.

(4) Noroozi, M.; Panahi-Sarmad, M.; Abrisham, M.; Amirkiai, A.; Asghari, N.; Golbaten-Mofrad, H.; Karimpour-Motlagh, N.; Goodarzi, V.; Bahramian, A. R.; Zahiri, B. Nanostructure of Aerogels and Their Applications in Thermal Energy Insulation. *ACS Appl. Energy Mater.* **2019**, *2*, 5319−5349.

(5) An, L.; Wang, J.; Petit, D.; Armstrong, J. N.; Hanson, K.; Hamilton, J.; Souza, M.; Zhao, D.; Li, C.; Liu, Y.; et al. An All-Ceramic, Anisotropic, and Flexible Aerogel Insulation Material. *Nano Lett.* **2020**, *20*, 3828−3835.

(6) Li, M.; Qin, Z.; Cui, Y.; Yang, C.; Deng, C.; Wang, Y.; Kang, J. S.; Xia, H.; Hu, Y. Ultralight and Flexible Monolithic Polymer Aerogel with Extraordinary Thermal Insulation by a Facile Ambient Process. *Adv. Mater. Interfaces* **2019**, *6*, No. 1900314.

(7) Zhu, J.; Xiong, R.; Zhao, F.; Peng, T.; Hu, J.; Xie, L.; Xie, H.; Wang, K.; Jiang, C. Lightweight, High-Strength, and Anisotropic Structure Composite Aerogel Based on Hydroxyapatite Nanocrystal and Chitosan with Thermal Insulation and Flame Retardant Properties. *ACS Sustainable Chem. Eng.* **2020**, *8*, 71−83.

(8) Oh, J.-H.; Kim, J.; Lee, H.; Kang, Y.; Oh, I.-K. Directionally Antagonistic Graphene Oxide-Polyurethane Hybrid Aerogel as a Sound Absorber. *ACS Appl. Mater. Interfaces* **2018**, *10*, 22650−22660.

(9) He, C.; Huang, J.; Li, S.; Meng, K.; Zhang, L.; Chen, Z.; Lai, Y. Mechanically Resistant and Sustainable Cellulose-Based Composite Aerogels with Excellent Flame Retardant, Sound-Absorption, and Superantiwetting Ability for Advanced Engineering Materials. *ACS Sustainable Chem. Eng.* **2018**, *6*, 927−936.

(10) Takeshita, S.; Yoda, S. Chitosan Aerogels: Transparent, Flexible Thermal Insulators. *Chem. Mater.* **2015**, *27*, 7569−7572.

(11) Si, Y.; Yu, J.; Tang, X.; Ge, J.; Ding, B. Ultralight Nanofibre-Assembled Cellular Aerogels with Superelasticity and Multifunctionality. *Nat. Commun.* **2014**, *5*, No. 5802.

(12) Krishnan, V. G.; Joseph, A. M.; Kuzhichalil Peethambharan, S.; Gowd, E. B. Nanoporous Crystalline Aerogels of Syndiotactic Polystyrene: Polymorphism, Dielectric, Thermal, and Acoustic Properties. *Macromolecules* **2021**, *54*, 10605−10615.

(13) Hrubesh, L.; Keene, L.; Latorre, V. Dielectric Properties of Aerogels. *J. Mater. Res.* **1993**, *8*, 1736−1741.

(14) Joseph, A. M.; Nagendra, B.; Shaiju, P.; Surendran, K.; Gowd, E. B. Aerogels of Hierarchically Porous Syndiotactic Polystyrene with a Dielectric Constant near to Air. *J. Mater. Chem. C* **2018**, *6*, 360−368.

(15) Meador, M. A. B.; Wright, S.; Sandberg, A.; Nguyen, B. N.; Van Keuls, F. W.; Mueller, C. H.; Rodríguez-Solís, R.; Miranda, F. A. Low Dielectric Polyimide Aerogels as Substrates for Lightweight Patch Antennas. *ACS Appl. Mater. Interfaces* **2012**, *4*, 6346−6353.

(16) Meador, M. A. B.; McMillon, E.; Sandberg, A.; Barrios, E.; Wilmoth, N. G.; Mueller, C. H.; Miranda, F. lA. Dielectric and Other

Properties of Polyimide Aerogels Containing Fluorinated Blocks. *ACS Appl. Mater. Interfaces* **2014**, *6*, 6062−6068.

(17) Guo, H.; Dewey, O. S.; McCorkle, L. S.; Meador, M. A. B.; Pasquali, M. Polyimide Aerogels as Lightweight Dielectric Insulators for Carbon Nanotube Cables. *ACS Appl. Polym. Mater.* **2019**, *1*, 1680−1688.

(18) Fischer, U.; Saliger, R.; Bock, V.; Petricevic, R.; Fricke, J. Carbon Aerogels as Electrode Material in Supercapacitors. *J. Porous Mater.* **1997**, *4*, 281−285.

(19) Pottathara, Y. B.; Tiyyagura, H. R.; Ahmad, Z.; Sadasivuni, K. K. Graphene Based Aerogels: Fundamentals and Applications as Supercapacitors. *J. Energy Storage* **2020**, *30*, No. 101549.

(20) Senokos, E.; Rana, M.; Vila, M.; Fernandez-Cestau, J.; Costa, R. D.; Marcilla, R.; Vilatela, J. J. Transparent and Flexible High-Power Supercapacitors Based on Carbon Nanotube Fibre Aerogels. *Nanoscale* **2020**, *12*, 16980−16986.

(21) Guo, W.; Liu, J.; Zhang, P.; Song, L.; Wang, X.; Hu, Y. Multi-Functional Hydroxyapatite/Polyvinyl Alcohol Composite Aerogels with Self-Cleaning, Superior Fire Resistance and Low Thermal Conductivity. *Compos. Sci. Technol.* **2018**, *158*, 128−136.

(22) Zheng, Q.; Cai, Z.; Gong, S. Green Synthesis of Polyvinyl Alcohol (PVA)−Cellulose Nanofibril (CNF) Hybrid Aerogels and Their Use as Superabsorbents. *J. Mater. Chem. A* **2014**, *2*, 3110−3118.

(23) Wang, L.; Sánchez-Soto, M.; Maspoch, M. L. Polymer/Clay Aerogel Composites with Flame Retardant Agents: Mechanical, Thermal and Fire Behavior. *Mater. Des.* **2013**, *52*, 609−614.

(24) Wang, X.; Pan, Y.; Liu, X.; Liu, H.; Li, N.; Liu, C.; Schubert, D. W.; Shen, C. Facile Fabrication of Superhydrophobic and Eco-Friendly Poly (Lactic Acid) Foam for Oil−Water Separation Via Skin Peeling. *ACS Appl. Mater. Interfaces* **2019**, *11*, 14362−14367.

(25) Maquet, V.; Blacher, S.; Pirard, R.; Pirard, J.-P.; Jérôme, R. Characterization of Porous Polylactide Foams by Image Analysis and Impedance Spectroscopy. *Langmuir* **2000**, *16*, 10463−10470.

(26) Song, J.; Chen, C.; Yang, Z.; Kuang, Y.; Li, T.; Li, Y.; Huang, H.; Kierzewski, I.; Liu, B.; He, S.; et al. Highly Compressible, Anisotropic Aerogel with Aligned Cellulose Nanofibers. *ACS Nano* **2018**, *12*, 140−147.

(27) De France, K. J.; Hoare, T.; Cranston, E. D. Review of Hydrogels and Aerogels Containing Nanocellulose. *Chem. Mater.* **2017**, *29*, 4609−4631.

(28) Zhao, S.; Malfait, W. J.; Guerrero-Alburquerque, N.; Koebel, M. M.; Nyström, G. Biopolymer Aerogels and Foams: Chemistry, Properties, and Applications. *Angew. Chem., Int. Ed.* **2018**, *57*, 7580−7608.

(29) Yildirim, N.; Shaler, S.; Gardner, D.; Rice, R.; Bousfield, D. Cellulose Nanofibril (CNF) Reinforced Starch Insulating Foams. *MRS Proc.* **2014**, *1621*, 177−189.

(30) Shen, P.; Zhao, H.-B.; Huang, W.; Chen, H.-B. Poly (Vinyl Alcohol)/Clay Aerogel Composites with Enhanced Flame Retardancy. *RSC Adv.* **2016**, *6*, 109809−109814.

(31) Shang, K.; Ye, D.-D.; Kang, A.-H.; Wang, Y.-T.; Liao, W.; Xu, S.; Wang, Y.-Z. Robust and Fire Retardant Borate-Crosslinked Poly (Vinyl Alcohol)/Montmorillonite Aerogel Via Melt-Crosslink. *Polymer* **2017**, *131*, 111−119.

(32) Simón-Herrero, C.; Gómez, L.; Romero, A.; Valverde, J. L.; Sanchez-Silva, L. Nanoclay-Based PVA Aerogels: Synthesis and Characterization. *Ind. Eng. Chem. Res.* **2018**, *57*, 6218−6225.

(33) Chen, H.-B.; Liu, B.; Huang, W.; Wang, J.-S.; Zeng, G.; Wu, W.-H.; Schiraldi, D. A. Fabrication and Properties of Irradiation-Cross-Linked Poly (Vinyl Alcohol)/Clay Aerogel Composites. *ACS Appl. Mater. Interfaces* **2014**, *6*, 16227−16236.

(34) Chen, H.-B.; Wang, Y.-Z.; Schiraldi, D. A. Preparation and Flammability of Poly(Vinyl Alcohol) Composite Aerogels. *ACS Appl. Mater. Interfaces* **2014**, *6*, 6790−6796.

(35) Wang, Y.-T.; Zhao, H.-B.; Degracia, K.; Han, L.-X.; Sun, H.; Sun, M.; Wang, Y.-Z.; Schiraldi, D. A. Green Approach to Improving the Strength and Flame Retardancy of Poly (Vinyl Alcohol)/Clay Aerogels: Incorporating Biobased Gelatin. *ACS Appl. Mater. Interfaces* **2017**, *9*, 42258−42265.

(36) Chen, H.-B.; Schiraldi, D. A. Flammability of Polymer/Clay Aerogel Composites: An Overview. *Polym. Rev.* **2019**, *59*, 1−24.

(37) Wang, Y.-T.; Liao, S.-F.; Shang, K.; Chen, M.-J.; Huang, J.-Q.; Wang, Y.-Z.; Schiraldi, D. A. Efficient Approach to Improving the Flame Retardancy of Poly (Vinyl Alcohol)/Clay Aerogels: Incorporating Piperazine-Modified Ammonium Polyphosphate. *ACS Appl. Mater. Interfaces* **2015**, *7*, 1780−1786.

(38) Sun, H.; Schiraldi, D. A.; Chen, D.; Wang, D.; Sánchez-Soto, M. Tough Polymer Aerogels Incorporating a Conformal Inorganic Coating for Low Flammability and Durable Hydrophobicity. *ACS Appl. Mater. Interfaces* **2016**, *8*, 13051−13057.

(39) Luo, Y.; Xie, D.; Chen, Y.; Han, T.; Chen, R.; Sheng, X.; Mei, Y. Synergistic Effect of Ammonium Polyphosphate and A-Zirconium Phosphate in Flame-Retardant Poly (Vinyl Alcohol) Aerogels. *Polym. Degrad. Stab.* **2019**, *170*, No. 109019.

(40) Sheng, X.; Li, S.; Zhao, Y.; Zhai, D.; Zhang, L.; Lu, X. Synergistic Effects of Two-Dimensional Mxene and Ammonium Polyphosphate on Enhancing the Fire Safety of Polyvinyl Alcohol Composite Aerogels. *Polymers* **2019**, *11*, 1964.

(41) Zhang, Q.; Wang, X.; Tao, X.; Li, Z.; Li, X.; Zhang, Z. Polyvinyl Alcohol Composite Aerogel with Remarkable Flame Retardancy, Chemical Durability and Self-Cleaning Property. *Compos. Commun.* **2019**, *15*, 96−102.

(42) Shang, K.; Yang, J.-C.; Cao, Z.-J.; Liao, W.; Wang, Y.-Z.; Schiraldi, D. A. Novel Polymer Aerogel toward High Dimensional Stability, Mechanical Property, and Fire Safety. *ACS Appl. Mater. Interfaces* **2017**, *9*, 22985−22993.

(43) Zhang, T.; Yan, H.; Shen, L.; Fang, Z.; Zhang, X.; Wang, J.; Zhang, B. Chitosan/Phytic Acid Polyelectrolyte Complex: A Green and Renewable Intumescent Flame Retardant System for Ethylene−Vinyl Acetate Copolymer. *Ind. Eng. Chem. Res.* **2014**, *53*, 19199−19207.

(44) Cai, X.; Chen, H.; Jiang, D.; Pan, M.; Mei, C. The Thermal Property and Flame Retardancy of Rpc with a Polyelectrolyte Complex of Nanocrystalline Cellulose and Ammonium Polyphosphate. *J. Therm. Anal. Calorim.* **2018**, *134*, 2089−2096.

(45) Zhang, Z.; Li, X.; Ma, Z.; Ning, H.; Zhang, D.; Wang, Y. A Facile and Green Strategy to Simultaneously Enhance the Flame Retardant and Mechanical Properties of Poly (Vinyl Alcohol) by Introduction of a Bio-Based Polyelectrolyte Complex Formed by Chitosan and Phytic Acid. *Dalton Trans.* **2020**, *49*, 11226−11237.

(46) Zhou, Y.; Tawiah, B.; Noor, N.; Zhang, Z.; Sun, J.; Yuen, R. K.; Fei, B. A Facile and Sustainable Approach for Simultaneously Flame Retarded, Uv Protective and Reinforced Poly (Lactic Acid) Composites Using Fully Bio-Based Complexing Couples. *Composites, Part B* **2021**, *215*, No. 108833.

(47) Cheng, X.-W.; Guan, J.-P.; Yang, X.-H.; Tang, R.-C.; Yao, F. A Bio-Resourced Phytic Acid/Chitosan Polyelectrolyte Complex for the Flame Retardant Treatment of Wool Fabric. *J. Cleaner Prod.* **2019**, *223*, 342−349.

(48) Lankalapalli, S.; Kolapalli, V. Polyelectrolyte Complexes: A Review of Their Applicability in Drug Delivery Technology. *Indian J. Pharm. Sci.* **2009**, *71*, 481.

(49) Verma, A.; Verma, A. Polyelectrolyte Complex-An Overview. *Int. J. Pharm. Sci. Res.* **2013**, *4*, 1684.

(50) Meka, V. S.; Sing, M. K.; Pichika, M. R.; Nali, S. R.; Kolapalli, V. R.; Kesharwani, P. A Comprehensive Review on Polyelectrolyte Complexes. *Drug Discovery Today* **2017**, *22*, 1697−1706.

(51) Haile, M.; Leistner, M.; Sarwar, O.; Toler, C. M.; Henderson, R.; Grunlan, J. C. A Wash-Durable Polyelectrolyte Complex That Extinguishes Flames on Polyester−Cotton Fabric. *RSC Adv.* **2016**, *6*, 33998−34004.

(52) Zhang, L.; Yi, D.; Hao, J. Poly (Diallyldimethylammonium) and Polyphosphate Polyelectrolyte Complex as Flame Retardant for Char-Forming Epoxy Resins. *J. Fire Sci.* **2020**, *38*, 333−347.

(53) Gong, X.; Wang, Y.; Zeng, H.; Betti, M.; Chen, L. Highly Porous, Hydrophobic, and Compressible Cellulose Nanocrystals/Poly (Vinyl Alcohol) Aerogels as Recyclable Absorbents for Oil−Water Separation. *ACS Sustainable Chem. Eng.* **2019**, *7*, 11118−11128.

(54) Chen, J.; Han, S.; Huang, M.; Li, J.; Zhou, M.; He, J. Green Crosslinked Nanofibers Membrane Based on CS/PVA Combined with Polybasic Organic Acid for Tympanic Membrane Repair. *Int. J. Polym. Mater. Polym. Biomater.* **2022**, *71*, 291−301.

(55) Wang, X.; Jana, S. C. Synergistic Hybrid Organic−Inorganic Aerogels. *ACS Appl. Mater. Interfaces* **2013**, *5*, 6423−6429.

(56) Wang, L.; Sanchez-Soto, M.; Maspoch, M. L. Polymer/Clay Aerogel Composites with Flame Retardant Agents: Mechanical, Thermal and Fire Behavior. *Mater. Des.* **2013**, *52*, 609−614.

(57) Rapisarda, M.; Malfense Fierro, G.-P.; Meo, M. Ultralight Graphene Oxide/Polyvinyl Alcohol Aerogel for Broadband and Tuneable Acoustic Properties. *Sci. Rep.* **2021**, *11*, No. 10572.

(58) Benzarti, K.; Colin, X. Understanding the Durability of Advanced Fibre-Reinforced Polymer (FRP) Composites for Structural Applications. In *Advanced Fibre-Reinforced Polymer (FRP) Composites for Structural Applications*, Elsevier, 2013; pp 361−439.

(59) Mouritz, A.; Mathys, Z.; Gibson, A. Heat Release of Polymer Composites in Fire. *Composites, Part A* **2006**, *37*, 1040−1054.

(60) Mouritz, A. Durability of Composites Exposed to Elevated Temperature and Fire. In *Durability of Composites for Civil Structural Applications*, Elsevier, 2007; pp 98−125.

(61) Javadi, A.; Zheng, Q.; Payen, F.; Javadi, A.; Altin, Y.; Cai, Z.; Sabo, R.; Gong, S. Polyvinyl Alcohol-Cellulose Nanofibrils-Graphene Oxide Hybrid Organic Aerogels. *ACS Appl. Mater. Interfaces* **2013**, *5*, 5969−5975.

(62) Feng, L.; Zhang, Y.; Xi, J.; Zhu, Y.; Wang, N.; Xia, F.; Jiang, L. Petal Effect: A Superhydrophobic State with High Adhesive Force. *Langmuir* **2008**, *24*, 4114−4119.

(63) Hu, H.; Zhao, Z.; Wan, W.; Gogotsi, Y.; Qiu, J. Polymer/Graphene Hybrid Aerogel with High Compressibility, Conductivity, and "Sticky" Superhydrophobicity. *ACS Appl. Mater. Interfaces* **2014**, *6*, 3242−3249.

Article

Thermoreversible Gels of Poly(L-lactide)/Poly(D-lactide) Blends: A Facile Route to Prepare Blend α-Form and Stereocomplex Aerogels

Vipin G. Krishnan, N. M. Praveena, R. B. Amal Raj, Kiran Mohan, and E. Bhoje Gowd*

Cite This: ACS Appl. Polym. Mater. 2023, 5, 1556−1564

Read Online

ACCESS | Metrics & More | Article Recommendations | SI Supporting Information

ABSTRACT: The demand for biodegradable polymer-based aerogels with superior comprehensive properties has escalated in various fields of application, such as packaging, tissue engineering, thermal insulation, acoustic insulation, and environmental remediation. In this work, we report a facile strategy for enhancing the thermal and mechanical properties of polylactide (PLA) aerogels through the stereocomplex (SC) formation between the opposite enantiomers. Thermoreversible gelation of poly(L-lactide) (PLLA)/poly(D-lactide) (PDLA) blend in crystal complex forming solvent and the subsequent thermal annealing of the gel resulted in crystalline pure SC gel, which, upon solvent exchange with water

PLLA/PDLA Blend Gel (ε form) / ANNEALING @ 70 °C / Stereocomplex Gel / Freeze-Drying / Blend Aerogel (α form) / Stereocomplex Aerogel (SC)

and freeze-drying, furnished robust SC aerogel. It was found that the SC content could be tuned by varying the annealing temperature of the blend gel and that we could prepare blend aerogels with pure α crystalline form and a mixture of α and SC. Crystalline pure blend α aerogel showed fibrillar morphology, whereas SC aerogel exhibited unique interwoven ball-like microstructures interconnected by PLLA and PDLA chains. The structural evolution during SC formation at the molecular level and the micrometer length scale instigated better properties in the PLA aerogels. When compared with the homopolymer aerogels, the crystalline pure SC aerogel showed an enhanced melting temperature of 227 ± 2 °C (50 °C higher), better thermal stability (onset of degradation was delayed by ∼40 °C), enhanced mechanical strength (compression modulus of 3.3 MPa), and better sound absorption ability. The biodegradability of PLA and the superior properties induced by stereocomplexation make these aerogels potential candidates for applications such as tissue engineering scaffolds, packaging, acoustic insulation, etc.

KEYWORDS: polylactide, stereocomplex, crystal complex, aerogel, solvent exchange, freeze-drying
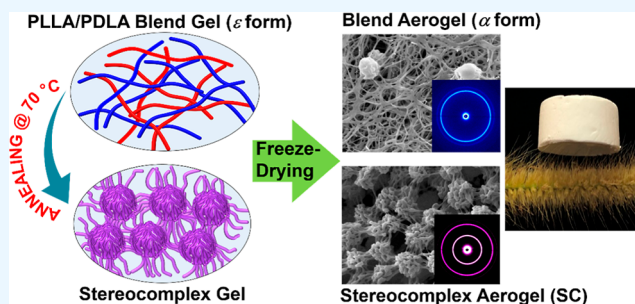
■ INTRODUCTION

Aerogels based on biodegradable polymers are the future of lightweight materials due to their comprehensive mechanical properties, easy processability, facile tunability, and environment-friendliness.[1−3] Among biopolymers, poly(L-lactide) (PLLA) and poly(D-lactide) (PDLA), are versatile and are commercially available. The aerogels of these polymers show great potential to replace fossil-based, nondegradable polymer aerogels and foams for different applications, from scaffolds for tissue regeneration to biodegradable packaging.[4−8] Stereocomplexation has been an efficient strategy for enhancing polylactide (PLA) properties, either in bulk or in aerogels/foams.[7,9−25] Blending the enantiomeric PLAs with the opposite enantiomer can introduce stereocomplex (SC) crystallites, resulting in enhanced crystallinity, thermal properties, and mechanical properties.[7,9−26] The SC formation in PLA mainly depends on the molecular weights of the homopolymers. Low molecular weight polymers (below 20,000 Da) readily favor the SC formation.[14,20,21,27] However, homopolymer crystallization dominates over the SC formation for PLLA/PDLA blends with high molecular weight polymers (above 20,000 Da).[14,20,21,28] Several strategies have been developed for the

exclusive SC formation in the high molecular weight PLLA/ PDLA blends. It was reported that the content of SC is sensitive to several factors, such as chain entanglements, chain diffusion, chain mobility, optical purity, and the mixing level of PLLA/PDLA.[11,15,20,23,29−33] In the conventional route, SC formation was achieved by melt blending and subsequent annealing of the blend at temperatures near the melting temperature of homopolymers.[34,35] However, no attempts were made to prepare the exclusive SC aerogels, as this procedure involves gel formation and subsequent solvent extraction.

Semicrystalline polymers are known to form thermoreversible gels through crystallization, where the small crystallites constitute the physical cross-links (junction zones) of the three-dimensional polymer networks.[36−43] In certain polymers,
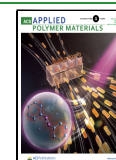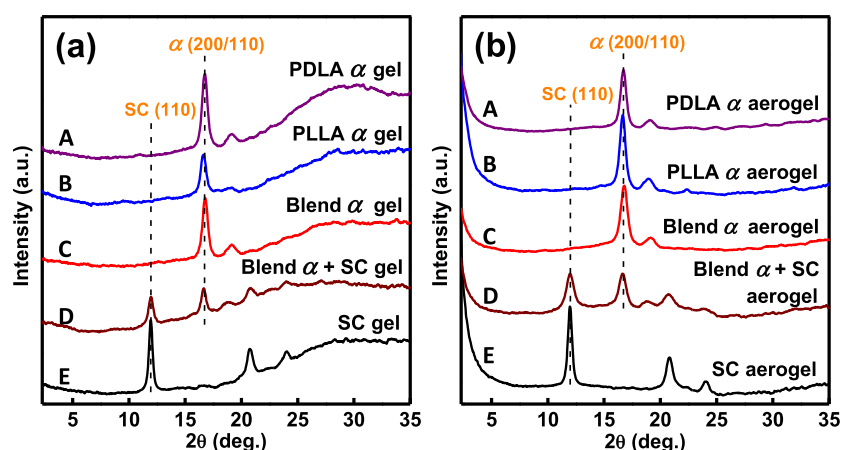
Figure 1. WAXD patterns of various (a) gels after the solvent exchange with water and (b) aerogels (gels after freeze-drying).

such as syndiotactic polystyrene (sPS) and poly(phenylene oxide) (PPO), the gelation solvent can form crystal complexes with polymers, that is, the polymer accommodates solvent molecules within its crystal lattice.[36,38,41,44−46] Similar to sPS and PPO, polylactides (PLLA and PDLA) are also known to form crystal complexes (ε-form) in certain solvents like *N,N*-dimethylformamide (DMF), tetrahydrofuran, cyclopentanone (CPO), and so forth.[15,47−51] PLLA has been demonstrated to form ε gel readily on cooling the polymer solution in DMF to below 0 °C. Matsuda et al. reported that the gelation of PLLA was induced by the solvents that form crystal complexes (ε crystals), and no such gel formation was observed in the solvents that cannot form PLLA crystal complexes.[40] These thermoreversible gels undergo a phase transition upon heating to form stable α-form gels at moderate temperatures. Even though much work has not been done on PDLA crystalline complexes, the same behavior was reported for PDLA in DMF.[15] ε gels of PLLA or PDLA could be converted to aerogels by extracting the gel solvent using techniques like supercritical drying or freeze-drying. However, the direct removal of organic solvents using these methods is tricky due to the high critical temperatures/pressures or low freezing points. Therefore, solvent exchange strategies should be adopted to facilitate the easy removal of gel solvents.[52,53] Matsuda et al. showed that DMF in PLLA ε gel is readily exchangeable with water without the disintegration of the gel network, and in the resultant gel, ε crystals transformed to α crystals bereft of any morphological changes.[40] However, there are no reports on homopolymer aerogels obtained by this method.

Though there is some understanding of the gel formation of homopolymers, the blending of PLLA and PDLA in crystal complex forming solvents for the preparation of aerogels has never been explored. Recent reports on SC PLA aerogel used 1,4-dioxane as the solvent for blending the enantiomers of PLA.[7,54] The blend solution was frozen and then freeze-dried to obtain the aerogels. It has to be noted that 1,4-dioxane does not induce typical thermoreversible gelation of PLA; hence, the resultant aerogels suffer from poor crystallinity. Praveena et al. tried the gel formation of PLLA/PDLA blends in DMF in the quest of SC crystallization and found that PLLA and PDLA chains in the blend gel crystallized independently into the corresponding crystal complexes (ε-form) rather than into the SC.[15] Although the SC formation was well studied in bulk, many questions are left unanswered in understanding the SC

formation in gels and aerogels. For example, is it possible to obtain pure SC gel without homopolymer crystals by blending PLLA and PDLA? Is it possible to convert the SC gel to SC aerogel without structural reorganization during solvent extraction? What happens to the structure of the blend gel in a hierarchical length scale on solvent extraction? So far, no one has attempted to answer the abovementioned questions, as gel formation and solvent exchange resulted in the structural change of PLAs.

In this work, we propose a simple strategy for the preparation of SC aerogels with crystalline purity by blending PLLA and PDLA in DMF. The PLLA/PDLA blend gel on solvent exchange with water resulted in the α-form gel, which, upon freeze-drying, furnished α-form aerogel. In order to instigate the chain diffusion and the alternate packing of the enantiomeric chains, the blend ε gel was thermally annealed at 70 °C. As a result, SC gel (without homocrystals) was obtained, which was then converted to aerogel by solvent exchange and freeze-drying. The degree of crystallinity was enhanced and unique morphologies were generated when the enantiomeric chains co-crystallized into the SC. These hierarchical structural changes resulted in the enhancement of the thermal, mechanical, and surface properties of aerogel.

■ RESULTS AND DISCUSSION

The PLLA/PDLA (1:1) blend gel was prepared by homogeneously mixing the equimolar PLLA and PDLA solutions prepared in DMF and cooling the mixed solution to below 0 °C. Similarly, homopolymer gels were also prepared. The total polymer concentration in the solution was 10 wt % in all the cases. The blend gel, similar to the PLLA and PDLA gels, crystallized into the ε-form with PLLA and PDLA chains adopting 10_7 helical conformations and accommodating DMF molecules within the orthorhombic lattice ($2\theta = 9.8°$ (111), 11.9° (200), 14.1° (020), 15.7° (121/114), 18.5° (123), 19.5° (223), 20.8° (116), and 23.8° (117)).[47] These gels were quite stable for a long duration even at room temperature, as evident from the wide-angle X-ray diffraction (WAXD) patterns in Figure S1. The gel solvent (DMF) of the blend as well as the homopolymer ε gels were exchanged with water (with a higher freezing temperature (0 °C) than DMF (−61 °C)) before the freeze-drying process to ease the solvent removal and obtain aerogels with negligible size reduction. However, solvent exchange resulted in a phase transition from ε-to-α form through a local disorder in the
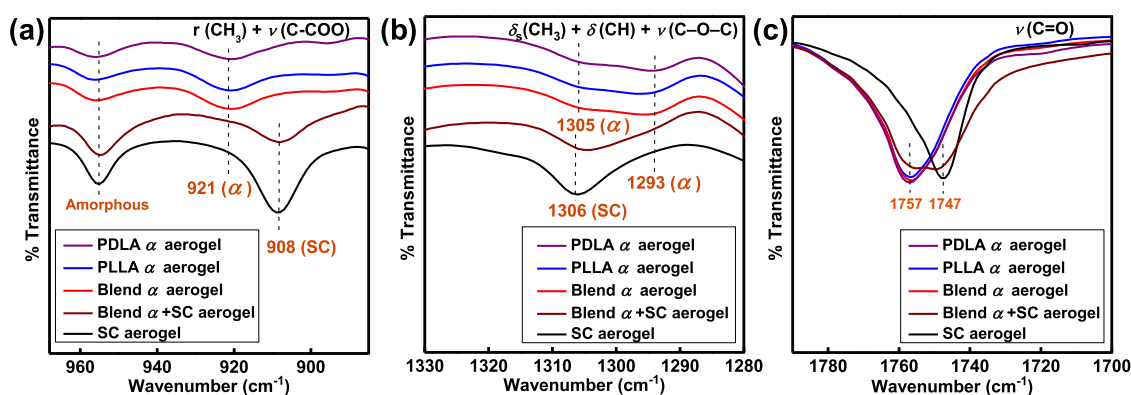
Figure 2. FTIR spectra of various aerogels in the regions of (a) 880−980, (b) 1280−1330, and (c) 1700−1800 cm^{-1}.

helical conformation within the crystal lattice following the solvent desorption from the crystal lattice to the amorphous region. The WAXD patterns of the PDLA, PLLA, and PLLA/PDLA blend gels after the solvent exchange (Figure 1a (A−C)) show characteristic reflections of the α-form ($2\theta = 16.7°$ (200/110) and 19.1° (203)).[55] Note that the PLLA/PDLA ratio in the blends is 1:1 throughout the entire work. The α crystalline form of PLA is stable, and therefore, solvent extraction from the gels resulted in α-form aerogels, as shown in Figure 1b (A−C). The degree of crystallinity of the obtained PLLA, PDLA, and PLLA/PDLA α aerogels was 51 ± 2, 49 ± 2, and $47 \pm 2\%$, respectively.

Variable temperature WAXD studies of the PLLA/PDLA blend ε gel (Figure S2a) show that on heating the gel, the ε form transformed to the α-form around 45 °C (this is an irreversible transition), and simultaneously, some of the disordered PLLA and PDLA chains reorganized to form SC crystals. Further heating resulted in the melting of α crystals (destabilization) and the formation of highly stable SC gel by chain reorganization. It has to be noted that the contents of the α and SC crystals remain the same after annealing the blend gel just above the ε-to-α transition temperature (50 °C) for 250 min (Figure S2b). These experiments suggested that annealing the blend gel at 70 °C is crucial because the α crystals are quite stable below this temperature. Based on the abovementioned observations, we planned two experiments. In the first experiment, we annealed the blend ε gel just above the ε-to-α transition temperature (50 °C) for 5 min, cooled it back to room temperature, and then aged it at < 0 °C for 12 h. The WAXD pattern (Figure S3) of the resultant gel shows new reflections at $2\theta = 11.9°$ (110), 20.8° (300/030), and 24.0° (220) along with the characteristic reflections of the α-form. The new peaks correspond to the SC crystals and this mixed α + SC structure prevailed even after the solvent exchange (Figure 1a (D)). At ~50 °C, as discussed earlier, the solvent molecules from the crystal lattice of the ε form are ejected to the amorphous phase, and some of the disordered PLLA and PDLA chains come close to each other due to the activated mobility. As a consequence, the ε crystals reorganize to form α crystals, and a fraction of the disordered chains reorganize into SC. The same crystal structure was retained in the aerogel, as shown in Figure 1b (D). In the second experiment, thermal annealing of the blend ε gel was carried out at around 70 °C. At this temperature, the whole of PLLA and PDLA α crystals (formed at 50 °C) melted, and the polymer chains achieved enough mobility and diffusion ability to discover opposite chains for the reorganization into SC crystals (3_1 helical

conformation) (Figure S3).[16] SC form shows the highest stability among all the crystalline forms of PLA, and therefore, the SC gel formed by the abovementioned experiment retained its crystal structure even after the solvent exchange (Figure 1a (E)) and solvent removal (Figure 1b (E)). Thus, we prepared pure SC crystalline PLA aerogels by thermally annealing the PLLA/PDLA blend ε gel at ~70 °C for a short duration (10 min) followed by solvent exchange with water and freeze-drying. It has to be noted that thermal annealing of the blend ε gel did not affect the gel stability, and no dimensional changes were observed after the annealing process. Freeze-drying resulted in only negligible shrinkage (~3%), and all the aerogels prepared in this study had a total porosity of ~90%. SC aerogel exhibited the highest degree of crystallinity of $54 \pm 2\%$.

The successful formation of aerogels with various crystalline forms was further confirmed by Fourier transform infrared (FTIR) analysis. The IR spectral region between 880 and 980 cm^{-1} corresponds to the $r(CH_3) + \nu(C-COO)$ vibrational modes, which are sensitive to the chain packing mode of PLA.[56,57] Similarly, another IR region, 1280−1330 cm^{-1} corresponding to the $\delta_s(CH_3) + \delta(CH) + \nu(C-O-C)$ vibrations was also found to be helpful in distinguishing between different structural forms of PLAs.[51,58] Figure 2a,b shows explicit spectral differences between the α-form (blend and homopolymers) aerogels and the SC aerogel. The latter exhibits a peak at 908 cm^{-1}, which is absent in all the α-form aerogels. The 921 cm^{-1} band is the characteristic band of the α-form,[16,19,57] and it was absent in the SC aerogel (Figure 2a). In the other spectral region (1280−1330 cm^{-1}) also, the peak positions were quite different for SC (1306 and 1318 cm^{-1}) and α-form (1293 and 1305 cm^{-1}) aerogels, as shown in Figure 2b. These observations substantiate the results obtained from the WAXD studies and confirm the crystal structure of all the aerogels prepared in this study. Figure 2c shows the carbonyl stretching region of various aerogels. Homopolymer and blend α-form aerogels showed identical carbonyl stretching frequencies (1757 cm^{-1}); however, in SC aerogel, there is a shift in the stretching peak towards the lower wavenumber (1747 cm^{-1}), which is attributed to the conformational change (from 10_7 to 3_1) of PLA chains and the strong interactions between the PLLA and PDLA chains. As expected, the α + SC aerogel exhibited two stretching frequencies in the intermediate region between 1757 and 1747 cm^{-1}, corresponding to the α and SC forms of PLA.

The homopolymer aerogels melted around 176 ± 2 °C, as shown in the differential scanning calorimetry (DSC) thermo-
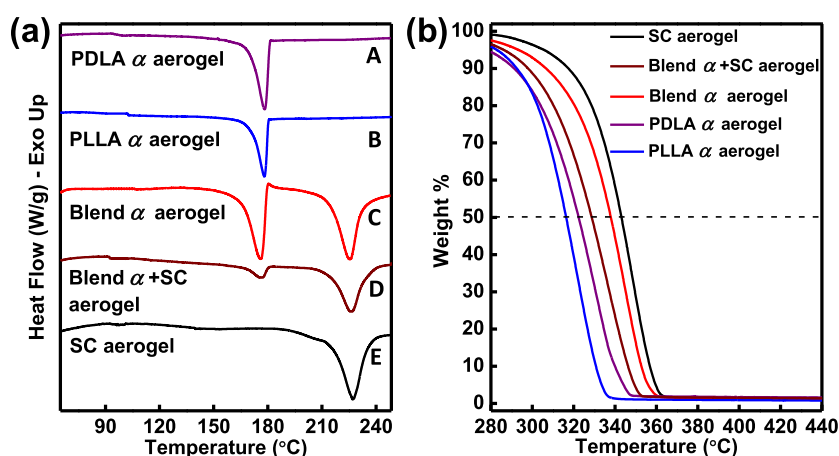
Figure 3. (a) DSC first heating curves and (b) TGA thermograms of various aerogels at a heating rate of 10 °C/min.
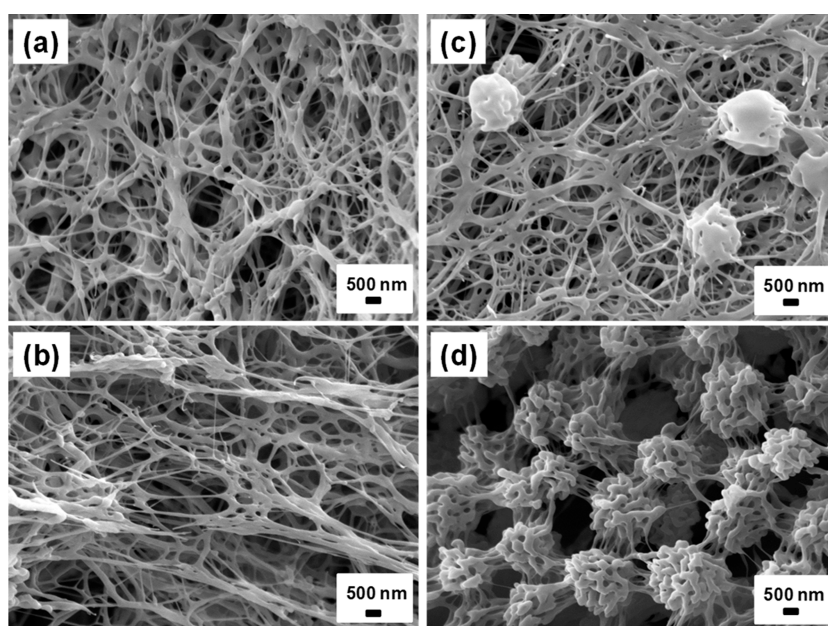

Figure 4. SEM images (magnification ×25,000) of (a) PDLA, (b) PLLA, (c) blend α-form, and (d) SC aerogels.

grams (Figure 3a (A, B)). The SC aerogel exhibited a higher melting temperature (227 ± 2 °C), and no homopolymer melting was observed in this case (Figure 3a (E)), which is absolute proof of the crystal purity of the prepared SC aerogel. However, in the blend α-form aerogel, endotherms corresponding to the melting of both α and SC crystals were observed in the DSC. This is because, just after melting all the α crystals, the disordered PLLA and PDLA chains in the blend aerogel attain sufficient mobility to form SC crystals.[17,20] Pan and co-workers reported that the entanglements degree in freeze-dried samples play a crucial role in SC crystallization.[32] We speculate here that the lesser chain entanglements in aerogels are responsible for the reorganization of molten chains into SC just above the melting of α crystals, which is different from the bulk samples.[18,20] The endotherm (α crystal melting) followed by a small exotherm in Figure 3a (C) is characteristic of such polymer chain reorganization and crystal to crystal transition.[18,59] It has to be noted that in the case of α + SC aerogel, no such exotherm following the first endotherm was observed (Figure 3a (D)) due to the low contents of the α crystals in the starting sample. The thermal stability of the

aerogels was also enhanced upon SC formation, as shown in Figure 3b. The temperature at 50% weight loss ($T_{50\%}$) for PLLA, PDLA, blend α-form, α + SC, and SC aerogels are 316, 322, 329, 337, and 343 °C, respectively. In the case of PLLA/PDLA blend aerogels, the pure crystalline forms (α-form and SC) exhibited better thermal stability than the assorted (α + SC) form.

PLLA and PDLA aerogels displayed typical interconnected fibrillar network morphologies, as shown in the scanning electron microscopy (SEM) images (Figure 4a,b). Transmission electron microscopy (TEM) image of PLLA xerogel (gel which is dried under ambient conditions) also shows similar morphology (Figure S4a). However, in the blend α-form aerogel, some of the polymer fibers agglomerated into dense spherical bundles (Figures 4c and S4b), and these globular species displayed a randomly scattered distribution on the fibrillar network, as given in Figure S5. However, in this case, the microstructure is more of the homopolymer structure, except for the agglomerated species. It has to be noted that the spherical bundles are more in the TEM image (Figure S4b) due to the ambient drying conditions compared to the aerogels
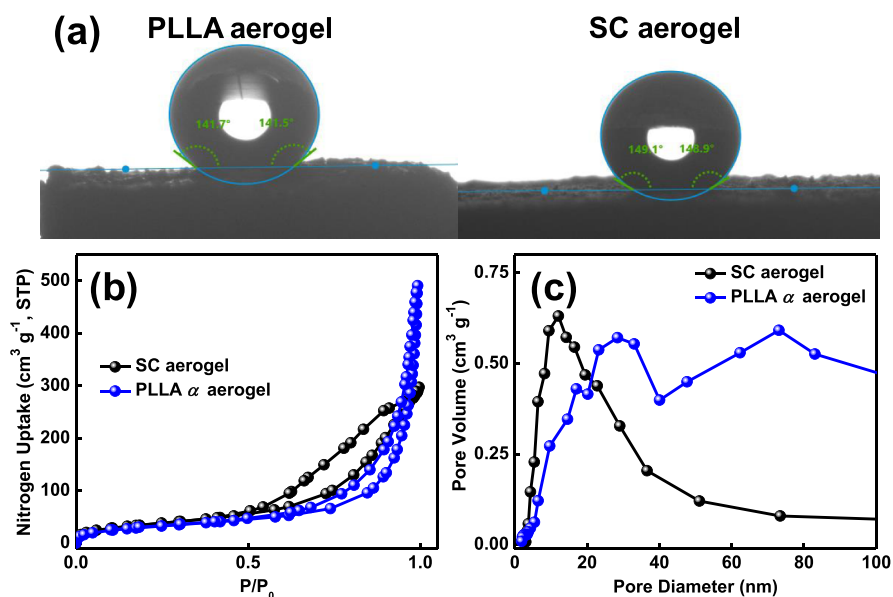
Figure 5. (a) Images of water droplets on the PLLA and SC aerogel surfaces and their contact angles. (b) N_2 adsorption−desorption isotherms and (c) pore size distributions of PLLA and SC aerogels.
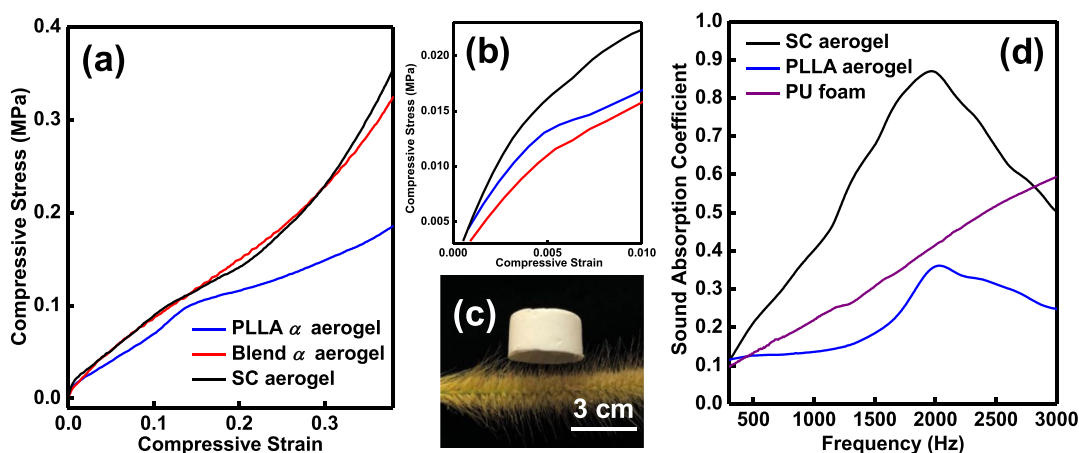

Figure 6. (a) Stress−strain plots of various aerogels under compression and (b) magnified linear elastic region. (c) Photographic image of SC aerogel on top of caterpillar grass. (d) Normal incident sound absorption coefficients of SC and PLLA aerogels measured in the frequency range of 300−3000 Hz.

prepared by the freeze-drying method (Figure 4c). On the other hand, SC aerogel exhibited a unique morphology that is different from the homopolymer and blend (α-form) aerogels. As seen in Figures 4d and S4c, most of the polymer fibrils were wrapped together into globular structures (nodular morphology) of micrometer dimensions upon SC formation, and the individual spheres were connected to each other by the short polymer fibers. For this to happen, during the thermal annealing of the blend gel, the PLLA and PDLA fibers have to unwind first to individual polymer chains, and then, the PLLA and PDLA chains have to come together at the molecular level. Unlike the blend α-form aerogel, the spherical structures in this case possess a certain level of porosity, owing to the loose winding of the polymer fibrils. Therefore, at the micrometer length scale, SC formation resulted in a major reorganization of the morphology from interconnected fibrillar structures to interconnected globular networks (nodular morphology). Such a difference in the microstructure is responsible for the enhancement of the aerogel thermal

properties. The observed morphologies of homopolymer and SC aerogels are different from that reported for PLA foams/aerogels.[60−64]

Several other properties were also elevated in the SC aerogel due to their unique morphological features, such as surface and mechanical properties. For example, the water contact angle (WCA) measured for SC aerogel was $149.0 \pm 1°$. WCA is a measure of the surface wettability of the aerogels. Since PLAs are inherently hydrophobic in nature, PLLA aerogel exhibited a very high WCA of $141.6 \pm 1°$. However, with the change in the surface morphology, more surface roughness was induced on the SC aerogel when compared to the PLLA aerogel, making it nearly superhydrophobic (Figure 5a). Similarly, the Brunauer−Emmett−Teller (BET) surface area was enhanced, and a narrow pore size distribution was obtained for SC aerogel when compared to the homopolymer aerogels. Figure 5b shows the nitrogen adsorption−desorption isotherms and pore size distribution curves of the PLLA and SC aerogels. Unlike the PLLA aerogel, the SC aerogel shows a typical Type

IV adsorption isotherm with a hysteresis loop (Figure 5b), characteristic of a mesoporous solid.[65] The pore size distribution in Figure 5c also validates the highly mesoporous structure of SC aerogel and the curve peaks around 12 nm. In the PLLA aerogel, the pore size distribution is broad and pore diameters above 50 nm dominate. Thus, it is appropriate to mention that the morphological switch has brought a shift from less mesoporous to highly mesoporous structures in PLA aerogels. The BET surface area was also enhanced in SC aerogel ($\sim$132 m^2 g^{-1}) in comparison with that of the PLLA aerogel ($\sim$113 m^2 g^{-1}).

Mechanical strength is of paramount importance for aerogels from the application point of view. PLA homopolymer aerogels are lagging in this department, and constant efforts have been put through to improve the mechanical properties of these aerogels.[7] The crystallinity of PLLA and SC aerogels prepared in this study are almost the same (52 ± 2%). However, there is a marked difference in the compression strength between these two aerogels, as shown in Figure 6a. The enlarged portion of Figure 6a (Figure 6b) shows the linear elastic region of the compressive stress−strain curve, the slope of which gives Young's modulus. All the aerogels used for the compression test have an overall porosity close to 90%. The compression moduli were calculated to be 2.0, 1.8, and 3.3 MPa for PLLA, blend α-form, and SC aerogels, respectively. The slight agglomeration of polymer fibrils in the blend α-form aerogel resulted in the lowering of modulus when compared to the homopolymer aerogels. However, the complete transformation of the blend into SC has furnished almost double the compression modulus. Even though PLLA and PDLA aerogels have interconnected fibrillar networks, these networks are not strong enough to withstand higher loads. However, in the SC aerogel, the winding of polymer fibrils into globular structures resulted in a muscular monolith. In addition, these spheres were connected to the neighboring spheres not by a single strand but by multiple polymer strands, hence making the interconnections quite strong. Thus, we could obtain PLA aerogels with superior load-bearing properties without compromising the high porosity by allowing the enantiomeric polymer chains to interact and form SC crystals (interconnected globular network). Figure 6c shows the SC aerogel being balanced on top of caterpillar grass; this indicates the ultra-lightweightness (density $\sim$ 0.09 g cm^{-3}) of the prepared aerogel.

The morphology switch has not just enhanced the mechanical properties of the aerogel but also improved its sound absorption ability. As demonstrated in our previous study on sPS aerogels, the differences in the pore structure, pore volume, and surface area can have significant effects on the sound insulation of aerogels.[52] The ratio of absorbed sound intensity in the material to the incident sound intensity is known as the normal incident sound absorption coefficient of a particular material. Figure 6c is the plot of the sound absorption coefficient of PLLA and SC aerogels at various frequencies (300−3000 Hz); for comparison, the data obtained for a commercial sound insulator [polyurethane (PU) foam] is also provided. Below 3000 Hz, the SC aerogel exhibited multifold enhancement in the sound absorption than the PLLA aerogel, and the absorption coefficients are way better than the PU foam. In the frequency range of 1800−2000 Hz, absorption coefficients as high as 0.85 were obtained for the SC aerogel. The excellence in the acoustic insulation performance of the SC aerogel is attributed to its largely

mesoporous structure. Sound waves get scattered multiple times inside the porous structure, resulting in the vibration of the pore walls. Also, the enhanced friction causes air viscosity consumption. In both these situations, the sound energy will be converted as heat within the material, resulting in a reduction of the sound pressure. As the market is looking for sustainable alternatives to the age-old sound insulation materials, these aerogels with superior comprehensive properties can be excellent candidates.

Based on the results obtained, we have clarified the development of hierarchical structures in PLLA/PDLA blend aerogels (Figure 7). Though the homopolymer gels crystallized
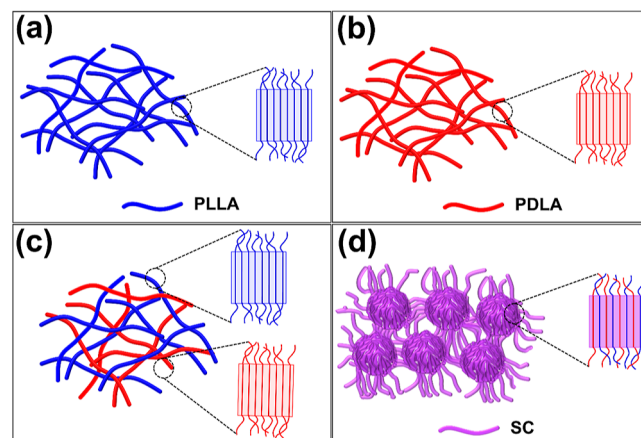

Figure 7. Schematic diagram showing the hierarchical structures of various aerogels (a) PLLA α aerogel, (b) PDLA α aerogel, (c) blend α aerogel, and (d) blend SC aerogel.

into the ε form, upon the aerogel preparation, the structure was transformed to the α-form, and higher-ordered structures show interconnected fibrillar networks in aerogels (Figure 7a,b). The PLLA/PDLA blend in DMF also crystallized into the ε-form on thermoreversible gelation. The blend ε-form gel transformed to the α-form upon solvent exchange, and the corresponding α-form aerogel showed an interdigitated fibrillar network with dense agglomerates at random positions (Figure 7c). Here, the interdigitating occurs between the fibrils of opposite enantiomeric chains, as there is only a local disorder of the helical chains during the ε-to-α transition. However, when the blend ε-form gel was annealed at 70 °C, the polymer chains attain enough diffusion ability to find opposite enantiomeric chains for the alternate packing into SC crystals. The higher-ordered structure in SC aerogel shows an interconnected network of globular structures, which is completely different from the blend α-form microstructure. In order to form such a morphology, the enantiomeric polymer fibrils have to unwind into individual chains first. Only then can the PLLA chains twine with the PDLA chains to form interwoven ball-like microstructures, as shown in Figure 7d. The untangled polymer strands form connections between the individual spheres to form a network structure. Thus, it is appropriate to mention that thermal stimulus has not only induced chain mobility and diffusion at the molecular level but has also instigated prodigious microstructural reorganization, resulting in perfect SC formation in PLLA/PDLA blend gels and aerogels.

CONCLUSIONS

In summary, using the thermoreversible gelation approach, we reported the formation of crystalline pure SC gels and aerogels of PLA. The crystal complex forming solvent was used for the PLLA/PDLA blend gel formation. In the initial blend gel, the homopolymers crystallized independently into the corresponding crystal complexes (ε-form) rather than co-crystallizing into the SC. When the gel solvent was exchanged with water and freeze-dried, blend α-form aerogel was obtained. Thermal treatment of the blend gel resulted in crystalline phase transitions; ε-to-α transition occurred around 50 °C due to the solvent desorption from the crystal lattice to the amorphous region, and the subsequent reorganization of the helical chains occurred through a disordered state. At a higher annealing temperature of blend gel (at 70 °C), polymer chains acquired enough energy to diffuse through the system and find the opposite chains for the alternate packing. As a result, gel with a complete SC crystal structure was obtained, resulting in SC aerogel upon solvent exchange and freeze-drying. The transitions at the molecular level were accompanied by hierarchical structural changes and microstructural evolution. The interconnected fibrillar morphology in the α-form aerogels was converted to unique interwoven globular network morphology upon the SC formation. These transitions, both at the molecular level and at the micrometer length scale, resulted in noteworthy enhancements of the thermal, mechanical, and acoustic properties of the aerogel.

EXPERIMENTAL SECTION

Materials. PLLA ($M_w \sim 101$ kg/mol, $Đ \sim 1.8$) and PDLA ($M_w \sim 124$ kg/mol, $Đ \sim 1.37$) were purchased from Sigma-Aldrich. The solvent DMF [purity $\geq 99.9\%$] was supplied by Merck and used as received.

Preparation of Homopolymer Gels and Aerogels. 10 wt % solution of PLLA or PDLA in DMF was prepared by heating the solvent at 120 °C. The solution was cooled to below 0 °C by keeping it in the freezer. Thermoreversible gelation occurred immediately, and the resulting gel was aged at the same temperature for 48 h. Then, DMF in the gel was exchanged with water by immersing the gel fully in water. This water was replaced with fresh water 4−5 times over a period of 30 h in order to ensure the complete exchange. The hydrogel thus obtained was first frozen at −40 °C and then freeze-dried for 24 h to obtain a homopolymer aerogel with an overall porosity of 90%.

Preparation of PLLA/PDLA Blend Gels and Aerogels. Equal quantities of PLLA and PDLA were used to separately prepare 10 wt % solutions in DMF. The PLLA and PDLA solutions were then mixed thoroughly, and the mixed solution was cooled to below 0 °C in the freezer to obtain a PLLA/PDLA (1:1) blend gel. This gel was aged at the same temperature for 48 h before further use.

In order to prepare blend α-form aerogel, the above gel was solvent exchanged with water as described earlier and then freeze-dried.

In order to prepare SC aerogel, the above gel was first subjected to thermal annealing at 70 °C. For this, an oil bath was preheated to 70 °C using a hot plate, and the vial containing the gel was immersed entirely in the oil for 5−10 min. Then, the gel was cooled back to the RT and aged in the freezer (<0 °C) for 12 h. This was followed by solvent exchange and freeze-drying as before to obtain a complete SC aerogel. Following the same procedure, except for a change in the annealing temperature to 50 °C, will result in an (α + SC) aerogel.

Characterization. The porosity of different aerogel samples was determined from the density values using the following equation

$$P = 100 \left[1 - \frac{\rho_{ap}}{\rho_{pol}} \right]$$

(1)

where ρ_{ap} is the mass/volume ratio (apparent density) of the prepared aerogel, the volume is determined theoretically from the dimensions of the samples, and ρ_{pol} is the density of the bulk polymer. The XEUSS SAXS/WAXS system from Xenocs, operating at 50 kV and 0.60 mA in the transmission mode using Cu Kα radiation with a wavelength of 1.54 Å, was used for WAXD measurements. The two-dimensional patterns were recorded on a Mar 345 image plate system (detector), and the Fit2D software was used for data processing. Variable temperature WAXD measurements were carried out with the aid of a Linkam THMS 600 hot stage connected to the LNP 95 cooling system. The infrared spectra of the aerogel samples were collected using a PerkinElmer Series FT-IR spectrum-2 at a resolution of 4 cm^{-1} over a wavenumber range of 4000−400 cm^{-1} in the attenuated total reflectance (ATR) mode. DSC measurements were performed using an advanced research-grade modulated differential scanning calorimeter TA Q2000 under a nitrogen atmosphere. The heating rate adopted was 10 °C/min. TGA was carried out under continuous nitrogen flow using TA Q50, a fourth-generation thermogravimetric analyzer. The surface morphologies of various aerogels were probed using a Zeiss EVO 18 cryo-SEM operated at an accelerating voltage of 12 kV. A JEOL 2010 transmission electron microscope operating at 300 kV was used to examine the morphology of the xerogels. The gels were dispersed in DMF, drop casted on a carbon-coated copper grid, and naturally dried under a dust-free atmosphere. An automated DSA30 Drop Shape Analyzer (KRÜSS, Germany) was used for the measurement of WCA. From the nitrogen adsorption−desorption isotherm (Gemini 2375, Micromeritics, Norcross, USA), the BET surface area of the aerogels was measured. The samples were degassed at room temperature for 24 h before the measurement. The pore size distributions were also obtained from the isotherms using the Barrett−Joyner−Halenda (BJH) method. A universal testing machine (Hounsfield, H5KS UTM, Redhill, UK) with a crosshead speed of 1.3 mm min^{-1} was used for the compressive strength analysis of the aerogels. Cylindrical samples with a diameter-to-height ratio of approximately 1.5:1 were used for these measurements. The normal incident sound absorption coefficient of all of the samples was obtained using a Brüel and Kjær impedance tube, type 4206 (Denmark), via the two-microphone method. Cylindrical samples with a diameter of 29 mm and thickness of 12 mm were used for the measurements.

ASSOCIATED CONTENT

ⓢ Supporting Information

The Supporting Information is available free of charge at https://pubs.acs.org/doi/10.1021/acsapm.2c02041.

> WAXD patterns of PLLA/PDLA gels, temperature- and time-dependent WAXD patterns of the PLLA/PDLA blend ε gel, WAXD patterns of the PLLA/PDLA blend ε gel annealed at different temperatures, TEM images of xerogels (PLLA, PLLA/PDLA blend, and SC), and SEM images of blend and SC aerogels (PDF)

AUTHOR INFORMATION

Corresponding Author

E. Bhoje Gowd − *Materials Science and Technology Division, CSIR-National Institute for Interdisciplinary Science and Technology, Trivandrum 695 019 Kerala, India; Academy of Scientific and Innovative Research (AcSIR), Ghaziabad 201 002, India;* ⓞ orcid.org/0000-0002-2878-5845; Phone: +91-471-2515474; Email: bhojegowd@niist.res.in; Fax: +91-471-2491712

Authors

Vipin G. Krishnan − *Materials Science and Technology Division, CSIR-National Institute for Interdisciplinary Science and Technology, Trivandrum 695 019 Kerala, India;*

Academy of Scientific and Innovative Research (AcSIR), Ghaziabad 201 002, India

N. M. Praveena − Materials Science and Technology Division, CSIR-National Institute for Interdisciplinary Science and Technology, Trivandrum 695 019 Kerala, India; Academy of Scientific and Innovative Research (AcSIR), Ghaziabad 201 002, India

R. B. Amal Raj − Materials Science and Technology Division, CSIR-National Institute for Interdisciplinary Science and Technology, Trivandrum 695 019 Kerala, India

Kiran Mohan − Chemical Sciences and Technology Division, CSIR-National Institute for Interdisciplinary Science and Technology, Trivandrum 695 019 Kerala, India

Complete contact information is available at:
https://pubs.acs.org/10.1021/acsapm.2c02041

Notes
The authors declare no competing financial interest.

■ REFERENCES

(1) Zhao, S.; Malfait, W. J.; Guerrero-Alburquerque, N.; Koebel, M. M.; Nyström, G. Biopolymer Aerogels and Foams: Chemistry, Properties, and Applications. *Angew. Chem., Int. Ed.* **2018**, *57*, 7580−7608.

(2) Ahankari, S.; Paliwal, P.; Subhedar, A.; Kargarzadeh, H. Recent Developments in Nanocellulose-Based Aerogels in Thermal Applications: A Review. *ACS Nano* **2021**, *15*, 3849−3874.

(3) Takeshita, S.; Zhao, S.; Malfait, W. J.; Koebel, M. M. Chemistry of Chitosan Aerogels: Three-Dimensional Pore Control for Tailored Applications. *Angew. Chem., Int. Ed.* **2021**, *60*, 9828−9851.

(4) Reverchon, E.; Pisanti, P.; Cardea, S. Nanostructured PLLA−Hydroxyapatite Scaffolds Produced by a Supercritical Assisted Technique. *Ind. Eng. Chem. Res.* **2009**, *48*, 5310−5316.

(5) Salerno, A.; Fernández-Gutiérrez, M.; San Román del Barrio, J.; Pascual, C. D. Macroporous and Nanometre Scale Fibrous PLA and PLA-HA Composite Scaffolds Fabricated by a Bio Safe Strategy. *RSC Adv.* **2014**, *4*, 61491−61502.

(6) Mader, M.; Jérôme, V.; Freitag, R.; Agarwal, S.; Greiner, A. Ultraporous, Compressible, Wettable Polylactide/Polycaprolactone Sponges for Tissue Engineering. *Biomacromolecules* **2018**, *19*, 1663−1673.

(7) Chen, P.; Bai, D.; Tang, H.; Liu, H.; Wang, J.; Gao, G.; Li, L. Polylactide Aerogel with Excellent Comprehensive Performances Imparted by Stereocomplex Crystallization for Efficient Oil-Water Separation. *Polymer* **2022**, *255*, 125128.

(8) Aragón-Gutierrez, A.; Arrieta, M. P.; López-González, M.; Fernández-García, M.; López, D. Hybrid Biocomposites Based on Poly(Lactic Acid) and Silica Aerogel for Food Packaging Applications. *Materials* **2020**, *13*, 4910.

(9) Ikada, Y.; Jamshidi, K.; Tsuji, H.; Hyon, S. H. Stereocomplex Formation between Enantiomeric Poly(Lactides). *Macromolecules* **1987**, *20*, 904−906.

(10) Okihara, T.; Tsuji, M.; Kawaguchi, A.; Katayama, K.-I.; Tsuji, H.; Hyon, S.-H.; Ikada, Y. Crystal Structure of Stereocomplex of Poly(L-Lactide) and Poly(D-Lactide). *J. Macromol. Sci., Part B: Phys.* **1991**, *30*, 119−140.

(11) Brochu, S.; Prud'homme, R. E.; Barakat, I.; Jerome, R. Stereocomplexation and Morphology of Polylactides. *Macromolecules* **1995**, *28*, 5230−5239.

(12) Brizzolara, D.; Cantow, H.-J.; Diederichs, K.; Keller, E.; Domb, A. J. Mechanism of the Stereocomplex Formation between Enantiomeric Poly(Lactide)S. *Macromolecules* **1996**, *29*, 191−197.

(13) Cartier, L.; Okihara, T.; Lotz, B. Triangular Polymer Single Crystals: Stereocomplexes, Twins, and Frustrated Structures. *Macromolecules* **1997**, *30*, 6313−6322.

(14) Tsuji, H. Poly(Lactide) Stereocomplexes: Formation, Structure, Properties, Degradation, and Applications. *Macromol. Biosci.* **2005**, *5*, 569−597.

(15) Praveena, N. M.; Virat, G.; Krishnan, V. G.; Gowd, E. B. Stereocomplex Formation and Hierarchical Structural Changes During Heating of Supramolecular Gels Obtained by Polylactide Racemic Blends. *Polymer* **2022**, *241*, 124530.

(16) Zhang, J.; Sato, H.; Tsuji, H.; Noda, I.; Ozaki, Y. Infrared Spectroscopic Study of $CH_3 \cdots OC$ Interaction During Poly(L-Lactide)/Poly(D-Lactide) Stereocomplex Formation. *Macromolecules* **2005**, *38*, 1822−1828.

(17) Zhang, J.; Tashiro, K.; Tsuji, H.; Domb, A. J. Investigation of Phase Transitional Behavior of Poly(L-Lactide)/Poly(D-Lactide) Blend Used to Prepare the Highly-Oriented Stereocomplex. *Macromolecules* **2007**, *40*, 1049−1054.

(18) Fujita, M.; Sawayanagi, T.; Abe, H.; Tanaka, T.; Iwata, T.; Ito, K.; Fujisawa, T.; Maeda, M. Stereocomplex Formation through Reorganization of Poly(L-Lactic Acid) and Poly(D-Lactic Acid) Crystals. *Macromolecules* **2008**, *41*, 2852−2858.

(19) Pan, P.; Yang, J.; Shan, G.; Bao, Y.; Weng, Z.; Cao, A.; Yazawa, K.; Inoue, Y. Temperature-Variable FTIR and Solid-State ^{13}C NMR Investigations on Crystalline Structure and Molecular Dynamics of Polymorphic Poly(L-Lactide) and Poly(L-Lactide)/Poly(D-Lactide) Stereocomplex. *Macromolecules* **2012**, *45*, 189−197.

(20) Pan, P.; Han, L.; Bao, J.; Xie, Q.; Shan, G.; Bao, Y. Competitive Stereocomplexation, Homocrystallization, and Polymorphic Crystalline Transition in Poly(L-Lactic Acid)/Poly(D-Lactic Acid) Racemic Blends: Molecular Weight Effects. *J. Phys. Chem. B* **2015**, *119*, 6462−6470.

(21) Tsuji, H. Poly(Lactic Acid) Stereocomplexes: A Decade of Progress. *Adv. Drug Delivery Rev.* **2016**, *107*, 97−135.

(22) Li, Z.; Tan, B. H.; Lin, T.; He, C. Recent Advances in Stereocomplexation of Enantiomeric Pla-Based Copolymers and Applications. *Prog. Polym. Sci.* **2016**, *62*, 22−72.

(23) Zhou, D.; Xu, M.; Li, J.; Tan, R.; Ma, Z.; Dong, X.-H. Effect of Chain Length on Polymer Stereocomplexation: A Quantitative Study. *Macromolecules* **2021**, *54*, 4827−4833.

(24) Zhou, W.; Wang, K.; Wang, S.; Yuan, S.; Chen, W.; Konishi, T.; Miyoshi, T. Stoichiometry and Packing Structure of Poly(Lactic Acid) Stereocomplex as Revealed by Solid-State NMR and 13^c Isotope Labeling. *ACS Macro Lett.* **2018**, *7*, 667−671.

(25) Tashiro, K.; Kouno, N.; Wang, H.; Tsuji, H. Crystal Structure of Poly(Lactic Acid) Stereocomplex: Random Packing Model of PDLA and PLLA Chains as Studied by X-Ray Diffraction Analysis. *Macromolecules* **2017**, *50*, 8048−8065.

(26) Chen, W.; Wang, S.; Zhang, W.; Ke, Y.; Hong, Y.-l.; Miyoshi, T. Molecular Structural Basis for Stereocomplex Formation of Polylactide Enantiomers in Dilute Solution. *ACS Macro Lett.* **2015**, *4*, 1264−1267.

(27) Tsuji, H.; Ikada, Y. Stereocomplex Formation between Enantiomeric Poly(Lactic Acids). 9. Stereocomplexation from the Melt. *Macromolecules* **1993**, *26*, 6918−6926.

(28) Xie, Q.; Bao, J.; Shan, G.; Bao, Y.; Pan, P. Fractional Crystallization Kinetics and Formation of Metastable B-Form Homocrystals in Poly(L-Lactic Acid)/Poly(D-Lactic Acid) Racemic Blends Induced by Precedingly Formed Stereocomplexes. *Macromolecules* **2019**, *52*, 4655−4665.

(29) Tsuji, H.; Horii, F.; Hyon, S. H.; Ikada, Y. Stereocomplex Formation between Enantiomeric Poly(Lactic Acid)s. 2. Stereocomplex Formation in Concentrated Solutions. *Macromolecules* **1991**, *24*, 2719−2724.

(30) Liu, J.; Qi, X.; Feng, Q.; Lan, Q. Suppression of Phase Separation for Exclusive Stereocomplex Crystallization of a High-

Molecular-Weight Racemic Poly(L-Lactide)/Poly(D-Lactide) Blend from the Glassy State. *Macromolecules* **2020**, *53*, 3493−3503.

(31) Brzeziński, M.; Biela, T. Supramolecular Polylactides by the Cooperative Interaction of the End Groups and Stereocomplexation. *Macromolecules* **2015**, *48*, 2994−3004.

(32) Sun, C.; Zheng, Y.; Xu, S.; Ni, L.; Li, X.; Shan, G.; Bao, Y.; Pan, P. Role of Chain Entanglements in the Stereocomplex Crystallization between Poly(Lactic Acid) Enantiomers. *ACS Macro Lett.* **2021**, *10*, 1023−1028.

(33) Bao, R.-Y.; Yang, W.; Wei, X.-F.; Xie, B.-H.; Yang, M.-B. Enhanced Formation of Stereocomplex Crystallites of High Molecular Weight Poly(L-Lactide)/Poly(D-Lactide) Blends from Melt by Using Poly(Ethylene Glycol). *ACS Sustainable Chem. Eng.* **2014**, *2*, 2301−2309.

(34) Bao, R.-Y.; Yang, W.; Jiang, W.-R.; Liu, Z.-Y.; Xie, B.-H.; Yang, M.-B.; Fu, Q. Stereocomplex Formation of High-Molecular-Weight Polylactide: A Low Temperature Approach. *Polymer* **2012**, *53*, 5449−5454.

(35) Tsuji, H.; Hyon, S. H.; Ikada, Y. Stereocomplex Formation between Enantiomeric Poly(Lactic Acid)s. 4. Differential Scanning Calorimetric Studies on Precipitates from Mixed Solutions of Poly(D-Lactic Acid) and Poly(L-Lactic Acid). *Macromolecules* **1991**, *24*, 5657−5662.

(36) Daniel, C.; Dammer, C.; Guenet, J.-M. On the Definition of Thermoreversible Gels: The Case of Syndiotactic Polystyrene. *Polymer* **1994**, *35*, 4243−4246.

(37) Guenet, J.*Thermoreversible Gelation of Polymers and Biopolymers*; Academic Press, 1992.

(38) Daniel, C.; Menelle, A.; Brulet, A.; Guenet, J.-M. Thermoreversible Gelation of Syndiotactic Polystyrene in Toluene and Chloroform. *Polymer* **1997**, *38*, 4193−4199.

(39) Talley, S. J.; Yuan, X.; Moore, R. B. Thermoreversible Gelation of Poly(Ether Ether Ketone). *ACS Macro Lett.* **2017**, *6*, 262−266.

(40) Matsuda, Y.; Fukatsu, A.; Wang, Y.; Miyamoto, K.; Mays, J. W.; Tasaka, S. Fabrication and Characterization of Poly(L-Lactic Acid) Gels Induced by Fibrous Complex Crystallization with Solvents. *Polymer* **2014**, *55*, 4369−4378.

(41) Gowd, E. B.; Tashiro, K.; Ramesh, C. Structural Phase Transitions of Syndiotactic Polystyrene. *Prog. Polym. Sci.* **2009**, *34*, 280−315.

(42) Kobayashi, M.; Nakaoki, T.; Ishihara, N. Molecular Conformation in Glasses and Gels of Syndiotactic and Isotactic Polystyrenes. *Macromolecules* **1990**, *23*, 78−83.

(43) Daniel, C.; Deluca, M. D.; Guenet, J. M.; Brûlet, A.; Menelle, A. Thermoreversible Gelation of Syndiotactic Polystyrene in Benzene. *Polymer* **1996**, *37*, 1273−1280.

(44) Daniel, C.; Longo, S.; Fasano, G.; Vitillo, J. G.; Guerra, G. Nanoporous Crystalline Phases of Poly(2,6-Dimethyl-1,4-Phenylene)-Oxide. *Chem. Mater.* **2011**, *23*, 3195−3200.

(45) Daniel, C.; Pellegrino, M.; Venditto, V.; Aurucci, S.; Guerra, G. Nanoporous-Crystalline Poly(2,6-Dimethyl-1,4-Phenylene)Oxide (Ppo) Aerogels. *Polymer* **2016**, *105*, 96−103.

(46) Immirzi, A.; de Candia, F.; Iannelli, P.; Zambelli, A.; Vittoria, V. Solvent-Induced Polymorphism in Syndiotactic Polystyrene. *Macromol. Rapid Commun.* **1988**, *9*, 761−764.

(47) Marubayashi, H.; Asai, S.; Sumita, M. Complex Crystal Formation of Poly(L-Lactide) with Solvent Molecules. *Macromolecules* **2012**, *45*, 1384−1397.

(48) Marubayashi, H.; Asai, S.; Sumita, M. Guest-Induced Crystal-to-Crystal Transitions of Poly(L-Lactide) Complexes. *J. Phys. Chem. B* **2013**, *117*, 385−397.

(49) Rizzo, P.; Ianniello, G.; Venditto, V.; Tarallo, O.; Guerra, G. Poly(L-Lactic Acid): Uniplanar Orientation in Cocrystalline Films and Structure of the Cocrystalline Form with Cyclopentanone. *Macromolecules* **2015**, *48*, 7513−7520.

(50) Shaiju, P.; Murthy, N. S.; Gowd, E. B. Molecular, Crystalline, and Lamellar Length-Scale Changes in the Poly(L-Lactide) (PLLA) During Cyclopentanone (CPO) Desorption in PLLA/CPO Cocrystals. *Macromolecules* **2016**, *49*, 224−233.

(51) Praveena, N. M.; Shaiju, P.; Raj, R. B. A.; Gowd, E. B. Infrared Bands to Distinguish Amorphous, Meso and Crystalline Phases of Poly(Lactide)s: Crystallization and Phase Transition Pathways of Amorphous, Meso and Co-Crystal Phases of Poly(L-Lactide) in the Heating Process. *Polymer* **2022**, *240*, 124495.

(52) Krishnan, V. G.; Joseph, A. M.; Kuzhichalil Peethambharan, S.; Gowd, E. B. Nanoporous Crystalline Aerogels of Syndiotactic Polystyrene: Polymorphism, Dielectric, Thermal, and Acoustic Properties. *Macromolecules* **2021**, *54*, 10605−10615.

(53) Joseph, A. M.; Nagendra, B.; Shaiju, P.; Surendran, K. P.; Gowd, E. B. Aerogels of Hierarchically Porous Syndiotactic Polystyrene with a Dielectric Constant near to Air. *J. Mater. Chem. C* **2018**, *6*, 360−368.

(54) Liu, X.; Zhang, M.; Hou, Y.; Pan, Y.; Liu, C.; Shen, C. Hierarchically Superhydrophobic Stereocomplex Poly (Lactic Acid) Aerogel for Daytime Radiative Cooling. *Adv. Funct. Mater.* **2022**, *32*, 2207414.

(55) Sasaki, S.; Asakura, T. Helix Distortion and Crystal Structure of the α-Form of Poly(L-Lactide). *Macromolecules* **2003**, *36*, 8385−8390.

(56) Kang, S.; Hsu, S. L.; Stidham, H. D.; Smith, P. B.; Leugers, M. A.; Yang, X. A Spectroscopic Analysis of Poly(Lactic Acid) Structure. *Macromolecules* **2001**, *34*, 4542−4548.

(57) Zhang, J.; Duan, Y.; Sato, H.; Tsuji, H.; Noda, I.; Yan, S.; Ozaki, Y. Crystal Modifications and Thermal Behavior of Poly(L-Lactic Acid) Revealed by Infrared Spectroscopy. *Macromolecules* **2005**, *38*, 8012−8021.

(58) Chao, Y.-K.; Praveena, N. M.; Yang, K.-C.; Gowd, E. B.; Ho, R.-M. Crystallization of Polylactides Examined by Vibrational Circular Dichroism of Intra- and Inter-Chain Chiral Interactions. *Soft Matter* **2022**, *18*, 2722−2725.

(59) Gowd, E. B.; Shibayama, N.; Tashiro, K. Structural Changes in Thermally Induced Phase Transitions of Uniaxially Oriented δ_e Form of Syndiotactic Polystyrene Investigated by Temperature-Dependent Measurements of X-Ray Fiber Diagrams and Polarized Infrared Spectra. *Macromolecules* **2006**, *39*, 8412−8418.

(60) Salerno, A.; Domingo, C. Making Microporous Nanometre-Scale Fibrous PLA Aerogels with Clean and Reliable Supercritical CO_2 Based Approaches. *Microporous Mesoporous Mater.* **2014**, *184*, 162−168.

(61) Yan, Z.; Liao, X.; He, G.; Li, S.; Guo, F.; Zou, F.; Li, G. Green and High-Expansion PLLA/PDLA Foams with Excellent Thermal Insulation and Enhanced Compressive Properties. *Ind. Eng. Chem. Res.* **2020**, *59*, 19244−19251.

(62) Wang, X.; Pan, Y.; Liu, X.; Liu, H.; Li, N.; Liu, C.; Schubert, D. W.; Shen, C. Facile Fabrication of Superhydrophobic and Eco-Friendly Poly(Lactic Acid) Foam for Oil−Water Separation Via Skin Peeling. *ACS Appl. Mater. Interfaces* **2019**, *11*, 14362−14367.

(63) Kanno, T.; Uyama, H. Unique Leafy Morphology of Poly(Lactic Acid) Monoliths Controlled Via Novel Phase Separation Technology. *RSC Adv.* **2017**, *7*, 33726−33732.

(64) Wang, L.; Lee, R. E.; Wang, G.; Chu, R. K. M.; Zhao, J.; Park, C. B. Use of Stereocomplex Crystallites for Fully-Biobased Microcellular Low-Density Poly(Lactic Acid) Foams for Green Packaging. *Chem. Eng. J.* **2017**, *327*, 1151−1162.

(65) Barton, T. J.; Bull, L. M.; Klemperer, W. G.; Loy, D. A.; McEnaney, B.; Misono, M.; Monson, P. A.; Pez, G.; Scherer, G. W.; Vartuli, J. C.; Yaghi, O. M. Tailored Porous Materials. *Chem. Mater.* **1999**, *11*, 2633−2656.